

INTERNATIONAL SOIL AND WATER CONSERVATION RESEARCH (ISWCR)

Volume 8, No. 3, September 2020

CONTENTS

- P. Chuenchum, M. Xu, W. Tang
Predicted trends of soil erosion and sediment yield from future land use and climate change scenarios in the Lancang-Mekong River by using the modified RUSLE model 213
- M. Hatefi, S.H. Sadeghi, R. Erfanzadeh, M. Behzadfar
Inhibiting soil loss and runoff from small plots induced by an individual freeze-thaw cycle using three rangeland species 228
- P. Hu, J. Tang, J. Fan, S. Shu, Z. Hu, B. Zhu
Incorporating a rainfall intensity modification factor γ into the I_a -S Relationship in the NRCS-CN method. 237
- R.I. Zoghalmi, H. Hamdi, S. Mokni-Tlili, S. Hechmi, M.N. Khelil, N. Ben Aissa, M. Moussa, H. Bousnina, S. Benzarti, N. Jedidi
Monitoring the variation of soil quality with sewage sludge application rates in absence of rhizosphere effect 245
- Y. Wang, Y. Dong, Z. Su, S.M. Mudd, Q. Zheng, G. Hu, D. Yan
Spatial distribution of water and wind erosion and their influence on the soil quality at the agropastoral ecotone of North China 253
- K. Teka, M. Haftu, M. Ostwald, C. Cederberg
Can integrated watershed management reduce soil erosion and improve livelihoods? A study from northern Ethiopia 266
- Z. Li, X. Xu, Y. Zhang, K. Wang
Fingerprinting sediment sources in a typical karst catchment of southwest China 277
- F. Rassaei, M. Hoodaji, S.A. Abtahi
Cadmium speciation as influenced by soil water content and zinc and the studies of kinetic modeling in two soils textural classes 286
- Y. Pang, B. Wu, Y. Cao, X. Jia
Spatiotemporal changes in terrestrial water storage in the Beijing-Tianjin Sandstorm Source Region from GRACE satellites. 295
- B. Ngangom, A. Das, R. Lal, R.G. Idapuganti, J. Layek, S. Basavaraj, S. Babu, G.S. Yadav, P.K. Ghosh
Double mulching improves soil properties and productivity of maize-based cropping system in eastern Indian Himalayas. 308
- E. Aytaç
Unsupervised learning approach in defining the similarity of catchments: Hydrological response unit based *k-means* clustering, a demonstration on Western Black Sea Region of Turkey 321

International Soil and Water Conservation Research (ISWCR) Vol. 8 (2020) 213-332

ISSN 2095-6339
CN 10-1107/P

International Soil and Water Conservation Research

Volume 8, No.3, September 2020

国际水土保持研究



Available online at www.sciencedirect.com

ScienceDirect



The *International Soil and Water Conservation Research (ISWCR)* is the official journal of World Association of Soil and Water Conservation (WASWAC), which is a non-governmental, non-profit organization. The mission of WASWAC is to promote the wise use of management practices, to improve and safeguard the quality of land and water resources. The Journal is co-owned by the International Research and Training Center on Erosion and Sedimentation, China Water & Power Press, and China Institute of Water Resources and Hydropower Research.



20 Chegongzhuang West Road
IRTCES Building 401-514
Beijing 100048, China
+86 10 68766413
irtces@iwhr.com
www.irtces.org

The International Research and Training Center on Erosion and Sedimentation (IRTCES) was jointly set up by the Government of China and UNESCO. It aims at the promotion of international exchange of knowledge and cooperation in the studies of erosion and sedimentation.



Building D, No. 1, South Yuyuantan Road,
Beijing 100038, China
+86 10 68545882
lk@waterpub.com.cn
<http://www.waterpub.com.cn>

China Water & Power Press (CWPP) is affiliated to the Ministry of Water Resources of China, which takes leadership of science and technology publishing in China.



A-1 Fuxing Road,
Beijing100038, China
+86 10 68781650
dic@iwhr.com
<http://www.iwhr.com>

China Institute of Water Resources and Hydropower Research is the largest and most comprehensive research institute in the field of water resources and hydropower in China.

Publishing services provided by Elsevier B.V. on behalf of KeAi

International Soil and Water Conservation Research (ISWCR)

Volume 8, Number 3, September 2020

International Research and Training Center on Erosion and Sedimentation
China Water and Power Press
China Institute of Water Resources and Hydropower Research

International Soil and Water Conservation Research

(Quarterly, since June 2013)

Volume 8, Number 3, September 2020

国际水土保持研究 (英文)

Guoji Shuitu Baochi Yanjiu (Yingwen)

(季刊, 2013 年6 月创刊)

第8卷第3期, 2020 年9月

ISSN 2095-6339
国际标准连续出版物号 2095-6339

CN 10-1107/P
国内统一连续出版物号 10-1107/P

Competent Authority Ministry of Water Resources, P.R. China
主管单位 中华人民共和国水利部

Sponsors International Research and Training Center on Erosion and Sedimentation
China Water & Power Press
China Institute of Water Resources and Hydropower Research
主办单位 国际泥沙研究培训中心
中国水利水电出版社有限公司
中国水利水电科学研究院

Published & Distributed by China Water & Power Press
(Building D, No. 1 South Yuyuantan Road, Haidian District,
Beijing 100038, China)
Tel: 86-10-68545882
E-mail: iswcr@foxmail.com

出版发行 中国水利水电出版社有限公司
(北京市海淀区玉渊潭南路1号D座, 邮编100038)
电话: (010) 68545882
信箱: iswcr@foxmail.com

Printed by Beijing Jinglu Digital Printing Co., Ltd.
印刷 北京京鲁数码快印有限责任公司

Editor-in-Chief Mark Nearing, Lei Tingwu
主编 Mark Nearing、雷廷武

Price RMB 240 Yuan per Issue (for the mainland of China only)
定价 240 元/期

INTERNATIONAL SOIL AND WATER CONSERVATION RESEARCH (ISWCR)

Volume 8, No. 3, September 2020

CONTENTS

P. Chuenchum, M. Xu, W. Tang Predicted trends of soil erosion and sediment yield from future land use and climate change scenarios in the Lancang–Mekong River by using the modified RUSLE model.	213
M. Hatef , S.H. Sadeghi, R. Erfanzadeh, M. Behzadfar Inhibiting soil loss and runoff from small plots induced by an individual freeze-thaw cycle using three rangeland species	228
P. Hu, J. Tang, J. Fan, S. Shu, Z. Hu, B. Zhu Incorporating a rainfall intensity modification factor γ into the I_a -S Relationship in the NRCS-CN method.	237
R.I. Zoghlami, H. Hamdi, S. Mokni-Tlili, S. Hechmi, M.N. Khelil, N. Ben Aissa, M. Moussa, H. Bousnina, S. Benzarti, N. Jedidi Monitoring the variation of soil quality with sewage sludge application rates in absence of rhizosphere effect	245
Y. Wang, Y. Dong, Z. Su, S.M. Mudd, Q. Zheng, G. Hu, D. Yan Spatial distribution of water and wind erosion and their influence on the soil quality at the agropastoral ecotone of North China	253
K. Teka, M. Haftu, M. Ostwald, C. Cederberg Can integrated watershed management reduce soil erosion and improve livelihoods? A study from northern Ethiopia	266
Z. Li, X. Xu, Y. Zhang, K. Wang Fingerprinting sediment sources in a typical karst catchment of southwest China	277
F. Rassaei, M. Hoodaji, S.A. Abtahi Cadmium speciation as influenced by soil water content and zinc and the studies of kinetic modeling in two soils textural classes	286
Y. Pang, B. Wu, Y. Cao, X. Jia Spatiotemporal changes in terrestrial water storage in the Beijing-Tianjin Sandstorm Source Region from GRACE satellites	295
B. Ngangom, A. Das, R. Lal, R.G. Idapuganti, J. Layek, S. Basavaraj, S. Babu, G.S. Yadav, P.K. Ghosh Double mulching improves soil properties and productivity of maize-based cropping system in eastern Indian Himalayas	308
E. Aytaç Unsupervised learning approach in defining the similarity of catchments: Hydrological response unit based <i>k-means</i> clustering, a demonstration on Western Black Sea Region of Turkey	321

AIMS AND SCOPE

The *International Soil and Water Conservation Research (ISWCR)*, the official journal of World Association of Soil and Water Conservation (WASWAC) www.waswac.org, is a multidisciplinary journal of soil and water conservation research, practice, policy, and perspectives. It aims to disseminate new knowledge and promote the practice of **soil and water conservation**.

The scope of *International Soil and Water Conservation Research* includes research, strategies, and technologies for prediction, prevention, and protection of soil and water resources. It deals with identification, characterization, and modeling; dynamic monitoring and evaluation; assessment and management of conservation practice and creation and implementation of quality standards.

Examples of appropriate topical areas include (but are not limited to):

- Σ Soil erosion and its control
- Σ Watershed management
- Σ Water resources assessment and management
- Σ Nonpoint-source pollution
- Σ Conservation models, tools, and technologies
- Σ Conservation agricultural
- Σ Soil health resources, indicators, assessment, and management
- Σ Land degradation
- Σ Sedimentation
- Σ Sustainable development
- Σ Literature review on topics related soil and water conservation research

© 2020 International Research and Training Center on Erosion and Sedimentation and China Water and Power Press. Production and hosting by Elsevier B.V.

Peer review under responsibility of IRTCES and CWPP.

Notice

No responsibility is assumed by the *International Soil and Water Conservation Research (ISWCR)* nor Elsevier for any injury and/or damage to persons, property as a matter of product liability, negligence, or otherwise, or from any use or operation of any methods, products, instructions, or ideas contained in the material herein.

Although all advertising material is expected to conform to ethical standards, inclusion in this publication does not constitute a guarantee or endorsement of the quality or value of such product or of the claims made of it by its manufacturer.

Full text available on ScienceDirect



Contents lists available at ScienceDirect

International Soil and Water Conservation Research

journal homepage: www.elsevier.com/locate/iswcr

Original Research Article

Predicted trends of soil erosion and sediment yield from future land use and climate change scenarios in the Lancang–Mekong River by using the modified RUSLE model

Pavisorn Chuenchum ^a, Mengzhen Xu ^b, Wenzhe Tang ^{a,*}

^a Institute of Hydraulic Structures Engineering and Project Management, and State Key Laboratory of Hydrosience Engineering, Tsinghua University, Beijing, 100084, PR China

^b River Research Institute, And State Key Laboratory of Hydrosience Engineering, Tsinghua University, Beijing, 100084, PR China

ARTICLE INFO

Article history:

Received 2 April 2020

Received in revised form

4 June 2020

Accepted 28 June 2020

Available online 9 July 2020

Keywords:

Soil erosion

Sediment

Land use change

Climate change

RUSLE

ABSTRACT

Soil erosion and sediments in the Lancang–Mekong River Basin as a result of climate change and changes in land use pose a threat to the existence of the riparian people, biodiversity and ecosystems. This study seeks to assess the annual soil erosion in terms of spatial distribution and the trends of sediment yield with the climate and land changes in future scenarios in 2030 and 2040 through the modified RUSLE model. Future lands were simulated by using the MLP artificial neural network and the Markov chain analysis. The future climate was examined by using the Max Planck Institute model, which showed a corrected bias and downscaled grid size under the Representative Concentration Pathways (RCPs). The simulated land use indicated that the forest areas were converted mostly to agricultural lands and urban areas. In the future, the average rainfall under all RCP scenarios is higher than that from the historical period. The R and C factors changed constantly, thereby affecting the soil erosion rate and sediment yield. The maximum erosion was estimated at approximately 21,000 and 21,725 t/km²/y under RCP8.5 in both years. Meanwhile, the results of sediment yield in 2030 and 2040 under RCP scenarios were much higher when compared to historical sediment data around 66.3% and 71.2%, respectively. Thailand's plateau, some parts of Cambodia and Laos PDR and the Mekong Delta are vulnerable to increase soil erosion and sediment yield. Measures to address these issues need to be planned to prepare and mitigate the possible effects, especially the loss of storage capacity in dams.

© 2020 International Research and Training Center on Erosion and Sedimentation and China Water and Power Press. Production and Hosting by Elsevier B.V. This is an open access article under the CC BY-NC-ND license (<http://creativecommons.org/licenses/by-nc-nd/4.0/>).

1. Introduction

Soil erosion and sediment process are among the effects of climate change because of the increase of rainfall and temperature and land use change from human activities may lead to the growing trends of soil erosion and sediment quantity into the river channel in the Lancang–Mekong River Basin. This specific area is one of the important basins that has posed challenges from both the changing climate and land, especially land use change from hydropower development and construction. Most studies have confirmed that soil erosion and sediment problems in the Lancang–Mekong River Basin is severe from the last 50 years to present; increased soil

erosion trends resulting from climate and land use changes will also occur in many areas in the future because of the high susceptibility of the soil structure to land deterioration and deforestation (Kondolf et al., 2018; MRC, 2010b, 2019a; Ta et al., 2002). Increased sediments may negatively affect the potential storage capacity of dams and the efficiency of hydraulic structures (Eroğlu, Çakır, Sivrikaya, & Akay, 2009; K.; Fu & He, 2007; Vaezi, Abbasi, Keesstra, & Cerdà, 2017).

Studies on soil erosion and sediment issues in the large catchment have applied various theories and applications, such as conceptual (Schuol, Abbaspour, Srinivasan, & Yang, 2008), empirical (Ferreira, Panagopoulos, Andrade, Guerrero, & Loures, 2015) and physical models (Nord & Esteves, 2005). The Revised Universal Soil Loss Equation (RUSLE) is widely used in estimating soil erosion and sediment (Peng, Li, & Zhang, 2007; Thuy & Lee, 2017; Yao, Yang, & Cui, 2006, 2005; Q. Zhou, Yang, Zhao, Cai, & Ya, 2014). This RUSLE is

* Corresponding author.

E-mail addresses: huw18@mails.tsinghua.edu.cn (P. Chuenchum), mz xu@mail.tsinghua.edu.cn (M. Xu), twz@mail.tsinghua.edu.cn (W. Tang).

regarded as one of the extensive models because the different characteristics of the large river basin were tested in the simulation with certain geographical tools (Kayet, Pathak, Chakrabarty, & Sahoo, 2018; Teng et al., 2018; Terranova, Antronico, Coscarelli, & Iaquinta, 2009). Recent studies have also indicated that the RUSLE model can be modified to analyse the sediment yield in interesting sites in terms of sediment deposition and erosion (Chuenchum, Xu, & Tang, 2019; Kaffas, Hrissanthou, & Sevasas, 2018; Rangsiwanichpong, Kazama, & Gunawardhana, 2018).

Previous studies on land use change have attempted to examine the conversion of land use dynamics in many regions affecting soil erosion, hydrological conditions and greenhouse gas emissions through linear models, regression analysis, cellular automata, Markov chain analysis, neural networks and agent-based models (Guan et al., 2011; Guo et al., 2019; Mandle et al., 2017; Mas, Kolb, Paegelow, Camacho Olmedo, & Houet, 2014; Verburg et al., 2002). Most studies indicated that the land change modeller (LCM) in TerrSet software is appropriate for simulating the future land use and analysing the difference between historical and future lands (Ansari & Golabi, 2019; Azimi Sardari, Bazrafshan, Panagopoulos, & Sardooi, 2019; Kamwi et al., 2018). This model is based on the neutral network for creating the transition potential maps and the Markov chain analysis for simulating possible land use map. The General Circulation Models or Global Climate Models (GCMs) have been applied generally in climate change studies under emission scenarios to analyse the future climate trends (IPCC, 2013; 2019; Johnson, Westra, Sharma, & Pitman, 2011). However, the products of raw GCMs need to be downscaled in terms of grid size and symmetrical error (biases) need to be corrected with the historical period for the study of regional climate and other hydrological purposes (Hoang et al., 2016; Kiem et al., 2008; Mandle et al., 2017). Most studies recommended that researchers apply GCMs that are completely downscaled and bias-corrected from the available data sources of relevant institutes and projects, such as WorldClim, CGIAR, CORDEX and IMPAC-T, to consider other concerns (Huang, Wang, Li, & Cai, 2014; Raghavan, Liu, Nguyen, Vu, & Liong, 2017; Ruan, Liu, Wang, & Yao, 2019).

The prediction of soil erosion and sediment yield from future land use and climate change scenarios must be focused to plan and arrange countermeasures and mitigate its effects on the Lancang–Mekong River Basin. The study objectives are as follows: (a) to consider the risk of soil erosion and sediment yield variations in 2030 and 2040 by using the RUSLE model under the effects of the future land use and climate change conditions, (b) to study and simulate the conversion of future land use by using artificial neural network and Markov chain analysis in TerrSet software to determine the cropping management factor (C) and support practice factor (P) in 2030 and 2040 and (c) to consider the changing trends of future rainfall and rainfall erosivity factor (R) from the GCMs under RCP2.6 (optimistic), RCP4.5 (intermediate) and RCP8.5 (pessimistic). The research outputs can help policymakers and related organizations in designating and fulfilling the suitable policies and measures towards the sustainable development of this river basin.

2. Study area

The Lancang–Mekong River is one of the largest and most important river systems in Southeast Asia (Fig. 1). This river drains from the Qinghai–Tibet Plateau to Mekong Delta and flows 4909 km (MRC, 2010b; 2019a) through six countries, including China, Myanmar, Thailand, Lao PDR, Cambodia and Vietnam. The basin covers an area of 795,000 km² (MRC, 2005; 2010b, 2011; 2019a). The elevation varies from 0 to 6549 m above sea level. In the upper Mekong River Basin, the geographical features of the

mainstream river and tributaries are the complex mountains and deep valleys (MRC, 2010b; 2019a). Most flat land and floodplain are in the lower Mekong River Basin, especially the Tonle Sap lake and the Mekong Delta. The Lancang–Mekong River's geomorphology can be divided into six zones depending on the geomorphological characteristics and tectonic movement of the mainstream and sub-river in a basin (Piman & Shrestha, 2017), including the Lancang River, China border to upstream Vientiane, upstream Vientiane to Klong Chiam, Klong Chaim to Kratie, Kratie to Chaktoumuk, Tonle Sap River and Great Lake and Phnom Penh to Mekong Delta. The most of soils in this river basin comprises of three soil properties, including Orthic Acrisols (Ao), Lithosols (I) and Ferric Acrisols (Af), which are approximately 59% of a whole river basin (Chuenchum et al., 2019). Soil erosion in a river basin has eroded at an average rate of 5350 t/km²/y, and it tends to increase in intensity continuously from climate change and land-use change (Anthony et al., 2015; Chuenchum et al., 2019).

From the 1960s to the present, this basin has encountered many challenges from climate change and rapid socio-economic development from human demand and the expansion of urban and rural areas. Climate change has a direct effect on the natural ecosystems and agriculture because the mean of the basin-wide temperature increases at approximately 0.79 °C (IPCC, 2019). The upper basin also increases considerably in the cold catchment areas. The annual precipitation increases by approximately 200 mm, especially in the upper basin during the dry season. Many water development projects from human activities, especially cascade hydropower dams, have been built and operated to respond to the demands for water, energy and food of each country. A study showed that 133 hydropower dams in all states of the mainstream and sub-basins (i.e. operation, under construction, and planned) have been built (ICEM, 2010; MRC, 2019a; WLE Graeter Mekong, 2016). These conditions can remodulated land use that may occur due to climate change and developments. Monitoring of land use change in 2003 was confirmed that the forest areas around 50% of total basin were decreased from the major issues of dams (MRC, 2019a). Moreover, the effects of the changing climate and land can increase high potential for sheet and gully erosion and sediment transfer during the intense rains of the early monsoon season. Therefore, soil erosion in the Lancang–Mekong River Basin has changed, thereby affecting the storage capacity in dams and hydropower production despite the effect of sedimentation (K. Fu & He, 2007; Vaezi et al., 2017; Wang, Wu, & Wang, 2007).

3. Materials and methods

3.1. The RUSLE and the technique of sediment yield estimation

The RUSLE model is an empirical erosion model utilized in calculating and monitoring the average soil loss risk on land. This model was developed from the Universal Soil Loss Equation by the United States Department of Agriculture. The RUSLE method can be implemented based on literature values or applied to empirical and statistical data by using the GIS techniques (B. J. Fu et al., 2005; Karaburun, 2009; Lufafa, Tenywa, Isabirye, Majaliwa, & Woomeer, 2003). The results are reliable in terms of assessing the risks of water erosion (Ozcan, Erpul, Basaran, & Erdogan, 2007). Equation (1) is presented as the RUSLE model:

$$A = R \times K \times LS \times C \times P, \quad (1)$$

where,

A is the average annual soil erosion (t/ha·y),

R is the rainfall erosivity factor (MJ·mm/ha·hr·y),

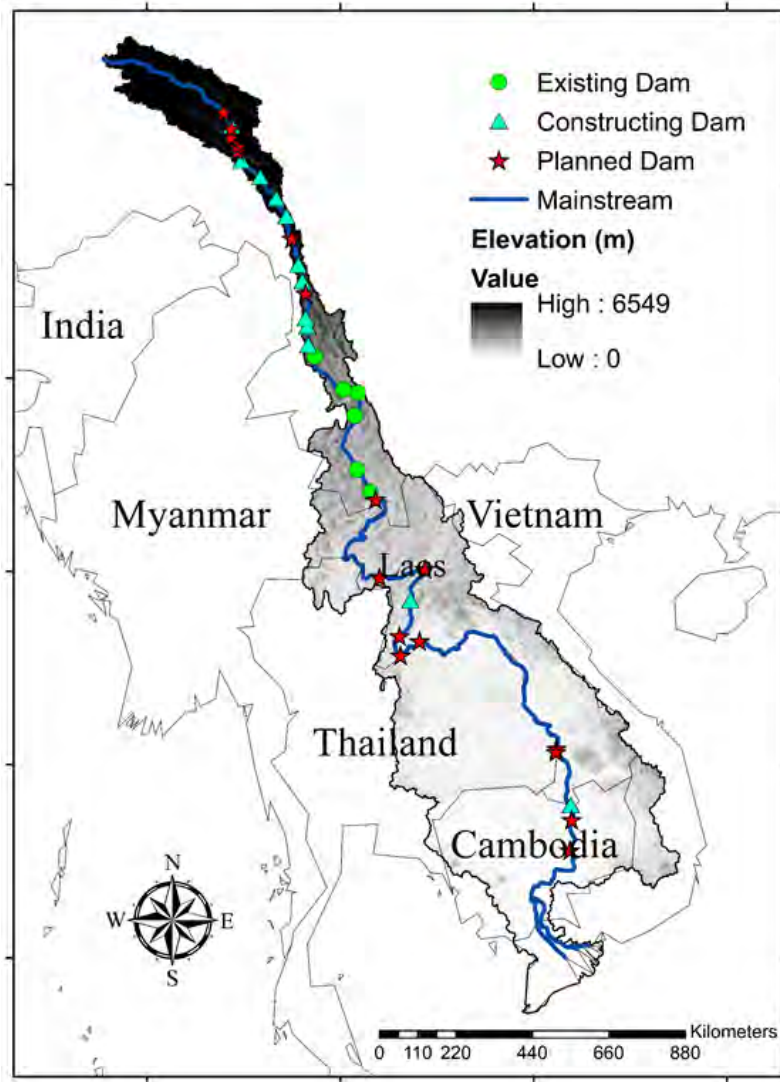


Fig. 1. Lancang–Mekong river basin.

K is the soil erodibility factor ($t \cdot hr/MJ \cdot mm$),
 LS is the topographic factor (dimensionless),
 C is the cropping management factor (dimensionless), and
 P is the support practice factor (dimensionless).

This study applied the RUSLE model for analysing soil erosion and sediment yield resulting from climate and land use changes that occurred due to global warming and the socio-economic development of human activities. The RUSLE model is appropriate for use in investigating soil erosion in the future through climate change scenarios by using the GCMs and land use change model (Arunyawat & Shrestha, 2016; Azimi Sardari et al., 2019; Plangoen, Babel, Clemente, Shrestha, & Tripathi, 2013). The R factor is applied by the GCMs. It has a corrected bias and downscaled grids of 1 km of the spatial resolution to analyse the future rainfall. The C and P factors are considered from the simulation of the LCM with FAO (2000) and Yang, Kanae, Oki, Koike, and Musiak (2003), respectively. The K and LS factors are determined as constant values because two factors cannot be predicted depending on time and space.

3.2. Climate change scenarios

Rainfall erosivity (R factor) is one of the vital factors in the study of soil erosion. Most studies have indicated that climate change has had considerable effect on the magnitude and variability of rainfall (IPCC, 2013; 2019; Moss et al., 2010). GCMs have been widely applied under the current Coupled Model Intercomparison Project Phase 5 (CMIP5) (Mehran, AghaKouchak, & Phillips, 2014; Taylor, Stouffer, & Meehl, 2012), which is the platform for simulated collaboration among international research groups worldwide. This step is carried out to consider future climate events. GCMs have been developed from the relationship between planetary atmosphere and ocean depending on the mathematical models and other related equations. The earth's atmosphere and ocean process were simulated to understand and forecast climate change.

The GCM rainfall dataset under CMIP5 was downloaded from the CGIAR Research Program on Climate Change, Agriculture and Food Security (<http://www.ccafs-climate.org/>). Such organisation provides future climate data in GCMs under the Earth System Grid online platform worldwide from the 2020s–2080s. The dataset

exhibited corrected symmetrical error (biases) because of the spatial resolution limitation in GCMs and was downscaled as a high spatial resolution of 1 km by applying the delta change method. This technique is used widely for the GCM output to analyse the catchment scale and hydrological modelling (Navarro-Racines, Tarapues, Thornton, Jarvis, & Ramirez-Villegas, 2020; Navarro & Tarapues, 2015; Ramirez Villejas & Jarvis, 2010).

We choose an appropriate GCM model in the Lancang–Mekong River Basin based on the literature and previous studies to investigate soil erosion and sediment yield. Most studies on changing climate analysis affirmed that the MPI-ESM-LR, which was developed by the Max Planck Institute (MPI) (Giorgetta et al., 2013), is appropriate for use in climate prediction in terms of the time and scale, such as the Lancang–Mekong River Basin (Hoang et al., 2016; Huang et al., 2014; Ruan et al., 2019) and Southeast Asia region (Hasson, Pascale, Lucarini, & Böhner, 2016; Kamworapan & Surussavadee, 2019; Raghavan et al., 2017), and global scale (Chhin & Yoden, 2018; Ruangrassamee, Khamkong, & Chuenchum, 2015; Tangang et al., 2019). The future rainfall data in 2015–2030 and 2015–2040 were simulated under three scenarios of greenhouse gas emissions, including RCP2.6 (optimistic), RCP4.5 (intermediate) and RCP8.5 (pessimistic). These scenarios were determined by the Representative Concentration Pathway (RCP) concept under the IPCC. The calculation of the R factor was applied according to Chuenchum et al. (2019); Li, Wang, and Liu (2013); F. J. Zhou, Chen, Lin, Huang, and Lu (1995), which is shown in Equation (2). This formula is appropriate for analysis because it was used in the assessment of the Lancang–Mekong River Basin as a case study before (Chuenchum et al., 2019).

$$R = \sum_{i=1}^{12} (-1.15527 + 1.792P_i) \quad (2)$$

where R is the rainfall erosivity factor ($\text{MJ} \cdot \text{mm}/(\text{ha} \cdot \text{hr} \cdot \text{y})$), and P_i is the monthly rainfall (mm).

3.3. Simulation of the land use change

Vegetation cover, such as the forest, grassland and agricultural area, is one of the influential factors affecting the soil erosion process. In the study of soil erosion, the cropping and management practices through the C factor are considered in terms of the vegetation cover. The soil erosion rate change is due to land use and cover changes by human activities. The prediction of land use change for the future period must be simulated by using the LCM compared with the baseline period (Anand, Gosain, & Khosa, 2018; Camacho Olmedo, Pontius, Paegelow, & Mas, 2015). LCM is one of the modules for the land planning and decision support system for ecological sustainability that is integrated fully into the TerrSet software developed by Clark Labs, Clark University. This software can also simulate with IDRISI software and the ArcGIS extension (Nor, Corstanje, Harris, & Brewer, 2017). LCM can analyse the present and future land use and cover changes and their implications by using the empirical model relationships to explanatory variables (slope and proximity to roads) and simulate future land use change scenarios (Pérez-Vega, Mas, & Ligmann-Zielinska, 2012). The simulated process in the LCM module can be divided into three processes, that is, change analysis (analysing previous land cover change), transition potentials (modelling the potential for land transitions) and change prediction (predicting the course of change into the future). These working processes are based on historical land change from a certain period to projected future land scenarios.

We need to understand the simulated process in TerrSet

software and LCM module to analyse the monitoring and prediction of land use and cover. The first step in the model is the change analysis that needs to be assessed for considering the difference between land cover maps in 1999, 2007 and 2015. The difference in land cover changes can be identified as the transitions from one land cover state to another with time. The effect of changing land use includes factors of urban area expansion, population growth and the human demand from natural resources. The second step is the transition potentials applied to the multilayer perceptron (MLP) artificial neural network. At this stage, the MLP artificial neural network is used to select transition variables for creating the transition potential maps appropriate for each transition in the sub model structure (Rumelhart, Hinton, & Williams, 1986). Each transition will be adjusted by decreasing the RMSE error to improve accuracy. The transition from one land use to another is simulated according to the explanatory variables, such as the elevation, slope and proximity to the road. The outcomes from this step will be the transition potential maps of each possible change.

Change prediction is the final step in the LCM module. The LCM can predict a future scenario for a specified future date by using the historical rates of change and the transition potential models. The change prediction will define the influential variables, constraints and incentives to the future changes, such as planned infrastructural modifications and zoning maps, between time steps i and j ; such process will then calculate the relative amount of transition to the future date by using the Markov chain analysis (Norris, 1997).

In this study, we applied the land use and cover in the Lancang–Mekong River Basin in 1999, 2007 and 2015 from the field survey of six riparian countries to analyse and detect the land change (MRC, 2010a). The land use and land cover data are 1 km of spatial resolution, which are obtained from the MRC (<https://portal.mrcmekong.org>). Nonetheless, the classification of land cover maps from each country must be adjusted by using the ArcGIS 10.5 extension to examine the land transition in each area. The six land use classes after the new classification in the LCM analysis are forest, grassland, agricultural land, bare land, urban area and water body. TerrSet software and the LCM module based on the MLP artificial neural network and the Markov chain analysis are applied to consider the land use change in the past and predict the future land use maps. This study focuses on the prediction of future land use in 2030 and 2040 that are based on the historical land use maps in 1999, 2007 and 2015.

The following six transition sub models were determined and inputted into the LCM module to analyse the sub models of the transition potentials by using the MLP artificial neural network: Forest to agriculture, forest to the urban area, grassland to agriculture, grassland to the urban area, water bodies to agriculture and water bodies to grassland. Six explanatory variables in land use change analysis (Figs. S1–S6) were also included. These variables include the digital elevation model (DEM), aspect, slope, distance from the road, distance from the mainstream river and distance from the residential land. Most studies affirmed that these explanatory variables have been applied to consider the land use change modelling.

The simulated result of the land use map in the future will then be calibrated and verified with the baseline land use maps using three Kappa index through the function of TerrSet software for accuracy assessment of land-use change models. The traditional Kappa index (K_{standara}) and the Kappa for no ability (K_{no}) show the consistency between two categorical datasets and two distribution of class sizes by using a stochastic model of random allocation of class transitions relative to the initial map, respectively (van Vliet, Bregt, & Hagen-Zanker, 2011). The Kappa for quantity and location (K_{location} & $K_{\text{location strata}}$) presents the consideration of the different accuracies in terms of quantity and location. Equations

(3)–(5) are presented as the $K_{standard}$, K_{no} , and $K_{location}$ & $K_{location}$ strata:

$$K_{standard} = \frac{p_o - p_e}{1 - p_e} \quad (3)$$

$$K_{no} = \frac{p_{Max} - p_e}{1 - p_e} \quad (4)$$

$$K_{location} = \frac{p_o - p_e}{p_{Max} - p_e} \quad (5)$$

where p_o is the observed fraction of agreement, p_e is the expected fraction of agreement, and p_{Max} is the maximum fraction of agreement. The maximum value of the Kappa index is usually set to 1.0 to mean absolute compliance. A decreasing Kappa index also means less matching. Hence, if the Kappa index values are consistent, then the simulated land use map can be applied in the study. Subsequently, the C factor is determined with our results of the predicted land use map by using the FAO (2000).

The C factor was analysed and the P factor determined. The support practice factor (P) reflects the effect of land use and cover on soil erosion, especially water erosion. The changing of potential erosion by flowing water can be explained through this factor, such as terraced contour farming, contouring, buffer strips and minimum tillage. After the C factor was simulated, the P factor was specified. Due the limitations in field observations in the Lancang–Mekong River Basin, the consideration of the P factor in this work is based on the study of Yang et al. (2003) that determined the land cover classification of the C factor to be the P factor (Table 1).

3.4. Soil erodibility and topographic factors

Soil erodibility (K factor) was considered from the physical soil properties in the Lancang–Mekong River Basin. The K factor was analysed by applying the free global data from the SoilGrids map at 1 km spatial resolution, which is developed and maintained by the ISRIC-World Soil Information (Hengl et al., 2014), according to Chuenchum et al. (2019) and the computation of the K method by Williams (1995); Williams, Renard, and Dyke (1983).

The topographic factor (LS factor) comprises the slope length (L) and steepness (S) factors. Both factors represent the topographical effect on the soil erosion process. This study used the DEM at 1 km of spatial resolution downloaded from the US Geological Survey (<https://earthexplorer.usgs.gov/>) and the GIS techniques by ArcGIS 10.5 software. The LS factor in each grid cell was analysed with the methods of Chuenchum et al. (2019); Panagos, Borrelli, and

Meusburger (2015); Renard, Foster, Weesies, McCool, and Yoder (1997); Van Remortel, Hamilton, and Hickey (2001); H. Zhang et al. (2017). Chuenchum et al. (2019) applied this method to calculate the LS factor in the Lancang–Mekong River Basin that was established in the analysis.

3.5. Consideration of the influential factors in the RUSLE model

Chuenchum et al. (2019) and Pham, Degener, and Kappas (2018) reported that the influential factors on soil erosion in the Lancang–Mekong River Basin can be identified by the relationship between the multiple linear regression and the logarithmic form. The five input factors in the RUSLE model were first converted into the logarithmic forms in Equations (6) and (7). The multiple linear regression was then used to analyse the influential factors on soil erosion in the basin under the climate and land change in future scenarios.

$$\ln(A) = \ln(R \times K \times LS \times C \times P), \quad (6)$$

$$\ln(A) = \ln(R) + \ln(K) + \ln(LS) + \ln(C) + \ln(P), \quad (7)$$

$$\ln(A) = \beta_0 + \beta_i(\ln R) + \beta_j(\ln K) + \beta_k(\ln LS) + \beta_l(\ln C) + \beta_h(\ln P), \quad (8)$$

where $\ln(A)$ represents the soil erosion rate in the logarithmic relationship, $\ln(R, K, LS, C$ and $P)$ represents the values of the RUSLE input factors in terms of the logarithmic form, β_0 denotes the intercept of soil erosion rate (constant values) and β_{i-h} is the regression coefficient of each explanatory variable from estimation. The standard coefficient (β) in Equation (8) can present the different units of the input factors. SPSS software was utilized to analyse the statistical results from the previous model. Statistical significance level at 95% is determined in this study.

3.6. Application of the modified RUSLE model for sediment yield estimation

After analysing soil erosion by applying original RUSLE model, the RUSLE factors were developed into the modified RUSLE model. This method can transform the estimation of the annual soil erosion to sediment yield based on the RUSLE input factors in each grid cell. The consideration of sediment yield of the modified RUSLE model in the climate and land changes under the future scenarios (2030 and 2040) was assessed and compared with the observed sediment data for the baseline period (1952–2011), which come from the MRC, LMC and related literature (He & Hsiang, 1997; Kummu, Lu, Rasphone, Sarkkula, & Koponen, 2008; Kummu & Varis, 2007; MRC, 2010b; Walling, 2008, 2011). Chuenchum et al.

Table 1
Land cover classification of the C and P factors.

Land Cover of the RUSLE	C factor (FAO, 2000)	P factor (Yang et al., 2003)
Urban area	0.1	1.0
Bare land	0.35	1.0
Dense forest	0.001	1.0
Sparse forest	0.01	1.0
Mixed forest and cropland	0.1	0.8
Cropland	0.5	0.5
Paddy field	0.1	0.5
Dense grassland	0.08	1.0
Sparse grassland	0.2	1.0
Mixed grassland and cropland	0.25	0.8
Wetland	0.05	1.0
Water body	0.01	1.0
Permanent ice and snow	0.001	1.0

Table 2
Evaluation of all sub models by using the MLP artificial neural network in transition.

Sub model	Accuracy Rate	Training RMSE	Testing RMSE
Forest to agricultural land	81.4%	0.0022	0.0024
Forest to urban area	73.9%	0.0020	0.0022
Rangeland to agricultural land	69.9%	0.0041	0.0043
Rangeland to urban area	83.4%	0.00198	0.00202
Water bodies to agricultural land	74.2%	0.0020	0.0021
Water bodies to rangeland	66.5%	0.0049	0.0050

(2019); Kaffas et al. (2018); Rangsiwanichpong et al. (2018) proposed the modified RUSLE model to estimate the sediment yield capacity or sediment deposition. Chuenchum et al. (2019) used this method to estimate the sediment yield in the Lancang–Mekong River Basin from 2000 to 2015. The results showed a high correlation (0.92) between the observed sediment yield and model output in the simulation.

The modified RUSLE model is described for the suspended sediment flow from a grid cell to other grid cells depending on the sediment yield of the initial grid cell (S_y) and the mean of sediment yield capacity of the sub-basin (S_c). Hence, if S_c is greater than S_y , then the sediment is deposited in a grid cell. Conversely, if S_y is more than S_c , then the sediment moves to the next grid. The calculation of the S_c in Equation (9) is computed by using the original RUSLE model with the area-averaged parameters. Equation (10) is calculated by using the individual parameters in each grid cell to consider S_y . The results from this method can be presented as the spatial distribution of the sediment yield capacity and sediment deposition and erosion mapping. Nonetheless, the method can be applied only during the estimation of the suspended sediment.

$$S_c = f \left(\frac{\sum_{i=1}^n I_1}{A_{basin}}, \frac{\sum_{i=1}^n I_2}{A_{basin}}, \dots, \frac{\sum_{i=1}^n I_5}{A_{basin}} \right), \quad (9)$$

$$S_y = f(I_1, I_2, \dots, I_5), \quad (10)$$

$$D_i \text{ if } S_y < S_c, \quad (11)$$

$$T_i \text{ if } S_y > S_c, \quad (12)$$

where S_c is the sediment yield capacity, S_y is the sediment yield, I_i represents the RUSLE parameters in the model (R , K , LS , C and P), A_{basin} is an area of the sub-basin, n is the number of data in each sub-basin, D_i is the sediment deposition in a cell i and T_i is the sediment transportation in cell i . In this method, S_y is the result of actual soil erosion in each cell and is obtained by considering the original RUSLE factors. Meanwhile, S_c is computed by adding the parameter values in the original RUSLE model divided by the area of the sub-basin. The five products are then multiplied to S_c .

Table 3
Probability of transition matrix from 1999 to 2015.

	Agricultural land	Forest	Rangeland	Urban area	Bare land	Waterbody
Agricultural land	0.992	0.002	0	0.006	0	0
Forest	0.048	0.950	0.002	0	0	0
Rangeland	0.030	0.006	0.964	0	0	0
Urban area	0	0	0	1	0	0
Bare land	0	0	0.006	0	0.994	0
Water body	0	0	0	0	0	0.987

4. Results & discussions

4.1. Climate change scenario

The outcomes of the rainfall projections of the MPI-ESM-LR model in all RCP scenarios in 2030 and 2040, which were down-scaled and bias-corrected using delta method, are shown in the Supplementary materials (Fig. S7). The average monthly rainfall (from 1990 to 2015) in the historical period was approximately 165 mm and the maximum and minimum rainfalls were 293 and 37 mm, respectively. The mean values of future rainfalls were 178.4, 176.4 and 180.7 mm and 177.3, 175.5, and 180.3 mm in 2030 and 2040 under the RCP scenarios, respectively. Accordingly, the trends of the future rainfalls demonstrated an increase in magnitude due to the effects of global warming and climate change. The probability of extreme rainfall in some sub-basins will also increase. Fig. S7 shows that the high values of rainfall were located mainly in Laos PDR, Cambodia, some parts of Vietnam and Mekong Delta because of the effects of the monsoon storms from the South China Sea and seasonal cycles of this region.

Fig. S8 show the comparison between the average of the monthly historical rainfall and the monthly future rainfalls in 2030 and 2040 under the RCP scenarios in the Lancang–Mekong River Basin. The results indicated that future rainfalls in 2030 and 2040 under the RCP scenarios presented similar patterns but differed in terms of the magnitude and peak rainfall in some months. The results show the characteristics of extreme events of rainfall projections affecting drought and flood. For instance, the number of rainfall projections in this river basin was lower than that of the historical rainfall during the dry season months. The peak rainfalls were also higher than the historical rainfall, especially under the RCP8.5 scenarios during most wet season months. Nevertheless, the results also indicated that the RCP4.5 scenarios in all years were underestimation mostly in terms of magnitude. Afterwards, future rainfalls were prepared and completely considered. Equation (2) was applied to compute the R factor in 2030 and 2040 under all RCP scenarios based on Chuenchum et al. (2019); Li et al. (2013); F. J. Zhou et al. (1995).

The R factor ranges in 2030 and 2040 were 160.7–997.7 and 163.2–993.1 MJ mm/(ha·hr·y) under all RCP scenarios, respectively. The spatial distribution of the R factor in 2030 and 2040 of all the scenarios in Fig. S9 exhibits a similar pattern but differ in terms of the magnitude of rainfall due to the effect of monsoon from the South China Sea in the seasonal cycles of this region. Previous research also indicated that the increasing rainfall (R factor) due to climate change resulted from the increased soil erosion rate, although climate conditions are different depending on each region (Plangoen et al., 2013; Pruski & Nearing, 2002; X. C.; Zhang, Liu, Li, & Zheng, 2009).

4.2. Simulation of land use change

4.2.1. Past land use change and transition potential modelling

Land use maps in 1999, 2007 and 2015 presented the changes

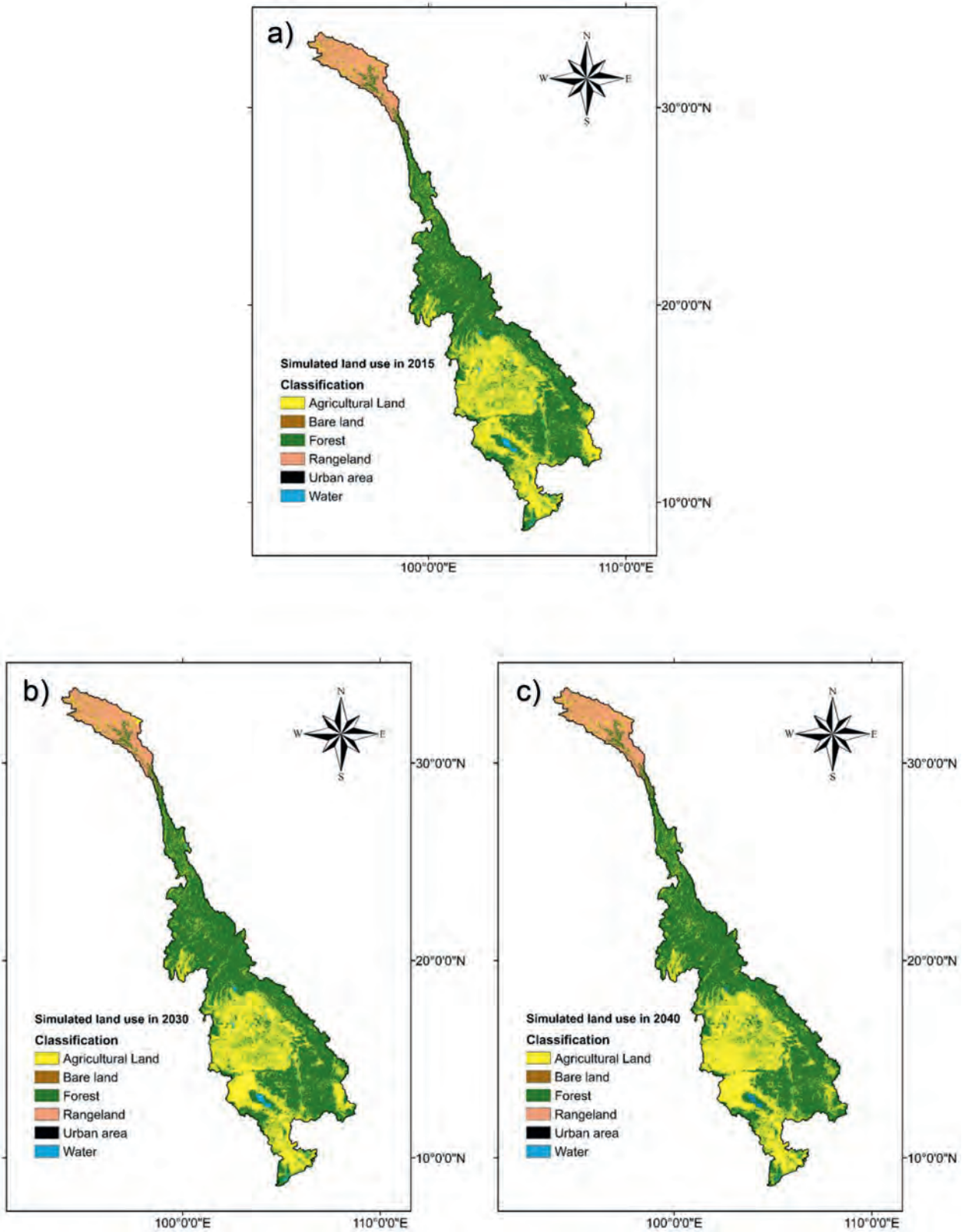


Fig. 2. Simulated land use map in (a) 2015, (b) 2030 and (c) 2040.

from the socio-economic development (Fig. S10), especially human activity and population growth. The baseline of the land use map in 1999 for LCM simulation is covered mainly by the forest (57.45%), followed by the agricultural lands (32.1%), rangelands (8.87%),

water bodies (1.45%), urban areas (0.08%) and bare lands (0.04%). The Kappa coefficient is considered in the analysis of land use maps in 1999, 2007 and 2015. The accuracy of the Kappa coefficients showed the produced land use maps can be applied to study the

land use change in this study. The Kappa coefficients were approximately 0.92, 0.86 and 0.91, thereby indicating that these values were high in all the years studied. The overall accuracies of the land use maps were 97.8%, 87% and 89.1% by using general accuracy assessment between observed land use maps and simulated land use maps in 1999, 2007, and 2015.

In this process, the LCM module simulated the transition potential maps by using the MLP artificial neural network from six explanatory variables, including the DEM, aspect, slope, distance from the road, distance from the mainstream river and distance from the residential land, for generating from one land use to another determined as six sub models. The evaluation results of the MLP artificial neural network for transition potential modelling are presented in Table 2. The table illustrates the values of accuracy rate, training RMSE and testing RMSE. The six sub models exhibited high accuracy and reliability ranging from 66.5% to 83.4%. Transition potential modelling by using the MLP artificial neural network in the LCM module is appropriate for this simulation of the land use change.

4.2.2. Land use projection using LCM

The change prediction process was computed from the transition potential maps, that is, the probability of transition from one land use in 1999 to another one in 2015 by using the Markov chain. The probability of the highest and lowest transition was the change of rangeland to an urban area and water body to rangeland, respectively, to simulate the land use projection in Table 3. The calibrations of the land use map in 2015 and the simulation of land use prediction in 2030 and 2040 were based on the probability of transition matrix from 1999 to 2015.

The calibration of the land use map in 2015 was used to test cell accuracy by using four Kappa statistics, including the $K_{standard}$, K_{no} and $K_{location}$ and $K_{location\ strata}$ according to Azimi Sardari et al. (2019); Plangoen et al. (2013); van Vliet et al. (2011). The $K_{standard}$, K_{no} and $K_{location}$ and $K_{location\ strata}$ were 0.958, 0.887 and 0.974, respectively. All Kappa statistics presented that the ability of the LCM module in TerrSet software in predicting the land use maps in 2030 and 2040 can be good in this case by using the Markov chain principle. The land use maps in 2015, 2030 and 2040 are shown in Fig. 2.

4.2.3. Trends of land use change using LCM

The LCM module in TerrSet software was used in the study of land use change. The results presented a relatively significant change in land use from 1999 to 2030 and 2040 (Fig. 2 and Table 4). The comparison results between the land use maps in 1999, 2030 and 2040 indicated that most areas were converted from forest and rangeland to agricultural land and urban area. The land use maps in 2030 and 2040 indicated that the forest area mostly decreased by approximately 2.27% and 3.27% or 18,065 and 26,030 km², respectively. The agricultural land constantly increases by 2.01% or 15,995 km² and 2.92% or 23,216 km² from 1999 to 2030 and 2040.

The urban area also rapidly expanded from 1999 by 0.38% or 2985 km² and 0.52% or 4113 km² from the socio-economic development in each country of the river basin. Nevertheless, the outcomes of land use simulation also showed that the rangeland, bare land and water body in the study area will change slightly in the near future.

The overall results indicated that the Lancang–Mekong River Basin has been facing that challenging issues such as deforestation, land degradation and population growth from developments in the future as areas change from agricultural land to urban areas. The conversion of land use affected the *C* and *P* factors in the RUSLE model because they reflect the ability of vegetation cover, especially forest area, to protect the soil surface from the erosion process and the change of potential water erosion through the supporting conservation practices. Consequently, if the forest area was destroyed, then the *C* factor values will increase despite the transformation to agricultural land and urban area. The trends of soil erosion rate will be high and may lead to extreme erosion in some specific areas.

4.3. Soil erosion analysis using the RUSLE model

The *C* factor values from the LCM module in TerrSet software were determined by using the FAO (2000) despite the limitation in the field investigation of the Lancang–Mekong River Basin. The *C* factor in 2030 and 2040 in Fig. S11 varies from 0 to 0.5, and its average was 0.25. The results indicated that the lower Mekong River Basin is more agricultural land than the upper one. The relatively high values of the *C* factor were shown (yellow). By contrast, the upper Mekong River, especially in China, is covered by the forest and rangeland, which reflected relatively low values of the *C* factor. The *P* factor values were specified following the recommendation by Yang et al. (2003) (Table 1). The range of the *P* factor in 2030 and 2040 was 0.5–1.0 (Fig. S11). The *P* value for cropland was assigned as 0.5, but the *P* values of paddy fields in many cases may be smaller than 0.5. Therefore, we suppose that the application of the *P* factor should depend on the researcher's discretion and suitability of research. Moreover, the further studies in soil erosion studies need to be cautious for configuration of the *P* value. Nevertheless, the *K* and *LS* factors in this study are constant in 2030 and 2040 in all the scenarios. The *K* factor was in the range of 0.012–0.0397 t h/MJ·mm (Fig. S12). The *K* factor values depended on the study area elevation. The areas with high elevation exhibited high *K* values, whereas the low *K* values were identified in the areas with low elevation. The range of the *LS* factor was 0–336 (Fig. S13). Most areas (65%) in the upper Mekong River Basin are steep and short length slopes. Accordingly, relatively high *LS* values were pointed out in the upper river basin from China to Laos PDR. The relatively low *LS* values were identified in the lower river basin from Laos PDR to Mekong Delta in Vietnam. The *LS* factor was analysed by using DEM 1 km of spatial resolution because this river basin is a large area for model simulation. However, the grid size is

Table 4
Land use change in 1999, 2007, 2015, 2030 and 2040.

Land use	1999		2007		2015		2030		2040	
	km ²	%								
Agricultural land	255,193	32.10	262,988	33.08	263,469	33.14	271,188	34.11	278,409	35.02
Forest	456,761	57.45	449,056	56.49	447,073	56.24	438,696	55.18	430,731	54.18
Rangeland	70,551	8.87	69,931	8.80	69,961	8.80	69,519	8.74	69,143	8.70
Urban area	633	0.08	1169	0.15	2352	0.30	3618	0.46	4746	0.60
Bare land	345	0.04	346	0.04	361	0.05	361	0.05	337	0.04
Water body	11,517	1.45	11,510	1.45	11,781	1.48	11,618	1.46	11,634	1.46

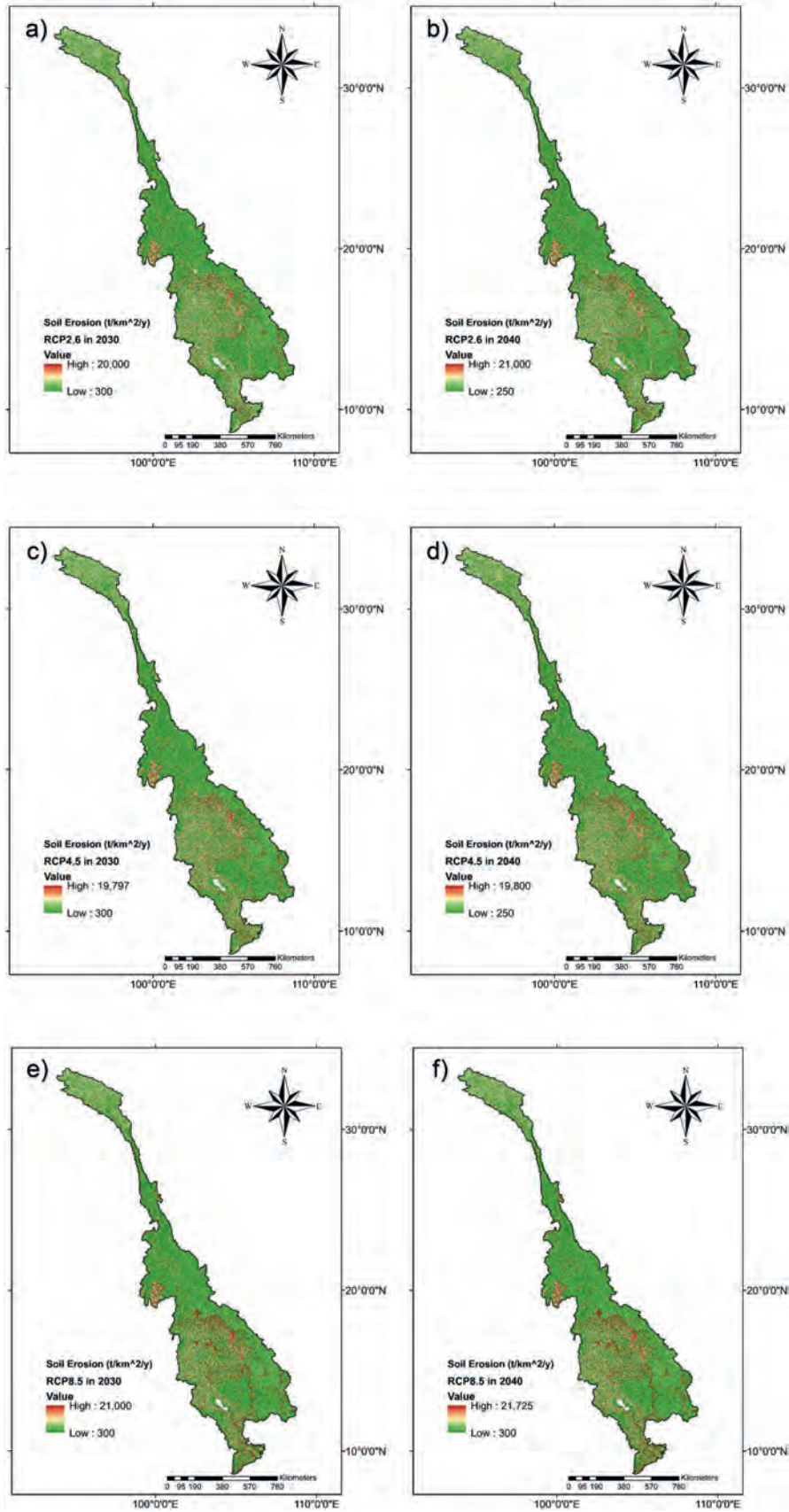


Fig. 3. Soil erosion rate in 2030 and 2040 under the (a, b) RCP2.6, (c, d) RCP4.5 and (e, f) RCP8.5 scenarios.

the coarse spatial resolution that may lead to error for the study of erosion rates. The study in the future need to be careful in this point for the further applications.

The results of the soil erosion prediction by using the RUSLE model can be divided into two cases in the near future, including soil erosion in 2030 and 2040 (Fig. 3). The first case shows that the mean soil erosion rates of all the RCP scenarios in 2030 were 10,150 t/km²/y (RCP2.6), 10,048.5 t/km²/y (RCP4.5) and 10,650 t/km²/y (RCP8.5). The second case presents that the average soil erosion rates of all the scenarios in 2040 were in the range of 9925 t/km²/y (RCP2.6), 9862.5 t/km²/y (RCP4.5) and 10,512.5 t/km²/y (RCP8.5). Both cases of soil erosion in 2030 and 2040 of all the RCP scenarios indicated that most lands in the lower Mekong River Basin were highly eroded by erosion agents. Most moderate and high erosion occurred in some parts of the upper river basin, Thailand's plateau, Tonle Sap and the Mekong Delta and most forest areas in Laos PDR and certain areas in Cambodia.

Chuenchum et al. (2019) were used as the baseline for the soil erosion rate for comparison with our research outcomes. The baseline of the maximum soil erosion rate was relatively at 10,000 t/km²/y from 2000 to 2015. Our results in 2030 and 2040 under the RCP scenarios and future lands indicated that the soil erosion rate was increasing around two times in some areas. The maximum of soil erosion in 2030 and 2040 was approximately 21,000 and 21,725 t/km²/y, respectively. The results indicated that the characteristics of soil erosion occurrence were changed on the spatial distribution and pattern from moderate to high and extreme levels. However, the minimum rate of soil erosion in the baseline (2000–2015) and future scenarios in 2030 and 2040 was also indicating a decrease of soil erosion rate in some areas from 700 t/km²/y to 250 t/km²/y, which was accounted for approximately 64.3% of the soil erosion rate. The central parts of the river basin and most areas in China have experienced decreasing soil erosion rates from the implementations of soil and water conservation (*P* factor) using structural and non-structural measures such as check dams and the application of vegetation cover (Barton et al., 2004; Chen, Zhang, Guo, Wang, & Wen, 2019; Duan et al., 2020).

4.4. Correlation analysis between the soil erosion rate and the RUSLE input factors

The results in a part of the correlation analysis between the soil erosion rate and the RUSLE input factors by using SPSS software were displayed in Table 5. The level of statistical significance in our hypothesis was specified at 95%. The results of the standardised coefficient can be considered as the logarithmic form of the multiple linear regression for analysis on the soil erosion rate and RUSLE input factors of the Lancang–Mekong River Basin. These equations can identify the influential factors on the rate of soil erosion occurrence.

All standardised coefficients of the RUSLE input factors in Table 5 can be substituted in Equation (7), and they represent a strong relationship with the RUSLE input factors of the soil erosion rate.

The results clearly show that the *C* factor was a strong influencing factor for soil erosion in the Lancang–Mekong River Basin, especially the lower Mekong River Basin, because of the direct land use change according to the socio-economic development. Some specified areas are transforming from forest areas to agricultural lands and urban areas. This area exhibits advancement in the hydropower construction and development in projects, especially the sub-basins in Lao PDR and Cambodia. Therefore, the increased rate of soil erosion likely occurs due to the land use change in the near future.

These results corresponded with those of Arunyawat and Shrestha (2016); Arunyawat and Shrestha (2018); Chuenchum et al. (2019) where in the dynamics and conversion of the vegetation cover are the effects of the soil erosion occurrence in the Lancang–Mekong River Basin and other areas because the ability of the *C* factor can protect topsoil from the erosion agents. The management options of soil–water conservation (*P* factor) that reduce vulnerability to soil erosion and nutrient loss include growing green manure crops and cover crops, crop residue retention, reduced tillage and maintenance of ground cover through improved grazing management. The relevant options also have mitigation co-benefits. The farming systems, including agroforestry, perennial pasture phases and usage of perennial grains, can substantially reduce soil erosion and nutrient leaching. The potential of cover crops can improve the soil conditions in some soil types and climate. Reducing deforestation and forest degradation can decrease greenhouse gas emissions by implementing sustainable forest management. The mechanism can reduce the extent of forest conversion to non-forest uses because this management aims to provide timber, fibre, biomass, non-timber resources and other ecosystem functions and services that can decrease greenhouse gas emissions and contribute to adaptation.

4.5. Sediment yield estimation using the modified RUSLE model

The modified RUSLE model was analysed according to Equations (8) and (9) to assess the sediment yield or sediment deposition areas in the Lancang–Mekong River Basin. Fig. 4 shows the simulated results of sediment deposition and erosion in each grid cell of the Lancang–Mekong River Basin in 2030 and 2040 under the RCP scenarios. The ranges of the potential sediment deposition and erosion in all years and RCP scenarios were approximately from <−5000 t/km²/y to >15,000 t/km²/y. All sediment deposition and erosion maps present that relatively high sediment erosion occurs along the Lancang–Mekong River's mainstream, especially in the lower Mekong River Basin. The north of the upper Mekong River Basin, the basin centre, Laos PDR, the lower Tonle Sap and the Mekong Delta are shown as the areas with high sediment erosion. The relatively high sediment deposition was observed in most areas in the upper Mekong River Basin (Qingshuilang and Weiyuanjiaing basin) and sub-basins in Thailand, Laos PDR and Cambodia.

The results of sediment deposition and erosion from modified RUSLE model can be analysed by using the specific sediment yield

Table 5

Analytical results of the correlation between soil erosion rate and input factors.

Multiple linear regression: $\ln(A) = \beta_0 + \beta_1(\ln R) + \beta_2(\ln K) + \beta_3(\ln LS) + \beta_4(\ln C) + \beta_5(\ln P)$						
Factors/Scenarios	RCP2.6 2030	RCP4.5 2030	RCP8.5 2030	RCP2.6 2040	RCP4.5 2040	RCP8.5 2040
<i>R</i>	0.193	0.202	0.203	0.209	0.208	0.213
<i>K</i>	0.100	0.102	0.103	0.086	0.080	0.075
<i>LS</i>	0.171	0.178	0.178	0.157	0.156	0.151
<i>C</i>	0.403	0.393	0.392	0.413	0.412	0.415
<i>P</i>	0.234	0.224	0.224	0.234	0.244	0.245

Remarks: all standardised coefficients were significant at 95% confidence.

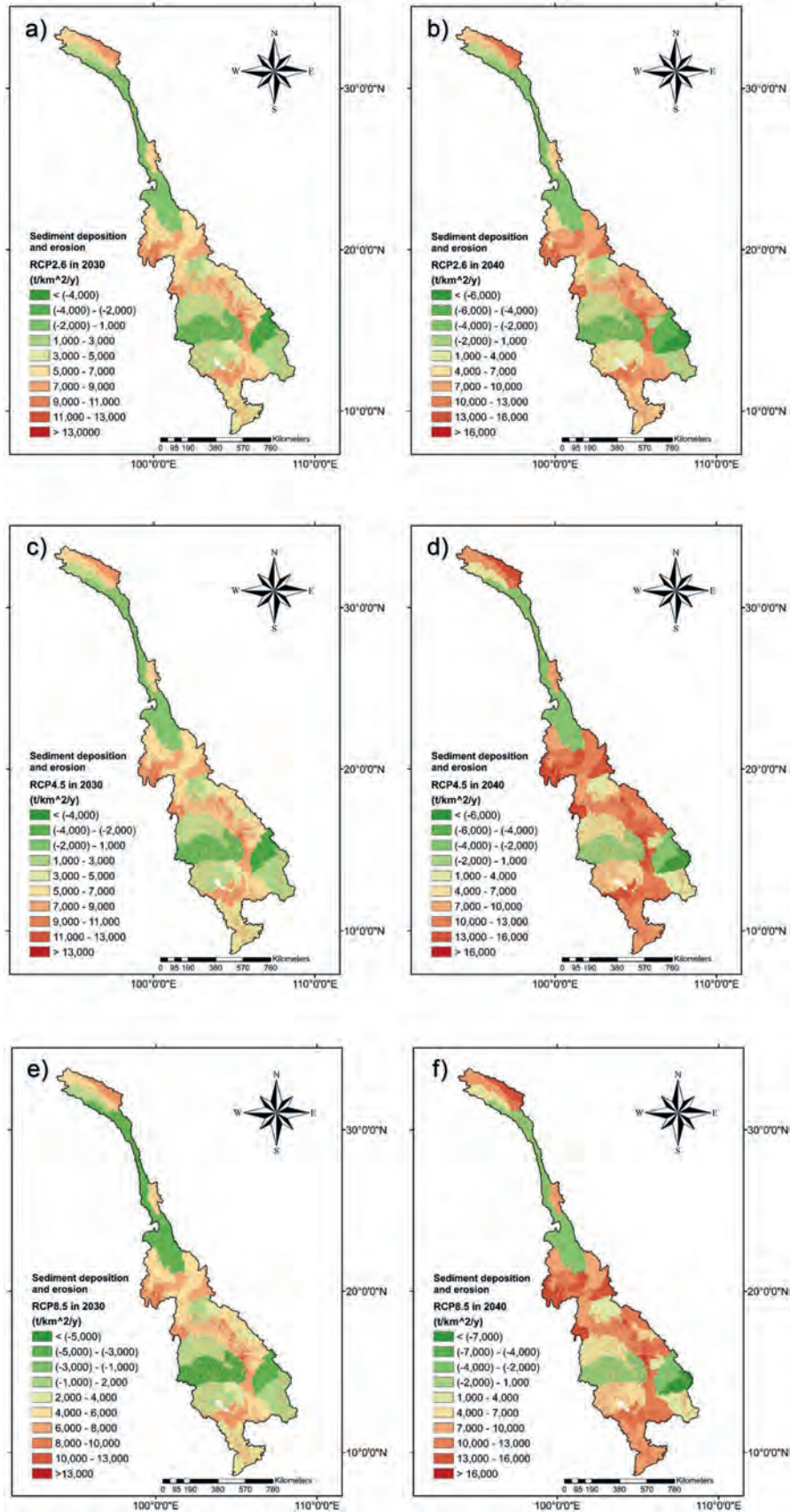


Fig. 4. Sediment deposition and erosion in 2030 and 2040 under the (a, b) RCP2.6, (c, d) RCP4.5 and (e, f) RCP8.5 scenarios.

Table 6

Comparison between observed and simulated SSY in 2030 under RCP scenarios.

Sub-basin	Observed SSY (t/km ² /y)	Model verification (Chuenchum et al., 2019)	Simulated SSY (t/km ² /y)			Percentage change comparing with observed SSY (%)		
			RCP2.6	RCP4.5	RCP8.5	RCP2.6	RCP4.5	RCP8.5
Qingshuilang	281	308	198	218	240	-42	-29	-17
Weiyuanjiang	382	412	302	332	365	-26	-15	-5
Nam Pho	489	525	540	594	653	9	18	25
Nam Chi	18	22	35	39	42	49	53	57
Nam Kam	35	42	57	63	69	39	44	49
Nam Khan	113	132	174	191	211	35	41	46
Nam Mae Ing	38	45	85	94	103	55	59	63
Nam Mun	27	34	59	65	71	54	58	62
Nam Ngum	36	44	88	97	106	59	63	66
Nam Ou	237	258	280	308	339	15	23	30
Nam Songkhram	31	40	86	95	104	64	67	70
Se Bang Fai	80	98	138	152	167	42	47	52
Se Bang Hieng	163	177	205	226	248	20	28	34
Se Done	206	218	278	306	336	26	33	39
St. Sen	33	40	99	109	120	67	70	72

(SSY) in each sub-basin compared with the observed sediment data from the 15 stations along the Lancang–Mekong River Basin. This study used the results of the estimated SSY from Chuenchum et al. (2019) to examine the model verification. The aforementioned study clearly showed that the modified RUSLE model can simulate the SSY in the Lancang–Mekong River Basin. The correlation result was approximately 0.92. The model verification of Chuenchum et al. (2019) compared with both results in 2030 and 2040 under the RCP scenarios indicated that the overall results were reasonable in terms of trends and spatial patterns. The comparison results between the observed sediment data and the simulated sediment in each year under the RCP scenarios are exhibited in Tables 6 and 7. All simulated results of the SSY in both years under the RCP scenarios clearly show the increasing trends, especially the lower Mekong River Basin (Nam Pho to St. Sen). St. Sen, Songkhram and Nam Ngum Basins were the third top ranks of the sub-basins to compute the percentage of the increased SSY rate in all years and the RCP scenarios compared with the observed sediment data. The average percentages in 2030 under all the RCP scenarios of these basins were approximately 69.6%, 67.1% and 62.1%. Meanwhile, the means of percentage in 2040 were relatively at 73.6%, 72% and 68.1%. The decreasing trends of the SSY show that the Qingshuilang and Weiyuanjiang Basins, which are located in the upper Mekong River Basin, reduced from the baseline sediment data at relatively 29.4% and 15.3% in 2030 and 20.3% and 9.9% in 2040 of all the RCP scenarios.

Table 7

Comparison between observed and simulated SSY in 2040 under RCP scenarios.

Sub-basin	Observed SSY (t/km ² /y)	Model verification (Chuenchum et al., 2019)	Simulated SSY (t/km ² /y)			Percentage change comparing with observed SSY (%)		
			RCP2.6	RCP4.5	RCP8.5	RCP2.6	RCP4.5	RCP8.5
Qingshuilang	281	308	213	234	258	-32	-20%	-9
Weiyuanjiang	382	412	317	349	384	-21	-10	0
Nam Pho	489	525	555	611	672	12	20	27
Nam Chi	18	22	50	55	61	64	67	70
Nam Kam	35	42	72	79	87	51	56	60
Nam Khan	113	132	189	208	229	40	46	51
Nam Mae Ing	38	45	100	110	121	62	65	69
Nam Mun	27	34	74	81	90	64	67	70
Nam Ngum	36	44	103	113	125	65	68	71
Nam Ou	237	258	295	325	357	20	27	34
Nam Songkhram	31	40	101	111	122	69	72	75
Se Bang Fai	80	98	153	168	185	48	52	57
Se Bang Hieng	163	177	220	242	266	26	33	39
Se Done	206	218	293	322	355	30	36	42
St. Sen	33	40	114	125	138	71	74	76

Therefore, the sediment trends in the upper Mekong River Basin were decreased from the soil conservation's policy in China using structural and non-structural measures and sediment trapping of hydropower dams. By contrast, the increased sediment in the lower Mekong River Basin occurred due to the land use change, especially the forest areas to agricultural lands or urban areas, and the development and construction of hydropower dams. Climate change also has considerable effects on rainfall and temperature conditions that effect soil erosion and sediments. Most studies affirm that the lower Mekong River Basin faces the risks posed by climate and land changes. MRC (2010b, 2019b) and Ingalls et al. (2018) reported that land use change in the Lancang–Mekong River Basin has occurred rapidly since 2000 because of the various developments and climate conditions in the upper and lower basins. Climate changes due to global warming have resulted in extreme events in this region, such as high temperature in the dry season and high rainfall rate in the wet season, resulting in certain changes to the long-term streamflow and sediments.

Furthermore, the conversion of soil erosion and sediments has a direct effect on morphological change and ecological system. Our study results indicated that sediment from the occurrence of soil erosion rate in the future had increasing trends in the lower Mekong River Basin, whereas the upper basin had significantly decreasing trends. Kondolf, Rubin, and Minear (2014) reported that the construction of hydropower dams and soil erosion change from

the changing climate and land use will cause a considerable change in the river and geomorphologies in the basin. The upper river basin has been eroding rapidly due to human factors, especially land use change as reflected by the deeply incised valleys and the active incision of river channels. Most parts in the lower Mekong River Basin also experience heavy rainfall and expeditious land use change that have a significant effect on riverbanks. Winemiller et al. (2016) reported that the construction of dams has caused not only a significant decrease in fish diversity but also blocked the movements of fish that connect populations and enable migratory species to complete their life cycles. Sediment alternation due to land use, climate and hydropower development and operation can alter the nutrient dynamics and other biochemical processes in the river channel, delta, estuary and marine-shelf ecosystems.

5. Conclusion

This study sought to investigate the changing trends of soil erosion and sediment yield from the effects of climate and land use changes in the Lancang–Mekong River Basin by using the modified RUSLE model. This river basin is known to have significant sediment problems from soil erosion that may cause obstructions to the storage capacity of hydropower dams, morphology and ecological system. The land use change in future scenarios demonstrated that most forest areas were transformed into agricultural lands and urban areas because of the pressures of socio-economic development in this region, which affected the increased C factor. The climate change factor increased the average rainfall of the whole basin and peak rainfall rate in some parts. Therefore, the R factor values in this study increased as compared with those in the historical periods. The findings from the changing climate and land use scenarios indicated increased soil erosion and sediment yield in most areas of the lower Mekong River Basin. In the meantime, China has implemented a soil conservation policy for protecting soil from the erosion agents in the upper Mekong River Basin. Hence, planning and implementation of the soil–water conservation policy should be in place in this river basin to promote sustainable management and control the land use change (P factor).

Funding

This research was funded by the National Key Research and Development Program of China (2016YFC0402407), National Natural Science Foundation of China (Grant Nos. 51779120, 51579135, 51379104 and 51079070), Chinese Academy of Sciences (XDA23090401) and State Key Laboratory of Hydrosience and Engineering (Grant Nos. 2013-KY-5 and 2015-KY-5).

Author contributions

Conceptualization: P.C., M.X. and W.T.; Methodology: P.C. M.X. and W.T.; Software: M.X. and W.T.; Formal analysis: P.C.; Investigation: M.X. and W.T.; Resources: P.C. and W.T.; Data curation: P.C. and W.T.; Writing, Original draft preparation: P.C.; Writing, Review and editing: P.C., M.X. and W.T.; Visualization: P.C.; Supervision: M.X. and W.T. and Funding acquisition: M.X. and W.T.

Data available statement

The data sets used and/or analysed during the current study are available from the corresponding author on reasonable request.

Declaration of competing interest

The authors declare no conflict of interest.

Acknowledgements

Our research team wishes to thank the Lancang–Mekong Cooperation and Mekong River Commission for helping us with the data needed in our analysis. We appreciate the help of the Clarks Labs at Clarks University in the development of the TerrSet software package. We also thank the beloved wife of the first author, Ms Usa Chuenchum, for the encouragement and the Chinese Government Scholarship for financial support as he pursued his Ph.D.

Appendix A. Supplementary data

Supplementary data to this article can be found online at <https://doi.org/10.1016/j.iswcr.2020.06.006>.

References

- Anand, J., Gosain, A. K., & Khosa, R. (2018). Prediction of land use changes based on Land Change Modeler and attribution of changes in the water balance of Ganga basin to land use change using the SWAT model. *The Science of the Total Environment*, 644, 503–519. <https://doi.org/10.1016/j.scitotenv.2018.07.017>.
- Ansari, A., & Golabi, M. H. (2019). Prediction of spatial land use changes based on LCM in a GIS environment for Desert Wetlands – a case study: Meighan Wetland, Iran. *International Soil and Water Conservation Research*, 7(1), 64–70. <https://doi.org/10.1016/j.iswcr.2018.10.001>.
- Anthony, E. J., Brunier, G., Besset, M., Goichot, M., Dussouillez, P., & Nguyen, V. L. (2015). Linking rapid erosion of the Mekong River delta to human activities. *Scientific Reports*, 5, Article 14745. <https://doi.org/10.1038/srep14745>.
- Arunyawat, S., & Shrestha, R. (2016). Assessing land use change and its impact on ecosystem services in northern Thailand. *Sustainability*, 8(8). <https://doi.org/10.3390/su8080768>.
- Arunyawat, S., & Shrestha, R. P. (2018). Simulating future land use and ecosystem services in Northern Thailand. *Journal of Land Use Science*, 13(1–2), 146–165. <https://doi.org/10.1080/1747423x.2018.1496157>.
- Azimi Sardari, M. R., Bazrafshan, O., Panagopoulos, T., & Sardooi, E. R. (2019). Modeling the impact of climate change and land use change scenarios on soil erosion at the Minab dam watershed. *Sustainability*, 11(12). <https://doi.org/10.3390/su11123353>.
- Barton, A. P., Fullen, M. A., Mitchell, D. J., Hocking, T. J., Liu, L., Wu Bo, Z., et al. (2004). Effects of soil conservation measures on erosion rates and crop productivity on subtropical Ultisols in Yunnan Province, China. *Agriculture, Ecosystems & Environment*, 104(2), 343–357. <https://doi.org/10.1016/j.agee.2004.01.034>.
- Camacho Olmedo, M. T., Pontius, R. G., Paegelow, M., & Mas, J.-F. (2015). Comparison of simulation models in terms of quantity and allocation of land change. *Environmental Modelling & Software*, 69, 214–221. <https://doi.org/10.1016/j.envsoft.2015.03.003>.
- Chen, G., Zhang, Z., Guo, Q., Wang, X., & Wen, Q. (2019). Quantitative assessment of soil erosion based on CSLE and the 2010 National soil erosion survey at regional scale in Yunnan Province of China. *Sustainability*, 11(12). <https://doi.org/10.3390/su11123252>.
- Chhin, R., & Yoden, S. (2018). Ranking CMIP5 GCMs for model ensemble selection on regional scale: Case study of the Indochina region. *Journal of Geophysical Research: Atmosphere*, 123(17), 8949–8974. <https://doi.org/10.1029/2017jd028026>.
- Chuenchum, P., Xu, M., & Tang, W. (2019). Estimation of soil erosion and sediment yield in the Lancang–Mekong River using the modified revised universal soil loss equation and GIS techniques. *Water*, 12(1), 135. <https://doi.org/10.3390/w12010135>.
- Duan, X., Rong, L., Bai, Z., Gu, Z., Ding, J., Tao, Y., et al. (2020). Effects of soil conservation measures on soil erosion in the Yunnan Plateau, southwest China. *Journal of Soil and Water Conservation*, 75(2), 131–142. <https://doi.org/10.2489/jswc.75.2.131>.
- Eroğlu, H., Çakır, G., Sivrikaya, F., & Akay, A. E. (2009). Using high resolution images and elevation data in classifying erosion risks of bare soil areas in the Hattila Valley Natural Protected Area, Turkey. *Stochastic Environmental Research and Risk Assessment*, 24(5), 699–704. <https://doi.org/10.1007/s00477-009-0356-5>.
- FAO. (2000). *Strategic environmental assessment: An assessment of the impact of cassava production and processing on the environment and biodiversity* (Paper presented at the FAO Proceedings of the validation forum on the global cassava development strategy).
- Ferreira, V., Panagopoulos, T., Andrade, R., Guerrero, C., & Loures, L. (2015). Spatial variability of soil properties and soil erodibility in the Alqueva reservoir watershed. *Solid Earth*, 6(2), 383–392. <https://doi.org/10.5194/se-6-383-2015>.
- Fu, K., & He, D. (2007). Analysis and prediction of sediment trapping efficiencies of the reservoirs in the mainstream of the Lancang River. *Chinese Science Bulletin*, 52(S2), 134–140. <https://doi.org/10.1007/s11434-007-7026-0>.
- Fu, B. J., Zhao, W. W., Chen, L. D., Zhang, Q. J., Lü, Y. H., Gulinck, H., et al. (2005). Assessment of soil erosion at large watershed scale using RUSLE and GIS: A case

- study in the loess plateau of China. *Land Degradation & Development*, 16(1), 73–85. <https://doi.org/10.1002/ldr.646>.
- Gorgetta, M. A., Jungclaus, J., Reick, C. H., Legutke, S., Bader, J., Böttinger, M., et al. (2013). Climate and carbon cycle changes from 1850 to 2100 in MPI-ESM simulations for the Coupled Model Intercomparison Project phase 5. *Journal of Advances in Modeling Earth Systems*, 5(3), 572–597. <https://doi.org/10.1002/jame.20038>.
- Guan, D., Li, H., Inohae, T., Su, W., Nagaie, T., & Hokao, K. (2011). Modeling urban land use change by the integration of cellular automaton and Markov model. *Ecological Modelling*, 222(20–22), 3761–3772. <https://doi.org/10.1016/j.ecolmodel.2011.09.009>.
- Guo, Y., Peng, C., Zhu, Q., Wang, M., Wang, H., Peng, S., et al. (2019). Modelling the impacts of climate and land use changes on soil water erosion: Model applications, limitations and future challenges. *Journal of Environmental Management*, 250, Article 109403. <https://doi.org/10.1016/j.jenvman.2019.109403>.
- Hasson, S.u., Pascale, S., Lucarini, V., & Böhner, J. (2016). Seasonal cycle of precipitation over major river basins in South and Southeast Asia: A review of the CMIP5 climate models data for present climate and future climate projections. *Atmospheric Research*, 180(1), 42–63. <https://doi.org/10.1016/j.atmosres.2016.05.008>.
- He, D. M., & Hsiang, T. K. (1997). Facilitating regional sustainable development through integrated multi-objective utilization, management of water resources in the Lancang-Mekong River Basin. *The Journal of Chinese Geography*, 7, 9–21. Retrieved from http://en.cnki.com.cn/Article_en/CJFDTOTAL-YNDL601.003.htm.
- Hengl, T., de Jesus, J. M., MacMillan, R. A., Batjes, N. H., Heuvelink, G. B., Ribeiro, E., et al. (2014). SoilGrids1km—global soil information based on automated mapping. *PLoS One*, 9(8), Article e105992. <https://doi.org/10.1371/journal.pone.0105992>.
- Hoang, L. P., Lauri, H., Kumm, M., Koponen, J., van Vliet, M. T. H., Supit, I., et al. (2016). Mekong River flow and hydrological extremes under climate change. *Hydrology and Earth System Sciences*, 20(7), 3027–3041. <https://doi.org/10.5194/hess-20-3027-2016>.
- Huang, Y., Wang, F., Li, Y., & Cai, T. (2014). Multi-model ensemble simulation and projection in the climate change in the Mekong River basin. Part I: temperature. *Environmental Monitoring and Assessment*, 186(11), 7513–7523. <https://doi.org/10.1007/s10661-014-3944-x>.
- ICEM. (2010). *MRC Strategic environmental assessment (SEA) of hydropower on the Mekong mainstream: Summary of the final report*. Retrieved from <http://www.mrcmekong.org/assets/Publications/Consultations/SEA-Hydropower/SEA-FR-summary-13oct.pdf>.
- Ingalls, M. L., Diepart, J. C., Truong, N., Hayward, D., Neil, T., Phomphakdy, C., et al. (2018). *State of land in the Mekong region*. Switzerland: Retrieved from Centre for Development and Environment (CDE), University of Bern. and Mekong Region Land Governance (MRLG), Vientiane, Lao PDR with Bern Open Publishing (BOP).
- IPCC. (2019). Special report on climate change and land. Retrieved from https://www.ipcc.ch/site/assets/uploads/2019/08/4.-SPM_Approved_Microsite_FINAL.pdf.
- Johnson, F., Westra, S., Sharma, A., & Pitman, A. J. (2011). An assessment of GCM skill in simulating Persistence across multiple time scales. *Journal of Climate*, 24(14), 3609–3623. <https://doi.org/10.1175/2011jcli3732.1>.
- Kaffas, K., Hrisanthou, V., & Sevastas, S. (2018). Modeling hydromorphological processes in a mountainous basin using a composite mathematical model and ArcSWAT. *Catena*, 162, 108–129. <https://doi.org/10.1016/j.catena.2017.11.017>.
- Kamwi, J., Cho, M., Kaetsch, C., Manda, S., Graz, F., & Chirwa, P. (2018). Assessing the spatial drivers of land use and land cover change in the protected and communal areas of the Zambezi region, Namibia. *Land*, 7(4). <https://doi.org/10.3390/land7040131>.
- Kamworapan, S., & Surussavadee, C. (2019). Evaluation of CMIP5 global climate models for simulating climatological temperature and precipitation for Southeast Asia. *Advances in Meteorology*, 1–18. <https://doi.org/10.1155/2019/1067365>, 2019.
- Karaburun, A. (2009). Estimating potential erosion risks in corlu using the Gis-based rusle method. *Fresenius Environmental Bulletin*, 18(9a), 1692–1700. Retrieved from <Go to ISI>://WOS:000270702400004.
- Kayet, N., Pathak, K., Chakrabarty, A., & Sahoo, S. (2018). Evaluation of soil loss estimation using the RUSLE model and SCS-CN method in hillslope mining areas. *International Soil and Water Conservation Research*, 6(1), 31–42. <https://doi.org/10.1016/j.iswcr.2017.11.002>.
- Kiem, A. S., Ishidaira, H., Hapuarachchi, H. P., Zhou, M. C., Hirabayashi, Y., & Takeuchi, K. (2008). Future hydroclimatology of the Mekong River basin simulated using the high-resolution Japan Meteorological Agency (JMA) AGCM. *Hydrological Processes*, 22(9), 1382–1394. <https://doi.org/10.1002/hyp.6947>.
- Kondolf, G. M., Rubin, Z. K., & Minear, J. T. (2014). Dams on the Mekong: Cumulative sediment starvation. *Water Resources Research*, 50(6), 5158–5169. <https://doi.org/10.1002/2013wr014651>.
- Kondolf, G. M., Schmitt, R. J. P., Carling, P., Darby, S., Arias, M., Bizzi, S., et al. (2018). Changing sediment budget of the Mekong: Cumulative threats and management strategies for a large river basin. *The Science of the Total Environment*, 625, 114–134. <https://doi.org/10.1016/j.scitotenv.2017.11.361>.
- Kummu, M., Lu, X. X., Rasphone, A., Sarkkula, J., & Koponen, J. (2008). Riverbank changes along the Mekong River: Remote sensing detection in the Vientiane–Nong Khai area. *Quaternary International*, 186(1), 100–112. <https://doi.org/10.1016/j.quaint.2007.10.015>.
- Kummu, M., & Varis, O. (2007). Sediment-related impacts due to upstream reservoir trapping, the Lower Mekong River. *Geomorphology*, 85(3–4), 275–293. <https://doi.org/10.1016/j.geomorph.2006.03.024>.
- Li, L., Wang, Y., & Liu, C. (2013). Effects of land use changes on soil erosion in a fast developing area. *International Journal of Environmental Science and Technology*, 11(6), 1549–1562. <https://doi.org/10.1007/s13762-013-0341-x>.
- Lufafa, A., Tenywa, M. M., Isabirye, M., Majaliwa, M. J. G., & Woomer, P. L. (2003). Prediction of soil erosion in a Lake Victoria basin catchment using a GIS-based Universal Soil Loss model. *Agricultural Systems*, 76(3), 883–894. [https://doi.org/10.1016/s0308-521x\(02\)00012-4](https://doi.org/10.1016/s0308-521x(02)00012-4).
- Mandle, L., Wolny, S., Bhagabati, N., Helsing, H., Hamel, P., Bartlett, R., et al. (2017). Assessing ecosystem service provision under climate change to support conservation and development planning in Myanmar. *PLoS One*, 12(9), Article e0184951. <https://doi.org/10.1371/journal.pone.0184951>.
- Mas, J.-F., Kolb, M., Paegelow, M., Camacho Olmedo, M. T., & Houet, T. (2014). Inductive pattern-based land use/cover change models: A comparison of four software packages. *Environmental Modelling & Software*, 51, 94–111. <https://doi.org/10.1016/j.envsoft.2013.09.010>.
- Mehran, A., AghaKouchak, A., & Phillips, T. J. (2014). Evaluation of CMIP5 continental precipitation simulations relative to satellite-based gauge-adjusted observations. *Journal of Geophysical Research: Atmosphere*, 119(4), 1695–1707. <https://doi.org/10.1002/2013jd021152>.
- Moss, R. H., Edmonds, J. A., Hibbard, K. A., Manning, M. R., Rose, S. K., van Vuuren, D. P., et al. (2010). The next generation of scenarios for climate change research and assessment. *Nature*, 463(7282), 747–756. <https://doi.org/10.1038/nature08823>.
- MRC. (2005). *Overview of the Hydrology of the Mekong basin*. Retrieved from <http://www.mekonginfo.org/assets/midocs/0001968-inland-waters-overview-of-the-hydrology-of-the-mekong-basin.pdf>.
- MRC. (2010a). *Databases of Mekong River Commission, Mekong River Commission (MRC)*. Retrieved from <http://portal.mrcmekong.org/search>.
- MRC. (2010b). *State of the basin report 2010*. Retrieved from <http://www.mrcmekong.org/assets/Publications/basin-reports/MRC-SOB-report-2010full-report.pdf>.
- MRC. (2011). *Assessment of basin-wide development scenarios - Main report*. Retrieved from <http://www.mrcmekong.org/assets/Publications/basin-reports/BDP-Assessment-of-Basin-wide-Dev-Scenarios-2011.pdf>.
- MRC. (2019a). *State of the basin report 2018*. Retrieved from http://www.mrcmekong.org/assets/Publications/SOBR-v8_Final-for-web.pdf.
- MRC. (2019b). *The study on the sustainable management and development of the Mekong River basin, including impacts of mainstream hydropower projects*. Retrieved from <http://www.mrcmekong.org/highlights/the-study-on-sustainable-management-and-development-of-the-mekong-river-including-impacts-of-mainstream-hydropower-projects/>.
- Navarro-Racines, C., Tarapues, J., Thornton, P., Jarvis, A., & Ramirez-Villegas, J. (2020). High-resolution and bias-corrected CMIP5 projections for climate change impact assessments. *Scientific Data*, 7(1), 7. <https://doi.org/10.1038/s41597-019-0343-8>.
- Navarro, C. E., & Tarapues, J. E. (2015). *Bias-correction in the CCAFS-climate Portal: A description of methodologies*. Columbia: Retrieved from Cali.
- Nor, A. N. M., Corstanje, R., Harris, J. A., & Brewer, T. (2017). Impact of rapid urban expansion on green space structure. *Ecological Indicators*, 81, 274–284. <https://doi.org/10.1016/j.ecolind.2017.05.031>.
- Nord, G., & Esteves, M. (2005). PSEM_2D: A physically based model of erosion processes at the plot scale. *Water Resources Research*, 41(8). <https://doi.org/10.1029/2004wr003690>.
- Norris, J. (1997). *Markov chains*. Cambridge, UK: Cambridge University Press.
- Ozcan, A. U., Erpul, G., Basaran, M., & Erdogan, H. E. (2007). Use of USLE/GIS technology integrated with geostatistics to assess soil erosion risk in different land uses of Indagi Mountain Pass—Çankırı, Turkey. *Environmental Geology*, 53(8), 1731–1741. <https://doi.org/10.1007/s00254-007-0779-6>.
- Panagos, P., Borrelli, P., & Meusburger, K. (2015). A new European slope length and steepness factor (LS-Factor) for modeling soil erosion by water. *Geosciences*, 5(2), 117–126. <https://doi.org/10.3390/geosciences5020117>.
- Peng, J., Li, D. D., & Zhang, Y. Q. (2007). Analysis of spatial characteristics of soil erosion in mountain areas of northwestern Yunnan based on GIS and RUSLE. *Journal of Mountain Science*, 25(5), 548–556 (In Chinese).
- Pérez-Vega, A., Mas, J.-F., & Ligmann-Zielinska, A. (2012). Comparing two approaches to land use/cover change modeling and their implications for the assessment of biodiversity loss in a deciduous tropical forest. *Environmental Modelling & Software*, 29(1), 11–23. <https://doi.org/10.1016/j.envsoft.2011.09.011>.
- Pham, T. G., Degener, J., & Kappas, M. (2018). Integrated universal soil loss equation (USLE) and Geographical Information System (GIS) for soil erosion estimation in A Sap basin: Central Vietnam. *International Soil and Water Conservation Research*, 6(2), 99–110. <https://doi.org/10.1016/j.iswcr.2018.01.001>.
- Piman, T., & Shrestha, M. (2017). Case study on sediment in the Mekong River Basin: Current state and future trends. Retrieved from www.sei-international.org.
- Plangoen, P., Babel, M., Clemente, R., Shrestha, S., & Tripathi, N. (2013). Simulating the impact of future land use and climate change on soil erosion and deposition in the Mae Nam nan sub-catchment, Thailand. *Sustainability*, 5(8), 3244–3274. <https://doi.org/10.3390/su5083244>.
- Pruski, F. F., & Nearing, M. A. (2002). Climate-induced changes in erosion during the 21st century for eight U.S. locations. *Water Resources Research*, 38(12). <https://doi.org/10.1029/2001wr000493>, 34-31-34-11.
- Raghavan, S. V., Liu, J., Nguyen, N. S., Vu, M. T., & Liong, S.-Y. (2017). Assessment of

- CMIP5 historical simulations of rainfall over Southeast Asia. *Theoretical and Applied Climatology*, 132(3–4), 989–1002. <https://doi.org/10.1007/s00704-017-2111-z>.
- Ramirez Villejas, J., & Jarvis, A. (2010). *Downscaling global Circulation model outputs*. Cali, CO: Retrieved from International Center for Tropical Agriculture (CIAT).
- Rangsiwanichpong, P., Kazama, S., & Gunawardhana, L. (2018). Assessment of sediment yield in Thailand using revised universal soil loss equation and geographic information system techniques. *River Research and Applications*, 34(9), 1113–1122. <https://doi.org/10.1002/rra.3351>.
- Ruangrassamee, P., Khamkong, A., & Chuenchum, P. (2015). 5–7 August, 2015). Assessment of precipitation simulations from CMIP5 climate models in Thailand. In *Paper presented at the 3rd Engineering institute of Thailand under H.M. The King's Patronage international Conference on water resources Engineering and the 6th National Convention on water resources Engineering*. Thailand: Udonthani.
- Renard, K. G., Foster, G. R., Weesies, G. A., McCool, D. K., & Yoder, D. C. (1997). *Predicting soil erosion by water: A Guide to conservation planning with the Revised Universal soil loss equation (RUSLE)*. USDA, Agricultural Research Service. *Agriculture Handbook Number 703*. Retrieved from.
- Ruan, Y., Liu, Z., Wang, R., & Yao, Z. (2019). Assessing the Performance of CMIP5 GCMs for projection of future temperature change over the lower Mekong basin. *Atmosphere*, 10(2). <https://doi.org/10.3390/atmos10020093>.
- Rumelhart, D. E., Hinton, G. E., & Williams, R. J. (1986). *Learning internal representation by error propagation* (Vol. 1). Cambridge, UK: MIT Press.
- Schuol, J., Abbaspour, K. C., Srinivasan, R., & Yang, H. (2008). Estimation of freshwater availability in the West African sub-continent using the SWAT hydrologic model. *Journal of Hydrology*, 352(1–2), 30–49. <https://doi.org/10.1016/j.jhydrol.2007.12.025>.
- IPCC. (2013). Summary for policymakers. In T. F. Stocker, D. Qin, G.-K. Plattner, M. Tignor, S. K. Allen, J. Boschung, et al. (Eds.), *Climate change 2013: The physical Science Basis. Contribution of working group I to the Fifth assessment Report of the Intergovernmental Panel on climate change*. Retrieved from https://archive.ipcc.ch/pdf/assessment-report/ar5/wg1/WG1AR5_SPM_FINAL.pdf.
- Tangang, F., Santisirisomboon, J., Juneng, L., Salimun, E., Chung, J., Supari, S., et al. (2019). Projected future changes in mean precipitation over Thailand based on multi-model regional climate simulations of CORDEX Southeast Asia. *International Journal of Climatology*, 39(14), 5413–5436. <https://doi.org/10.1002/joc.6163>.
- Ta, T. K. O., Nguyen, V. L., Tateishi, M., Kobayashi, I., Tanabe, S., & Saito, Y. (2002). Holocene delta evolution and sediment discharge of the Mekong River southern Vietnam. *Quaternary Science Reviews*, 21(16–17), 1807–1819. [https://doi.org/10.1016/S0277-3791\(02\)00007-0](https://doi.org/10.1016/S0277-3791(02)00007-0).
- Taylor, K. E., Stouffer, R. J., & Meehl, G. A. (2012). An overview of CMIP5 and the experiment design. *Bulletin of the American Meteorological Society*, 93(4), 485–498. <https://doi.org/10.1175/bams-d-11-00094.1>.
- Teng, H., Liang, Z., Chen, S., Liu, Y., Viscarra Rossel, R. A., Chappell, A., et al. (2018). Current and future assessments of soil erosion by water on the Tibetan Plateau based on RUSLE and CMIP5 climate models. *The Science of the Total Environment*, 635, 673–686. <https://doi.org/10.1016/j.scitotenv.2018.04.146>.
- Terranova, O., Antronico, L., Coscarelli, R., & Iaquinia, P. (2009). Soil erosion risk scenarios in the Mediterranean environment using RUSLE and GIS: An application model for Calabria (southern Italy). *Geomorphology*, 112(3–4), 228–245. <https://doi.org/10.1016/j.geomorph.2009.06.009>.
- Thuy, H. T., & Lee, G. (2017). Soil loss vulnerability assessment in the Mekong River basin. *Journal of the Korean Geo-Environmental Society*, 18(1), 37–47. <https://doi.org/10.14481/jkges.2017.18.1.37>.
- Vaezi, A. R., Abbasi, M., Keesstra, S., & Cerdà, A. (2017). Assessment of soil particle erodibility and sediment trapping using check dams in small semi-arid catchments. *Catena*, 157, 227–240. <https://doi.org/10.1016/j.catena.2017.05.021>.
- Van Remortel, R. D., Hamilton, M. E., & Hickey, R. J. (2001). Estimating the LS factor for RUSLE through iterative slope length processing of digital elevation data within arcInfo grid. *Cartography*, 30(1), 27–35. <https://doi.org/10.1080/00690805.2001.9714133>.
- Verburg, P. H., Soepboer, W., Veldkamp, A., Limpiada, R., Espaldon, V., & Mastura, S. S. (2002). Modeling the spatial dynamics of regional land use: the CLUE-S model. *Environmental Management*, 30(3), 391–405. <https://doi.org/10.1007/s00267-002-2630-x>.
- van Vliet, J., Bregt, A. K., & Hagen-Zanker, A. (2011). Revisiting Kappa to account for change in the accuracy assessment of land-use change models. *Ecological Modelling*, 222(8), 1367–1375. <https://doi.org/10.1016/j.ecolmodel.2011.01.017>.
- Walling, D. E. (2011). Human impact on the sediment loads of Asian rivers. *Sediment Problems and Sediment Management in Asian River Basins*, 349, 37–51. Retrieved from <Go to ISI>://WOS:000304975300004.
- Walling, D. E. (2008). The changing sediment load of the Mekong River. *Ambio*, 37(3), 150–157. [https://doi.org/10.1579/0044-7447\(2008\)37\[150:tcslot\]2.0.co;2](https://doi.org/10.1579/0044-7447(2008)37[150:tcslot]2.0.co;2). <https://search.crossref.org/?q=equals;Walling%2C+D.+E.+%282008%29.+The+changing+sediment+load+of+the+Mekong+River.+Ambio%2C+37%283%29%2C+150-157>.
- Wang, Z. Y., Wu, B., & Wang, G. (2007). Fluvial processes and morphological response in the Yellow and Weihe rivers to closure and operation of sanmenxia dam. *Geomorphology*, 91(1–2), 65–79. <https://doi.org/10.1016/j.geomorph.2007.01.022>.
- Williams, J. R. (1995). Chapter 25: The epic mode. In V. P. Singh (Ed.), *Computer models of Watershed Hydrology* (pp. 909–1000). Water Resource Publications.
- Williams, J. R., Renard, K. G., & Dyke, P. T. (1983). Epic - a new method for assessing erosions effect on soil productivity. *Journal of Soil and Water Conservation*, 38(5), 381–383. Retrieved from <Go to ISI>://WOS:A1983RM90400004.
- Winemiller, K. O., McIntyre, P. B., Castello, L., Fluet-Chouinard, E., Giarrizzo, T., Nam, S., et al. (2016). DEVELOPMENT AND ENVIRONMENT. Balancing hydro-pow and biodiversity in the Amazon, Congo, and Mekong. *Science*, 351(6269), 128–129. <https://doi.org/10.1126/science.aac7082>.
- WLE Graeter Mekong. (2016). *Dams in the Mekong River basin: Commissioned, under construction, and planned dams*. Retrieved from https://wle-mekong.cgiar.org/wp-content/uploads/Mekong_A0_2016_Final.pdf.
- Yang, D., Kanai, S., Oki, T., Koike, T., & Musiak, K. (2003). Global potential soil erosion with reference to land use and climate changes. *Hydrological Processes*, 17(14), 2913–2928. <https://doi.org/10.1002/hyp.1441>.
- Yao, H. R., Yang, Z. F., & Cui, B. S. (2005). Soil erosion and its environmental background at Lancang basin of Yunnan Province. *Bulletin of Soil and Water Conservation*, 25(4), 5–14 (In Chinese).
- Yao, H. R., Yang, Z. F., & Cui, B. S. (2006). Spatial analysis on soil erosion of Lancang River watershed in Yunnan Province under the support of GIS. *Geographical Research*, 25(3), 421–429 (In Chinese).
- Zhang, X. C., Liu, W. Z., Li, Z., & Zheng, F. L. (2009). Simulating site-specific impacts of climate change on soil erosion and surface hydrology in southern Loess Plateau of China. *Catena*, 79(3), 237–242. <https://doi.org/10.1016/j.catena.2009.01.006>.
- Zhang, H., Wei, J., Yang, Q., Baartman, J. E. M., Gai, L., Yang, X., et al. (2017). An improved method for calculating slope length (λ) and the LS parameters of the Revised Universal Soil Loss Equation for large watersheds. *Geoderma*, 308, 36–45. <https://doi.org/10.1016/j.geoderma.2017.08.006>.
- Zhou, F. J., Chen, M. H., Lin, F. X., Huang, Y. H., & Lu, C. L. (1995). The rainfall erosivity index in Fujian Province. *Journal of Soil and Water Conservation*, 9(1), 13–18.
- Zhou, Q., Yang, S., Zhao, C., Cai, M., & Ya, L. (2014). A soil erosion assessment of the upper Mekong River in Yunnan Province, China. *Mountain Research and Development*, 34(1), 36–47. <https://doi.org/10.1659/mrd-journal-d-13-00027.1>.



Contents lists available at ScienceDirect

International Soil and Water Conservation Research

journal homepage: www.elsevier.com/locate/iswcr

Original Research Article

Inhibiting soil loss and runoff from small plots induced by an individual freeze-thaw cycle using three rangeland species

Milad Hatefi^a, Seyed Hamidreza Sadeghi^{a,*}, Reza Erfanzadeh^b, Morteza Behzadfar^a^a Department of Watershed Management Engineering, Faculty of Natural Resources, Tarbiat Modares University, Iran^b Department of Rangeland Management, Faculty of Natural Resources, Tarbiat Modares University, Noor, Iran

ARTICLE INFO

Article history:

Received 2 April 2020

Received in revised form

21 May 2020

Accepted 22 May 2020

Available online 17 June 2020

Keywords:

Biological measures

Frosted soil

Plant binding effects

Soil hydrology

ABSTRACT

This study investigated the role of three rangeland species viz. *Agropyron trichophorum*, *Medicago sativa*, and *Lolium preenne* on mitigating of effects of a freeze-thaw (FT) cycle on runoff generation and soil loss from small experimental plots. Small plots (0.5 × 0.5m) were prepared in three replicates for control (i.e., under a FT cycle only) and treatments (i.e., individually planted with the study species and subject to a FT cycle). The treated plots were then placed at a slope of 20% and subjected to simulated rainfall with intensity of 70 mm h⁻¹ and 30 min duration. The results of the study showed a significant effect (P < 0.05) of the plants on controlling runoff and soil loss after a FT cycle. Also, the detrimental effects of the FT cycle due to performance of ice lenses and formation of an active melting layer in the soil surface were ameliorated by the presence of litter on the soil and root-binding effect of the plants. Time to runoff increased by 54, 111 and 10%, runoff volume decreased by 27, 68 and 0.4% and soil loss changed by -34, -62, and +6.5% in the plots planted with *A. trichophorum*, *L. preenne* and *M. sativa*, respectively. The results of the current study indicated that *L. preenne* had the maximum benefit on reducing runoff and soil loss from the plots undergoing a FT cycle.

© 2020 International Research and Training Center on Erosion and Sedimentation and China Water and Power Press. Production and Hosting by Elsevier B.V. This is an open access article under the CC BY-NC-ND license (<http://creativecommons.org/licenses/by-nc-nd/4.0/>).

1. Introduction

Soil erosion is recognized as a serious environmental problem, which is gradually intensified due to over exploitation of soil and water resources (Hazbavi & Sadeghi, 2017; Hu et al., 2018; Sadeghi et al., 2020). In addition, freeze-thaw (FT) cycle greatly affects soil properties such as bulk density and aggregate stability in high latitudes and highlands. During the FT Cycle in natural conditions, as air temperature drops, heat is lost from the soil surface. When sufficient heat is lost, the water in the soil begins freezing (Ferrick & Gatto, 2005). The soil particles are then rearranged due to the FT cycle occurring in soil, which has an important effect on the physical and mechanical properties of soil (Zhou et al., 2018). The results of various experiments showed that the number of FT cycles is so important and has permanent effects on the mechanical properties of the soil particles and facilitates the soil particles

detachment during runoff generation (Liu et al., 2016). So far, many researches have reported the effect of FT cycles on physical properties (Van Klaveren & McCool, 2010; Li et al., 2013; Zhang et al., 2016; Liu et al., 2016), aggregate size (Oztas & Fayetorbay, 2003), aggregate stability (Kværnø and Øygarden, 2006; Staricka & Benoit, 1995; Wang et al., 2012; Zhou et al., 2018), detachment capacity (Sun et al., 2018) and performance of soil amendment (Behzadfar et al., 2017; Sadeghi et al., 2016; Zaimoglu, 2010).

The pioneer study by Johnson and McArthur (1973) about the effects of FT cycles on soil loss showed that soil erosion was often influenced by snow melting and glaciers. Edwards and Burney (1987, pp. 109–115) studied the soil loss under FT cycles and concluded that the content of soil loss due to the FT cycle increased by 90% in bare soils, while soil loss decreased by 70–80% in soils cultivated with winter rye seed when compared with no FT cycle conditions. The laboratory simulation on soils under a FT cycle by Frame et al. also verified a higher sediment concentration at rate of some 25% compared to that reported for the soils with no FT cycle. Ferrick and Gatto (2005) performed three replications of six experiments to determine the soil erosion in bare soils after an individual FT cycle. Kværnø and Øygarden (2006) studied the

* Corresponding author.

E-mail addresses: miladhatefi72@yahoo.com (M. Hatefi), sadeghi@modares.ac.ir (S.H. Sadeghi), Erfanzadeh@yahoo.com (R. Erfanzadeh), mbehzadfar@gmail.com (M. Behzadfar).

influences of FT cycles on aggregate stability of three types of loam-silty soil in Norway and reported that the FT cycle decreased the rainfall stability of all soils, but it has more effects on silty soil. Wang et al. (2007) investigated the effect of 21 successive FT cycles on mechanical properties of clay in the Tibetan Region of China. Results showed a significant changes in moisture content, shear strength behavior, fracture toughness, elasticity modulus, adhesion, and angle of friction in soil due to induction of FT cycles. Wang et al. (2009) studied the effects of soil surface layer on the FT cycle on runoff generation in a Chinese experimental watershed. The results showed that the active layer of FT at a depth of less than 60 cm had a significant effect on surface runoff generation. Bing et al. studied the effect of the FT cycle on physical and mechanical properties of salty soils in Lanzhou region, China. The results of this study illustrated that FT decreased soil resistance. In the other words, induction of the FT cycles caused disturbance of soil dynamics equilibrium index which finally led to a constant conditions after six successive FT cycles. Gui-Yuan et al. reported that the effects of the FT cycle on aggregate stability depended on the initial soil moisture content. There are also evidences that the FT cycle in black soils with initial moisture content in northeastern China increased detachment of aggregates up to 36.5% under laboratory conditions (Liu et al., 2017). Sadeghi et al. (2018) investigated the effect of the FT cycle on splash erosion. They found that only freezing reduced upward, downward and net splash erosion in splash cups in comparison with plots under whole FT cycle. Sun et al. (2018) proved using the Taguchi method that the detachment capacity of aggregates after a FT cycle initially decreased and then increased as number of the FT cycle and moisture content increased. Fu et al. (2019) explored the effects of biochar amendment on nitrogen mineralization in black soil with different moisture contents under FT cycles. The results showed that FT cycles promoted the fragmentation and decomposition of soil aggregates. Wang et al. (2020) have recently conducted an experiment on freeze-thaw meltwater compound erosion and runoff energy consumption on loessal slopes. The experiments were performed over frozen, shallow-thawed, and unfrozen soil-filled flumes under 1, 2, and 4 L min⁻¹ flow rates. The results showed that soil erosion became more severe with increasing flow rate and therefore frozen slope displayed the highest runoff and sediment yield at the equal flow rate.

Numerous studies (e.g., Battany & Grismer, 2000; Da Silva et al., 2018; Feng et al., 2018; Garcia-Rodeja & Gil-Sotres, 1997; Gyssels et al., 2005; Lotfalian et al., 2019; Mohammad & Adam, 2010; Neave & Abrahams, 2002; Nunes et al., 2011; Yu et al., 2019; Zhang et al., 2011; Zhou et al., 2016) investigated the relationships between different characteristics of vegetation cover and hydrologic and hydraulic responses. Accordingly, Rasse et al. (2000) specifically investigated the effects of the litter from aerial parts and roots of *M. sativa* on the hydraulic properties of aggregate particles. The results showed that the root system of *M. sativa* increased moisture penetration up to 57% in soil profiles. Zhou and Shangguan (2005) and De Baets et al. (2006) investigated the effects of plant roots on concentrated flow erosion using a hydraulic flume. They wholly reported a decrease in soil erosion with increasing root biomass. They also indicated the efficiency of roots in controlling soil erosion varied with different root types. Zheng-Chao and Shangguan, 2008 studied the influence of living roots and canopies of ryegrasses (*Lolium preenne*) during the growing season on soil loss and runoff of a silt loam soil. The results indicated that during the growing season, runoff volume and soil loss decreased with time. In addition, the results showed that the roots contributed up to 96% in reducing soil loss in the late stage of the growing season. Many other pioneer studies (e.g., Chu et al., 2010; Gyssels et al., 2005; Iwasaki et al., 2013; Shinohara et al., 2016; Toy et al., 2002) also reported the significant inverse relationship between the vegetation cover

density with soil erosion. Jordán et al. (2010) reported that vegetation litter widely improved the physical and chemical characteristics of the soil against erosion. El Kateb et al. (2013) investigated the effectability of soil erosion and surface runoff on different vegetation covers. The results demonstrated that the rate of erosion was substantially influenced by changes in vegetation cover. Wang et al. (2014) studied soil detachment by overland flow under different vegetation restoration approaches in the Loess Plateau of China. Results showed that the measured soil detachment capacities were controlled significantly by the restoration measures and mean detachment capacity of cultivated farmland was greater than those of the restored areas. Duan et al. (2016) reported that the vegetation canopy could intercept the precipitation and reduce the velocity of rain drops led to reduce soil erosion. The effects of moisture absorption by the litter in corn and soybean cultivated soils was reported Kutlu et al. (2018).

Reviewing of literatures showed that there have been many individual studies about effects of FT on soil properties including soil erosion. The results showed that the FT cycle often affected the mechanical and engineering properties of the soil and specially decrease the stability of the soil aggregates. Many simulated laboratory experiments reported the negative effect of FT cycle as a periodic factor on soil characteristics. Further researches were also documented to verify the high controlling roles of vegetation cover on soil and water conservation. However, the impact of the vegetation cover as one of the factors influencing creation and control of the FT effect has not been considered yet. Besides, Iran is a mountainous country half of which is distributed in the highlands where soils are highly exposed to the FT cycle. Whilst, it is hypothesized that the existence of vegetation cover on the soil surface significantly affects and controls runoff generation, and as a result, reduces soil erosion through affecting controlling factors like FT cycle. The current study tried to characterize the effects of some native rangeland species on controlling runoff generation and soil erosion at small plot scale induced by a FT cycle and under laboratory simulation condition. The present study was formulated at plot scale to better control the governing conditions and possibility for inducing the FT cycle. All study plots were planted with three rangeland species. They were then subjected to rainfall simulations for the proper assessment of the effectiveness on controlling runoff generation and soil loss.

2. Materials and methods

To achieve the study purposes, the small plots were prepared in three replicates for control and treated conditions. The plots subject to an individual FT cycle were considered as control to show the effects a FT cycle on hydrological behavior of the study plots. Whereas, plots initially planted with three individual plants and subject to a FT cycle were regarded as the treatment to indicate the role of the study rangeland species in changing hydrological responses of the study treated plots. During the present study, it was tried to compare the impact of vegetation reclamation as a common approach in rangeland management on controlling soil and water loss from the plots, which underwent through a FT cycle. Here, we did not intend to compare the role of FT cycle on soil and water loss to need having a control situation of plots without FT cycle. Though, the incremental effect of a FT cycle on soil and water loss from the same experimental design and soil from the same soil origin has already been reported by Behzadfar, Sadeghi, Khangani, and Hazbavi (2012 and 2017). The detailed procedure has been given in the following.

2.1. Soil characteristics

Soil samples were collected from the top-30 cm layer of a mountainous summer rangeland with a general slope of 20% in Badranlou Region (57° 11' E and 37° 29' N) located at 10 km from Bojnourd City, the capital of Northern Khorasan Province, northeast of Iran. The soil samples were then transferred to the laboratory and sifted by a 3-mm sieve after air-drying according to previous research (Behzadfar et al., 2017) conducted in the same field of study with similar soil. According to the hydrometer method, the soil samples were characterized as a silt loam soil. The soil bulk density, organic matter, electrical conductivity (EC) and pH of soil samples determined in a soil:water suspension of 1:2 by pH and EC meters (Sadeghi et al., 2018) were 1.2 g cm⁻³, 0.15%, 123.4 μS cm⁻¹ and 7.9, respectively.

2.2. Experimental setup

The study was conducted under controlled conditions with a simulated rainfall at the Soil Erosion and Rainfall Simulation Laboratory, Tarbiat Modares University, Iran. The small sized plots were also used for better control, facilitation, and adaptation of experimental conditions. The sieved soil was poured in small erosion plots with 0.5 × 0.5 × 0.3 m in dimensions. A 10-cm thick layer of soil was placed over a 20-cm thick layer of crushed pumice considered for draining the lower portion of the soil profile. The prepared soil sample was evenly packed into the soil plots with the help of a hand-made, small and PVC-pipe roller filled with cement (Behzadfar et al., 2017) until reaching a bulk density of 1.2 g cm⁻³ similar to that measured under field conditions. The designed plots contained three replicates for control and treatments were firstly transferred to the greenhouse to plant species. Fig. 1 shows a general view of preparation of experimental plots.

2.3. Freezing induction system

In order to induce freezing conditions in the soil, a cooling system with dimensions of 1.70 × 1.5 m, with capacity of producing cold temperatures of some -30 °C, air rotation, manual and digital temperature control and timing (Behzadfar et al., 2017) was applied. Accordingly, the freezing depth of soil was set to 10 cm. In this regards, the whole temperature data recorded in 6 intervals of soil depths viz. 5, 10, 20, 30, 50 and 100 cm at local times of 3, 9 and 15 h during 1992–2007 were obtained from the Bojnourd Synoptic Station and then analyzed. Based on the analysis of freezing temperature at various soil depths at the study climatological station, the maximum soil frost depth of 10 cm with frequency of 92% (Behzadfar et al., 2012; 2017) was used as target point for simulation processes. According to the analyses, the maximum frequency of freezing temperature occurred in 0 °C (488 times; 86.2%), -2.0 °C

(362 times, 34.2%) and -4.0 °C (337 times; 28.1%), respectively. The temperature of some -10 °C was then considered for inducing the freezing process in the whole FT cycle in the study plots.

2.4. Selection of plant species

In order to select appropriate plant species for the study purposes, initially seven rangeland gramineous and forbs species viz. *Agropyron trichophorum*, *Chenopodium murale*, *Eurotia ceratoides*, *Festuca ovina*, *Medicago sativa*, *Lolium preenne* and *Poa bulbosa* with higher biomass and more extended root systems were initially selected according to phytosociological reports for the study area and their potential usage for rangeland reclamation and development activities in the region (Consulting Engineering company of Saz-Ab Shargh). In the next step, seeds of selected species were obtained from the Isfahan Pakanbazzr Company. The Tetrazolium solution prepared using distilled water and placed in Petri dishes was consequently applied for evaluating germination power of the study seeds. The seeds of the study rangeland species were then immersed in the solution to assess the germination rates (Mohammadi et al., 2011, p. 252) whose results have been shown in Table 1. Nonetheless, according to the existing routine methodology being often used in the rangeland reclamation projects, some 0.5 g (≈ 50–100) seeds were sown in each study plot. Of course, they germinated, grew, and produced biomass differently based on their own inherent characteristics and similar to what usually occurs under real conditions.

2.5. Freeze-thaw setting and rainfall experiments

After cultivating seven rangeland species in the greenhouse, three species of *A. trichophorum*, *M. sativa*, and *L. preenne* almost completed the phenological stages and ultimately were selected for the successor experiments. The planted plots were then set aside in order to wither the plants and to maximally mimic the non-growing season governing the region. Three plant species consisting of 18 total plots were ultimately considered for the study. For all treatments, the FT cycle was performed in the form of freezing conditions at some -10 °C for three days and then two days of thawing as per conditions often occur in the study area. The freezing air was induced to the plots surfaces from the top as taken place in real conditions through isolating all sides and bottom of the plots with the help of thick (≈ 3 cm) unolite impervious plastic sheets (Behzadfar et al., 2012). The plots were then left for three days in the laboratory under ambient temperature between 10 and 15 °C to be thawed as occurred in the real condition of the soil origin. The soil moisture in the study plots were also measured before the rainfall experiment and found within a range of 35–40% in plots with *L. preenne*, 20–30% for *A. trichophorum*, 17–35% for *M. sativa* and less than 10% in control plots.

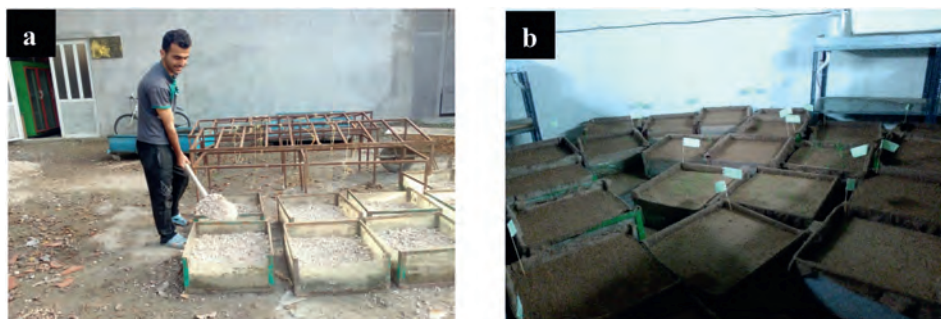


Fig. 1. A view of soil placement in the small plots (left) and preparing plots for cultivating species (right).

Table 1
Results of germination test for the study rangeland plant species.

Plant species	Number of seeds	Number of alive seeds	Germination rate (%)
<i>Agropyron trichophorum</i>	20	18	90
<i>Chenopodium murale</i>		15	75
<i>Eurotia ceratoides</i>		16	80
<i>Festuca ovina</i>		14	70
<i>Lolium preenne</i>		17	85
<i>Medicago sativa</i>		18	90
<i>Poa bulbosa</i>		16	80

The erosion plots were placed at a slope of 20% as reported for soil origin and exposed to rainfall with intensity of some 70 mm h^{-1} for 30 min based on the analysis of intensity-duration-frequency curves of the Bojnourd climatological Station (Behzadfar et al., 2017). After starting the rainfall event, the time to runoff of the plots was recorded after the onset of reaching the first drop of runoff to the collector apparatus installed at the lower part of the plots. Runoff sampling was performed consequently at intervals of 2-min (for the first three time steps after beginning of the runoff), 3-min (the second three time steps of the event), 5-min steps until the end of the rainfall event and one sample on 5 min after stopping the rainfall event (Hazbavi & Sadeghi., 2017). The volume of runoff was measured at different time stages by a graduated cylinder. Moreover, the content of soil loss was also calculated using decantation technique (Saeidi et al., 2016) in which sediment laden runoff was left for 24 h and upper clear water was then discharged and the disposal was finally kept in the oven with 105°C for 24 h to get the entire soil loss during each measurement. A general view of the designed cooling system and rainfall simulation and runoff measurement setup has been shown in Fig. 2.

2.6. Determination of phyto-biomass

The phyto-biomass in the study plots was measured through the clipping and weighing method (Catchpole & Wheeler, 1992) and air dried. The clipped plants were placed for 72 h and then weighed again to determine the dry weight. Some 2 g of the clipped plants were also placed in the oven with 72°C for 24 h and re-weighed to determine dry matter of the study species. Some stems of each species were also randomly selected to measure the average height of species under consideration as shown in Table 2.

2.7. Data analyses

The effectiveness of the study treatments on mitigating the

effects of the FT cycle on runoff and soil loss from the study plants was statistically compared. The data normality and homogeneity of variances were initially tested using the Kolmogrov–Smirnov and Levene tests, respectively. The analysis of variance (ANOVA) under factorial design were also used to compare the mean values of the treatments to investigate the independent and significant effects of the study treatments on runoff generation and soil loss from the plots (Behzadfar et al., 2017). The entire statistical analyses and graphical presentation were performed using SPSS 23 and Microsoft Excel 2016.

3. Results

The present study was conducted to evaluate potential effects of three rangeland species to control the impacts of the FT cycle on runoff and soil loss. The entire results for the selected treatment and study variables have been summarized in Table 3.

3.1. Effect of study treatments on runoff commencement

After starting the rainfall event, the time for the surface runoff to reach the lower collector was recorded as runoff commencement whose corresponding results and statistical analyses have been shown in Fig. 3 and Table 4, respectively.

According to the results of the statistical analyses, *A. trichophorum*, *L. preenne*, and *M. sativa* increased time to runoff by 54.0, 111.5, and 10.1% compared to those recorded for the control condition, respectively. Despite a significant difference ($P < 0.05$) among the study group (Table 4), the statistical analyses (Fig. 3) did not confirm significant effects ($P > 0.05$) of *M. sativa* and *A. trichophorum* treatments on runoff commencement in comparison with their corresponding control plots. While, *L. preenne* had a significant ($P < 0.05$) effect on runoff commencement. It seems that the presence of vegetation cover provides more time for the rainfall drops to penetrate into soil depth (Zhang et al., 2015).



Fig. 2. Simulation of the study FT cycle in designed cooling system (left), and rainfall simulation and runoff measurement (right).

Table 2
Dry weight and height of study plant species.

Treatment	Mean height (cm)	Wet weight (g m^{-2})			Mean \pm Standard deviation	Dry matter (%)			Mean \pm Standard deviation
		1	2	3		1	2	3	
Replication	—	1	2	3	—	1	2	3	—
<i>A. trichophorum</i>	38.2	74.4	53.7	56.6	61.5 \pm 11.2	70.0	78.3	60.2	69.5 \pm 9.0
<i>L. prene</i>	34.0	77.8	78.8	82.0	79.5 \pm 2.1	72.2	74.4	82.5	76.3 \pm 5.4
<i>M. sativa</i>	12.9	50.6	26.6	31.8	36.3 \pm 12.6	70.0	60.2	62.6	64.2 \pm 5.1

Table 3
Entire results for the selected treatment and study variables.

Treatment	Time to runoff (min)			Mean \pm Standard deviation	Runoff volume (L)			Mean \pm Standard deviation	Soil loss (g)			Mean \pm Standard deviation
	1	2	3		1	2	3		1	2	3	
	<i>A. trichophorum</i>	5.97	3.05		5.11	4.71 \pm 1.5	0.23		0.34	0.26	0.27 \pm 0.05	
Control	3.18	2.21	3.75	3.04 \pm 0.77	0.38	0.38	0.37	0.37 \pm 0.00	1.17	1.41	1.1	1.2 \pm 0.16
<i>L. prene</i>	6.41	6.66	6.24	6.43 \pm 0.21	0.11	0.10	0.12	0.11 \pm 0.01	0.27	0.16	0.22	0.21 \pm 0.05
Control	4.07	2.11	3.87	3.35 \pm 1.07	0.32	0.40	0.32	0.34 \pm 0.04	0.61	0.59	0.53	0.57 \pm 0.04
<i>M. sativa</i>	4.12	3.32	2.78	3.40 \pm 0.67	0.32	0.33	0.36	0.33 \pm 0.02	0.77	0.73	0.48	0.66 \pm 0.15
Control	3.15	4.31	2.27	3.24 \pm 1.02	0.34	0.30	0.38	0.34 \pm 0.04	0.97	0.5	0.51	0.66 \pm 0.26

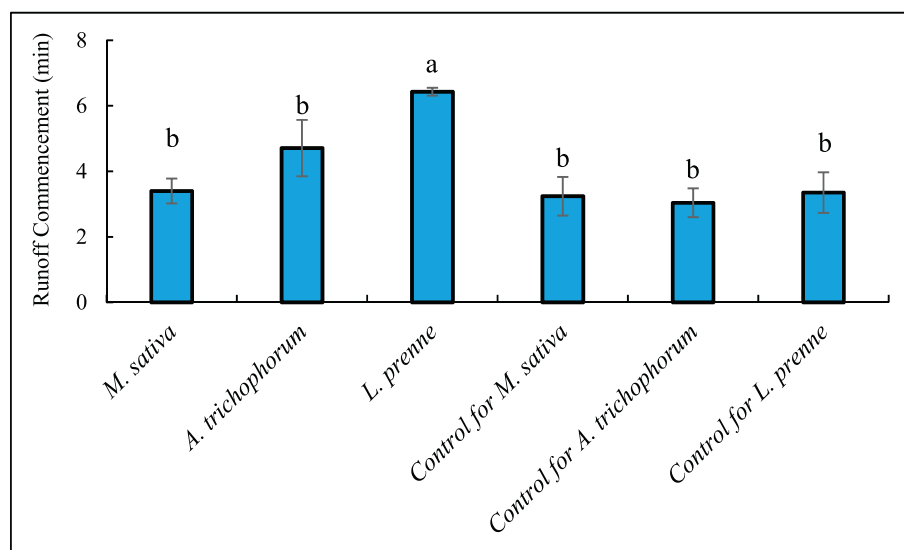


Fig. 3. Statistical comparison of mean values of runoff commencement time (min) in control and treated plots under the study FT cycle.

Table 4
Analysis of variance (ANOVA) for runoff commencement in plots treated by rangeland species and control under the study freeze-thaw cycle.

Examined Factor	Sum of squares	Degree of freedom	Mean squares	F-value	Level of significance
Between Groups	26.07	5	5.21	5.62	0.00
Within Groups	11.13	12	0.92		
Total	37.20	17			

3.2. Effect of study treatments on runoff volume

The runoff was collected at the specific intervals during the rainfall event as explained earlier and the total volume of runoff was finally recorded for each experimental treatment whose associated results have been depicted in Fig. 4. The results of ANOVA has also been given in Table 5.

The results of the study, while confirming different behaviors, showed that *A. trichophorum*, *L. prene* and *M. sativa* reduced the runoff volume by 26.6, 67.7 and 0.4% compared to those of control plots. Statistical analysis confirmed that the runoff volumes at the plot planted with *A. trichophorum* and *L. prene* were significantly

($P < 0.05$) different from both *M. sativa*, and the control treatments.

3.3. Effect of study treatments on soil loss

The entire runoff was also analyzed to determine the soil washed out from the study plots with different treatments during soil erosion process. The results of soil loss in different experimental treatments and corresponding statistical comparisons have been shown in Fig. 5 and Table 6, respectively. Based on the analyses, *A. trichophorum*, *L. prene* and *M. sativa* treatments changed soil losses by -34.1 , -62.4 , and $+6.5\%$, respectively. Statistical analyses further indicated that *M. sativa* had no significant effect

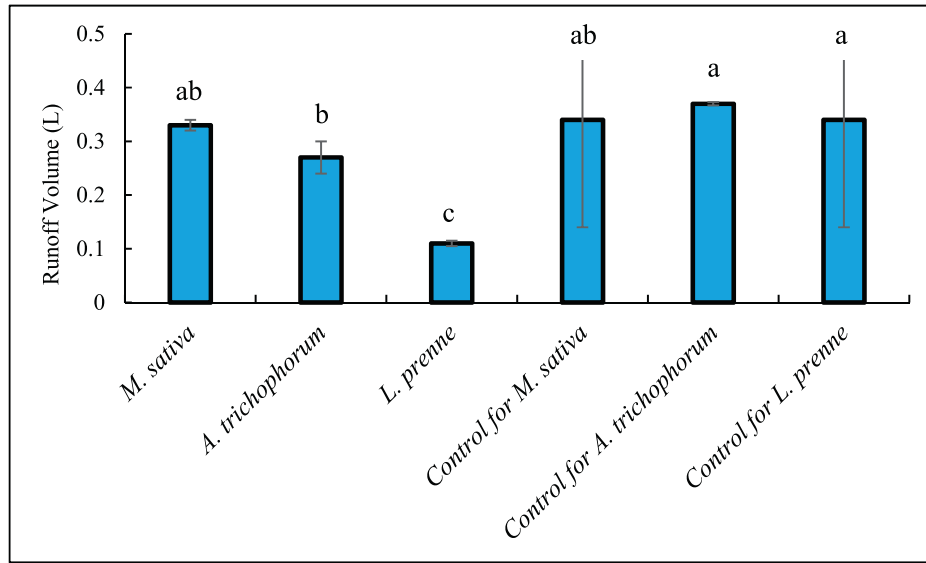


Fig. 4. Statistical comparison of mean values of runoff volume (L) in control and rangeland species plots under the study FT cycle.

Table 5

Analysis of variance (ANOVA) of runoff volume in plots treated by rangeland species and control under the study freeze-thaw cycle.

Examined Factor	Sum of squares	Degree of freedom	Mean squares	F-value	Level of significance
Between Groups	0.14	5	0.029	22.75	0.00
Within Groups	0.01	12	0.00		
Total	0.15	17			

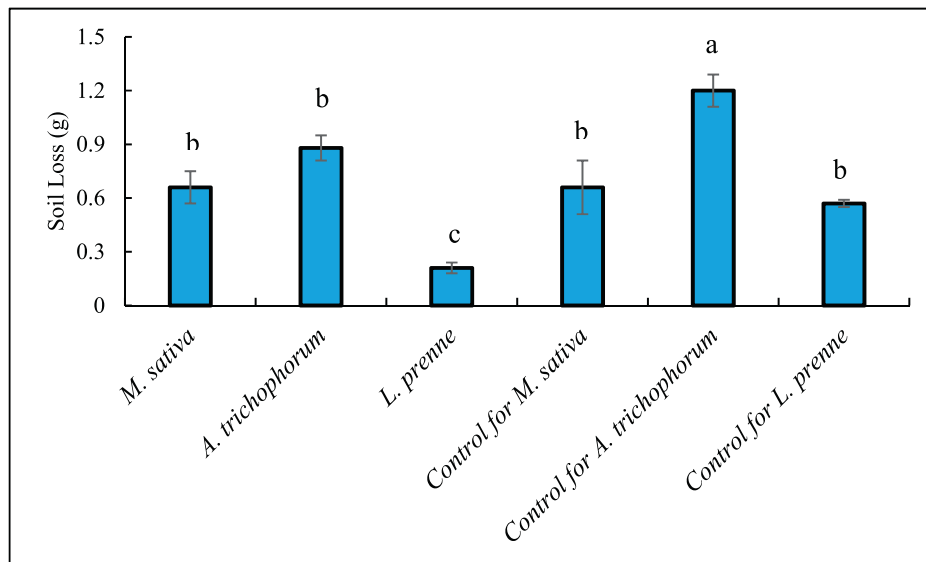


Fig. 5. Statistical comparison of mean values of soil loss (g) in control and rangeland species plots under the study FT cycle.

Table 6

Analysis of variance (ANOVA) of soil loss in plots treated by rangeland species and control under the study freeze-thaw cycle.

Examined Factor	Sum of squares	Degree of freedom	Mean squares	F-value	Level of significance
Between Groups	1.62	5	0.32	13.44	0.00
Within Groups	0.29	12	0.02		
Total	1.91	17			

($P > 0.05$) on reduction of soil loss. Whilst, *A. trichophorum* and *L. preenne* significantly ($P < 0.05$) decreased soil loss from the plots induced by the FT cycle.

4. Discussion

This study aimed to indicate how three rangeland species could mitigate the effect of FT cycle on runoff generation and soil loss. The main reason for decreasing the time to runoff and increasing the runoff in unplanted plots was the complete presence of active thawing layer in the surface of the soil and, in particular, the better formation of a lowered permeable concrete frosty soil profile as noted by former researches (e.g., Ban et al., 2016; Ferrick & Gatto, 2005; Sadeghi et al., 2015).

As seen in Table 3, the runoff volumes for the only study initial simulated rain event were extremely low against the amount of some 9 L of total rain applied on the plots. However, as it was mentioned before, the soil is silt loam with low bulk density of 1.2 g cm⁻³ with inherent high infiltration rate and further increased by puffy (Ferrick & Gatto, 2005) and cracked/ruptured surface of thawed soil allowing preferential flow (Doerr et al., 2000) through providing efficient conduits for enhanced infiltration (Watanabe & Kugisaki, 2017) and consequent less runoff. Besides, no significant hydrophobicity was found based on water drop penetration tests applied on soil surface of all treated and control plots. So that the times of water drop penetration were <7 s, which is mainly classified as non-hydrophobic soil (Steenhuis et al., 2001). Fig. 6 also shows the cracked soil surface of the control and treated plots significantly improved the water infiltration into the soil. Of course the hydrologic behavior of the soil for the consequent rains and more FT cycles might be totally different (Liu et al., 2016; Sadeghi et al., 2016; Wang et al., 2007). Some other sources of uncertainties like lowering rain intensity during the experiments might also be as another reason for low runoff volumes. Though the conditions were comparative and therefore could not significantly affect the reduction benefit of role of vegetation cover on runoff generation.

On the other hand, comparative increase in the runoff generation and soil loss may be attributed to the disintegration of soil surface made by FT cycle compared to that without FT cycle. The reason of this phenomenon is possibly to increase the sensitivity of crusting due to formation of fine-grained elements under different freezing processes, which reduce porosity content of soil profile and soil permeability but led to larger extended cracks and ruptures facilitating more preferential flow into the soil. So that the total soil loss from the study plots for an individual rain event varied within low amounts of some 0.3 and 1.4 g (i.e., 0.01–0.06 t ha⁻¹event⁻¹).

These results are similar to Ferrick and Gatto (2005) who proved increases in soil loss in frozen and thawed soils because of presence of ice lenses on the border of the frozen front, soil swelling, and soil surface collapse. Though, Gatto (2000), Turcotte et al. (2011), and Ban et al. (2016) reported differently due to the small size and dimensions of the experimental plots and absence of ruptures on the soil surface.

Minute considerations of mechanisms governing the FT process induced soils and determinant factor which affects the processes may partially or wholly control the runoff and soil loss generation in different aspects. In this study, the results illustrated that the presence of plant species generally reduced soil losses and runoff generation and increased runoff commencement time. Although, some previous studies (e.g., Behzadfar et al., 2017; Watanabe & Kugisaki, 2017; Wu et al., 2018; Zhang et al., 2016; Zheng et al., 2018) have shown that FT cycles increase runoff generation and soil loss, any study has not been carried out on potential of biologic methods in areas exposed to FT cycles. In addition, it is obvious that vegetation cover increases the content of organic matter and litter in the soil surface. According to Table 2, more dry matter of *L. preenne* and the more height of *A. trichophorum* leading to more litter on the soil and might affect more in controlling runoff generation and soil loss rather than *M. sativa*. It can be attributed to the greater physical impediment of these species on the soil surface against rainfall drops to produce runoff and soil loss. In this regard, Kavianpour et al. (2015) also emphasized the positive effects of vegetation cover with higher content on runoff generation and soil loss. Additionally, the texture and structure of the litters were definitely different in *L. preenne* and *M. sativa*, so that the contiguity of stem and the length of litters of *L. preenne* was a serious obstacle to the runoff generation and soil loss rather than *M. sativa*. Different studies (i.e., Arzani et al., 2015; Ashrafzadeh et al., 2015) proved that the percentage of fibrous parts in the gramineous family are more than those in forbs. So that, more fiber in gramineous litters and more resistance are efficacious factors in reduction of runoff generation. The whole effectiveness of the study species on runoff and soil loss control may not be attributed to the aboveground characteristics of the study species, since there was no statistical significant differences ($P > 0.05$) among the study variables.

Plant roots in the soil also improve soil permeability and, as a result, decrease runoff generation and soil loss. Of course, different vegetation covers affect runoff and soil loss in various aspects and extents. On the other hand, differences between pattern and engineering of the root systems were also found as important factors affecting the performance of the species as noted by Forde and Lorenzo (2001) and Hodge et al. (2009). The positive effects of plant roots in this study might affect aggregate stability including



Fig. 6. Cracked soil surface of the control and treated plots after undergoing a FT cycle.

the greater binding of soil particles by root net as similarly reported by Amezketa (1999). Besides, the roots of planted species could affect the shear stress of the soil, which is defined as the ability to adhere and resist the soil particles against forces such as gravity, fluid motion, and mechanical loads (Pimental et al., 1995). On the other hand, in the current study, the great importance of plant roots, which increase soil adhesion and decrease runoff generation and soil losses rather than those of plant stems was proved (Zhang et al., 2014). The roots of most of the gramineous species are fibrous and mainly developed near to the soil surface (Hodge et al., 2009; Weaver, 1958), while the roots of the forbs are deep and even extend up to a depth of 2.5–4.5 m from the soil surface. Plants with tap root systems are generally less effective at limiting soil erosion than plants with fibrous root systems. In the present study and based on the measurement, *M. sativa* had a high root depth of 7–9 cm in average. However, *A. trichophorum* and *L. preenne* had root depths of 3.5–5.5 and 2.5–4.5 cm, respectively. According to the observations, the major part of the roots of the last two species were expanded on the soil surface. Therefore, *L. preenne* had most significant effect on reducing the effect of the FT cycle on runoff generation and soil loss. In addition, due to the fact that the erosion occurred in topsoil surface and pointing to the fact that *L. preenne* had more superficial roots (Guerrero-Campo & Fitter, 2001) and dry matter (Table 2), it is likely that the soil surface adhesion in the depth of freezing would increase and had a greater impact in reduction of soil loss in comparison with other two species.

5. Conclusion

The present initiative study successfully reported the eco-hydrologic effects of three rangeland plant species on soil loss and runoff characteristics from small experimental plots subjected to a freeze-thaw cycle. It can be concluded from the results that the study rangeland species had significant positive effect on runoff commencement, runoff volume and soil loss in the experimental plots and under FT cycle. In general, the results of this study showed that *L. preenne* performed better in conserving water and soil in the plots induced by a FT cycle. As a result, runoff volume and soil loss following the FT cycle was well managed in experiments under consideration. The present study, while providing a suitable platform for performing other related research, emphasizes the importance of the FT cycle on runoff generation and soil loss and its inhibitory effect of gramineous species for conservation of soil and water resources. Though the effects were resulted from the experiments at small sized plots scales, one phonological period, an individual rain event, and a single freeze-thaw cycle. Hence, more insight, long spanned and extensive studies under different spatial scales with further prolonged monitoring of effectiveness of various plant species and subsequent rain events and more freeze-thaw cycles are crucial to allow drawing comprehensive and of course more practical conclusion for better conserving soil and water resources. The findings of this study would be practically applied by local ranchers in order to reclaim and restore the vegetation cover of the study region to strengthen soil and water resources against destructive effects of freeze-thaw.

Declaration of competing interest

The authors declare that they have no known competing financial interests or personal relationships that could have appeared to influence the work reported in this paper.

Acknowledgement

The present research has been prepared based on the facilities

provided by Tarbiat Modares University, Iran. The partial support of the Agrohydrology Research Group of Tarbiat Modares University (grant No. IG-39713), Iran, with regards to the corresponding author is also appreciated.

References

- Amezketa, E. (1999). Soil aggregate stability: A review. *Journal of Sustainable Agriculture*, 14, 83–151. https://doi.org/10.1300/J064v14n02_08
- Arzani, H., Miraki, F., & Erfanzadeh, R. (2015). The effect of elevation from the sea level and phonological stages on the quality of forage in three rangelands in Kurdistan Province (Saral region). *Research in Agriculture and Technology*, 20(1), 156–167. (In Persian).
- Ashrafzadeh, M., Erfanzadeh, R., & Hosseini Kahnouj, H. (2015). Effects of soil chemical properties on forage quality in dry rangelands in the south of Fars Province. *Iranian Journal of Range and Desert Research*, 22(2), 382–391 (In Persian).
- Ban, Y., Lei, T., Liu, Z., & Chen, C. (2016). Comparison of rill flow velocity over frozen and thawed slopes with electrolyte tracer method. *Journal of Hydrology*, 534, 630–637. <https://doi.org/10.1016/j.jhydrol.2016.01.028>
- Battany, M. C., & Grismer, M. E. (2000). Rainfall runoff and erosion in napa valley vineyards: Effects of slope, cover and surface roughness. *Hydrological Processes*, 14(7), 1289–1304. [https://doi.org/10.1002/\(SICI\)1099-1085\(200005\)14:7<1289::AIDHY43>3.0.CO;2-R](https://doi.org/10.1002/(SICI)1099-1085(200005)14:7<1289::AIDHY43>3.0.CO;2-R)
- Behzadfar, M., Sadeghi, S. H. R., Khangani, M. J., & Hazbavi, Z. (2012). Effectability of runoff and sediment yield from soils induced by freezing and thawing cycle under simulated rainfall condition. *Journal of Soil and Water Resources Conservation*, 2(1), 13–23. (In Persian).
- Behzadfar, M., Sadeghi, S. H., Khanjani, M. J., & Hazbavi, Z. (2017). Effects of rates and time of zeolite application on controlling runoff generation and soil loss from a soil subjected to a freeze-thaw cycle. *International Soil and Water Conservation Research*, 5(2), 95–101. <https://doi.org/10.1016/j.iswcr.2017.04.002>
- Catchpole, W. R., & Wheeler, C. J. (1992). Estimating plant biomass: A review of techniques. *Australian Journal of Ecology*, 17(2), 121–131. <https://doi.org/10.1111/j.1442-9993.1992.tb00790.x>
- Chu, L., Ishikawa, Y., Shiraki, K., Wakahara, T., & Uchiyama, Y. (2010). Relationship between forest floor cover percentage and soil erosion rate on the forest floor with an impoverished understory grazed by deer (*Cervus nippon*) at Doudaira, Tanzawa mountains. *Journal of the Japanese Forestry Society*, 92(5), 261–268. <https://doi.org/10.4005/jjfs.92.261>
- Da Silva, R. M., Santos, C. A. G., & Dos Santos, J. Y. G. (2018). Evaluation and modeling of runoff and sediment yield for different land covers under simulated rain in a semiarid region of Brazil. *International Journal of Sediment Research*, 33(2), 117–125. <https://doi.org/10.1016/j.ijsrc.2017.04.005>
- De Baets, S., Poesen, J., Gysels, G., & Knape, A. (2006). Effects of grass roots on the erodibility of topsoils during concentrated flow. *Geomorphology*, 76(1–2), 54–67. <https://doi.org/10.1016/j.geomorph.2005.10.002>
- Doerr, S. H., Shakesby, R. A., & Walsh, R. P. D. (2000). Soil water repellency: Its causes, characteristics, and hydro-geomorphological significance. *Earth-Science Reviews*, 51(1–4), 33–65. [https://doi.org/10.1016/S0012-8252\(00\)00011-8](https://doi.org/10.1016/S0012-8252(00)00011-8)
- Duan, L., Huang, M., & Zhang, L. (2016). Differences in hydrological responses for different vegetation types on a steep slope on the Loess Plateau, China. *Journal of Hydrology*, 537, 356–366. <https://doi.org/10.1016/j.jhydrol.2016.03.057>
- Edwards, L. M., & Burney, J. R. (1987). *Soil erosion losses under freeze/thaw and winter ground cover using a laboratory rainfall simulator*. National Research Council, Division of Building Research. Agriculture Engineering.
- El Kateb, H., Zhang, H., Zhang, P., & Mosandl, R. (2013). Soil erosion and surface runoff on different vegetation covers and slope gradients: A field experiment in southern shaanxi Province, China. *Catena*, 105, 1–10. <https://doi.org/10.1016/j.catena.2012.12.012>
- Feng, T., Wei, W., Chen, L., Rodrigo-Comino, J., Die, C., Feng, X., & Yu, Y. (2018). Assessment of the impact of different vegetation patterns on soil erosion processes on semiarid loess slopes. *Earth Surface Processes and Landforms*, 43(9), 1860–1870. <https://doi.org/10.1002/esp.4361>
- Ferrick, M. G., & Gatto, L. W. (2005). Quantifying the effect of a freeze-thaw cycle on soil erosion: Laboratory experiments. *Earth Surface Processes and Landforms*, 30(10), 1305–1326. <https://doi.org/10.1002/esp.1209>
- Forde, B., & Lorenzo, H. (2001). The nutritional control of root development. *Plant and Soil*, 232, 51–68. <https://www.jstor.org/stable/42951196>
- Fu, Q., Yan, J., Li, H., Li, T., Hou, R., Liu, D., & Ji, Y. (2019). Effects of biochar amendment on nitrogen mineralization in black soil with different moisture contents under freeze-thaw cycles. *Geoderma*, 353, 459–467. <https://doi.org/10.1016/j.geoderma.2019.07.027>
- García-Rodeja, I., & Gil-Sotres, F. (1997). Prediction of parameters describing phosphorus-desorption kinetics in soils of Galicia (Northwest Spain). *Journal of Environmental Quality*, 26(5), 1363–1369. <https://doi.org/10.2134/jeq1997.00472425002600050023x>
- Gatto, L. W. (2000). Soil freeze-thaw-induced changes to a simulated rill: Potential impacts on soil erosion. *Geomorphology*, 32(1–2), 147–160. [https://doi.org/10.1016/S0169-555X\(99\)00092-6](https://doi.org/10.1016/S0169-555X(99)00092-6)
- Guerrero-Campo, J., & Fitter, A. H. (2001). Relationships between root characteristics and seed size in two contrasting floras. *Acta Oecologica*, 22(2), 77–85. [https://doi.org/10.1016/S1146-609X\(00\)01101-2](https://doi.org/10.1016/S1146-609X(00)01101-2)

- Gyssels, G., Poesen, J., Bochet, E., & Li, Y. (2005). Impact of plant roots on the resistance of soils to erosion by water: A review. *Progress in Physical Geography*, 29(2), 189–217. <https://doi.org/10.1191/0309133305pp443ra>
- Hazbavi, Z., & Sadeghi, S. H. R. (2017). Watershed health characterization using reliability–resilience–vulnerability conceptual framework based on hydrological responses. *Land Degradation & Development*, 28(5), 1528–1537. <https://doi.org/10.1002/ldr.2680>
- Hodge, A., Berta, G., Doussan, C., Merchan, F., & Crespi, M. (2009). Plant root growth, architecture, and function. *Plant and Soil*, 321(1–2), 153–187. <https://doi.org/10.1007/s11104-009-9929-9>
- Hu, F., Liu, J., Xu, C., Wang, Z., Liu, G., Li, H., & Zhao, S. (2018). Soil internal forces initiate aggregate breakdown and splash erosion. *Geoderma*, 320, 43–51. <https://doi.org/10.1016/j.geoderma.2018.01.019>
- Iwasaki, T., Shinohara, Y., Otani, S., & Kubota, T. (2013). *Effects of sampling sites on soil erosion for slope revegetation using forest topsoil* (Vol. 94, pp. 18–22). Food and Agriculture Organization of the United Nations.
- Johnson, C. W., & McArthur, R. P. (1973). Winter storm and flood analysis, northwest interior. In *Hydraulic engineering and the environment* (Vols. 15–17, pp. 359–369). New York: ASCE.
- Jordán, A., Zavala, L. M., & Gil, J. (2010). Effects of mulching on soil physical properties and runoff under semi-arid conditions in southern Spain. *Catena*, 81(1), 77–85. <https://doi.org/10.1016/j.catena.2010.01.007>
- Kavianpour, A. H., Jafarian, Z., Asmali, A., & Kavian, A. (2015). The effect of vegetation cover on reducing runoff generation and soil loss by rainfall simulation in Nasho rangeland of Mazandaran County. *Geographic and Environmental Planning*, 26(2), 179–190. <https://doi.org/10.1155/2019/7043428>
- Kutlu, T., Guber, A. K., Rivers, M. L., & Kravchenko, A. N. (2018). Moisture absorption by plant residue in soil. *Geoderma*, 316, 47–55. <https://doi.org/10.1016/j.geoderma.2017.11.043>
- Kværnø, S. H., & Øygarden, L. (2006). The influence of freeze–thaw cycles and soil moisture on aggregate stability of three soils in Norway. *Catena*, 67(3), 175–182. <https://doi.org/10.1016/j.catena.2006.03.011>
- Li, Q., Liu, G. B., & Xu, M. G. (2013). Effect of seasonal freeze–thaw on soil anti-scourability and its related physical property in hilly loess plateau. *Transactions of the Chinese Society of Agricultural Engineering*, 29(17), 105–112. <https://doi.org/10.3969/j.issn.1002-6819.2013.17.014>
- Liu, J., Chang, D., & Yu, Q. (2016). Influence of freeze–thaw cycles on mechanical properties of a silty sand. *Engineering Geology*, 210, 23–32. <https://doi.org/10.1016/j.enggeo.2016.05.019>
- Liu, H., Yang, Y., Zhang, K., & Sun, C. (2017). Soil erosion as affected by freeze–thaw regime and initial soil moisture content. *Soil Science Society of America Journal*, 81(3), 459–467. <https://doi.org/10.2136/sssaj2016.08.0271>
- Lotfalian, M., Babadi, T. Y., & Akbari, H. (2019). Impacts of soil stabilization treatments on reducing soil loss and runoff in cutslope of forest roads in Hyrcanian forests. *Catena*, 172, 158–162. <https://doi.org/10.1016/j.catena.2018.08.023>
- Mohammad, A. G., & Adam, M. A. (2010). The impact of vegetative cover type on runoff and soil erosion under different land uses. *Catena*, 81(2), 97–103. <https://doi.org/10.1016/j.catena.2010.01.008>
- Mohammadi, G. H., Jalalihanarmand, S., Mohammadkhah, A., & Ahmadi, G. H. (2011). *Seed germination*. Publication of Education and Agricultural Promotion.
- Neave, M., & Abrahams, A. D. (2002). Vegetation influences on water yields from grassland and shrubland ecosystems in the Chihuahuan Desert. *Earth Surface Processes and Landforms*, 27(9), 1011–1020. <https://doi.org/10.1002/esp.389>
- Nunes, A. N., De Almeida, A. C., & Coelho, C. O. (2011). Impacts of land use and cover type on runoff and soil erosion in a marginal area of Portugal. *Applied Geography*, 31(2), 687–699. <https://doi.org/10.1016/j.apgeog.2010.12.006>
- Oztas, T., & Fayetorbay, F. (2003). Effect of freezing and thawing processes on soil aggregate stability. *Catena*, 52(1), 1–8. [https://doi.org/10.1016/S0341-8162\(02\)00177-7](https://doi.org/10.1016/S0341-8162(02)00177-7)
- Pimentel, D., Harvey, C., Resosudarmo, P., Sinclair, K., Kurz, D., McNair, M., & Blair, R. (1995). Environmental and economic costs of soil erosion and conservation benefits. *Science*, 267, 1117–1123. <https://doi.org/10.1126/science.267.5201.1117>
- Rasse, D. P., Smucker, A. J., & Santos, D. (2000). Alfalfa root and shoot mulching effects on soil hydraulic properties and aggregation. *Soil Science Society of America Journal*, 64(2), 725–731. <https://doi.org/10.2136/sssaj2000.642725x>
- Sadeghi, S. H. R., Ghaffari, G. A., Rangavar, A., Hazbavi, Z., & Singh, V. P. (2020). Spatiotemporal distribution of soil moisture in gully facies. *International Soil and Water Conservation Research*, 8, 15–25. <https://doi.org/10.1016/j.iswcr.2019.10.001>
- Sadeghi, S. H. R., Raeisi, M. B., & Hazbavi, Z. (2018). Influence of freeze–only and freeze–thawing cycles on splash erosion. *International Soil and Water Conservation Research*, 6(4), 275–279. <https://doi.org/10.1016/j.iswcr.2018.07.0042095-63>
- Sadeghi, S. H. R., Raisi, M. B., & Hazbavi, Z. (2015). Effects of polyacrylamide in controlling of splash erosion from a soil induced freeze–thaw cycle. *Journal of Water and Soil*, 29(6), 1601–1611. <https://doi.org/10.22067/jsw.v29i6.36782>
- Sadeghi, S. H. R., Sharifi Moghadam, E., & Khaledi Darvishan, A. V. (2016). Effects of subsequent rainfall events on runoff and soil erosion components from small plots treated by vinasse. *Catena*, 138, 1–12. <https://doi.org/10.1016/j.catena.2015.11.007>
- Saeidi, P., Sadeghi, S. H. R., & Talori, A. (2016). Simulation of sediment graph by hydrograph. *Journal of Watershed Engineering and Management*, 8(1), 28–41 (In Persian).
- Shinohara, Y., Otani, S., Kubota, T., Otsuki, K., & Nanko, K. (2016). Effects of plant roots on the soil erosion rate under simulated rainfall with high kinetic energy. *Hydrological Sciences Journal*, 61(13), 2435–2442. <https://doi.org/10.1080/02626667.2015.1112904>
- Staricka, J. A., & Benoit, G. R. (1995). Freeze–drying effects on wet and dry soil aggregate stability. *Soil Science Society of America Journal*, 59(1), 218–223. <https://doi.org/10.2136/sssaj1995.03615995005900010033x>
- Steenhuis, T. S., Rivera, J. C., Hernández, C. M., Walter, M. T., Bryant, & R. B., & Nektarios, P. (2001). Water repellency in New York State soils. *International Turfgrass Society Research Journal*, 9, 624–628.
- Sun, B. Y., Xiao, J. B., Li, Z. B., Ma, B., Zhang, L. T., Huang, Y. L., & Bai, L. F. (2018). An analysis of soil detachment capacity under freeze–thaw conditions using the Taguchi method. *Catena*, 162, 100–107. <https://doi.org/10.1016/j.catena.2017.11.025>
- Toy, T. J., Foster, G. R., & Renard, K. G. (2002). *Soil erosion: Process, prediction, measurement, and control*. New York: John Wiley & Sons.
- Turcotte, B., Morse, B., Bergeron, N. E., & Roy, A. G. (2011). Sediment transport in ice-affected rivers. *Journal of Hydrology*, 409, 561–577. <https://doi.org/10.1016/j.jhydrol.2011.08.009>
- Van Klaveren, R. W., & McCool, D. K. (2010). Freeze–thaw and water tension effects on soil detachment. *Soil Science Society of America Journal*, 74(4), 1327–1338. <https://doi.org/10.2136/sssaj2009.0360>
- Wang, E., Cruse, R. M., Chen, X., & Daigh, A. (2012). Effects of moisture condition and freeze/thaw cycles on surface soil aggregate size distribution and stability. *Canadian Journal of Soil Science*, 92(3), 529–536. <https://doi.org/10.4141/cjss2010-044>
- Wang, G., Hu, H., & Li, T. (2009). The influence of freeze–thaw cycles of active soil layer on surface runoff in a permafrost watershed. *Journal of Hydrology*, 375, 438–449. <https://doi.org/10.1016/j.jhydrol.2009.06.046>
- Wang, T., Li, P., Liu, Y., Hou, J., Li, Z., Ren, Z., & Hinkelmann, R. (2020). Experimental investigation of freeze–thaw meltwater compound erosion and runoff energy consumption on loessal slopes. *Catena*, 185, 104310. <https://doi.org/10.1016/j.catena.2019.104310>
- Wang, G. X., Li, Y. S., Wang, Y. B., & Shen, Y. P. (2007). Impacts of alpine ecosystem and climate changes on surface runoff in the headwaters of the Yangtze River. *Journal of Glacial Geocryology*, 29(2), 159–168.
- Wang, B., Zhang, G. H., Shi, Y. Y., & Zhang, X. C. (2014). Soil detachment by overland flow under different vegetation restoration models in the Loess Plateau of China. *Catena*, 116, 51–59. <https://doi.org/10.1016/j.catena.2013.12.010>
- Watanabe, K., & Kugisaki, Y. (2017). Effect of macropores on soil freezing and thawing with infiltration. *Hydrological Processes*, 31(2), 270–278. <https://doi.org/10.1002/hyp.10939>
- Weaver, J. E. (1958). Classification of root systems of forbs of grassland and a consideration of their significance. *Ecology*, 39(3), 393–401. <https://doi.org/10.2307/1931749>
- Wu, X., Xiang, X., Qiu, C., & Li, L. (2018). Impacts of the thawing–freezing process on runoff generation in the sources area of the yellow river on the northeastern Qinghai–Tibet plateau. *Proceedings of the International Association of Hydrological Sciences*, 379, 211–215. <https://doi.org/10.5194/piahs-379-211-2018>
- Yu, Y., Wei, W., Chen, L., Feng, T., & Daryanto, S. (2019). Quantifying the effects of precipitation, vegetation, and land preparation techniques on runoff and soil erosion in a Loess watershed of China. *The Science of the Total Environment*, 652, 755–764. <https://doi.org/10.1016/j.scitotenv.2018.10.255>
- Zaimoglu, A. S. (2010). Freezing–thawing behavior of fine-grained soils reinforced with polypropylene fibers. *Cold Regions Science and Technology*, 60(1), 63–65. <https://doi.org/10.1016/j.coldregions.2009.07.001>
- Zhang, G. H., Guo-Bin, Liu, Guo-Liang, Wang, & Yu-Xia, Wang (2011). Effects of vegetation cover and rainfall intensity on sediment-bound nutrient loss, size composition, and volume fractal dimension of sediment particles. *Pedosphere*, 21(5), 676–684. [https://doi.org/10.1016/S1002-0160\(11\)60170-7](https://doi.org/10.1016/S1002-0160(11)60170-7)
- Zhang, L., Wang, J., Bai, Z., & Lv, C. (2015). Effects of vegetation on runoff and soil erosion on reclaimed land in an opencast coal-mine dump in a loess area. *Catena*, 128, 44–53. <https://doi.org/10.1016/j.catena.2015.01.016>
- Zhang, Z., Wei, M. A., Wenjie, Feng, Donghui, Xiao, & Xin, Hou (2016). Reconstruction of soil particle composition during freeze–thaw cycling: A review. *Pedosphere*, 26(2), 167–179. [https://doi.org/10.1016/S1002-0160\(15\)60033-9](https://doi.org/10.1016/S1002-0160(15)60033-9)
- Zhang, X., Yu, G. Q., Li, Z. B., & Li, P. (2014). Experimental study on slope runoff, erosion and sediment under different vegetation types. *Water Resources Management*, 28(9), 2415–2433. <https://doi.org/10.1007/s11269-014-0603-5>
- Zheng-Chao, Zhou, & Shangguan, Z. P. (2008). Effect of ryegrasses on soil runoff and sediment control. *Pedosphere*, 18(1), 131–136. [https://doi.org/10.1016/S1002-0160\(07\)60111-8](https://doi.org/10.1016/S1002-0160(07)60111-8)
- Zheng, D., Van der velde, R., Su, Z., Wen, J., Wang, X., & Yang, K. (2018). Impact of soil freeze–thaw mechanism on the runoff dynamics of two Tibetan rivers. *Journal of Hydrology*, 563, 382–394. <https://doi.org/10.1016/j.jhydrol.2018.06.024>
- Zhou, J., Fu, B., Gao, G., Lü, Y., Liu, Y., Lü, N., & Wang, S. (2016). Effects of precipitation and restoration vegetation on soil erosion in a semi-arid environment in the Loess Plateau, China. *Catena*, 137, 1–11. <https://doi.org/10.1016/j.catena.2015.08.015>
- Zhou, Z., Ma, W., Zhang, S., Mu, Y., & Li, G. (2018). Effect of freeze–thaw cycles in mechanical behaviors of frozen loess. *Cold Regions Science and Technology*, 146, 9–18. <https://doi.org/10.1016/j.coldregions.2017.11.01>
- Zhou, Z. C., & Shangguan, Z. P. (2005). Soil anti-scourability enhanced by plant roots. *Journal of Integrative Plant Biology*, 47(6), 676–682. <https://doi.org/10.1111/j.1744-7909.2005.00067.x>



Contents lists available at ScienceDirect

International Soil and Water Conservation Research

journal homepage: www.elsevier.com/locate/iswcr

Original Research Article

Incorporating a rainfall intensity modification factor γ into the I_a-S Relationship in the NRCS-CN methodPengcheng Hu^{a, b}, Jialiang Tang^a, Jihui Fan^a, Shumiao Shu^{a, b}, Zhaoyong Hu^{a, b}, Bo Zhu^{a, *}^a Key Laboratory of Mountain Environment Evolution and Regulation, Institute of Mountain Hazards and Environment, Chinese Academy of Sciences, Chengdu, 610041, China^b University of Chinese Academy of Sciences, Beijing, China

ARTICLE INFO

Article history:

Received 26 November 2019

Received in revised form

18 May 2020

Accepted 14 July 2020

Available online 18 July 2020

Keywords:

Climate change

Rainfall intensity

Runoff

NRCS-CN method

CN sensitivity

ABSTRACT

The Natural Resources Conservation Service runoff curve number (NRCS-CN) method is widely used to simulate direct runoff, but the impact of rainfall intensity has not been considered. In this study, a rainfall intensity modification factor (γ) was incorporated into the I_a-S relationship of the NRCS-CN method, and the modified method (NRCS-CN- γ) was compared with the NRCS-CN method with $\lambda = 0.2$ and $\lambda = 0.05$ in three watersheds of the Walnut Gulch Experimental Watershed (WGEW). The results showed that for 2016–2018 period, the simulation performance of the NRCS-CN- γ method was close to the NRCS-CN ($\lambda = 0.05$) method and better than the NRCS-CN ($\lambda = 0.2$) method. When the new data (2009 data with high variance) was added, the significant improvement was observed by NRCS-CN- γ method with all the evaluation parameters being the best in the three watersheds, indicating a more adapted capability of the modified method with highly uneven rainfall intensities. The covariance between rainfall intensity and the simulated runoff were 19.01, 15.14, and 16.35 for the three methods, respectively. When the optimal CN changed, the relative errors representing CN sensitivity were 6.25, 6.49 and 17.39 for the methods, respectively. It is suggested that the NRCS-CN- γ method outperformed the other two methods and could contribute to a more accurate estimation of direct runoff where rainfall intensity greatly varied, especially in monsoon region or under the context of climate change.

© 2020 International Research and Training Center on Erosion and Sedimentation and China Water and Power Press. Production and Hosting by Elsevier B.V. This is an open access article under the CC BY-NC-ND license (<http://creativecommons.org/licenses/by-nc-nd/4.0/>).

1. Introduction

Rainfall intensity, as an important factor in rainfall-runoff and sediment yield processes, has often been studied worldwide (Foley & Silburn, 2002; Fu et al., 2019; Hewlett et al., 1977; Kim & Lee, 2008; Mandal et al., 2010; Renard & Osborn, 1966). A basic aspect of such studies is the determination of the amount of rainfall that flows into infiltration or direct runoff from rainfall intensity (Mein & Larson, 1973). Mein and Larson (1973) further noted that infiltration has the greatest impact on watershed runoff in the hydrologic cycle. The infiltration process has been included in many popular hydrologic methods (Singh, 2010), including theoretical

(Green & Ampt, 1911; Philip, 1957) and empirical (Holtan, 1961; Kostiaikov, 1932; SCS, 1985) methods. Therefore, rainfall intensity has a large influence on the simulation results of these hydrologic methods.

Among these methods, the Natural Resources Conservation Service runoff curve number (NRCS-CN) method, formerly called the Soil Conservation Service curve number (SCS-CN) method, is one of the most widely used methods to estimate the direct surface runoff (Mishra & Singh, 2003; SCS, 1985). Due to its simplicity and stability, the NRCS-CN method has been applied to standard hydrological models, such as the agricultural nonpoint source pollution (AGNPS) model (Young et al., 1989), the erosion-productivity impact calculator (EPIC) (Sharpley, 1990), the Soil and Water Assessment Tool (SWAT) (Arnold et al., 1994) and the global flood monitoring system (GFMS) (Yilmaz et al., 2010). The NRCS-CN method has also been used to compute the sediment yield (Mishra et al., 2006), estimate the soil moisture (Reshmidevi et al.,

* Corresponding author.

E-mail addresses: hpc0813@imde.ac.cn (P. Hu), jltang@imde.ac.cn (J. Tang), jhfan@imde.ac.cn (J. Fan), longdun2101@foxmail.com (S. Shu), huzy418@imde.ac.cn (Z. Hu), bzhu@imde.ac.cn (B. Zhu).

2008) and quantify runoff in ungauged watersheds (Ajmal et al., 2016).

However, the NRCS-CN method does not contain any expression of storm time and ignores the impact of rainfall intensity (Mishra et al., 2018). This means that the NRCS-CN simulation results will be uncertain in areas or periods where rainfall characteristics change significantly, even if previous studies are satisfactory. Hence, the objective of this study is to expand the applicability of the NRCS-CN method by incorporating a rainfall intensity modification factor (γ) into the I_a - S relationship.

2. Materials and methods

2.1. Existing NRCS-CN method

The NRCS-CN method consists of one water balance equation and two fundamental hypotheses (SCS, 1985):

$$P = I_a + F + Q \quad (1)$$

$$\frac{Q}{P - I_a} = \frac{F}{S} \quad (2)$$

$$I_a = \lambda S \quad (3)$$

The NRCS-CN method can be expressed as:

$$Q = \frac{(P - I_a)^2}{P - I_a + S}, \quad P > I_a \quad (4)$$

Parameter S is derived from:

$$S = 254 \left(\frac{100}{CN} - 1 \right) \quad (5)$$

where P is the volume of rainfall, mm; I_a is initial abstraction, mm; F is cumulative infiltration from the beginning of runoff, mm; Q is the volume of runoff, mm; S is the potential maximum retention, mm; λ is the initial abstraction ratio, dimensionless; and CN is the curve number.

Parameter λ was regarded as a geologic and climatic factor varying from 0 to ∞ (Mishra & Singh, 1999, 2003). The CN value ranged from 0 to 100 and depended on soil type, vegetation cover, land use/treatment, hydrologic condition, antecedent moisture condition, and climate of the watershed (Mishra & Singh, 2003).

2.2. Modified NRCS-CN method

In the existing NRCS-CN method, I_a is calculated by accumulating rainfall from the beginning to the generation of runoff, including interception, surface storage, and infiltration (SCS, 1985). The infiltration prior to the start of runoff can be derived from a modified Green-Ampt equation by Mein and Larson (1973) as follows:

$$F_s = S_{av} M_d \left(\frac{R_c}{K_s} - 1 \right) \quad (6)$$

where F_s is the infiltration prior to runoff, mm; S_{av} is capillary suction at the wetting front, cm; M_d is the initial moisture deficit for the range of moisture content, cm^3/mm^3 ; K_s is saturated hydraulic conductivity, cm/min; and R_c is a constant intensity of rainfall, mm/h.

The constant rainfall intensity (R_c) and the infiltration prior to runoff (F_s) can be inferred to exhibit a negative correlation from Eq. (6). Zhu et al. (2006) also found the same negative correlation

between F_s and R_c from indoor laboratory experiments. F_s showed no significant difference under unsteady or steady rainfall during one rainfall-runoff event (Chen & Young, 2006; Horton, 1941). Furthermore, Ponce and Hawkins (1996) noted that infiltration (F_s) was the most important abstraction for short-term evaluation (storm analysis) between the different parts of initial abstraction (I_a). Therefore, each initial abstraction ($I_{a(i)}$) is considered to be inversely related to the average rainfall intensity (R_i) during a rainfall-runoff event. To avoid increasing the structural complexity of the NRCS-CN method, the relationship between $I_{a(i)}$ and R_i can be assumed to be an inversely proportional function:

$$I_{a(i)} = R_i^{-1} k \quad (7)$$

where k is a constant, mm^2/h . Intuitively, Eq. (7) has the correct form, as if it rains, $R_i \neq 0$; and $I_{a(i)} \neq 0$ ($k \neq 0$), since infiltration certainly occurs regardless of whether runoff is generated.

As $I_{a(i)}$ is also a function of S (SCS, 1985), Eq. (7) can be rewritten with Eq. (3) as follows:

$$I_{a(i)} = R_i^{-1} \alpha (\lambda S) \quad (8)$$

where α is a constant, mm/h. Considering dimensional harmony and the stability of the formula, the saturated hydraulic conductivity (K_s) can be used to represent α . K_s is a relatively stable rainfall characteristic factor that indicates the basic condition of generated runoff (Mein & Larson, 1973). In this study, K_s is assumed to be the minimum rainfall intensity (R_{min}) inducing runoff during the whole simulation period in the watershed. The R_{min} concept in this method is not a constant, but a physical parameter that can change over time. For traditional applications, λ is suggested to be 0.2 as in the official manual (Mishra & Singh, 2003; SCS, 1985). To be more practical, we also added the NRCS-CN method with $\lambda = 0.05$ as the control group (Blair et al., 2014; Walega et al., 2020). These substitutions are made into Eq. (8), which results in the following equation:

$$I_{a(i)} = R_i^{-1} R_{min} (0.2S) \quad (9)$$

Compared with the original NRCS-CN method, the different portion of $R^{-1} R_{min}$ in Eq. (9) is called the rainfall intensity modification factor (γ), and the modified method is called the NRCS-CN- γ method.

3. Data collection and processes

3.1. Study watersheds

To verify the efficiency of the NRCS-CN- γ method, this study selected the small watersheds 102, 103 and 104 at the Lucky Hills of the Walnut Gulch Experimental Watershed (WGEW), which were designed to quantify the effect of rainfall intensity on runoff and sediment production (Keefer et al., 2008; Stone et al., 2008). The three watersheds are 1.46, 3.68, and 4.53ha, respectively. The small-scale landforms of the WGEW are individual hills, fan terraces, basins, alluvial fans, and recent alluvial sediment (Osterkamp, 2008). Annual rainfall is concentrated between July and September, with high intensity and short duration (Simanton et al., 1996). The soil type is mainly composed of well-drained sandy loam and relatively fine sand (Heilman et al., 2008). The vegetation cover of the three basins is mainly shrubs and sparse grasses (Skirvin et al., 2008). The three catchments use a V notch weir (VNW) and a Santa Rita or Smith flume (SRF) to measure runoff (Stone et al., 2008). The daily data from 2016 to 2019 were downloaded from the Southwest Watershed Research Center website at <http://www.>

tucson.ars.ag.gov/dap/(the statistical data are provided in the Appendices).

3.2. Data processing

Data preprocessing is mainly used to calculate summary statistics for the data on the day of rainfall-runoff events. Data statistics were calculated using Microsoft Excel. Data were fitted via the nls function (Team, 2019), Nash-Sutcliffe efficiency (NSE), root mean square error (RMSE), and coefficient of determination (R^2) were calculated by hydroGOF (Zambrano-Bigiarini, 2014), and graphs were drawn with the ggplot2 package (Wickham, 2016) within the R platform (Team, 2018).

3.3. Estimation of parameters

CN is set to a sequence from 60 to 94 to avoid the influence of different CNs on the NRCS-CN- γ method, the NRCS-CN method with $\lambda = 0.05$ and the NRCS-CN method with $\lambda = 0.2$ (Mishra & Singh, 2003), according to a previous study that suggested a median CN of 80 in the WGEW (Simanton et al., 1996). Based on the runoff data from 2016 to 2019, the optimal CN was considered as the value when the best simulation result was obtained. In the watersheds 102, 103, and 104, the optimal CNs are 69, 69, and 78 for the NRCS-CN- γ method, 70, 72, and 81 for the NRCS-CN ($\lambda=0.05$) method, 64, 67, and 77 for the NRCS-CN ($\lambda=0.2$) method, respectively.

According to the hypotheses of the NRCS-CN method, the calculated initial abstraction ($I_{a(i)}^*$) can be derived from Eq. (1) and Eq. (2):

$$I_{a(i)}^* = \begin{cases} (2P_i - Q_i - \sqrt{Q_i^2 + 4Q_i S}) / 2 \\ (2P_i - Q_i + \sqrt{Q_i^2 + 4Q_i S}) / 2 \end{cases} \quad (10)$$

According to Zhou (2011), the exact expression of $I_{a(i)}^*$ is as follows:

$$I_{a(i)}^* = (2P_i - Q_i - \sqrt{Q_i^2 + 4Q_i S}) / 2 \quad (11)$$

where S can be calculated from Eq. (5) when the optimal CN is available. Fig. 1 shows the simulated initial abstraction ($I_{a(i)}$) and the calculated initial abstraction ($I_{a(i)}^*$) from 2016 to 2019 in watersheds 102, 103 and 104. The CN is the optimal value of the three methods in each watershed. The distributions of $I_{a(i)}$ and $I_{a(i)}^*$ from 2016 to 2018 are basically the same. Compared with the other methods, the $I_{a(i)}$ curve of the NRCS-CN- γ method is more consistent with the distribution trend of $I_{a(i)}^*$ points.

3.4. Method evaluation indicators

The performance of runoff simulation was evaluated by the NSE (Nash 1970), RMSE (Loague & Green, 1991), R^2 and a second-order variant of Akaike information criterion (AIC_c) (Anderson & Burnham, 2004; Hurvich & Tsai, 1989). AIC_c is expressed as:

$$AIC_c = 2K + n \ln \left(\frac{SSR}{n} \right) + \frac{2K(K+1)}{n-K-1} \quad (12)$$

where n is the number of rainfall-runoff events; K is the total number of unknown parameters; and SSR is the sum of squared

residuals. The lower AIC_c indicates the better performance of the corresponding method.

Because rainfall intensity exhibits an abnormal distribution, Cov is taken to represent the correlation between rainfall intensity and simulated runoff. A higher absolute value of Cov indicates a stronger response of the method to rainfall intensity, and vice versa. This result is calculated via the cov function (Team, 2019).

The sensitivity of CN is evaluated by the relative error (ε), which shows the variation range of NSE when CN is floating. The greater the value of ε is, the higher the sensitivity of CN.

4. Results

4.1. Runoff simulation

Figs. 2 and 3 show the observed runoff and the simulated runoff. In watersheds 102, 103 and 104, R_{min} in Figs. 2 and 3 are 3.33 and 2.26, 3.53 and 1, 3.23 and 1 mm/h, respectively. The simulation results of the NRCS-CN- γ method and the NRCS-CN ($\lambda = 0.05$) method using 2016–2018 data are similar. When adding data for 2019 with different rainfall characteristics from 2016 to 2018, the NRCS-CN- γ method is significantly better than the NRCS-CN ($\lambda = 0.05$) method. The simulation performance of the NRCS-CN ($\lambda = 0.2$) method is the worst of the three methods. From Figs. 2 and 3, the NRCS-CN- γ method has relatively high NSE and R^2 and relatively low RMSE and AIC_c in the simulation results of each watershed, indicating that this method performs best among the three methods.

4.2. Correlation between rainfall intensity and simulated runoff

Tables 1 and 2 show the correlation between rainfall intensity and simulated runoff in watersheds 102, 103 and 104 from 2016 to 2018 and 2016 to 2019, respectively. In each watershed, the NRCS-CN- γ method mainly produces a higher Cov than the other methods, which indicates that the modification factor γ can make the simulation results have a strong response to rainfall intensity.

4.3. CN sensitivity

From Table 3, the relative error (ε) of the NRCS-CN- γ method is the lowest among the three methods when CN varies within the same range in each watershed. In particular, the relative error of the NRCS-CN- γ method is less than one third of the NRCS-CN method with $\lambda = 0.2$. This result indicates that changes in CN have less of an impact on the simulation results of the NRCS-CN- γ method, which is beneficial for the simulation of future rainfall events.

5. Discussion

5.1. Performance of runoff simulation

In each of the three watersheds, the performance of the NRCS-CN method with $\lambda = 0.05$ is close to the NRCS-CN- γ method. The fitness of the NRCS-CN method with $\lambda = 0.2$ is the worst. However, the simulated initial abstraction of the NRCS-CN method with $\lambda = 0.05$ or $\lambda = 0.2$ is only a fixed estimate (Fig. 1). Conversely, the NRCS-CN- γ method can simulate the trend of the initial abstraction using the rainfall intensity. Thus, the runoff simulation results of the NRCS-CN- γ method should be superior to those of the other methods. This finding is consistent with the results shown in Fig. 1.

According to a discriminant method for the selection of multiple models (Anderson & Burnham, 2004), AIC_c of the NRCS-CN- γ method also outperforms the other methods in terms of model

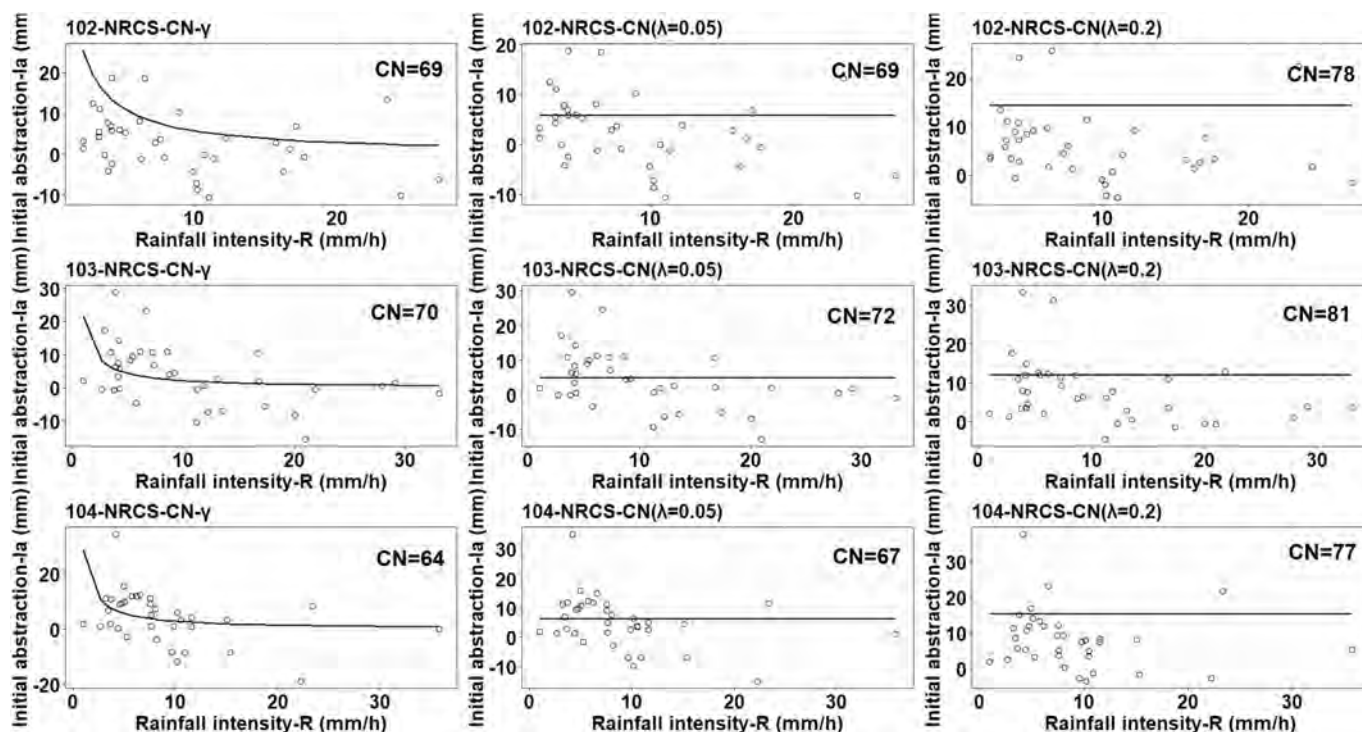


Fig. 1. The simulated initial abstraction ($I_{a(t)}$) and the calculated initial abstraction ($I_{a(t)}^*$). The solid line is $I_{a(t)}$. $I_{a(t)}^*$ are represented by hollow points.

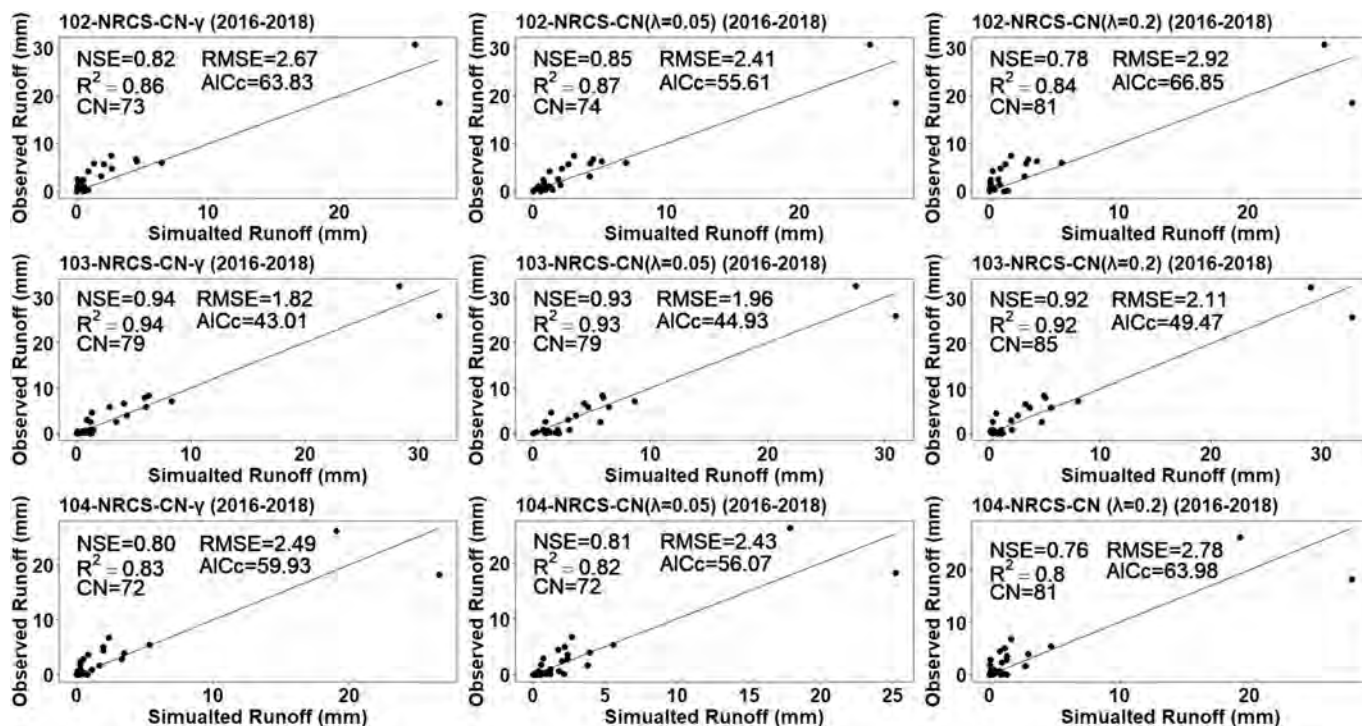


Fig. 2. Observed and simulated runoff depths from 2016 to 2018 at watersheds 102, 103 and 104.

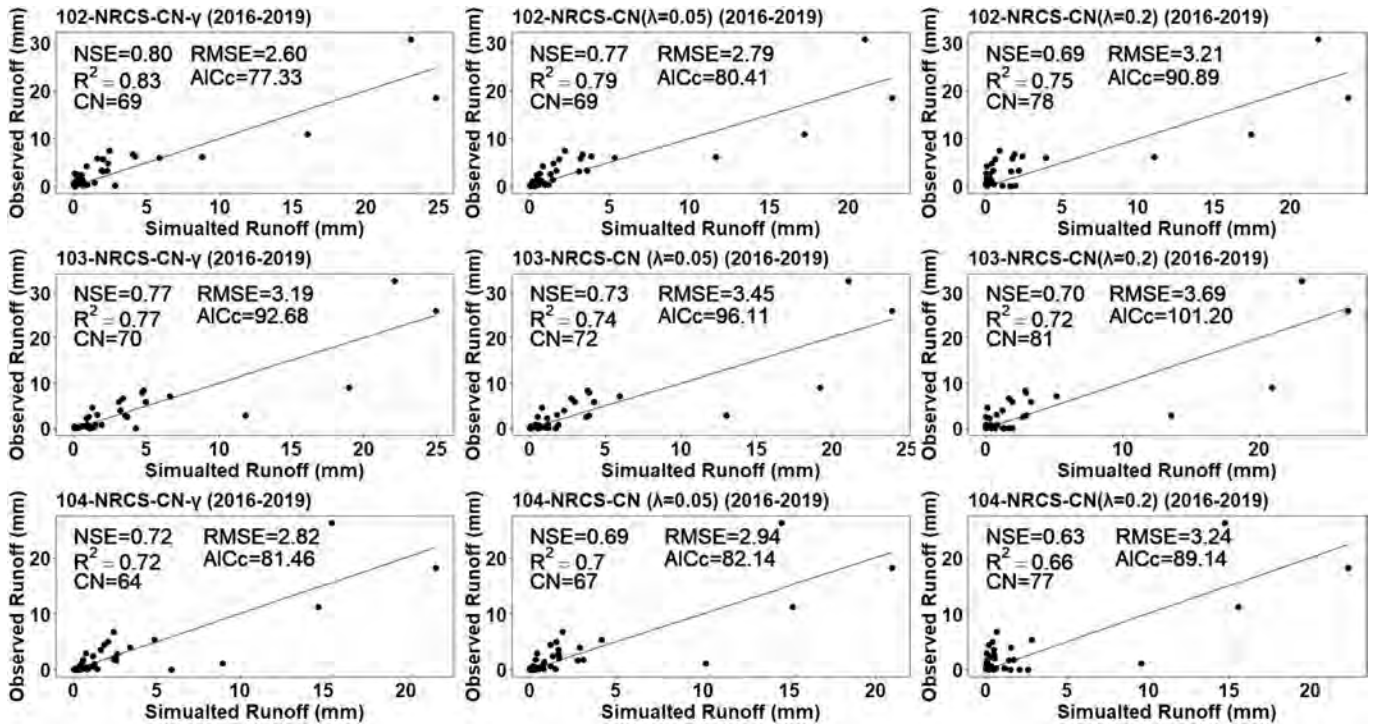


Fig. 3. Observed and simulated runoff depths from 2016 to 2019 at watersheds 102, 103 and 104.

Table 1

The covariance between rainfall intensity and the simulated runoff from 2016 to 2018.

Watershed numbers	NRCS-CN- γ			NRCS-CN ($\lambda = 0.05$)		NRCS-CN ($\lambda = 0.2$)	
	R_{min}	CN	Cov	CN	Cov	CN	Cov
102	3.33	73	28.40	74	24.85	81	26.87
103	3.53	79	21.87	79	16.72	85	19.29
104	3.23	72	24.11	72	20.14	81	22.40

Note: R_{min} is the minimum rainfall intensity of the rainfall-runoff events from 2016 to 2018, mm/h; CN is the optimal value for each method in each watershed.

Table 2

The covariance between rainfall intensity and the simulated runoff from 2016 to 2019.

Watershed numbers	NRCS-CN- γ			NRCS-CN ($\lambda = 0.05$)		NRCS-CN ($\lambda = 0.2$)	
	R_{min}	CN	Cov	CN	Cov	CN	Cov
102	2.26	69	19.01	69	15.14	78	16.35
103	1.00	70	10.45	72	8.98	81	10.59
104	1.00	64	13.17	67	12.21	77	11.82

Note: R_{min} is the minimum rainfall intensity of the rainfall-runoff events from 2016 to 2019, mm/h; CN is the optimal value for each method in each watershed.

complexity and the goodness of fit even after increasing variance by adding new dataset from 2019 (Figs. 2 and 3). It is shown that NRCS-CN- γ method could have highest adaptivity for runoff simulation under more complex rainfall conditions.

5.2. Impact of rainfall intensity

The NRCS-CN method has only two fixed parameters (CN and λ) that can reflect rainfall characteristics (Mishra & Singh, 2003), which means that the method requires stable climatic conditions to

ensure accuracy. However, the climate has undergone great changes as a result of global warming (Jaeger & Clark, 1988). For instance, Zhang et al. (2003) found that the intensity and duration of rainfall in the eastern and western parts of Northwest China changed inversely. Alexander et al. (2006) noted that precipitation has exhibited a broad and significant increase. Moreover, Trenberth (2011) found that the dry areas have become drier and the wet areas have become wetter. Hence, the NRCS-CN method needs to be modified to cope with the increasingly unstable rainfall climatic conditions.

To improve the response of the method to changes in rainfall characteristics, the rainfall intensity was incorporated into the I_a -S relationship as a modification factor γ . As a result, the correlation between the simulated runoff and rainfall intensity was stronger for the NRCS-CN- γ method than for the other methods (Tables 1 and 2). Therefore, by considering the greater variation of I_a induced by rainfall intensity, the NRCS-CN- γ method may be more accurate and useful for the simulation of monsoon regions where greater rainfall intensity variations were found, especially under the impact of global climate change.

5.3. CN sensitivity and applications

The curve number (CN) is the most important parameter in the NRCS-CN method. This value can be selected from the tables in the National Engineering Handbook (Section 4) (NEH-4) or estimated from measured rainfall-runoff data. However, studies have shown that CN is a variable parameter (Banasik et al., 2014; Banasik & Hejduk, 2012; Bondelid et al., 2010; Soulis & Valiantzas, 2012). Therefore, the sensitivity of CN is critical when simulating future rainfall-runoff events based on previous or existing research results.

In this study, rainfall intensity was extracted as a separate modification factor that can reduce the impact of uncertainty in rainfall characteristics on CN sensitivity. As shown in Table 3, the

Table 3The range of ϵ when the optimal CN changes with ± 5 .

Watershed numbers	Methods	2016–2018			2016–2019		
		CNs	NSEs	ϵ	CNs	NSEs	ϵ
102	NRCS–CN– γ	73 \pm 5	0.82–0.78	4.88%	69 \pm 5	0.80–0.75	6.25%
102	NRCS–CN ($\lambda = 0.05$)	74 \pm 5	0.85–0.78	8.24%	69 \pm 5	0.77–0.72	6.49%
102	NRCS–CN ($\lambda = 0.2$)	81 \pm 5	0.78–0.66	15.38%	78 \pm 5	0.69–0.57	17.39%
103	NRCS–CN– γ	79 \pm 5	0.94–0.87	7.45%	70 \pm 5	0.77–0.73	5.19%
103	NRCS–CN ($\lambda = 0.05$)	79 \pm 5	0.93–0.84	9.68%	72 \pm 5	0.73–0.69	5.48%
103	NRCS–CN ($\lambda = 0.2$)	85 \pm 5	0.92–0.72	21.74%	81 \pm 5	0.70–0.52	25.71%
104	NRCS–CN– γ	72 \pm 5	0.81–0.75	7.41%	64 \pm 5	0.72–0.68	5.56%
104	NRCS–CN ($\lambda = 0.05$)	72 \pm 5	0.81–0.76	6.17%	67 \pm 5	0.69–0.63	8.70%
104	NRCS–CN ($\lambda = 0.2$)	81 \pm 5	0.76–0.58	23.68%	77 \pm 5	0.63–0.48	23.81%

relative error (ϵ) used to represent CN sensitivity in the NRCS–CN– γ method is lower than that in the NRCS–CN ($\lambda = 0.05$) method and less than one third of that in the NRCS–CN ($\lambda = 0.2$) method. This means that the NRCS–CN– γ method has a more stable CN and can be better used for future simulations considering different rainfall intensities, especially in monsoon affected regions.

In terms of usage in un-gauged areas, we suggested the new CN as the recommended value in NEH-4 should be reduced by 10%. On the one hand, the new CN must be smaller than the value recommended in NEH-4, as γ is less than or equal to 1 from Eq. (9). On the other hand, when the optimal CN in the NRCS–CN ($\lambda = 0.2$) method is reduced by 10% and used in the NRCS–CN– γ method, the relative error of the simulation accuracy is within 10%.

6. Conclusions

As a result of the changes in rainfall and temperature under the context of global changes, the problem of nonstationary parameters in hydrological models has received great attention, especially for the NRCS–CN method, which does not contain rainfall intensity factors. The following conclusions can be derived: Compared with the original NRCS–CN method, the NRCS–CN– γ method took the minimum rainfall intensity inducing runoff over years and average rainfall intensity as important parameters. On a temporal scale, the CN sensitivity of the NRCS–CN– γ method is much lower than that of the original method, which will reduce the prediction errors in future studies by combining the new γ factor. As the NRCS–CN method is originated from the United States, and the data in this study are also derived from the WGEW, the NRCS–CN– γ method has only limited improvement compared with NRCS–CN methods of $\lambda = 0.2$ or $\lambda = 0.05$, but this also means that the modified method may be particularly useful in monsoon regions where rainfall intensity varies greatly, especially in response to climate change. Because the new parameters are relatively fixed, and the required CN can be derived from the NEH-4, the NRCS–CN– γ method can have great application potential in un-gauged areas.

Acknowledgments

This work was jointly supported by the Strategic Priority Research Program of the Chinese Academy of Sciences (XDA23040202) and the National Natural Science Foundation (Grant No. 41430750). The original data are downloaded from the Southwest Watershed Research Center website at <http://www.tucson.ars.ag.gov/dap/>. The statistical data displayed in this paper are available in the Appendices.

Appendices

Table.A.1

Statistical data of 102 watershed.

Date	Tq	Q	Tp	P	R	γ
6/29/2016	22.5	0.2048	41	11.68	17.10	7.57
6/30/2016	28.5	0.5574	157	16.26	6.21	2.75
7/1/2016	60.5	4.7107	43	19.43	27.11	12.00
7/16/2016	28.5	1.6038	126	13.21	6.29	2.78
7/17/2016	38.5	1.3641	238	19.05	4.80	2.13
8/2/2016	37.5	0.6891	263	14.73	3.36	1.49
8/9/2016	24.5	1.0029	78	10.29	7.91	3.50
9/12/2016	63.5	6.6616	99	26.80	16.24	7.19
9/29/2016	23.5	2.3081	79	13.08	9.93	4.40
10/2/2016	19.5	0.4584	31	8.64	16.71	7.40
7/3/2017	17.5	0.3269	111	16.51	8.92	3.95
7/10/2017	16.5	0.0050	207	11.81	3.42	1.51
7/13/2017	91.5	5.9764	163	33.15	12.20	5.40
7/16/2017	9.5	0.0221	17	4.45	15.69	6.94
7/23/2017	28.5	0.5603	92	11.18	7.29	3.23
7/27/2017	20.5	0.5004	191	13.59	4.27	1.89
7/28/2017	62.5	30.6643	163	66.29	24.40	10.80
7/30/2017	21.5	5.6132	124	21.08	10.20	4.51
8/1/2017	26.5	2.5874	296	18.42	3.73	1.65
8/10/2017	29.5	7.4881	123	22.61	11.03	4.88
8/12/2017	159.5	18.4358	177	69.22	23.46	10.38
7/15/2018	34.5	0.5495	224	12.45	3.33	1.48
7/20/2018	24.5	0.3094	210	13.84	3.96	1.75
9/2/2018	32.5	1.0868	121	15.37	7.62	3.37
9/19/2018	85.5	6.1882	151	28.58	11.35	5.02
10/21/2018	35.5	4.2147	91	15.49	10.22	4.52
10/22/2018	23.5	0.1131	20	3.56	10.67	4.72
10/23/2018	182.0	3.1907	300	26.04	5.21	2.30
12/7/2018	93.3	5.7980	369	26.29	4.27	1.89
8/3/2019	74.5	3.2692	69	20.32	17.67	7.82
9/24/2019	559.5	10.8178	547	59.44	6.52	2.88
11/19/2019	189.5	3.2403	396	27.81	4.21	1.86
11/21/2019	154.5	0.2277	358	17.65	2.96	1.31
11/27/2019	461.3	6.1740	685	48.51	4.25	1.88
11/29/2019	236.5	2.6165	217	14.48	4.00	1.77
12/8/2019	84.5	0.7126	287	10.80	2.26	1.00
12/9/2019	22.5	0.0700	161	6.10	2.27	1.01

Note: Tq means the duration of runoff, min; Q means the volume of runoff, mm; Tp means the time period of rainfall, mm; P means the volume of rainfall, mm; R means the rainfall intensity, mm/h; γ means the rainfall modification factor, unitless, Red font means R_{min} , mm/h.

Table.A.2

Statistical data of 103 watershed.

Date	Tq	Q	Tp	P	R	γ
6/29/2016	21.5	0.0377	45	12.57	16.76	16.76
6/30/2016	29.5	0.2366	157	16.13	6.16	6.16
7/1/2016	74.5	3.9567	38	20.96	33.09	33.09
7/16/2016	22.5	0.6305	84	12.95	9.25	9.25
7/17/2016	50.5	0.8334	215	19.43	5.42	5.42
8/2/2016	45.5	0.4706	206	13.46	3.92	3.92
8/9/2016	35.5	0.8051	23	11.18	29.15	29.15
9/12/2016	91.25	8.4027	79	26.42	20.06	20.06

TableA.2 (continued)

Date	Tq	Q	Tp	P	R	γ
9/27/2016	4.5	0.0002	51	3.56	4.18	4.18
9/29/2016	36.5	2.5435	42	12.19	17.42	17.42
February 10, 2016	28.5	0.3431	29	8.13	16.82	16.82
7/3/2017	43.25	0.1944	108	15.49	8.61	8.61
7/10/2017	56.5	0.0167	205	12.07	3.53	3.53
7/13/2017	142.25	7.1457	163	32.26	11.87	11.87
7/16/2017	19.5	0.0189	18	3.94	13.12	13.12
7/23/2017	60.5	0.4617	78	11.43	8.79	8.79
7/27/2017	51.5	0.4768	184	13.21	4.31	4.31
7/28/2017	100.25	32.4985	178	62.36	21.02	21.02
7/30/2017	45.25	6.5628	111	22.73	12.29	12.29
8/1/2017	49.25	2.9312	267	19.18	4.31	4.31
8/10/2017	54.25	7.9645	118	26.67	13.56	13.56
8/12/2017	275.25	25.8256	184	67.06	21.87	21.87
7/15/2018	22.5	0.0484	237	16.64	4.21	4.21
7/20/2018	30.5	0.0929	115	13.84	7.22	7.22
9/2/2018	38.5	0.7578	132	16.26	7.39	7.39
9/19/2018	97.5	5.7664	147	27.69	11.30	11.30
10/21/2018	53.5	4.5085	76	14.22	11.23	11.23
10/22/2018	17.5	0.0476	6	2.79	27.94	27.94
10/23/2018	175	2.4848	296	26.04	5.28	5.28
12/7/2018	88.5	5.7695	246	23.62	5.76	5.76
9/24/2019	349	8.9356	535	59.18	6.64	6.64
9/25/2019	6.5	0.0003	129	2.16	1.00	1.00
11/19/2019	121.5	2.8864	383	26.67	4.18	4.18
11/21/2019	93.5	0.0184	379	18.67	2.96	2.96
11/27/2019	430.5	2.8779	740	47.88	3.88	3.88
11/29/2019	136.5	2.2318	255	16.00	3.77	3.77
12/9/2019	56	0.4050	143	6.35	2.66	2.66

Note: Tq means the duration of runoff, min; Q means the volume of runoff, mm; Tp means the time period of rainfall, mm; P means the volume of rainfall, mm; R means the rainfall intensity, mm/h, γ means the rainfall modification factor, unitless, Red font means R_{min} , mm/h.

Table.A.3

Statistical data of 104 watershed.

Date	Tq	Q	Tp	P	R	γ
6/29/2016	9.5	0.0014	76	9.53	7.52	7.52
6/30/2016	33.5	0.1311	171	16.38	5.75	5.75
7/1/2016	56.5	2.8263	36	21.46	35.77	35.77
7/16/2016	34.5	0.9562	85	16.38	11.56	11.56
7/17/2016	47.5	0.6393	241	19.05	4.74	4.74
8/2/2016	45.5	0.2713	202	15.37	4.56	4.56
8/9/2016	44.5	0.6122	84	10.67	7.62	7.62
9/12/2016	77.5	4.4147	74	18.92	15.34	15.34
9/29/2016	44.5	1.7090	92	12.57	8.20	8.20
10/2/2016	33.5	0.1937	50	8.76	10.52	10.52
7/3/2017	24.5	0.0833	116	14.61	7.55	7.55
7/10/2017	9.5	0.0011	215	11.56	3.23	3.23
7/13/2017	116.5	5.3881	162	31.24	11.57	11.57
7/16/2017	13.5	0.0005	42	5.33	7.62	7.62
7/23/2017	53.5	0.3409	77	13.08	10.19	10.19
7/27/2017	35.5	0.2908	230	13.21	3.45	3.45
7/28/2017	88.5	26.1315	153	56.77	22.26	22.26
7/30/2017	35.5	4.9729	114	20.70	10.90	10.90
8/1/2017	43.25	2.3544	271	19.81	4.39	4.39
8/10/2017	41.5	6.7101	133	22.61	10.20	10.20
8/12/2017	234.5	18.1218	177	68.96	23.38	23.38
7/15/2018	33.5	0.1696	249	20.57	4.96	4.96
7/20/2018	16.5	0.0009	118	12.19	6.20	6.20
9/2/2018	32.5	0.3785	110	14.73	8.04	8.04
9/19/2018	60.5	3.9079	163	26.67	9.82	9.82
10/21/2018	37.5	2.8582	84	13.46	9.62	9.62
10/22/2018	3.5	0.0005	21	3.68	10.52	10.52
10/23/2018	135	1.6763	310	26.16	5.06	5.06
12/7/2018	77.5	3.5596	244	21.46	5.28	5.28

Table.A.3 (continued)

Date	Tq	Q	Tp	P	R	γ
8/3/2019	32.5	2.0550	86	21.59	15.06	15.06
9/24/2019	444.5	11.1211	531	58.17	6.57	6.57
9/25/2019	85.5	0.0032	145	2.41	1.00	1.00
11/19/2019	49.5	1.7257	438	27.43	3.76	3.76
11/27/2019	245.5	1.1077	676	47.37	4.20	4.20
11/29/2019	82.5	1.4027	271	16.64	3.68	3.68
12/9/2019	32.5	0.2009	146	6.48	2.66	2.66

Note: Tq means the duration of runoff, min; Q means the volume of runoff, mm; Tp means the time period of rainfall, mm; P means the volume of rainfall, mm; R means the rainfall intensity, mm/h, γ means the rainfall modification factor, unitless, Red font means R_{min} , mm/h.

Table.A.4

Table of Symbols.

Symbols	Means	Unites
P	the volume of rainfall	Mm
Q	the volume of runoff	Mm
F	the volume of infiltration	Mm
S	the potential maximum retention	Mm
Ia	the volume of initial abstraction	Mm
$I_{a(i)}^*$	the volume of calculated initial abstraction	Mm
$I_{a(i)}$	the volume of simulated initial abstraction	Mm
CN	the curve number	Unitless
λ	the initial abstraction ratio	unitless
γ	the rainfall intensity modification factor	unitless
Tq	the duration of runoff	min
Tp	the time period of rainfall	min
R	the rainfall intensity	mm/h

References

Ajmal, M., Ahn, J. H., & Kim, T. W. (2016). Excess stormwater quantification in ungauged watersheds using an event-based modified NRCS model. *Water Resources Management*, 30, 1433–1448.

Alexander, L. V., Zhang, X., Peterson, T. C., Caesar, J., Gleason, B., Klein Tank, A. M. G., ... Tagipour, A. (2006). Global observed changes in daily climate extremes of temperature and precipitation. *Journal of Geophysical Research-Atmospheres*, 111, 22.

Anderson, D., & Burnham, K. (2004). Model selection and multimodel inference. *Technometrics*, 45, 181–81.

Arnold, J. G., Williams, J. R., Srinivasan, R., King, K. W., & Griggs, R. H. (1994). SWAT (soil and water assessment Tool) user's manual. Temple, Texas: Usda. In *Agricultural research Service, grassland, soil, and water research laboratory* accessed <http://www.brc.tamus.edu/swat/>. (Accessed 13 December 2005).

Banasik, K., & Hejduk, L. (2012). Variation of curve number with storm depth. In *EGU general assembly conference abstracts*, 13468.

Banasik, K., Hejduk, L., Banasik, J., & Rutkowska, A. (2014). Influence of Curve Number variation on peak discharge of small catchment. In *EGU general assembly conference abstracts*.

Blair, A., Sanger, D., White, D., Holland, A. F., Vandiver, L., Bowker, C., et al. (2014). Quantifying and simulating stormwater runoff in watersheds. *Hydrological Processes*, 28(3), 559–569.

Bondelid, T. R., McCuen, R. H., & Jackson, T. J. (2010). Sensitivity of SCS models to curve number Variation 1. *JAWRA Journal of the American Water Resources Association*, 18, 111–116.

Chen, L., & Young, M. H. (2006). Green-Ampt infiltration model for sloping surfaces. *Water Resources Research*, 42, 887–896.

Foley, J. L., & Silburn, D. M. (2002). Hydraulic properties of rain impact surface seals on three clay soils - influence of raindrop impact frequency and rainfall intensity during steady state. *Soil Research*, 40(7), 1069–1083.

Fu, X. T., Zhang, L. P., & Wang, Y. (2019). Effect of slope length and rainfall intensity on runoff and erosion conversion from laboratory to field. *Water Resources*, 46, 530–541.

Green, W. H., & Ampt, G. A. (1911). Studies on soil physics. *The Journal of Agricultural Science*, 4, 1–24.

- Heilman, P., Nichols, M. H., Goodrich, D. C., Miller, S. N., & Guertin, D. P. (2008). 'Geographic information systems database, Walnut Gulch experimental watershed, Arizona, United States'. *Water Resources Research*, 44, 61–74.
- Hewlett, J. D., Fortson, J. C., & Cunningham, G. B. (1977). The effect of rainfall intensity on storm flow and peak discharge from forest land. *Water Resources Research*, 13, 259–266.
- Holtan, H. N. (1961). Concept for infiltration estimates in watershed engineering. *AIChE Journal*, 150(1), B16–B25.
- Horton, R. E. (1941). An approach toward a physical interpretation of infiltration-capacity 1. *Soil Science Society of America Journal*, 5, 399–417.
- Hurvich, C. M., & Tsai, C. L. (1989). 'Regression and time series model selection in small samples. *Biometrika*, 76, 297–307.
- Jaeger, J., & Clark, W. C. (1988). *Developing policies for responding to climatic change*. Geneva: WMO Secretariat.
- Keefer, T. O., Moran, M. S., & Paige, G. B. (2008). Long-term meteorological and soil hydrology database, Walnut Gulch Experimental Watershed, Arizona, United States. *Water Resources Research*, 44, 570–575.
- Kim, N. W., & Lee, J. (2008). Temporally weighted average curve number method for daily runoff simulation. *Hydrological Processes*, 22, 4936–4948.
- Kostiakov, A. N. (1932). On the dynamics of the coefficient of water percolation in soils and the necessity of studying it from the dynamic point of view for the purposes of amelioration. In *Trans. Sixth Comm. Int. Soc. Soil Sci.*, 1 pp. 7–21.
- Loague, K., & Green, R. E. (1991). Statistical and graphical methods for evaluating solute transport models: Overview and application. *Journal of Contaminant Hydrology*, 7, 51–73.
- Mandal, U. K., Rao, K. V., Mishra, P. K., Vittal, K. P. R., Sharma, K. L., Narsimlu, B., et al. (2010). Soil infiltration, runoff and sediment yield from a shallow soil with varied stone cover and intensity of rain. *European Journal of Soil Science*, 56, 435–443.
- Mein, R. G., & Larson, C. L. (1973). Modeling infiltration during a steady rain. *Water Resources Research*, 9, 384–394.
- Mishra, S. K., & Singh, V. P. (1999). Another look at SCS-CN method. *Journal of Hydrologic Engineering*, 4(3), 257–264.
- Mishra, S. K., & Singh, V. P. (2003). *Soil conservation Service curve number (SCS-CN) methodology*. Water Science and Technology Library. <https://doi.org/10.1007/978-94-017-0147-1>
- Mishra, S. K., Singh, V. P., & Singh, P. K. (2018). Revisiting the soil conservation Service curve number method. In *Hydrologic modeling* (pp. 667–693). Singapore: Springer.
- Mishra, S. K., Tyagi, J. V., Singh, V. P., & Singh, R. (2006). SCS-CN-based modeling of sediment yield. *Journal of Hydrology*, 324, 301–322.
- Nash, J. E., & Sutcliffe, J. V. (1970). River flow forecasting through conceptual models part I - A discussion of principles. *Journal of Hydrology*, 10, 282–290.
- Osterkamp, W. R. (2008). 'Geology, soils, and geomorphology of the Walnut Gulch experimental watershed, Tombstone, Arizona. *Journal of the Arizona-Nevada Academy of Science*, 40, 136–154.
- Philip, J. R. (1957). The theory of infiltration: 1. The infiltration equation and its solution. *Soil Science*, 83, 345–358.
- Ponce, V. M., & Hawkins, R. H. (1996). Runoff curve number: Has it reached maturity? *Journal of Hydrologic Engineering*, 1, 11–19.
- Renard, K. G., & Osborn, H. B. (1966). Rainfall intensity comparisons from adjacent 6-Hour and 24-hour recording rain gages. *Water Resources Research*, 2, 145–146.
- Reshmidevi, T. V., Jana, R., & Eldho, T. I. (2008). Geospatial estimation of soil moisture in rain-fed paddy fields using SCS-CN-based model. *Agricultural Water Management*, 95, 447–457.
- Scs, U. (1985). *National engineering handbook, section 4: Hydrology*. Washington, DC: US Soil Conservation Service, USDA.
- Sharpley, A. N. (1990). EPIC-erosion/productivity impact calculator: 1, model documentation. In *USDA Techn. Bull.*, 1759 p. 235).
- Simanton, J. R., Hawkins, R. H., Mohseni-Saravi, M., & Renard, K. G. (1996). Runoff curve number variation with drainage area, Walnut Gulch, Arizona. *Transactions of the ASAE*, 39, 1391–1394.
- Singh, V. P. (2010). Entropy theory for derivation of infiltration equations. *Water Resources Research*, 46(3).
- Skirvin, S., Kidwell, M., Biedenkemper, S., Henley, J. P., King, D., Collins, C. H., ... Weltz, M. (2008). Vegetation data, Walnut Gulch experimental watershed, Arizona, United States. *Water Resources Research*, 44, 61–74.
- Soulis, K. X., & Valiantzas, J. D. (2012). SCS-CN parameter determination using rainfall-runoff data in heterogeneous watersheds. The two-CN system approach. *Hydrology and Earth System Sciences*, 16, 1001–1015.
- Stone, J. J., Nichols, M. H., Goodrich, D. C., & Buono, J. (2008). 'Long-term runoff database, Walnut Gulch experimental watershed, Arizona, United States'. *Water Resources Research*, 44(5).
- Team, R. S. (2018). *RStudio: Integrated development environment for R*. Boston, MA: RStudio, Inc.
- Team, R. C. (2019). *R: A language and environment for statistical computing*. Vienna, Austria: R Foundation for Statistical Computing.
- Trenberth, K. E. (2011). Changes in precipitation with climate change. *Climate Research*, 47, 123–138.
- Walega, A., Amatya, D. M., Caldwell, P. V., Marion, D., & Panda, S. (2020). Assessment of storm direct runoff and peak flow rates using improved SCS-CN models for selected forested watersheds in the Southeastern United States'. *Journal of Hydrology: Regional Studies*, 27, 100645.
- Wickham, H. (2016). *ggplot2: Elegant graphics for data analysis*. New York: Springer-Verlag.
- Yilmaz, K. K., Adler, R. F., Tian, Y., Hong, Y., & Pierce, H. F. (2010). Evaluation of a satellite-based global flood monitoring system. *International Journal of Remote Sensing*, 31, 3763–3782.
- Young, R. A., Onstad, C. A., Bosch, D. D., & Anderson, W. P. (1989). Agnps: A nonpoint-source pollution model for evaluating agricultural watersheds. *Journal of Soil and Water Conservation*, 44, 168–173.
- Zambrano-Bigiarini, M. (2014). hydroGOF: Goodness-of-fit functions for comparison of simulated and observed hydrological time series. In *R package version 0.3-8*.
- Zhang, C., Gao, X., & Zhao, H. (2003). Impact of global warming on autumn precipitation in Northwest China. *Journal of Glaciology and Geocryology*, 25(2), 157–164.
- Zhou, S., & Lei, T. (2011). 'Calibration of SCS-CN initial abstraction ratio of a typical small watershed in the Loess Hilly-Gully region. *Scientia Agricultura Sinica*, 44, 4240–4247.
- Zhu, W., Chen, X. D., & Zhong, X. C. (2006). Observation and analysis of rainfall infiltration. *Rock and Soil Mechanics*, 27, 1873–1879.



Contents lists available at ScienceDirect

International Soil and Water Conservation Research

journal homepage: www.elsevier.com/locate/iswcr

Original Research Article

Monitoring the variation of soil quality with sewage sludge application rates in absence of rhizosphere effect



Rahma Inès Zoghlami ^{a, b}, Helmi Hamdi ^{c, *}, Sonia Mokni-Tlili ^b, Sarra Hechmi ^b, Mohamed Naceur Khelil ^d, Nadhira Ben Aissa ^e, Mohamed Moussa ^a, Habib Bousnina ^e, Saoussen Benzarti ^f, Naceur Jedidi ^b

^a Arid Regions Institute, University of Gabès, Médenine, 4119, Tunisia

^b Water Research and Technology Center, University of Carthage, P.O. Box 273, Soliman, 8020, Tunisia

^c Center for Sustainable Development, College of Arts and Sciences, Qatar University, P.O. Box 2713, Doha, Qatar

^d National Institute for Research in Rural Engineering, Water and Forestry, P.O. Box 10, Ariana, 2080, Tunisia

^e National Institute of Agronomy, 43 Av. Charles Nicolle, Tunis, 1082, Tunisia

^f College of Agriculture at Mograne, University of Carthage, 1121, Mograne, Tunisia

ARTICLE INFO

Article history:

Received 3 April 2020

Received in revised form

29 July 2020

Accepted 30 July 2020

Available online 31 July 2020

Keywords:

Sandy loam soil

Urban sewage sludge

Structural stability

Soil degradation

Aggregation

Magnetic susceptibility

ABSTRACT

Agricultural soils in semi-arid regions have frequently been degraded due to adverse climatic conditions, organic matter depletion, and poor farming practices. To enhance soil quality, this study examines the reuse of sewage sludge (SS) as an available source of organic matter in a typical Mediterranean sandy-loam soil. Accordingly, we studied the cumulative effect of two annual applications of 40, 80 and 120 tons of sludge per ha on soil quality in absence of vegetation. The dose-dependent improvement of organic matter content was the most significant event that reflected sludge application rates, and consequently influenced other soil properties. Accordingly, soil structural stability increased by 13.3%, 28.8% and 59.4% for treatments SS-40, SS-80 and SS-120 respectively as compared to unamended control. Structural stability improvement was also confirmed by the dose-dependent variation of other edaphic factors including calcium content, the microbial quotient as well as Welt and C:N ratios. These parameters are involved in cementing soil aggregates by cation bridging, the formation of microbial mucilage, and clay-humic complexes. Soil magnetic susceptibility (SMS) was measured in situ as a possible rapid tool to evaluate soil condition. SMS showed significant correlation with sludge dose and stability amelioration testifying to the aggregation role that can play Al_2O_3 and particularly Fe_2O_3 minerals added by the hematite-rich sludge. Besides, analytical results and field observations revealed no trends of soil salinization or acidification by excessive sludge amounts. By avoiding the rhizosphere effect, outcomes could reflect the resilience and intrinsic capacity of the soil to cope with excessive sludge loads.

© 2020 International Research and Training Center on Erosion and Sedimentation and China Water and Power Press. Production and Hosting by Elsevier B.V. This is an open access article under the CC BY-NC-ND license (<http://creativecommons.org/licenses/by-nc-nd/4.0/>).

1. Introduction

Degradation of productive croplands has been of a great economic concern due to its impact on current and future production and implications on food security. Global estimates of total degraded lands vary from less than 1 billion ha to over 6 billion ha, with equally wide disagreement in their spatial distribution (Gibbs & Salmon, 2015). In any case, improving soil quality contributes to

minimize arable land degradation and allows for better sustainable agricultural practices. On the other hand, semi-arid soils in particular are more vulnerable to degradation because they store little organic carbon (Janzen, 2004); whereas these soils possess a great potential for carbon sequestration after organic amendments (Lal, 2009). Therefore, enriching soils with exogenous organic matter is a major practice that restores degraded soils in semi-arid regions (Masciandaro et al., 2013; Zoghlami et al., 2016).

It has historically been proved that the valorization of agricultural wastes such as farm manures or plant residues improves the fertility of soils by enhancing their structure, nutrient content, hydrodynamics properties, and biological activities (Adediran et al.,

* Corresponding author.

E-mail address: hhamdi@qu.edu.qa (H. Hamdi).

2003; Zoghlami et al., 2016). In addition, nutrient inputs from organic wastes to croplands is a way to reduce the need for chemical fertilizers (Siebielec et al., 2018). In recent years, agricultural intensification has led to greater input requirements, which resulted in high demand for traditional farm manure and raised the need of seeking organic matter supply from unconventional sources. For instance, urban sewage sludge (SS) is an organic by-product continuously generated during domestic wastewater treatment. Urban sludge is naturally rich in organic carbon, N, P, and micro-nutrients, which gives it unique fertilizing benefits (Fytili & Zabaniotou, 2008). Sludge addition to croplands has been a promising practice for farmers in semi-arid regions because it equilibrates soil humic balance, supplies nitrogen and phosphorus at lower costs, and most importantly, copes with farm manure shortages (Lu et al., 2012; Siebielec et al., 2018). While the improvement of crop yield and the changes of soil chemical properties including contaminant accumulation have extensively been studied (Delibacak & Ongon, 2016; Siebielec et al., 2018; Tejada & Gonzalez, 2007), less is known about changes in other soil properties following repetitive or mismanaged SS applications. In this regard, soil physical degradation may occur depending on sludge quality, applied dose, amendment frequency, and pedo-environmental conditions (Hamdi et al., 2007; Singh & Agrawal, 2008).

Physical degradation has generally been monitored by addressing soil pH and electrical conductivity, which reflect acidification and salinization risks after sludge application (Eid et al., 2018; Hamdi et al., 2007; Singh & Agrawal, 2008). These factors affect soil aggregate stability resulting in dispersive soils with poor structure (Odeh & Onus, 2008). On the other hand, most of studies that monitor sludge effect on soil have been conducted under cropped conditions (Delibacak & Ongon, 2016; Eid et al., 2018; Kayikcioglu et al., 2019). Consequently, the intrinsic capacity of soils to cope with degradation is likely to be influenced by plant roots referred to as the rhizosphere effect (Kobierski et al., 2018). Therefore, the aim of this study was to monitor soil indicators that reflect changes in global soil quality after two annual amendments with increasing rates of sewage sludge. Conducted in complete unvegetated soil conditions, this study could be then carried out by ascertaining the effect of sewage sludge addition on: (i) soil organic matter quality, (ii) soil structural stability, (iii) soil pH and salinity, and (iv) whether these properties were influenced or not by moderate to excessive rates of sludge. Accordingly, our hypotheses were as follows: (i) appropriate sludge reuse is a suitable practice for the restoration of semi-arid agricultural soils by improving soil fertility, (ii) the quality of organic matter (fulvic and humic acids) would affect structural stability, and (iii) the absence of vegetal cover would ultimately reflect soil resilience and intrinsic capacity to cope with excessive sludge loads.

2. Materials and methods

2.1. Experimental design

The field study was conducted in an Agricultural Experiment Station located in the city of Nabeul (northeastern Tunisia, 36° 27' 15" N, 10° 44' 5" E). The region has a southern semi-arid Mediterranean climate characterized by prolonged dry summers, warm winters, moderate and irregular precipitation (350–400 mm). The experimental soil is typical light-textured agricultural soil of the region classified as sandy loam, having moderate organic matter and low N contents (Table 1). Soil X-ray diffraction (XRD) pattern shows a dominance of quartz and calcite minerals (71%), while the smaller clay fraction (~12%) is composed mostly of kaolinite and

Table 1
Physico-chemical properties of experimental soil and sewage sludge.

	Soil (sandy loam)	Sewage sludge
Sand (%)	70.9	–
Clay (%)	11.9	–
Silt (%)	17.2	–
SSA ($m^2 g^{-1}$)	27	–
Bulk density ($g cm^{-3}$)	1.31	–
pH (1:2.5)	7.72	7.7
EC ($\mu S cm^{-1}$) (1:5)	155	1702
TOC (%)	0.76	18.5
OM (%)	1.30	31.8
N (%)	0.071	1.18
C:N	10.7	15.7
P Olsen ($mg kg^{-1}$)	14.1	220
K ($mg kg^{-1}$)	58.8	9.54
Na ($mg kg^{-1}$)	19.6	1231
Ca ($g kg^{-1}$)	9.56	113.5
Fe ₂ O ₃ (%)	0.95	2.08
CaCO ₃ (%)	1.8	11.8
Al ₂ O ₃ (%)	1.91	4.41

All values are given on dry weight basis.

illite. Consequently, the soil has a relatively small specific surface area of $27 m^2 g^{-1}$ (Table 1). The mean topsoil annual temperature is 18 °C but varies largely with seasons (9.7–31.7 °C). Aerobically digested SS was directly collected from the drying beds of a close urban wastewater treatment plant. It was further air dried at the experimental farm for three weeks to reach a final water content of about 10%. The urban sludge had a C:N ratio of 15 and complied with Tunisian guidelines (NT 106-20) for biosolids reuse in agriculture.

The experimental protocol consisted of four soil treatments with four replicates distributed in four completely randomized blocks. Each replicate plot had a surface area of $4 m^2$ ($2 m \times 2 m$) separated from other neighbouring plots by a pathway of 2 m. Treatments were: control C (without sludge), and SS added at moderate to excessive rates calculated in equivalent metric ton per ha per year as follows: SS-40 ($40 t ha^{-1} year^{-1}$), SS-80 ($80 t ha^{-1} year^{-1}$), and SS-120 ($120 t ha^{-1} year^{-1}$). Since 2012, sewage sludge has been yearly added during the fall season (October–November) by uniform spreading onto amended plots followed by incorporation into the topsoil (~10 cm). Control plots were hand-hoed similarly without SS addition. Outcomes described in this study represent changes in soil quality after two annual successive amendments. To this end, soil samples were collected from each replicate plot at 0–20 cm depth, composited and then stored until analysis. Throughout the experimental period, emerging weeds had regularly been removed to avoid the rhizosphere effect on soil dynamics. Consequently, changes in soil properties were exclusively influenced by sludge dose and prevailing climatic conditions.

2.2. Physico-chemical analysis

Physico-chemical properties were determined using air-dried soil samples sieved through 2 mm mesh. Soil pH and EC were measured in soil-water slurries of 1:2.5 and 1:5, respectively. Aluminium and iron oxides were analysed by X-ray fluorescence (XRF). Total organic carbon (TOC) was determined using dichromate oxidation method (Walkley & Black, 1934). Total nitrogen was analysed by the Kjeldahl method (Bremner, 1996). Extractable phosphorus was determined according to the Olsen method (Olsen et al., 1954). Exchangeable bases were extracted from the soil with ammonium acetate (1 M) and analysed by flame photometer (Pauwels et al., 1992, p. 180).

2.3. Soil structural stability

Soil structural stability was determined by the Henin and Monnier method (1956) using aggregate size fraction ≤ 2 mm. The proportions (% w/w) of stable Ag , Ag_a and Ag_b aggregates (corresponding to untreated, alcohol-treated, and benzene-treated aggregates, respectively) were calculated, and the instability index (Is) was obtained using the following equation:

$$Is = \frac{(\% < 20\mu m)_{max}}{(Ag + Ag_a + Ag_b) - 0.9 (\% C_s)}$$

where numerator indicates the largest proportion of suspended particles $< 20 \mu m$ for each soil sample, and $\%C_s$ is the largest proportion of coarse sand fraction (0.2–2 mm) forming part of the stable aggregates (Tejeda & Gonzalez, 2007).

2.4. Biomass C and N

Microbial biomass C and N (BC and BN) were estimated by the fumigation-extraction of fresh soil samples (Vance et al., 1987). To this end, a moist soil sample was divided into two portions equivalent to 10 g of oven-dry soil. One portion was fumigated for 24 h at 25 °C with ethanol-free $CHCl_3$. Following fumigant removal, the soil was extracted with 40 mL K_2SO_4 (0.5 M) by horizontal shaking for 60 min (Joergensen & Brookes, 1990). The non-fumigated portion was extracted similarly at the time fumigation had started. After organic C and N analysis in extracts, microbial biomass C or N were calculated as follows:

$$BC \text{ or } BN \text{ (mg kg}^{-1}\text{)} = E/ke$$

where E = (organic C or N extracted from fumigated soils) - (organic C or N extracted from non-fumigated soils)
 $ke = 0.45$ (Joergensen & Brookes, 1990).

2.5. Humic substances

Humic compounds in soil samples were analysed according to Shnitzer (1982) modified by Fourti et al. (2010). Accordingly, 10 g of soil were extracted with 100 mL of NaOH (0.1N) for 24 h until the calcium-containing humic compounds are exhausted. The mixture was separated by centrifugation 4000 rpm for 20 min, then sulphuric acid (2N, pH = 1) was added to the supernatant. After breather for 24 h at ambient temperature and centrifugation of 4000 rpm for 20 min, the collected supernatant represented fulvic acids (FA) and the pelleted fraction humic acids (HA).

The quality of soil organic matter was estimated using a colorimetric method described by Shnitzer (1982). As such, before the final extraction of FA and HA, absorbance of the mixture (pH 7–8) was measured at two wavelengths ($E_4 = 465$ nm; $E_6 = 665$ nm). The rate of E_4/E_6 known as the Welt ratio reflects organic matter quality and represents the humification index (Chen et al., 1977).

2.6. Magnetic susceptibility

Soil magnetic susceptibility (SMS) was measured in situ onto the surface of each replicate plot by means of a shirt-pocket size magnetic susceptibility meter (SM-20; ZH instruments, Czech Republic). This device operates at a frequency of 10 kHz and measures SMS on an average depth of 10 cm. Readings are displayed as values $\times 10^{-3}$ SI and indicate the content of ferromagnetic minerals in soil (Yoshida et al., 2003).

2.7. Statistical analysis

As previously mentioned, the experimental protocol consisted of four completely randomized blocks, each containing four treatments (C, SS-40, SS-80 and SS-120). ANOVA analysis with *post hoc* Duncan's multiple range test ($P \leq 0.05$) was used for quadruplicate mean separation (SPSS statistics 17.0, SPSS Inc., Chicago, USA). Relationships between different measured parameters were estimated with Pearson product-moment correlation coefficients ($P \leq 0.05$).

3. Results and discussion

This study aimed to examine the interaction effect of sewage sludge dose and intrinsic soil properties on soil quality under semi-arid pedo-climatic conditions. In particular, soil fertility is characterized by the influence of three soil components namely, (i) physical properties (ii), chemical properties, and (iii) biological properties (Delgado & Gómez, 2016). Accordingly, two annual successive SS applications increased soil TOC in a dose-dependent manner (Table 2). Therefore, the highest significant TOC content was observed in treatment SS-120 (1.88%) with respect to the rest of treatments and unamended soil (0.86%). Moreover, all sludge-treated soils had a soil organic matter (SOM) content greater than 2% (Table 2), a reference value considered as the highest in semi-arid Mediterranean croplands (Ryan & Pala, 2007). It has already been proven that the agricultural reuse of sewage sludge improves SOM and enriches amended soils with macro and micronutrients (Masciandro et al., 2013; Zoghlami et al., 2016; Kayikcioglu et al., 2019). This is related to the richness of urban sludge with organic carbon (18.5%) and its stability (maturity) at the time of application (C:N = 15, Table 1). In this regard, soil carbon to nitrogen ratio (C:N) is one of the most important parameters reflecting soil quality and ecological functions. For instance, Bird et al. (2002) found that this ratio was the best predictor of aggregate stability in a semiarid rangeland in New Mexico, USA. Besides, C:N reflects carbon and nitrogen cycling and nutrition balance in soils (Sun et al., 2017). In this study, C:N ratio decreased significantly with SS dose reaching the lowest value of 9.9 in treatment SS-120 as illustrated in Table 2. This value matches C:N ratios of stabilized humus (10), which allows for beneficial slow releases of bioavailable forms of nitrogen (Bengtsson et al., 2003). Consequently, increasing SS dose to 120 t ha^{-1} year $^{-1}$ created better conditions in terms of N mineralization under the described pedo-climatic conditions. In contrast, unamended control showed the highest C:N ratio (29) among treatments, which also significantly increased with respect to that calculated for the experimental soil (13.5) as illustrated in Table 1.

Table 2

Variation of soil properties after two annual successive amendments with urban sewage sludge (SS).

Treatments	C	SS-40	SS-80	SS-120
pH	8.17 ^a	8.19 ^{ab}	7.99 ^b	7.88 ^b
EC ($\mu S \text{ cm}^{-1}$)	313 ^a	480 ^{ab}	650 ^{bc}	722 ^c
TOC, %	0.86 ^a	1.21 ^{ab}	1.30 ^b	1.88 ^c
SOM, %	1.48 ^a	2.08 ^{ab}	2.24 ^b	3.23 ^c
N, %	0.04 ^a	0.09 ^b	0.12 ^b	0.19 ^c
C/N	21.5	13.4	10.8	9.9
P (mg kg^{-1})	14.77 ^a	15.54 ^b	18.19 ^c	20.02 ^d
Na ⁺ (mg kg^{-1})	48.2 ^a	55.5 ^b	63.5 ^c	75.7 ^d
Ca ²⁺ (g kg^{-1})	6.08 ^a	6.47 ^{ab}	7.01 ^b	7.14 ^b
Fe ₂ O ₃ , %	1.15 ^a	1.15 ^a	1.16 ^{ab}	1.19 ^b
Al ₂ O ₃ , %	2.52 ^a	2.51 ^a	2.51 ^a	2.56 ^b

Numbers associated to treatment names represent SS application rates in t ha^{-1} year $^{-1}$. C: unamended soil control. For each soil parameter, means with the same lowercase letters are not statistically different at $P \leq 0.05$.

Soil depletion in absence of organic amendments is in direct connection with degradation caused by “N-hunger” and the subsequent incapacity of microorganisms to mineralize organic carbon (Atkins et al., 1989).

Depending on prevailing conditions, organic matter mineralization affects directly soil physical properties (Hamdi et al., 2007; Abdollahi et al., 2014). The observed pH decrease and EC increase with sludge application rates were previously reported in a sandy soil under the same experimental conditions (Zoghlami et al., 2016). Under oxic and warm temperature environments that characterize light-textured topsoils in semi-arid regions, the aerobic biodegradation of organic matter has always been reported to be rapid (Rey et al., 2008). Part of the released CO₂ reacts with H₂O of the soil solution to form a weak acid called carbonic acid (H₂CO₃) (Hamdi et al., 2007). The latter will release H⁺ protons by double dissociation causing gradual soil pH decrease over time (Stevenson, 1994, p. 496). Despite the slight dose-dependent decrease of soil pH in the current study, values remained within neutral range (7.88–8.17) as shown in Table 2. This indicates that SS-amended soils were still able to buffer against acidification resulting from TOC transformation and cycling over two years (Bolan et al., 2005; Hajnos, 2011). In addition, it is likely that the prevailing semi-arid conditions of the region did not allow for maintaining adequate soil moisture that accelerates the formation of H₂CO₃. In fact, particularly low and irregular pluviometry of 263 and 370 mm was respectively recorded during the two years of study.

After two successive SS amendments, soil salinity increased significantly with application rates as reflected by the variation of EC and Na⁺ (Table 2). However, salinization did not occur since EC values and exchangeable Na⁺ concentrations remained low enough to cause substantial soil degradation even for the highest sludge dose of 120 t ha⁻¹ (722 μS cm⁻¹ and 76 mg kg⁻¹, respectively) as compared to control (313 μS cm⁻¹ and 48 mg kg⁻¹, respectively) (Yan & Marschner, 2013). In addition, no visible signs of saline/sodic soils were ever observed on the surface of all SS-treated plots throughout the experimental period (Choudhary & Kharche, 2015). This was also evidenced by the consistent emergence of same weed species in both unamended and amended soils testifying to the absence of any salinity-induced phytotoxicity caused by sludge addition (Wu et al., 2015). It is likely that the joint effect of rainfall and soil permeability could have resulted in the partial leaching of accumulated salts, which reduce the extent of soil salinization as well.

Soil instability index (Is) is another important physical

parameter that reflects the relative state of aggregate water stability. This index has extensively been used for assessing changes in soil structural stability after organic amendments (Dimoyiannis et al., 1998; Tejada & Gonzalez, 2007). Fig. 1 illustrates the variation of log₁₀(Is) with soil treatments after two annual successive SS applications. There was a significant dose-dependent amelioration of soil structure reflected by substantial decreases of instability index with respect to unamended control. Improvement rates were +13.3%, +28.8% and +59.4% for SS-40, SS-80 and SS-120, respectively. This was further highlighted by a significant correlation between Is and TOC content ($r = -0.89$) as indicated in Table 3. García-Orenes et al. (2005) reported that successive biosolids amendments significantly improved the aggregate stability percentage. Under comparable dryland conditions, Tejada and Gonzalez (2007) observed also a structural stability improvement by 9% in soils treated for two years with SS at 25.6 t ha⁻¹ year⁻¹. In general, enriching agricultural soils with organic matter affects soil mineralogy and particle-size distribution, resulting in soil cementing by flocculating particles to form stable aggregates (Spaccini et al., 2004; Tejada & Gonzalez, 2007; Abdollahi et al., 2014; Shahbaz et al., 2017). As revealed before, the dose-dependent improvement of structural stability (Fig. 1) was also confirmed by the absence of signs of clay and/or organic matter dispersion in situ as well as by pH values consistently below the alkalinity range (<8.5) (Choudhary & Kharche, 2015).

In addition to organic matter effect, soil aggregation occurs also in presence of aluminium or iron oxides, colloidal silica or calcium carbonate (Braver et al., 1972, p. 498; Igwe et al., 2013). Several

Table 3
Pearson product-moment correlation coefficients (r) of soil parameters.

	Is	E ₄ /E ₆	BN	BC	SMS	TOC	Ca ²⁺	Fe ₂ O ₃	Al ₂ O ₃
Is	-	<i>-0.99</i>	<i>-0.89</i>	<i>-0.99</i>	<i>-0.96</i>	<i>-0.89</i>	<i>-0.98</i>	0.78	0.51
E ₄ /E ₆		-	0.94	0.99	0.97	0.94	0.93	0.96	0.78
BN			-	0.92	0.88	0.99	0.87	0.85	0.67
BC				-	0.96	0.91	0.91	0.97	0.80
SMS					-	0.83	0.99	0.86	0.61
TOC						-	0.75	0.99	0.94
Ca ²⁺							-	0.79	0.49
Fe ₂ O ₃								-	0.92
Al ₂ O ₃									-

Italic correlation coefficients are significant at $P \leq 0.05$. Is: Soil instability index; E₄/E₆: Welt ratio; BN: Biomass nitrogen; BC: Biomass carbon; SMS: Soil magnetic susceptibility; TOC: Total organic carbon.

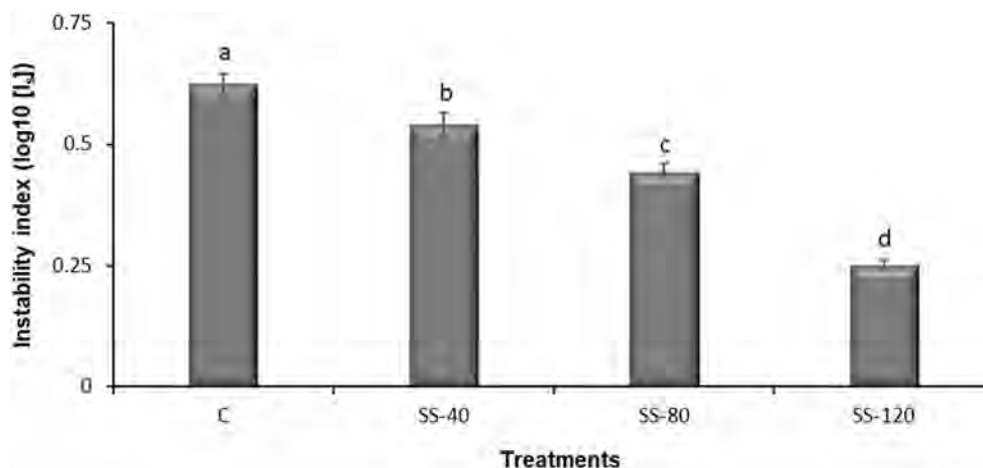


Fig. 1. Variation of soil instability index (Is) with soil treatments after two annual successive amendments with urban sewage sludge (SS). Numbers associated to treatment names represent sludge application rates in t ha⁻¹ year⁻¹. C: unamended soil control. Means with the same lowercase letters are not statistically different at $P \leq 0.05$.

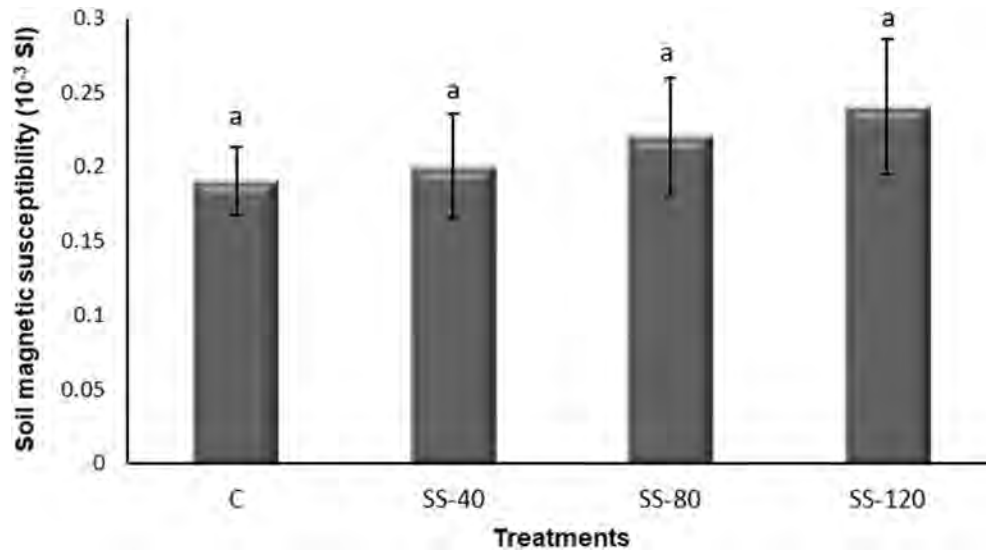


Fig. 2. Variation of soil magnetic susceptibility (SMS) with soil treatments after two annual successive amendments with urban sewage sludge (SS). Numbers associated to treatment names represent sludge application rates in $t\ ha^{-1}\ year^{-1}$. C: unamended soil control. Means with the same lowercase letters are not statistically different at $P \leq 0.05$.

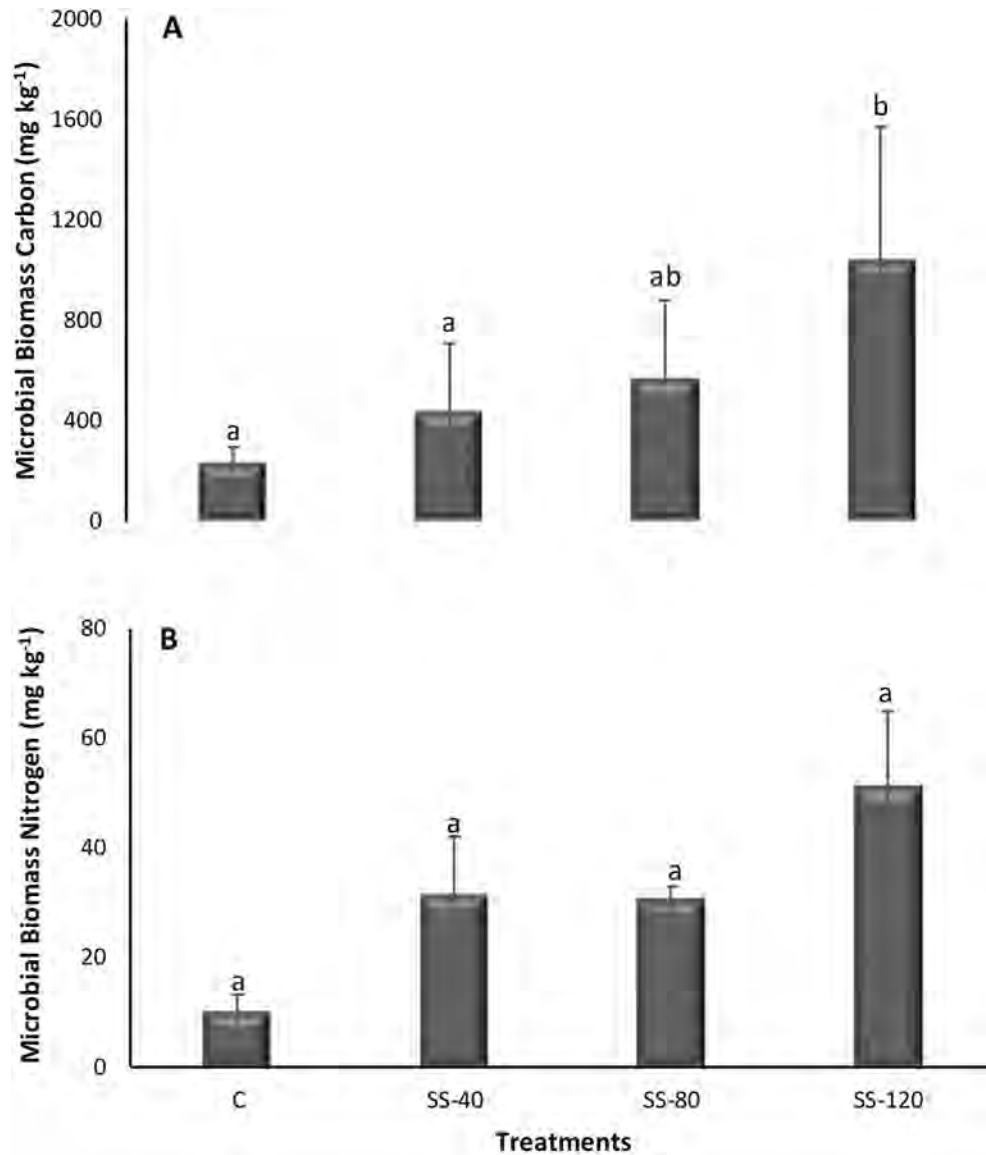


Fig. 3. Variation of microbial biomass carbon (A) and nitrogen (B) with soil treatments after two annual successive amendments with urban sewage sludge (SS). Numbers associated to treatment names represent sludge application rates in $t\ ha^{-1}\ year^{-1}$. C: unamended soil control. Means with the same lowercase letters are not statistically different at $P \leq 0.05$.

studies have highlighted the cation “bridging” effect of calcium between polycarboxylic molecules (humic acids) and clays, which results in additional soil aggregate stability (Muneer & Oades, 1989; Wuddivira & Camps-Roach, 2007). Interestingly, the current sludge had a substantial CaCO_3 content (11.8%) that caused a significant dose-dependent accumulation of calcium ions in amended soils, reaching 7.14 g kg^{-1} in SS-120 as compared to 6.1 g kg^{-1} in control soil (Table 2). The contribution of SS to Ca^{2+} accumulation in soil was also evidenced by significant correlation with TOC as illustrated in Table 3 ($r = 0.75$). On the other hand, an increase of soil magnetic susceptibility with SS rate was measured in situ (Fig. 2), showing strong correlations to TOC content and instability index (0.83 and -0.96 , respectively) (Table 3). SMS reflects the presence of ferrimagnetic minerals in soil and is correlated to magnetite $\beta\text{-Fe}_3\text{O}_4$ and maghemite $\gamma\text{-Fe}_2\text{O}_3$ (Ramos et al., 2017; Yoshida et al., 2003). Consequently, the richness of SS in Fe_2O_3 (Table 1) was likely to further improve soil aggregation in a dose-dependent manner as well (Table 2). As compared to our findings (Tables 2 and 3), Sokolowska et al. (2016) observed also a linear relationship ($r = 0.76$) between SMS and Al_2O_3 content in soil after irrigation with wastewater. Goldberg (1989) explained the stabilizing role of iron and aluminium oxides in soil by decreasing critical coagulation concentration, clay dispersion and modulus of rupture; and by increasing micro-aggregation and hydraulic conductivity. These oxides precipitate on clay surfaces and play the role of stable coatings at high pH levels. The lowest SMS and structural stability in control treatment are indicators of degradation trends in absence of organic matter input under the current experimental conditions.

The microbiological assessment of agricultural soils is also important for quality monitoring (Wall et al., 2019). In this study, microbial biomass carbon and nitrogen increased as function of SS addition rates (Fig. 3). More precisely, BC (Fig. 3A) and BN (Fig. 3B) increased by almost five-fold in SS-120 treatment comparing to unamended control. This shows that excessive SS rates had no detrimental effects on the proliferation of biomass C and N (Fernandes et al., 2005). In general, the addition of biowastes provides exogenous microorganisms to soil and stimulates indigenous populations simultaneously, which increases aggregate formation and stabilization (Annabi et al., 2007). This contribution to

structural stability is due to the production of microbial mucilage that act as soil binding agents (Caesar-Tonthat, 2002; Six et al., 2004; Tejada & Gonzalez, 2007). On the other hand, 1–5% of total soil organic matter is represented by microbial biomass, which is a more sensitive indicator of changing soil conditions than direct analysis of organic carbon (Leita et al., 1999). Soil BC/TOC ratio, or microbial quotient, has widely been used as an indicator for future changes in organic matter due to alterations of soil conditions (Leita et al., 1999; Yang et al., 2010). This ratio is also used for comparison of soil quality across soils with different organic matter contents (Joergensen & Scheu, 1999). In other words, the microbial quotient is interpreted as substrate available and the portion of total soil carbon immobilized in microbial cells (Yang et al., 2010). In this study, TOC and BC were significantly correlated ($r = 0.91$) as shown in Table 3. Calculated BC/TOC ratios increased significantly with SS dose reaching 1.04%, 2.12%, 4.32% and 5.48% for control, SS-40, SS-80 and SS-120, respectively. This increase confirms the consistent dose-dependent improvement of soil quality with respect to unamended control under the described pedo-climatic conditions (Leita et al., 1999; Powlson, 1994; Zoghalmi et al., 2016).

The quality of soil organic matter could be evaluated by determining the Welt ratio as well (Stevenson, 1994, p. 496), which is calculated to characterize soil HA and FA. Similar to BC/TOC, we observed a significant increase of E_4/E_6 ratio with sludge dose after two successive annual amendments (Fig. 4). As such, E_4/E_6 ratio passed from 1.45 in control to 3.48 in SS-120 implying significant correlation to TOC build up in soil as indicated in Table 3 ($r = 0.94$). Welt ratio is the parameter indicative of decomposition status and molecular size of soil organic matter. It mirrors the carbon fraction associated with humic acids in soil, which represent the major forms of stabilized carbon (Angelova et al., 2013; Zhao et al., 2013). According to Hevia et al. (2003), E_4/E_6 quotients lower than 5 indicate that humic rather than fulvic acids exist in the organic fraction of soils. This corresponds to ratios observed in all SS-amended soils (Fig. 4), which implies higher humus polymerization degree that favours organic matter adsorption onto the mineral matrix of the soil (Liu et al., 2015). This adsorption implicates a strong complexation between soil minerals and organic acid ligands especially those associated with aromatic structures

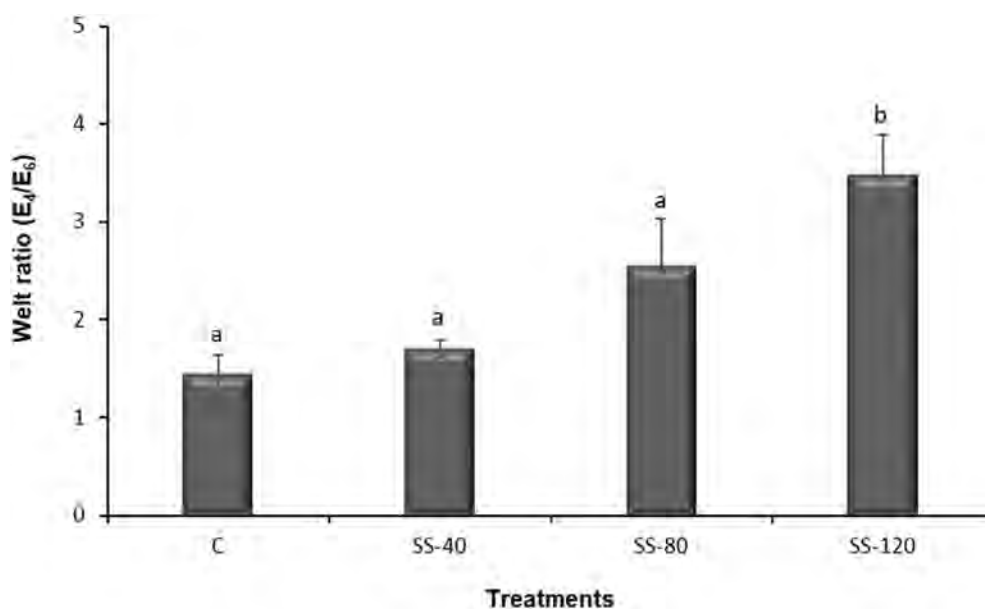


Fig. 4. Variation of the Welt ratio (E_4/E_6) with soil treatments after two annual successive amendments with urban sewage sludge (SS). Numbers associated to treatment names represent sludge application rates in $\text{t ha}^{-1} \text{ year}^{-1}$. C: unamended soil control. Means with the same lowercase letters are not statistically different at $P \leq 0.05$.

(Verchot et al., 2011). In this study, the strong negative correlation between the Welt ratio and soil instability index ($r = -0.99$) evidences the beneficial effect of humic acids on soil structural stability through their contribution to the formation of clay-humic complexes, which prevents soil degradation (Wang and Xing, 2005). The lowest E_4/E_6 value calculated for unamended soil indicates that its small “aged” organic fraction has a higher degree of humification than the fresh one added with sludge.

4. Conclusions

The current field study investigated the quality of a semi-arid agricultural soil treated twice with increasing sludge amounts. Under the described pedo-climatic conditions, this practice resulted in a significant dose-dependent variation of all studied parameters. Overall, organic matter accumulation and its subsequent mineralization over two years improved soil structural stability in proportion to sludge dose. In this regard, soil magnetic susceptibility could be an interesting parameter in situ that correlates with soil quality. From a pure pedological point of view, excessive sludge rates of $120 \text{ t ha}^{-1} \text{ year}^{-1}$ did improve soil structure and fertility without causing physical degradation. By conducting the field trials in absence of rhizosphere effect, we could highlight the intrinsic capacity of the agricultural soil in mitigating possible negative effects of sludge reuse.

Acknowledgments

This study was financially supported by a research grant from the Tunisian Ministry of Higher Education and Scientific Research. The authors would like to thank the National Sanitation Utility (ONAS) for providing urban sewage sludge. The technical support of Rym Ghrib is hereby acknowledged.

References

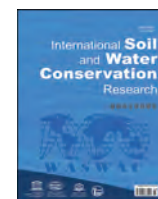
- Abdollahi, L., Schjøning, P., Elmholt, S., & Munkholm, L. J. (2014). The effects of organic matter application and intensive tillage and traffic on soil structure formation and stability. *Soil and Tillage Research*, 36, 28–37.
- Adediran, J. A., De Baets, N., Mkeni, P. N. S., Kiekens, L., Muyima, N. Y. O., & Thys, A. (2003). Organic waste materials for soil fertility improvement in the border region of the Eastern Cape, South Africa. *Biological Agriculture & Horticulture*, 20, 283–300.
- Angelova, V. R., Akova, V. I., Artinova, N. S., & Ivanov, K. I. (2013). The effect of organic amendments on soil chemical characteristics. *Bulg. J. Agric. Sci.*, 19, 958–971.
- Annabi, M., Houot, S., Francou, C., Poiraud, M., & Le Bissonnais, Y. (2007). Soil aggregate stability improvement with urban composts of different maturities. *Soil Science Society of America Journal*, 71, 413–423.
- Atkins, C. A., Pate, J. S., Sanford, P. J., Dakora, F. D., & Mathews, I. (1989). Nitrogen nutrition of nodules in relation to ‘N-hunger’ in cowpea (*Vigna unguiculata* L. Walp). *Plant Physiology*, 90, 1644–1649.
- Bengtsson, G., Bengtson, P., & Månsson, K. F. (2003). Gross nitrogen mineralization-, immobilization-, and nitrification rates as a function of soil C/N ratio and microbial activity. *Soil Biology and Biochemistry*, 35, 143–154.
- Bird, S. B., Herrick, J. E., Wander, M. M., & Wright, S. F. (2002). Spatial heterogeneity of aggregate stability and soil carbon in semi-arid rangeland. *Environment and Pollution*, 116, 445–455.
- Bolan, N. S., Curtin, D., & Adriano, D. C. (2005). Acidity. In D. Hillel (Ed.), *Encyclopedia of soils in the environment* (pp. 11–17). New York, NY, USA: Columbia University.
- Braver, L. D., Gardner, W. H., & Gardner, W. R. (1972). *Soil physics* (p. 498). New Delhi: Wiley Eastern Limited.
- Bremner, J. M. (1996). Nitrogen total. In D. L. Sparks (Ed.), *Methods of soil analysis Part 3: Chemical methods, SSSA book series 5* (pp. 1085–1122). Madison, Wisconsin, USA: Soil Science Society of America.
- Caesar-Tonthat, T. C. (2002). Soil binding properties of mucilage produced by a basidiomycete fungus in a model system. *Mycological Research*, 106, 930–937.
- Chen, Y., Senesi, N., & Schnitzer, M. (1977). Information provided on humic substances by E_4/E_6 ratios. *Soil Science Society of America Journal*, 41, 352–358.
- Choudhary, O. P., & Kharche, V. K. (2015). Soil salinity and sodicity. In *Soil science: An introduction (chapter 12)* (pp. 353–384). Indian Society of Soil Science.
- Delgado, A., & Gómez, J. A. (2016). The soil. Physical, chemical and biological properties. Chapter 2. In F. J. Villalobos, & E. Fereres (Eds.), *Principles of agronomy for sustainable agriculture* (p. 555).
- Delibacac, S., & Ongun, A. I. (2016). Influence of treated sewage sludge applications on corn and second crop wheat yield and some properties of sandy clay soil. *Turk. J. Field Crops*, 21, 1–9.
- Dimoyiannis, D., Tsadilas, C. D., & Valmis, S. (1998). Factors affecting aggregate instability of Greek agricultural soils. *Communications in Soil Science and Plant Analysis*, 29, 1239–1251.
- Eid, E. M., Alrumman, S. A., El-Bebany, A. F., Fawy, K. F., Taher, M. A., Hesham, A. L., El-Shaboury, G., & Ahmed, M. T. (2018). The evaluation of sewage sludge application as a fertilizer for broad bean (*Faba sativa* Bernh.) crops. *Food Energy Secur.*, 7, Article e00142.
- Fernandes, S. A. P., Bettiol, W., & Cerri, C. C. (2005). Effect of sewage sludge on microbial biomass, basal respiration, metabolic quotient and soil enzymatic activity. *Applied Soil Ecology*, 30, 65–77.
- Fourti, O., Jedidi, N., & Hassen, A. (2010). Humic substances change during the co-composting process of municipal solid wastes and sewage sludge. *World Journal of Microbiology and Biotechnology*, 26, 2117–2122.
- Fytilli, D., & Zabanitoulou, A. (2008). Utilization of sewage sludge in EU application of old and new methods - a review. *Renewable and Sustainable Energy Reviews*, 12, 116–140.
- García-Orenes, F., Guerrero, C., Mataix-Solera, J., Navarro-Pedreño, J., Gómez, I., & Mataix-Beneyto, J. (2005). Factors controlling the aggregate stability and bulk density in two different degraded soils amended with biosolids. *Soil and Tillage Research*, 82, 65–76.
- Gibbs, H. K., & Salmon, J. M. (2015). Mapping the world’s degraded lands. *Applied Geography*, 57, 12–21.
- Goldberg, S. (1989). Interaction of aluminium and iron oxides and clay minerals and their effect on soil physical properties: A review. *Communications in Soil Science and Plant Analysis*, 20, 1181–1207.
- Hajnos, M. (2011). Buffer capacity of soils. In J. Gliński, J. Horabik, & J. Lipiec (Eds.), *Encyclopedia of agrophysics* (pp. 94–95). Netherlands: Publishing Springer.
- Hamdi, H., Benzarti, S., Manusadzian, L., Aoyama, I., & Jedidi, N. (2007). Solid-phase bioassays and soil microbial activities to evaluate PAH-spiked soil ecotoxicity after a long-term bioremediation process simulating landfarming. *Chemosphere*, 70, 135–143.
- Henin, S., & Monnier, G. (1956). *Evaluation de la Stabilité de la Structure du* (pp. 49–52). Paris, France: Sol. 4^{ème} Sciences du Sol.
- Hévia, G. G., Buschiazzo, D. E., Hepper, E. N., Urioste, A. M., & Antón, E. L. (2003). Organic matter in size fractions of soils of the semiarid Argentina. Effects of climate, soil texture and management. *Geoderma*, 116, 265–277.
- Igwe, C. A., Zarei, M., & Stahr, K. (2013). Stability of aggregates of some weathered soils in south-eastern Nigeria in relation to their geochemical properties. *J. Earth Syst. Sci.*, 122, 1283–1294.
- Janzen, H. H. (2004). Carbon cycling in earth systems. *Agriculture, Ecosystems & Environment*, 104, 397–417.
- Joergensen, R., & Brookes, P. (1990). N-hydrin-reactive nitrogen measurements of microbial biomass in 0.5 M K_2SO_4 soil extracts. *Soil Biology and Biochemistry*, 22, 1023–1027.
- Joergensen, R. G., & Scheu, S. (1999). Depth gradients of microbial and chemical properties in moder soils under beech and spruce. *Pedobiologia*, 43, 134–144.
- Kayikcioglu, H. H., Yener, H., Ongun, A. R., & Okur, B. (2019). Evaluation of soil and plant health associated with successive three-year sewage sludge field applications under semi-arid biodegradation condition. *Archives of Agronomy and Soil Science*, 65, 1659–1676.
- Kobierski, M., Kondratowicz-Maciejewska, K., Banach-Szott, M., Wojewódzki, P., & Peñas Castejón, J. M. (2018). Humic substances and aggregate stability in rhizospheric and non-rhizospheric soil. *Journal of Soils and Sediments*, 18, 2777–2789.
- Lal, R. (2009). Sequestering carbon in soils of arid ecosystems. *Land Degradation & Development*, 20, 441–454.
- Leita, L., De Nobili, M., Mondini, C., Muhlbachova, G., Marchiol, L., Bragato, G., & Contin, M. (1999). Influence of inorganic and organic fertilization on soil microbial biomass, metabolic quotient and heavy metal bioavailability. *Biology and Fertility of Soils*, 28, 371–376.
- Liu, W. L., Ma, L., Wu, J. G., & Liang, Y. J. (2015). Contents and elemental composition of various humus components in orchard soils according to different cultivation years in the northern China. In Scholz (Ed.), *Water resources and environment* (pp. 395–402). CRC Press, Taylor and Francis Group.
- Lu, Q., He, Z. L., & Stoffella, P. J. (2012). Land application of biosolids in the USA: A review. *Appl. Environ. Soil Sci.* <https://doi.org/10.1155/2012/201462>
- Masciandaro, G., Macci, C., Peruzzi, E., Ceccanti, B., & Doni, S. (2013). Organic matter-microorganism-plant in soil bioremediation: A synergic approach. *Reviews in Environmental Science and Biotechnology*, 12, 399–419.
- Muneeb, M., & Oades, J. M. (1989). The role of Ca-organic interactions in soil aggregate stability. III. Mechanisms and models. *Soil Research*, 27, 411–423.
- Odeh, I. O. A., & Onus, A. (2008). Spatial analysis of soil salinity and soil structural stability in a semiarid region of New South Wales, Australia. *Environmental Management*, 42, 265. <https://doi.org/10.1007/s00267-008-9100-z>
- Olsen, S. R., Cole, C. V., Watanabe, F. S., & Dean, L. A. (1954). In A. D. Banderis, D. H. Barter, K. A. Anderson, & Advisor (Eds.), *Estimation of available phosphorus in soils by extraction with sodium bicarbonate*. U.S. Department of agriculture. Circular No. 939.
- Pauwels, J., Van Ranst, E., Verloo, M., & Mvondo Ze, A. (1992). *Manuel de Laboratoire de Pédologie - Méthodes d’analyses de sols et de plantes; Equipment et gestion des stocks de verrerie et de produits chimiques* (p. 180). Brussels, Belgium: A.G.C.D. Publications Agricoles No. 28.

- Powlson, D. S. (1994). The soil microbial biomass: Before, beyond and back. In K. Ritz, J. Dighton, & K. E. Giller (Eds.), *Beyond the biomass* (pp. 3–20). Chichester: Wiley.
- Ramos, P. V., Dalmolin, R. S. D., Marques Júnior, J., Siqueira, D. S., Almeida, J. A., & Moura-Bueno, J. M. (2017). Magnetic susceptibility of soil to differentiate soil environments in southern Brazil. *Rev Bras Cienc Solo*, 41, Article e0160189.
- Rey, A., Pegoraro, E., & Jarvis, P. G. (2008). Carbon mineralization rates at different soil depths across a network of European forest sites (FORCAST). *European Journal of Soil Science*, 59, 1049–1062.
- Ryan, J., & Pala, M. (2007). Syria's long-term rotation and tillage trials: Potential relevance to carbon sequestration in central Asia. In R. Lal, M. Suleimenov, B. A. Stewart, D. O. Hansen, & M. P. Doraiswamy (Eds.), *Climate change and terrestrial carbon sequestration in central Asia rotation* (pp. 223–234). London, UK: Taylor & Francis Group.
- Shahbaz, M., Kuzyakov, Y., & Heitkamp, F. (2017). Decrease of soil organic matter stabilization with increasing inputs: Mechanisms and controls. *Geoderma*, 304, 76–82.
- Shnitzer, M. (1982). Organic matter characterization. In *Methods of soil analysis. Part 2. Chemical and microbiological properties-agronomy*. Madison, USA. Monograph No. 9.
- Siebielec, G., Siebielec, S., & Lipski, D. (2018). Long-term impact of sewage sludge, digestate and mineral fertilizers on plant yield and soil biological activity. *Journal of Cleaner Production*, 187, 372–379.
- Singh, R. P., & Agrawal, M. (2008). Potential benefits and risks of land application of sewage sludge. *Waste management*, 28, 347–358.
- Six, J., Bossuyt, H., Degryze, S., & Deneef, K. (2004). A history of research on the link between (micro) aggregates, soil biota, and soil organic matter dynamics. *Soil and Tillage Research*, 79, 7–31.
- Sokolowska, Z., Alekseev, A., Skic, K., & Brzezinska, M. (2016). Impact of wastewater application on magnetic susceptibility in Terric Histosol soil. *International Agrophysics*, 30, 89–94.
- Spaccini, R., Mbagwu, J. S. C., Igwe, C. A., Conte, P., & Piccolo, A. (2004). Carbohydrates and aggregation in lowland soils of Nigeria as influenced by organic inputs. *Soil and Tillage Research*, 75, 161–172.
- Stevenson, F. J. (1994). *Humus chemistry: Genesis, composition, reactions* (2nd ed., p. 496). New York, USA: John Wiley and Sons.
- Sun, G., Li, W., Zhu, C., & Chan, Y. (2017). Spatial variability of soil carbon to nitrogen ratio and its driving factors in Ili River valley, Xinjiang, Northwest China. *Chinese Geographical Science*, 27, 529–538.
- Tejeda, M., & Gonzalez, J. L. (2007). Application of different organic wastes on soil properties and wheat yield. *Agronomy Journal*, 99, 1597–1606.
- Vance, E. D., Brookes, P. C., & Jenkinson, D. S. (1987). An extraction method for measuring soil microbial biomass C. *Soil Biology and Biochemistry*, 19, 703–707.
- Verchot, L. V., Dutaur, L., Shepherd, K. D., & Albrecht, A. (2011). Organic matter stabilization in soil aggregates: Understanding the biogeochemical mechanisms that determine the fate of carbon inputs in soils. *Geoderma*, 161, 182–193.
- Walkley, A., & Black, I. A. (1934). An examination of the Degtjareff method for determining soil organic matter, and a proposed modification of the chromic acid titration method. *Soil Science*, 37, 29–38.
- Wall, L. G., Gabbarini, L. A., Ferrari, A. E., Frene, J. P., Covelli, J., Reyna, D., & Robledo, N. B. (2019). Changes of paradigms in agriculture soil microbiology and new challenges in microbial ecology. *Acta Oecologica*, 95, 68–73.
- Wang, K., & Xing, B. (2015). Structural and sorption characteristics of adsorbed humic acid on clay minerals. *Journal of Environmental Quality*, 34, 342–349.
- Wuddivira, M. N., & Camps-Roach, G. (2007). Effects of organic matter and calcium on soil structural stability. *European Journal of Soil Science*, 58, 722–727.
- Wu, G. Q., Jiao, Q., & Shui, Q. Z. (2015). Effect of salinity on seed germination, seedling growth, and inorganic and organic solutes accumulation in sunflower (*Helianthus annuus* L.). *Plant Soil and Environment*, 5, 220–226.
- Yang, K., Zhu, J., Zhang, M., Yan, Q., & Sun, O. J. (2010). Soil microbial biomass carbon and nitrogen in forest ecosystems of northeast China: A comparison between natural secondary forest and larch plantation. *Journal of Plant Ecology*, 3, 175–182.
- Yan, N., & Marschner, P. (2013). Response of soil respiration and microbial biomass to changing EC in saline soils. *Soil Biology and Biochemistry*, 65, 322–328.
- Yoshida, M., Jedidi, N., Hamdi, H., & Ayari, F. (2003). Magnetic susceptibility variation of MSW compost-amended soils: *In situ* method for monitoring heavy metal contamination. *Waste Management & Research*, 21, 155–160.
- Zhao, A., Zhang, M., & He, Z. (2013). Spectroscopic characteristics and biodegradability of cold and hot water extractable soil organic matter under different land uses in subarctic Alaska. *Communications in Soil Science and Plant Analysis*, 44, 3030–3048.
- Zoghlami, R. I., Hamdi, H., Mokni-Tlili, S., Khelil, M. N., Ben Aissa, N., & Jedidi, N. (2016). Changes in light-textured soil parameters following two successive annual amendments with urban sewage sludge. *Ecological Engineering*, 95, 604–611.



Contents lists available at ScienceDirect

International Soil and Water Conservation Research

journal homepage: www.elsevier.com/locate/iswcr

Original Research Article

Spatial distribution of water and wind erosion and their influence on the soil quality at the agropastoral ecotone of North China

Yanzai Wang^c, Yifan Dong^{a,*}, Zhengan Su^b, Simon M. Mudd^d, QiuHong Zheng^e, Gang Hu^f, Dong Yan^g^a Institute of International Rivers and Eco-Security, Yunnan University, Kunming, 650091, PR China^b Key Laboratory of Mountain Hazards & Surface Process, Institute of Mountain Hazards and Environment, Chinese Academy of Sciences, Chengdu, 610041, PR China^c College of Geography and Tourism, Chongqing Normal University, Chongqing, 401331, PR China^d School of GeoSciences, University of Edinburgh, Edinburgh, EH8 9XP, UK^e China Meteorological Administration Training Center, CMA, Beijing, 100081, PR China^f School of Tourism and Geography Sciences, Qingdao, 266071, Shandong, PR China^g National Institute for Radiological Protection, Chinese Center for Disease Control and Prevention, Beijing, 100088, PR China

ARTICLE INFO

Article history:

Received 29 July 2019

Received in revised form

10 April 2020

Accepted 6 May 2020

Available online 18 May 2020

Keywords:

Soil erosion

Soil quality

Spatial distribution

Agropastoral ecotone

a b s t r a c t :

In semiarid regions, wind and water erosion are serious environmental and ecological problems around world. They have different impacts on soil quality over a range of spatial scales. Analyzing the spatial distribution of soil erosion and understanding the impacts of wind and water erosion on soil quality at the regional scale is vital for mitigating soil erosion risk. In this study we explore the spatial distributions of water and wind erosion around Zhangjiakou city which suffers both water and wind erosion contemporaneously, and detect the influence of soil erosion on soil quality. We find that annual wind erosion intensities range 4.99–10.05 t ha⁻¹ yr⁻¹, and annual water erosion intensities range 2.92–4.14 t ha⁻¹ yr⁻¹. Areas with higher potential wind and total erosion risk occur mainly in northwest and southeast Zhangjiakou city, whereas potential water erosion risk is highest in the southwest and central regions. The highest erosion rates are concentrated in gentle parts of the landscape, where agriculture has led to low vegetation cover. Steeper portions of the landscape, which remain forested, have lower erosion rates. These spatial patterns are dominated by higher wind erosion, which correlates with surface soil coarsening and higher water infiltration, whereas the soil water holding capacity decreases with increasing wind erosion rates. In regions with high water infiltration rates, we find the intensity of water erosion weakened. To mitigate risks of soil degradation, suitable erosion measures should be implemented according to the dominant erosion type, which varies in space.

© 2020 International Research and Training Center on Erosion and Sedimentation and China Water and Power Press. Production and Hosting by Elsevier B.V. This is an open access article under the CC BY-NC-ND license (<http://creativecommons.org/licenses/by-nc-nd/4.0/>).

1. Introduction

Accelerated soil erosion has numerous environmental and ecological effects. Where soil erosion occurs, it leads to deterioration of soil health because it degrades soil quality and disrupts both mechanical and chemical processes in the soil (Lal, 2001). Eroded soil can result in sedimentation of reservoirs and waterways, non-point source pollution, emission of greenhouse gases and a decline in the quality of both water and air (Lal, 2018; Shi, Yan, Yuan, &

Nearing, 2004).

Soil and nutrient losses are dominated by water and wind erosion (e.g., Tuo, Xu, & Gao, 2018). In semiarid regions, wind and water erosion may occur contemporaneously (Du, Dou, Deng, Xue, & Wang, 2016; Tuo, Xu, Zhao, & Gao, 2015; Van Pelt et al., 2017; Visser, Sterk, & Ribolzi, 2004; Zhang et al., 2011b). Visser et al. (2004) argued that to better understand the impact of wind and rainfall on soil degradation in semi-arid areas, processes should be studied simultaneously. Despite the potential importance of mechanisms of erosion in dryland environments, limited studies have quantified the absolute and relative magnitudes of wind and water erosion at the same site over the same time period

* Corresponding author.

E-mail address: yifan@ynu.edu.cn (Y. Dong).

(Breshears, Whicker, Johansen, & Pinder, 2003). Tuo et al. (2015) argued that effective mitigation of erosion risk requires controls of water and wind erosion because the two mechanisms amplify each other. A key factor in the effectiveness of these measures is coeval assessment of wind and water erosion.

To understand appropriate mitigation strategies for soil erosion, one must determine the relative influence of water and wind, which varies between regions. Soil erosion is a scale-dependent phenomenon, the small-scale and large-scale effects on the soil quality can vary widely (Berhe, Barnes, Six, & Marín-Spiotta, 2018; Lal, 2001). Zhang et al. (2011b) reported that the soil erosion rate caused by the combined effects of water and wind in southern Arizona was $7.60 \text{ t ha}^{-1} \text{ yr}^{-1}$, although wind was responsible for only $0.08 \text{ t ha}^{-1} \text{ yr}^{-1}$. Van Pelt et al. (2017) reported that wind erosion was responsible for about 75% of the total soil loss in semiarid regions of the USA. Tuo et al. (2018) recently reported the contributions of water and wind erosion in Chinese Loess Plateau were different on slopes with different aspect, different gradient, and different soil physical and chemical properties. These variations also modulated the total soil erosion.

As for the impact of soil erosion on soil nutrients, Visser, Stroosnijder, and Chardon (2005) observed that nutrient losses by water erosion were small compared with those by wind erosion in the Sahelian zone of West-Africa. This small contribution, however, could have serious impacts to soil health because nutrients lost by water were permanently transported away from the area. In addition, Visser et al. (2005) found that sediment transport by wind in which grains were saltating resulted in the largest soil and nutrient loss on the event timescale. Subsequently, Visser and Sterk (2007) found that water and wind erosion had different impacts on nutrient losses when looking at different spatial scales: the nutrient losses caused by soil erosion at the village scale were considerably smaller than at the plot scale. However, the impacts of water and wind erosion on soil nutrients at the regional scale, and how the water and wind erosion affected other soil qualities such as soil texture have not been reported in past studies.

Numerous studies have documented the soil erosion risk in semiarid China (Fu et al., 2011; Shi et al., 2004; Wei, Chen, Fu, Lü, & Gong, 2009). These authors predominantly studied wind and water erosion as two separate processes. Meanwhile, most studies featuring combined assessments of water and wind erosion in China have focused on the Loess Plateau and Inner Mongolia (Du et al., 2016; Jiang, Zhang, Zhang, & Wang, 2019; Tuo et al., 2015, 2018), due to the regions' importance for agricultural production. However, the semiarid regions north of Beijing, of which the Zhangjiakou city area is one, have received little attention. Zhangjiakou city sits at the boundary of Inner Mongolia, which experiences severe wind erosion region (Zhang et al., 2018), and the Loess Plateau, which experiences severe water erosion (Fu et al., 2011). We anticipate strong spatial variations in the relative magnitude of these two erosion mechanisms around Zhangjiakou city, making it an ideal site to explore the relative impacts of water and wind erosion. In addition, the expected intensive land use changes associated with the 2022 Olympic Games means it is imperative to assess the soil erosion potential risk and discuss its influence on the regional environment (Cyranoski, 2015.; Liu et al., 2018; Song et al., 2018).

Zhang, Yang, Pan, and Zhang (2011a) have calculated the wind erosion rate of farm land in the north region of Zhangjiakou city using the ^{137}Cs tracer technique, and calculated an average rate of $89.5 \text{ t ha}^{-1} \text{ yr}^{-1}$. However, Zhang, Zhang, Chang, Wang, and Liu (2017) recently reported that the wind erosion rate of farm land in the same area was lower, from $40.1 \text{ t ha}^{-1} \text{ yr}^{-1}$ to $47.9 \text{ t ha}^{-1} \text{ yr}^{-1}$ using SWEEP model (Zhang et al., 2017). In general, these assessments of wind erosion did not cover the whole area of Zhangjiakou

city. Meanwhile, water erosion in Zhangjiakou city has not been reported previously. Furthermore, Zhang et al. (2011a) found that surface soils of farmland in Zhangjiakou city became coarser because of wind erosion, the proportion of sand particles larger than 0.05 mm exceeded 67% in the plough layer and higher than that in grasslands. However, the impact of soil erosion in Zhangjiakou city on other soil quality parameters such as soil nutrients (e.g., organic carbon and nitrogen) was not quantified, even though these parameters would affect the soil nutrient availability and ecosystem's provisioning service (Bilotta, Grove, & Mudd, 2012).

In this study, we use soil erosion models and ^{137}Cs inventories to estimate annual water and wind erosion intensity and long-term soil erosion, respectively. We also detect the influence of soil erosion on soil quality such as soil grain size, soil hydraulic and soil nutrient indices in Zhangjiakou city. The objectives of this study are (a) to explore the spatial distribution of water and wind erosion intensity in Zhangjiakou city, and quantify the contributions to total erosion over the whole study area; (b) to reveal the influences of soil erosion on various parameters of soil quality on regional scales.

2. Materials and methods

2.1. Study area

Zhangjiakou city is a prefectural level city (i.e., a regional administrative unit including both urbanized and non-urbanized areas) situated in the northwest of the Hebei province, China, bordering Beijing to the southwest, Inner Mongolia to the north and northwest, and the Loess Plateau to the southwest (Fig. 1a). The main construction efforts for the 2022 Olympic venues and supporting facilities will occur in Chongli, which is a small county in central Zhangjiakou city (Fig. 1b–c) (Song et al., 2018).

Zhangjiakou city has a continental monsoon climate, with high annual temperature variation, and less rainfall (Table 1). The dominant wind direction in Zhangjiakou is from northwest to southeast. Gales, defined as wind speeds higher than 17 m s^{-1} , mostly occur in the northern part of Zhangjiakou city between March and May (Zhang et al., 2011a). Zhangjiakou city lies at the transition zone between the Inner Mongolia Plateau and the North China Plain (Fig. 1b,d). The elevation has a general trend of increasing elevations from southeast to northwest. Zhangjiakou city can be classified into three different geomorphic units, each one of them has different landform characteristics (Table 1). Zhangjiakou city itself belongs to the agropastoral ecotone, grass, forestry and arable land are the main land use types (Fig. 1e–f).

2.2. Data preparation and statistical analysis

(1) modelling data preprocess

In this study, DEM (Digital elevation model) data, land use data, NDVI (Normalized difference vegetation index) data, and two types of daily meteorological data (gridded data of daily precipitation, and daily wind speed data) were used to assess water and wind annual erosion rates in Zhangjiakou city. The meteorological data from weather stations were interpolated into raster data with spatial resolution of 60 m using Kriging method. We resampled all spatial data with non- 60 m spatial resolution into grid pixels with a spatial resolution of 60 m . To assess the total erosion rate in decade scale, ^{137}Cs data in southern Zhangjiakou city was collected from Zhao, Yan, Zhang, Zhan, and Hu (2012) (Fig. 1i). Details of ^{137}Cs data collection and preparation follow standard procedures but details can be found in Zhao et al. (2012).

(2) field sampling and laboratory test of soil quality data

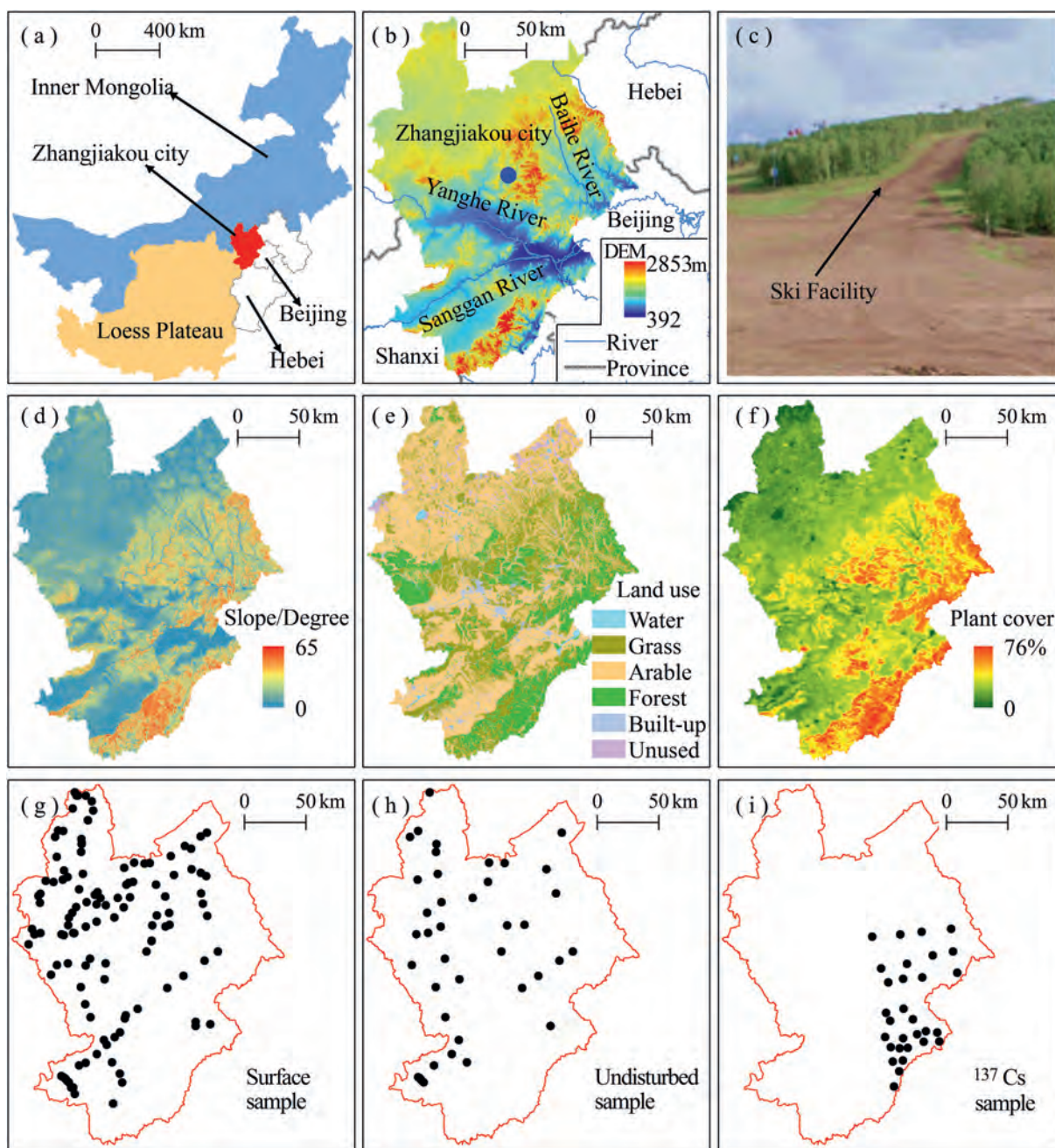


Fig. 1. The study area and the sampling sites of soil quality data.

Table 1
The geographic characteristics in Zhangjiakou city.

Characteristics		Description
Climate	Temperature	average annual value:6.9 °C; the highest monthly value:22.4 °C; the lowest monthly value: 11.4 °C;
	Precipitation	average annual value:393.4 mm; 93.2% happens from April to October
	Wind	the dominant direction: from northwest to southeast; 66.3% of daily maximum wind speed >5.5 m s ⁻¹
Landforms	Elevation	ranges from 392 m to 2853 m above sea level, with an increasing trend from southeast to northwest
	Slope	the average slope:9.8°; more than 24.2% of land area> 5°
	River	Yanghe River and Sanggan River cross Zhangjiakou city
	Geomorphic units (Yuan, Niu, & Wang, 2006)	eastern part: mountainous region with a steeper slopes; southwest part: a part of Loess Plateau, is comprised of alluvial and diluvial plain, loess hill and fringe mountains;
		northwest part: a part of Inner Mongolia Plateau, with an elevation 1000–1700 m and very low gradients.
Land use	Forest	are dominated by temperate broad-leaved deciduous species (Yuan et al., 2006)
	Grassland	are various species of shrubs, perennial and annual herbaceous plants
	Arable land	are mainly located in the region with gentle gradients

128 surface soil samples and 42 undisturbed soil samples were collected in the study area in June of 2018 (Fig. 1g–h). The collection depth of surface samples were 0–5 cm, and each sample has a weight about 1 kg. Undisturbed soil samples were collected by cutting ring, with a height of 5 cm, and a volume of 100 cm³.

Two soil quality parameters that are of primary interest with regard to ecosystem services are soil texture and nutrient availability (Bilotta et al., 2012). In this study, particle size distribution data (PSD, unit: %), field capacity of soil moisture (unit: %), soil saturated hydraulic conductivity (K_s , unit: cm h⁻¹). Soil organic carbon (SOC, unit: g kg⁻¹) and total nitrogen (N, unit: g kg⁻¹) were chosen as soil quality parameters. The particle size distributions (PSDs) in this study were analyzed using the EOF method to extract the sensitive grain size fraction (GSF) (Wang, Wu, Lu, & Pan, 2018c). We found that the sensitive grain size fraction here is > 0.099 mm. Hence, for particle size, we performed the regression the content of GSF > 0.099 mm and the total soil erosion in 2015. After surface samples were dried naturally, gravels were removed using a 2 mm aperture sieve. The remaining samples were used to measure PSD, SOC and N. PSD data of surface soil was measured using Malvern Mastersizer 2000 Particle size Analyzer in the School of Geography, Southwest University, China. SOC and N were measured using elemental analyzer (Elementar, Vario Max CN, Germany) in Institute of Mountain Hazards and Environment, Chinese Academy of Sciences (Li et al., 2017a). Undisturbed soil samples were used to measure field capacity of soil moisture and K_s . The field capacity of soil moisture was measured using the centrifugation method, and soil saturated hydraulic conductivity was tested using the constant head method (Wang, Shao, Han, & Liu, 2015). The field capacity of soil moisture and K_s were measured in the College of Urban & Environmental Sciences, Central China Normal University.

(3) data statistics analysis method

After soil erosion calculation, we classified soil erosion intensity following the scheme of Du et al. (2016), and extracted the land area fraction within Zhangjiakou city for each soil erosion intensity (Table 2). In addition, to better understand the spatial distribution of water and wind erosion, we compiled the water and wind erosion intensities in terms of environmental and anthropogenic factors.

After laboratory test of soil samples, we spatially interpolated data of each soil quality parameter into a raster format using the kriging method. Following the method introduced by Jiang et al. (2019), the value range of each soil quality parameter was divided into twenty intervals, and we extracted the average value for each interval and its corresponding estimated soil erosion in 2015. Finally, we used regression to explore whether the measured soil quality parameters were correlated with predicted erosion rates or not. In addition, the relationships between soil erosion and soil quality would be strongly affected by land use type, thus, we performed the regression analysis between soil erosion and soil quality for arable land and non-arable land, respectively.

Table 2

The land area proportion of different soil erosion intensity.

Soil erosion intensity/t ha ⁻¹ yr ⁻¹	Water erosion			Wind erosion		
	2005	2010	2015	2005	2010	2015
<2.0	64.7	53.6	54.0	37.6	26.6	45.2
2.0–25.0	33.3	43.8	43.3	58.7	63.5	54.8
25.0–50.0	1.7	2.2	2.4	3.6	10.0	0
50.0–80.0	0.3	0.3	0.3	0	0	0
80.0–150.0	0.1	0.1	0	0	0	0
>150.0	0	0	0	0	0	0

The unit of land area proportion is: %.

2.3. Water erosion assessment

A number of methods have been used to model water erosion over areas with mixed land use. The USLE (The universal soil loss equation) and RUSLE (The revised universal soil loss equation) are amongst the most frequently used due to several advantages: simple modelling processes; fewer input parameters; and well tested predictions (e.g., Aksoy & Kavvas, 2005; Jiang et al., 2019; Tuo et al., 2018). The USLE model has been applied in estimation soil erosion for many regions worldwide (e.g., Aksoy & Kavvas, 2005), frequently supported by GIS and remote sensing (e.g., Fu et al., 2011). Ongoing improvements have been made for the calculation of various factors of USLE based on the erosion environment for specific regions: a number of authors have developed local USLE factors in the semiarid regions of China (Fu et al., 2011; Jiang et al., 2019; Nearing, Xie, Liu, & Ye, 2017).

In this study, we used a modified version of the USLE model to calculate water erosion. It can be defined as follows (Wischmeier & Smith, 1978):

$$A = R \times K \times LS \times C \times P \quad (1)$$

Where A is the calculated water erosion rate (t ha⁻¹ yr⁻¹); R is the rainfall-runoff erosivity factor (MJ mm ha⁻¹ h⁻¹ yr⁻¹); K is the soil erodibility factor (t h MJ⁻¹ mm⁻¹); LS is the slope-length and steepness factor, dimensionless; C is the cover management factor, dimensionless; and P is the conservation support practice factor, dimensionless.

The rainfall-runoff erosivity factor, R , is an indicator of the potential that precipitation will detach and transport soil particles (Teng et al., 2018). In this study, gridded daily rainfall data was used to calculate R using the power function model of (Zhang et al., 2003), which they successfully tested against field data in northern China and which has been used successfully in subsequent studies (Wu et al., 2018).

$$R_i = \alpha \sum_{j=1}^k (d_j^i)^\beta \quad (2)$$

where R_i is the i half-month value (MJ mm ha⁻¹ h⁻¹); k is the number of days in the i half-month; and d_j^i is the erosive rainfall for j day of the i half-month, which is ≥ 12 mm. The parameters α and β are calculated with:

$$\alpha = 21.586 \times \beta^{-7.1891} \quad (3)$$

$$\beta = 0.8363 + \frac{18.114}{d_{12}} + \frac{24.455}{y_{12}} \quad (4)$$

where d_{12} is the average daily erosive rainfall (mm), y_{12} is the average annual erosive rainfall (mm). Annual rainfall erosivity, R , is the total rainfall erosivity within a year, can be aggregated by summing all half-month R_i values in the year.

The soil erodibility factor, K , describes the vulnerability of the soil to raindrop detachment and runoff wash (Fu et al., 2011). In this study, the K factor data was derived from Gao et al. (2012). They calculated K factor values using a soil erodibility nomograph which estimated the erodibility at a specific site by analyzing soil condition and soil types (Efthimiou, 2018; Liu, Bi, & Fu, 2010; Wischmeier & Smith, 1978).

Topographical factors, such as slope length and steepness, substantially affect the rate of water erosion (Liu, Nearing, & Risse, 1994; Visser et al., 2004; Wischmeier & Smith, 1978). In this

study, two topographic factors, slope length factor L and slope steepness factor S are calculated with (Liu et al., 1994; Renard et al., 1997):

$$L = (\lambda/22.1)^m \tag{5}$$

$$S = 10.8 \sin\theta + 0.03 \quad \theta < 5^0 \tag{6}$$

$$S = 16.8 \sin\theta - 0.50 \quad 10^0 > \theta \geq 5^0 \tag{7}$$

$$S = 21.9\sin\theta - 0.96 \quad \theta \geq 10^0 \tag{8}$$

where λ is the slope length (m) measured along a horizontal projection, m is a variable slope length exponent which is related to the ratio, $\bar{\beta}$, of rill erosion to inter-rill erosion, and θ is the slope angle.

The variable slope-length exponent m and the ratio $\bar{\beta}$ of rill erosion to inter-rill erosion is computed using the following equations:

$$m = \bar{\beta}/(1 + \bar{\beta}) \tag{9}$$

$$\bar{\beta} = (\sin\theta / 0.0896) / [3(\sin\theta)^{0.8} + 0.56] \tag{10}$$

The cover and management factor C in the USLE measures the combined effect of all interrelated cover and management variables (Wischmeier & Smith, 1978). Previous studies developed a series of methods to estimate the C factor value using vegetation cover based on simulated and natural rainfall on experimental plots (Fu et al., 2011). In this study, we calculate C with the following (Jiang, Wang, & Liu, 1996; Liu et al., 2010):

$$C = e^{-0.0418(vc-5)} \tag{11}$$

$$C = 0.988 e^{-0.11vc} \tag{12}$$

$$C = 1.029e^{-0.0235vc} \tag{13}$$

Eq. (11) is applied to grassland (Jiang et al., 1996) and Eq. (12) is applied to forests (Liu et al., 2010). As for arable land, considering the monthly change in effectiveness of crop cover within the crop year, the C factor of arable land was evaluated using Eq. (11), Eq. (12) and Eq. (13) for three different crop stage periods, a stage from April to June, a stage from July to September, and a stage of October to March in the following year, respectively (Liu et al., 2010). The annual C value was calculated using a weighted mean with the monthly rainfall erosivity as the weights.

Vegetation coverage (vc ,%) was calculated using $NDVI$ data (Fu et al., 2011).

$$vc = \frac{(NDVI - NDVI_{soil})}{(NDVI_{max} - NDVI_{soil})} \tag{14}$$

where $NDVI_{soil}$ is $NDVI$ of bare soil; $NDVI_{max}$ stands for regional maximum $NDVI$. We obtained $NDVI$ data from the Chinese Academy of Sciences.

The factor P is the ratio of soil loss with a specific cropping practice to the corresponding loss with cropping that is perpendicular to topographic contours (i.e., up-and-down cropping) (Wischmeier & Smith, 1978). At large spatial scales, it is difficult to capture the effects of soil and water conservation measures (such as terrace systems, contour tillage and strip-cropping on the contour) with land use maps (Fu et al., 2011). A recent study found the soil loss ratio, P , is greater with greater topographic gradient (Zhao,

Yang, & Govers, 2019). In addition, the practice of narrow strip-cropping using a strips of approximately 2 m width has frequently been used in Zhangjiakou city (Fig. 2) as an erosion mitigation measure on slopes with topographic gradients greater than 0.27 (i.e., $>15^\circ$). In these areas we calculated the P factor using annual rainfall data. Given the above considerations, two statistical formulas were used to determine the value of the P :

$$P = 0.2 + 0.03\bar{\theta} \quad \bar{\theta} \leq 27 \tag{15}$$

$$P = 0.0039 \times y_{20}^{0.6772} \quad \bar{\theta} > 27 \tag{16}$$

where $\bar{\theta}$ is the slope gradient in %, calculated directly from the DEM data. y_{20} is sum of the daily rainfall above > 20 mm over the whole year (an integer value that represents then number of days).

2.4. Wind erosion assessment

We used a statistical wind erosion equation to estimate the wind erosion rate in Zhangjiakou city. The equation was developed for semiarid environments using wind tunnel experiments and field observations (Gao et al., 2012). The equation has been applied to estimate wind erosion rates and dust emissions in previous studies; it was expressed using the following:

$$Q_1 = 10 \cdot \hat{C} \cdot \sum_{j=1} < T_j \cdot \exp \left\{ a_1 + \frac{b_1}{z_0} + c_1 \cdot \left[(A \cdot u_j)^{\frac{1}{2}} \right] \right\} > \tag{17}$$

$$Q_2 = 10 \cdot \hat{C} \cdot \sum_{j=1} < T_j \cdot \exp \left\{ a_2 + b_2 \cdot vc^2 + \frac{c_2}{A \cdot u_j} \right\} > \tag{18}$$

where, Q_1 ($t \text{ ha}^{-1} \text{ yr}^{-1}$) is the wind erosion rate in arable land with no vegetation cover; Q_2 ($t \text{ ha}^{-1} \text{ yr}^{-1}$) is the wind erosion rate in areas with plant cover, $t \text{ ha}^{-1} \text{ yr}^{-1}$; \hat{C} is a scaling parameter that in our sites is 0.0018; T_j is the accumulated time of wind speed u_j (u'_j), minute; A is a conversion parameter of wind speed between field stations and data derived from wind tunnels, which in our study is 0.893; z_0 is the aerodynamic roughness length, here is 0.55 cm; vc is the plant coverage (%); other parameters a_1 and a_2 , b_1 and b_2 , c_1 and c_2 are -9.208 and 2.4869 , 0.018 and -0.0014 , 1.955 and -54.9472 ; u_j is station wind speed greater than sand particle's threshold wind under lower plant coverage, here the threshold wind speed is 5.5 m s^{-1} ; u'_j is station wind speed greater than sand particle's threshold wind with plant coverage. According to wind tunnel experiments, the threshold wind speed u_t can be expressed as a function of plant coverage:

$$u_t = 5.56158 + 1.63299 \times \exp\left(\frac{vc}{38.6747}\right) \tag{19}$$

We used Eq. (18) To compute the wind erosion rate for grassland and forests. Because crop cover that is present before harvesting is effective in reducing wind erosion, we also use Eq. (18) For arable land in the crop-stage periods between April and September. In contrast, we use Eq. (17) To calculate the wind erosion rate for arable land during other periods of the year.

2.5. Total erosion assessment

In previous studies, total soil erosion was defined as the sum of water and wind erosion (Du et al., 2016; Jiang et al., 2019), meanwhile, the Cesium-137 (^{137}Cs) tracing technique was also used to estimate total soil erosion (Tuo et al., 2018; Van Pelt et al., 2017). In



Fig. 2. Soil erosion control practices in Zhangjiakou city.

this study, we use both of these methods to calculate total soil erosion in Zhangjiakou city, and we test these two predictions against each other.

In this study, we synthesized published ^{137}Cs inventories data in northern China and their corresponding soil erosion rate data (Li, Li, Liu, & Yao, 2005; bib_Qi_et_al_2008Qi, Liu, Shi, Hu, & Zhuang, 2008; Yan et al., 2000, 2003; bib_Yan_et_al_2000; bib_Yan_et_al_2003; Zhang et al., 2007a). Deposition of ^{137}Cs is not homogenous in space and time, so we normalize the different ^{137}Cs inventories with a reference inventory (i.e., we divide ^{137}Cs values at each site with their local reference inventory). Our results are not sensitive to the selected reference inventory, but we selected the inventory from the site closest to our field site. reference ^{137}Cs inventory we use in the results presented here is $1602.79 \text{ Bq m}^{-2}$ (Qi et al., 2008) and divided all ^{137}Cs inventories in our dataset to create a standardized inventory across all sites. We then regressed the standardized ^{137}Cs inventories against measured soil erosion rates using a variety of regressions (linear, logarithmic, polynomial) and found that the relationship between total soil erosion rate in northern China and standardized ^{137}Cs inventories is best described by a logarithmic relationship (Fig. 3).

We then aggregated the ^{137}Cs inventory data in southern Zhangjiakou city, which have been published in (Zhao et al., 2012). From these data, we employed the logarithmic regression formula to compute the total soil erosion in southern Zhangjiakou city, and described the spatial distribution of the total erosion rate inferred

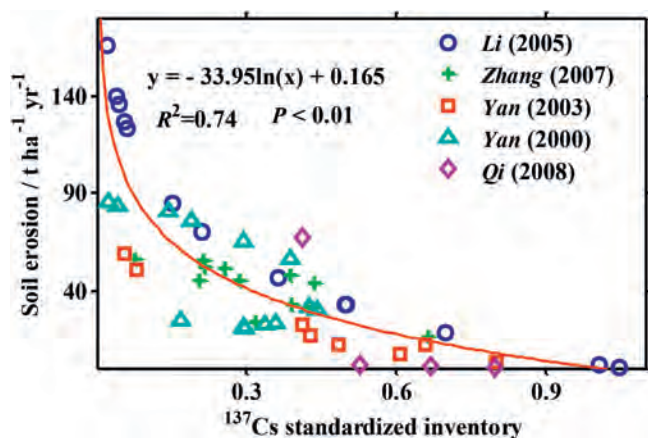


Fig. 3. The relationship between ^{137}Cs standardized inventories and soil erosion rate.

from ^{137}Cs inventories in the decade scale.

3. Results

3.1. Water and wind erosion

In Zhangjiakou city, our modelling predicts that annual water erosion rates are 2.9, 3.9, and 4.1 $\text{t ha}^{-1} \text{ yr}^{-1}$, respectively for the years 2005, 2010 and 2015. We calculate annual wind erosion rates of 7.5, 10.1, and 5.0 $\text{t ha}^{-1} \text{ yr}^{-1}$ in the same years (Fig. 4), suggesting that the wind erosion rate exceeds the water erosion rate in Zhangjiakou city for each year. In addition, we find that the wind erosion in Zhangjiakou city peaks in 2010 and is twice of the value in 2015. The changing trend of wind erosion in Zhangjiakou city is similar to assessments of wind erosion in Inner Mongolia which lies on the north of Zhangjiakou city (Zhang et al., 2018). They reported that the wind erosion rates were 23, 42 and 23 $\text{t ha}^{-1} \text{ yr}^{-1}$, respectively for 2005, 2010 and 2015.

We found that the fraction of land area experiencing erosion intensity $< 2 \text{ t ha}^{-1} \text{ yr}^{-1}$ in Zhangjiakou city are 54.0%–64.7% (water erosion), 26.6%–45.2% (wind erosion) (Table 2). The fraction of land area experiencing erosion intensity 2–25 $\text{t ha}^{-1} \text{ yr}^{-1}$ are 33.3%–43.8% (water erosion), 54.8%–63.5% (wind erosion). Our calculations suggest that greater than 80% of the land area in Zhangjiakou city has soil erosion rates of less than 25 $\text{t ha}^{-1} \text{ yr}^{-1}$. The region has erosion hot spots, however. In particular, we predict minimal water erosion intensity $< 2 \text{ t ha}^{-1} \text{ yr}^{-1}$ as the dominant intensity category, whereas the erosion intensity of 2–25 $\text{t ha}^{-1} \text{ yr}^{-1}$ is dominant for wind erosion. This, to some extent, explains the difference of average erosion rate between water and wind erosion. We aim to explain this discrepancy and explore how it correlates with soil quality measurements.

The spatial distribution of soil erosion intensities are similar for the years 2005, 2010 and 2015 (Fig. 4). Compared to other regions, wind erosion rates are higher in the northwest region and south-east corner of Zhangjiakou city. In the northwest region, the wind erosion rates reach 8.7–15.7 $\text{t ha}^{-1} \text{ yr}^{-1}$ over the three years, whereas the wind erosion rates in southwest region account for 2.7–4.4 $\text{t ha}^{-1} \text{ yr}^{-1}$. Calculations of water erosion stand in contrast to wind erosion: they have larger values in southwestern Zhangjiakou city, displaying a banded pattern from southwest to northeast (Fig. 4). In the southwestern Zhangjiakou city, water erosion rates reach 4.2–4.4 $\text{t ha}^{-1} \text{ yr}^{-1}$ over the three studies years, the value in northwest region accounts for 2.3–4.3 $\text{t ha}^{-1} \text{ yr}^{-1}$.

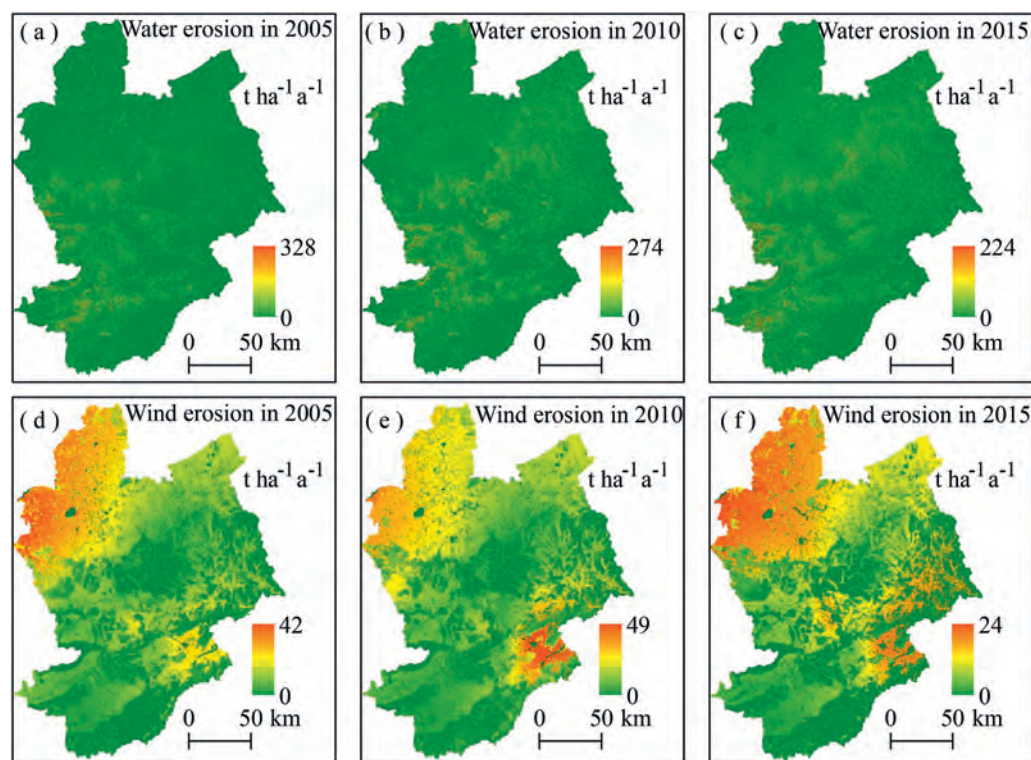


Fig. 4. The spatial distribution of water and wind erosion in Zhangjiakou city.

3.2. Total erosion derived from the models and from ^{137}Cs inventories

Using the logarithmic regression formula between soil erosion and ^{137}Cs inventory (collected in 2008), the average soil erosion rate in southeast Zhangjiakou city was calculated to be $16.7 \text{ t ha}^{-1} \text{ yr}^{-1}$. In the same area, the average value of modelled total erosion rates were 7.4, 15.3 and $7.2 \text{ t ha}^{-1} \text{ yr}^{-1}$ for the year 2005, 2010 and 2015, respectively. In general, the erosion rate derived from ^{137}Cs is of the same order of magnitude as modelled erosion rates, and is close to the estimated total erosion rate of $15.3 \text{ t ha}^{-1} \text{ yr}^{-1}$ in 2010. Meanwhile, the spatial distribution of total erosion in southeastern Zhangjiakou city inferred from ^{137}Cs inventories is similar to that of the modelled erosion rates in 2010: both predict a hotspot of erosion in the southeastern corner of Zhangjiakou city (Fig. 5).

Fig. 5 shows that the modelled total erosion in the whole area of Zhangjiakou city presents a spatial pattern with relatively high erosion rates in northwest and southeast regions of Zhangjiakou city. The spatial pattern of total erosion for each year is similar to that of wind erosion in Zhangjiakou city (Fig. 4) because wind erosion dominates the total erosion signal compared to water erosion.

3.3. Relations between soil erosion and soil quality

The proportion of the grain size distribution greater than 0.099 mm, and soil saturated hydraulic conductivity (K_s), and the total N content are positively correlated with modelled wind and total erosion (Fig. 6). In contrast, the field capacity of soil water is negatively correlated with wind and total erosion (Fig. 6). However, for some soil quality parameters the direction of correlation differs between water and wind erosion. Total erosion follows the same pattern as wind erosion because, as previously stated, wind erosion dominates the total erosion across the study area. Water erosion

has a positive relationship with the content of SOC, and a negative relationship with soil saturated hydraulic conductivity (K_s). Moreover, the regression coefficient, R^2 , between wind erosion and soil quality parameters range from 0.57 to 0.85, and correlation coefficients are higher than that between water erosion and soil quality parameters, as well as between total erosion and soil quality parameters.

We found that the relationships between soil erosion and soil quality in arable land and in non-arable land are similar to that in the whole study area (Fig. 7). The correlation between soil particle size and water erosion, and the correlation between K_s and total erosion are significant in arable land, however, these two correlations are not significant in non-arable land ($P < 0.01$), indicates that the relationships between soil erosion and soil quality in arable land are more reliable than them in non-arable land. In addition, among five soil quality parameters, four parameters have significant correlation with wind erosion ($P < 0.01$), while three parameters and two parameters significantly correlate with water erosion and total erosion, respectively ($P < 0.01$).

4. Discussion

4.1. The influence factors on soil erosion

Zhang et al. (2018) claimed that climate variation was the dominant factor controlling changes in wind erosion, as it drives changes in wind speeds. The dominant wind direction over Zhangjiakou city is from the northwest to the southeast. Driving the patterns in wind erosion is physiography. The distribution of blown sand and dust events in 2015 shows that the cumulative duration of blown sand and dust events in northern Zhangjiakou city are much higher than other regions (Fig. 8). The distribution pattern of blown sand and dust events is similar to that of wind erosion. However, rainfall-runoff erosivity factor (R) in 2015 exhibits high values in the

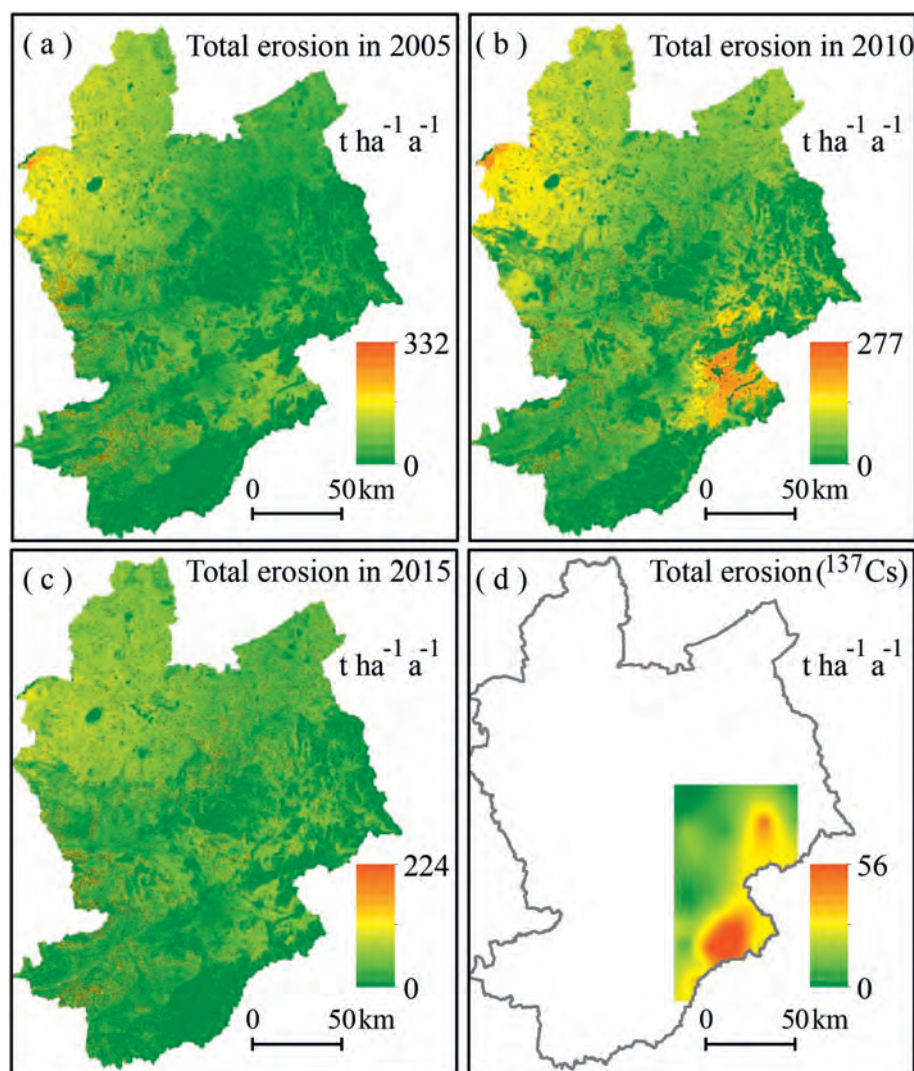


Fig. 5. The spatial distribution of total erosion in Zhangjiakou city.

east region of Zhangjiakou city, and the distribution pattern is different from that of water erosion (Fig. 8), implies that the distribution of water erosion would be more affected by other factors such as landscape, land use and plant cover, rather than mostly affected by the rainfall-runoff erosivity factor.

From the perspective of landscape, we found that high water erosion rates mainly occur at elevations between 800 and 1300 m (Table 3), which are the elevations that represent a transition zone between the Inner Mongolia Plateau and North China Plains. Water erosion rates are also high at slopes of 5° – 15° , grassland and arable land, and areas with plant coverage 10–30%. High wind erosion rates mainly present at elevations <800 m (alluvial plain of Yanghe river and Sanggan river) and elevations between 1300 and 2000 m (on the Inner Mongolian Plateau), slopes less than 15° and especially in very gentle areas with the slope less than 5° , arable land, and areas with plant coverage 10–30%.

Furthermore, we extracted the land area ratio of different land use types, as well as plant coverage in different topographic gradient grades. Fig. 9 shows that, arable land are primary land use types in slope grades 0° – 5° and 5° – 15° , with land area ratio of 68.9% and 46.4%, respectively. However, in slope grades 15° – 25° and $>25^{\circ}$, forest and grass land are primary land use types. In addition, the plant coverage increase from 30.5% in slope grade 0° – 5° to 51.4% in

slope grade $>25^{\circ}$. These results above indicate that human activities which relate to farming and deforestation activities are the most important factors to decide the distribution of water and wind erosion. Topographic gradient might still be driving the pattern of soil erosion, but indirectly as it determines the land use pattern and plant coverage around Zhangjiakou city.

4.2. Spatial scale effect on the relations between soil erosion and soil quality

It is commonly thought that soil erosion creates distinct spatial variations in soil quality. However, soil erosion is a scale-dependent phenomenon, and the different spatial scale effects on soil quality can vary widely (Berhe et al., 2018). At the small spatial scale, such as the hillslope scale, soil erosion process and other factors that influence soil quality such as topography and land use type, are relatively homogeneous, and the effects of soil erosion on the soil quality distribution would be more significant (Visser & Sterk, 2007). At the regional scale, the factors that influence the soil quality distribution are various and heterogeneous, and so they may weaken the relations between soil erosion and soil quality.

In this study, we found that grain size fraction >0.099 mm, field capacity of soil water, and total nitrogen (N) do not have significant

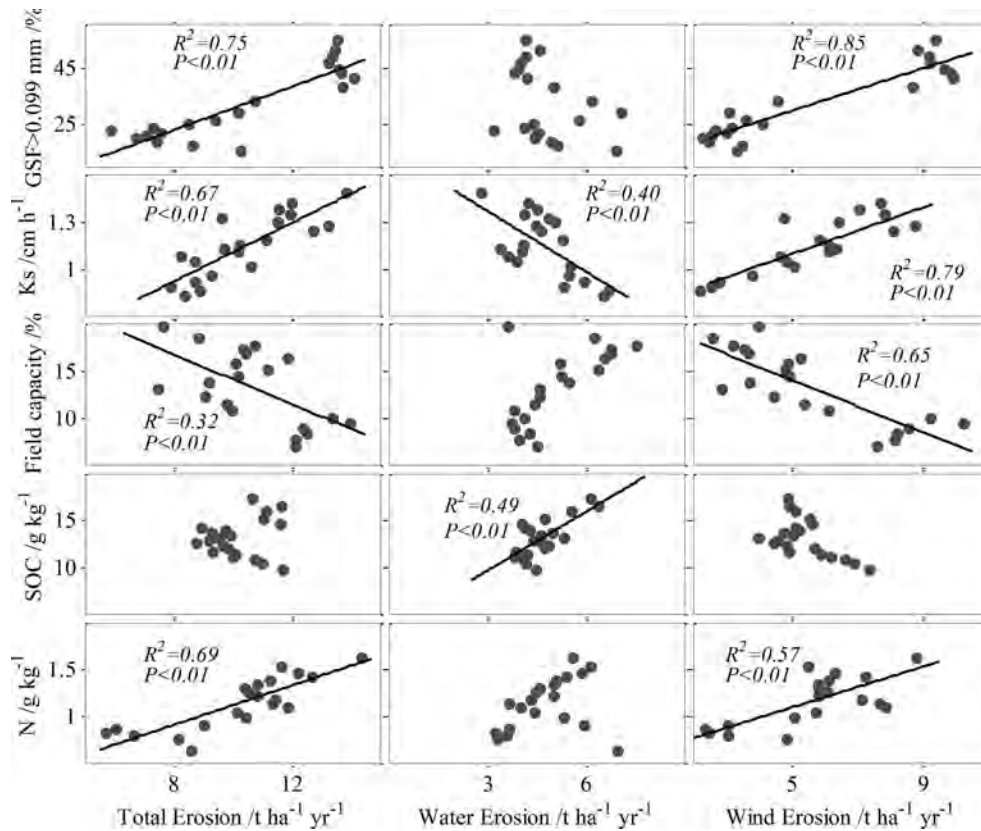


Fig. 6. The relationship between soil erosion and soil quality.

correlations with water erosion, and SOC does not have significant correlation with wind erosion ($P < 0.01$). In addition, different soil erosion mechanisms at the regional scale may have a distinct spatial distribution, their influence on the distribution of soil quality could interact to each other, thus increase the uncertainty of single soil erosion impact on soil quality at the regional scale. In this study, we found that the correlation direction may differs between water and wind erosion. We also found because wind erosion in Zhangjiakou city dominates the total erosion across the study area, total erosion in simple linear regressions follow the same pattern as wind erosion.

Therefore, our observed relationships between soil quality and soil erosion may be a function of the spatial scales of observation, with some relationships potentially due to the small scale or in-situ observation, and we may not be capturing these relationships at regional spatial scales.

4.3. Soil erosion and soil degradation

In this study, the proportion of the grain size fraction >0.099 mm has a positive correlation with wind and total erosion ($P < 0.01$), which is consistent with predicted coarsening of the soil surface by aeolian winnowing. Li, Okin, and Epstein (2009b) has reported that soil particles in the fractions of <0.125 mm were significantly depleted after wind erosion seasons. Yan et al. (2013) also found that the most reduction occurs between grain sizes of 0.05–0.09 mm after wind erosion experiments. In this study, the relationship between soil erosion and the change in soil grain size in surface soil is consistent with previous studies.

Soil saturated hydraulic conductivity (K_s) and field capacity of soil water not only are important parameters to assess the effect of soil and water conservation but also are key factors to affect the soil

hydrological process (Duan et al., 2018). K_s reflects the water infiltration and determines water distribution (Wang et al., 2018a). In this study, K_s has a positive relation with wind and total erosion, but a negative relation with water erosion. We hypothesize that this is because the surface soil becomes coarser with accelerated wind erosion, leading to greater porosity and water infiltration rates (Duan et al., 2018; Zhang, Chan, Oates, Heenan, & Huang, 2007b). In addition, severe wind erosion rates occur in northern Zhangjiakou city where there is relatively low water erosion (Fig. 4). This causes a negative relationship between water erosion and K_s at the regional scales. Furthermore, increasing water infiltration in severe wind erosion region would weaken the water erosion process by decreasing runoff, thus, larger water infiltration also leads to lower water erosion intensity (Ruiz-Colmenero, Bienes, Eldridge, & Marques, 2013; Zhang et al., 2007b). Therefore, the difference between spatial distributions of wind erosion and water erosion may enhance negative relation between water erosion and K_s at the regional scale. The field capacity of soil water has a negative correlation with wind and total erosion, indicating that the soil water holding capacity becomes greater with slower rates of wind erosion.

Soil organic carbon (SOC) and nitrogen (N) are two important nutrients related to biogeochemical cycling (Quinton, Govers, Van Oost, & Bardgett, 2010). Previous studies argued that SOC and N were preferentially removed by water and wind erosion (Lal, 2018). The loss of SOC and N have positive relationships with soil erosion intensity (Yan, Wang, Wang, Zhang, & Patel, 2005, 2013), and SOC and N contents in the residue soil have a negative relationship with soil erosion intensity (Su et al., 2017; Zou et al., 2018). However, a recent study argued that SOC content in sediments are minimally affected by the amount of soil loss because of soil zonality which relates to how the soils formation and evolve (Li et al., 2017c). Li

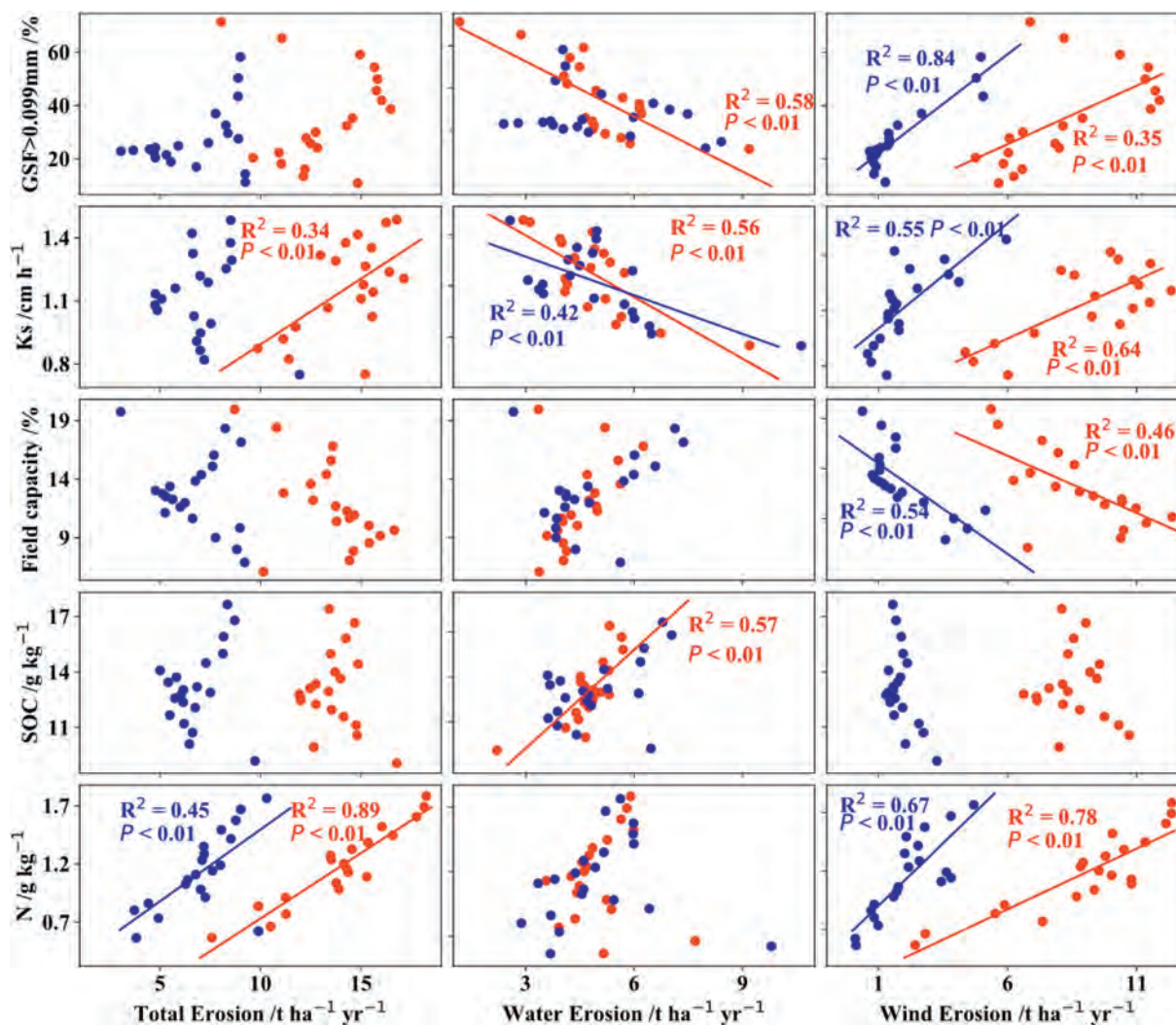


Fig. 7. The relationship between soil erosion and soil quality for arable land and non-arable land, respectively.

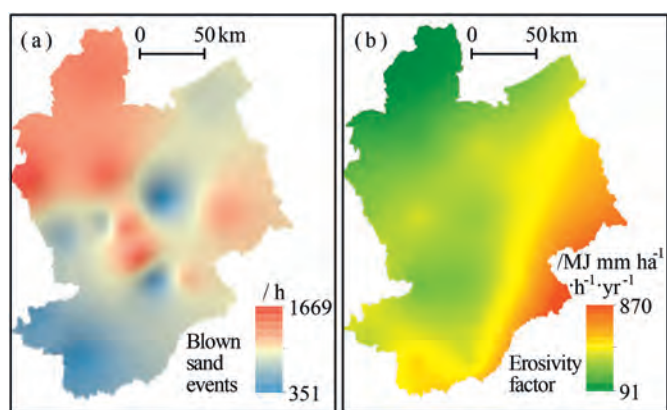


Fig. 8. The rainfall-runoff erosivity factor and cumulative duration of blown sand and dust events in Zhangjiakou city.

et al. (2017b) reported that the contents of SOC and total N have no significant correlation with soil erosion in artificial grassland in semiarid China. In addition, Parfitt et al. (2013) found that gains in soil carbon and nitrogen under hill country pasture are probably

largely due to the ongoing input from carbon and nitrogen in the grass-legume pastures rather than erosion or depositional of soil. Therefore, the relations between soil erosion and soil nutrient (SOC and N) may not follow the negative rule due to different processes of soil nutrient input. In this study, the content of SOC has a positive relationship with water erosion ($P < 0.01$) (Fig. 6). Severe water erosion in Zhangjiakou city occurs in the southwest and central regions (Fig. 4) where surface soil particles are finer compared to areas with severe wind erosion rates: fine particles in soil are conducive to increase SOC contents (e.g., Doetterl et al., 2016; Eusterhues, Rumpel, & Kogel-Knabner, 2005; Wang et al., 2018b). In addition, both plants and erosion may play an important role in redistributing soil nutrients (Eger et al., 2018; Li, Zhao, Liu, & Huang, 2009a). We found severe water erosion in Zhangjiakou city occur in grass land as well as areas with vegetation (30–50%) (Table 3), the plant material that is either emplaced by roots or dropped and buried within the sediment would enrich the content of SOC.

In our case, the total N content is positively correlated with wind and total erosion. Severe wind erosion occurs in arable land and regions with lower vegetation coverage (10–30%) (Table 3). The total N were mainly concentrated in the uppermost soil layer (0–10 cm) in a semiarid region (Li et al., 2017a). Hence, soil erosion

Table 3
Water and wind erosion intensity within different influencing factors.

		Water erosion			Wind erosion		
		2005	2010	2015	2005	2010	2015
Elevation/m	<800	2.7 ± 5.1	3.0 ± 6.0	2.5 ± 4.9	7.9 ± 5.9	14.1 ± 14.2	5.4 ± 5.1
	800–1300	4.9 ± 9.1	5.3 ± 9.0	5.1 ± 8.5	5.1 ± 5.4	7.7 ± 8.0	3.4 ± 4.1
	1300–2000	2.4 ± 5.1	3.9 ± 6.5	4.4 ± 7.0	9.3 ± 8.8	11.3 ± 9.7	6.2 ± 5.7
	>2000	1.9 ± 2.6	3.3 ± 5.1	3.3 ± 6.0	0.8 ± 1.1	2.8 ± 2.2	0.7 ± 1.1
Slope/Degree	<5	2.6 ± 5.1	3.0 ± 5.1	3.2 ± 5.1	10.8 ± 7.8	14.0 ± 10.5	7.2 ± 5.3
	5–15	5.0 ± 8.9	6.4 ± 9.5	6.8 ± 9.4	7.8 ± 7.5	10.2 ± 9.2	5.2 ± 5.1
	15–25	2.6 ± 6.6	4.1 ± 7.7	3.8 ± 7.6	2.5 ± 3.8	4.5 ± 6.0	1.7 ± 3.0
	>25	1.0 ± 2.9	2.0 ± 3.9	1.8 ± 3.5	1.2 ± 2.0	3.0 ± 4.1	0.7 ± 1.7
Land use/%	Forest	0.3 ± 1.5	0.6 ± 1.9	2.2 ± 5.1	1.6 ± 2.8	3.4 ± 3.4	1.0 ± 1.7
	Grass	5.5 ± 9.9	7.8 ± 10.9	6.3 ± 10.0	3.0 ± 4.2	3.9 ± 4.3	1.8 ± 2.6
	Arable	2.8 ± 5.6	3.9 ± 5.9	4.4 ± 6.7	12.2 ± 7.3	16.8 ± 9.2	9.0 ± 4.5
	Other	2.3 ± 6.4	2.3 ± 6.8	1.3 ± 4.1	5.4 ± 7.7	6.7 ± 10.4	3.0 ± 5.3
Plant coverage/%	<10	1.3 ± 5.2	2.1 ± 8.9	0.4 ± 1.9	6.0 ± 13.5	6.5 ± 14.4	2.0 ± 6.3
	10–30	4.4 ± 8.2	4.7 ± 8.4	5.0 ± 8.1	10.3 ± 8.0	13.7 ± 10.0	8.0 ± 5.9
	30–50	1.9 ± 3.9	4.8 ± 7.5	5.0 ± 7.7	3.5 ± 4.4	9.7 ± 9.5	4.3 ± 4.3
	>50	0.2 ± 0.6	0.9 ± 2.3	1.5 ± 3.1	0.7 ± 1.3	2.7 ± 4.5	0.7 ± 2.0

The unit of water and wind erosion intensity is: $t\ ha^{-1}\ yr^{-1}$.

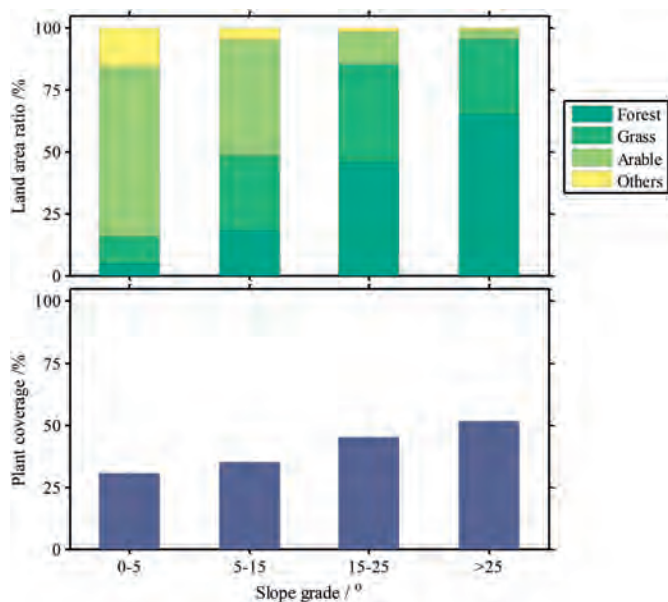


Fig. 9. Land use types and plant coverage in different slope grades.

could lead to the mixing of carbon-poor or nutrient-poor subsoil into the layer mixed by tillage, and if the newly exposed mineral surfaces bind organic matter, soil carbon and nutrient inventories may also increase (Quinton et al., 2010). In northern Zhangjiakou city with severe wind erosion intensity, total N could be lost from bare unprotected soils towards areas with sufficient vegetation or mulch cover because of wind erosion process at the local scale. However, in a balance between deposition on fields and denudation from fallow areas, and the long-term N import or export due to wind erosion on the scale of a village or cluster of farms can be assumed zero (Visser & Sterk, 2007). In addition, we predict a low intensity of wind erosion in the southwest region of Zhangjiakou city (Fig. 4), but this area exhibits higher than average water erosion. Nutrients transported by water are always directed in a down-slope direction and cannot be transported upslope again as is possible with wind erosion. Total N lost by water erosion are forever lost for the upslope area (Visser & Sterk, 2007). Thus, these mechanism above would explain the positive relationship between wind erosion and soil nutrient at the regional scale.

Overall, the relationship between soil quality and soil erosion varies on regional scales, and the correlations between them, can be caused by many different processes: i.e., we cannot make a definitive causal link between these two datasets. The data does show that, compared to water erosion, wind erosion displays higher correlation coefficients with soil quality parameters in Zhangjiakou city possibly because of its dominance compared to water erosion in contributing to total erosion.

5. Conclusion

In this study, we calculated annual soil erosion rates using USLE and a wind erosion model, as well as calculated long-term soil erosion rates in decade scale based on ^{137}Cs inventories, to assess the spatial distribution of soil erosion intensity and its influence on soil degradation in Zhangjiakou city.

We find that soil erosion rates in Zhangjiakou city in the decade before 2015 were 2.92–4.14 $t\ ha^{-1}\ yr^{-1}$ for water erosion and 4.99–10.05 $t\ ha^{-1}\ yr^{-1}$ for wind erosion. More than 80% of the land area in the Zhangjiakou city region are eroding at less than 25 $t\ ha^{-1}\ yr^{-1}$. Areas with higher potential wind and total erosion risk occur mainly in northwest and southeast Zhangjiakou city, whereas potential water erosion risk is highest in the southwest and central regions. The spatial distribution of total erosion rates in decade scale, which calculated based on ^{137}Cs inventories, is similar to the spatial distribution of annual soil erosion in 2005, 2010 and 2015.

Higher soil erosion intensities in Zhangjiakou city occur primarily in areas with gentle slope, lower plant coverage and areas of arable land. Topographic slope plays an important role in determining erosion rates, but in an indirect fashion. Areas with high topographic slopes have not been used for farming, and are primarily forested. In the Zhangjiakou city region, the dominant erosion mechanism is wind erosion, driven by low plant cover on fallow fields, and so human modification of the landscape, partially determined by topographic gradient, is the primary driver of soil erosion in Zhangjiakou city.

We find complex relationships between soil erosion and soil quality parameters in Zhangjiakou city. However, some clear trends do emerge. Surface soil becomes coarser and water infiltration is enhanced as wind erosion is greater, whereas the soil water holding capacity decreases with increasing wind erosion rates. However, in regions with higher water infiltration rates, the intensity of water erosion is lower. The relations between the distributions of soil

nutrient and soil erosion present positive patterns, which are varied, and likely caused by a suite of different processes. Our analysis of the relationships of soil nutrient parameters with soil erosion may be a function of the spatial scales of observation. Meanwhile, compared to water erosion, wind erosion has more significant correlations with soil quality in Zhangjiakou city possibly because of its dominance compared to water erosion in contributing to total erosion. To mitigate risks of soil degradation, suitable erosion measures should be implemented according to the dominant erosion type, which varies in space. The measures will protect the regional environment in advance of the 2022 Winter Olympics.

Acknowledgments

This work was supported by National Major Science and Technology Program for Water Pollution Control and Treatment (2017ZX07101001) of China; Scientific and Technological Research Program of Chongqing Municipal Education Commission (KJ110608) of China, and the Chinese Government Scholarship from China Scholarship Council (CSC). We would like to thank National Earth System Science Data Center, National Science & Technology Infrastructure of China (<http://www.geodata.cn>), the National Meteorological Information Center of China (<http://data.cma.cn>), the Geospatial Data Cloud website (<http://www.gscloud.cn>), and the Data Center for Resources and Environmental Sciences, Chinese Academy of Science (RESDC) to give us data support including the daily meteorological data, NDVI, DEM, and the land use dataset. We thank Dr. Wu Yongqiu and Dr. Zhang Chunlai at the Beijing Normal University for their assistance with soil erosion calculation. We thank Dr. Wei Jie and Li Shasha at the Chongqing Normal University for their assistance during the field work. We also acknowledge Dr. Liu Muxing and Dr. Yi Jun and Lou Shulan at the Central China Normal University, as well as Dr. Wang Yong and Liu Chuan at the Southwest University for their assistance with measurements of soil parameters.

References

- Aksoy, H., & Kavvas, M. L. (2005). A review of hillslope and watershed scale erosion and sediment transport models. *Catena*, *64*, 247–271. <https://doi.org/10.1016/j.catena.2005.08.008>.
- Berhe, A. A., Barnes, R. T., Six, J., & Marín-Spiotta, E. (2018). Role of soil erosion in biogeochemical cycling of essential elements: Carbon, nitrogen, and phosphorus. *Annual Review of Earth and Planetary Sciences*, *46*, 521–548. <https://doi.org/10.1146/annurev-earth-082517-010018>.
- Bilotta, G. S., Grove, M., & Mudd, S. M. (2012). Assessing the significance of soil erosion: Boundary Crossings. *Transactions of the Institute of British Geographers*, *37*, 342–345. <https://doi.org/10.1111/j.1475-5661.2011.00497.x>.
- Breshears, D. D., Whicker, J. J., Johansen, M. P., & Pinder, J. E. (2003). Wind and water erosion and transport in semi-arid shrubland, grassland and forest ecosystems: Quantifying dominance of horizontal wind-driven transport. *Earth Surface Processes and Landforms*, *28*, 1189–1209. <https://doi.org/10.1002/esp.1034>.
- Cyranoski, D. (2015). Chinese biologists lead Olympics outcry. *Nature*, *524*, 278–279.
- Doetterl, S., Berhe, A. A., Nadeu, E., Wang, Z., Sommer, M., & Fiener, P. (2016). Erosion, deposition and soil carbon: A review of process-level controls, experimental tools and models to address C cycling in dynamic landscapes. *Earth-Science Reviews*, *154*, 102–122. <https://doi.org/10.1016/j.earscirev.2015.12.005>.
- Duan, X., Deng, Y., Tao, Y., He, Y., Lin, L., & Chen, J. (2018). Variation in soil saturated hydraulic conductivity along the hillslope of collapsing granite gullies. *Hydrological Sciences Journal*, *63*, 803–817. <https://doi.org/10.1080/02626667.2018.1453610>.
- Du, H., Dou, S., Deng, X., Xue, X., & Wang, T. (2016). Assessment of wind and water erosion risk in the watershed of the Ningxia-Inner Mongolia Reach of the Yellow River, China. *Ecological Indicators*, *67*, 117–131. <https://doi.org/10.1016/j.ecolind.2016.02.042>.
- Efthimiou, N. (2018). The importance of soil data availability on erosion modeling. *Catena*, *165*, 551–566. <https://doi.org/10.1016/j.catena.2018.03.002>.
- Eger, A., Yoo, K., Almond, P. C., Boitt, G., Larsen, I. J., Condron, L. M., et al. (2018). Does soil erosion rejuvenate the soil phosphorus inventory? *Geoderma*, *332*, 45–59. <https://doi.org/10.1016/j.geoderma.2018.06.021>.
- Eusterhues, K., Rumpel, C., & Kogel-Knabner, I. (2005). Organo-mineral associations in sandy acid forest soils: Importance of specific surface area, iron oxides and micropores. *European Journal of Soil Science*, *56*, 753–763. <https://doi.org/10.1111/j.1365-2389.2005.00710.x>, 0, 050912034650049.
- Fu, B., Liu, Y., Lü, Y., He, C., Zeng, Y., & Wu, B. (2011). Assessing the soil erosion control service of ecosystems change in the Loess Plateau of China. *Ecological Complexity*, *8*, 284–293. <https://doi.org/10.1016/j.ecocom.2011.07.003>.
- Gao, S., Zhang, C., Zou, X., Wu, Y., Wei, X., Huang, Y., et al. (2012). *Benefits of Beijing-Tianjin sand source control engineering*. Beijing: China Science Publishing & Media Ltd (in Chinese).
- Jiang, Z., Wang, Z., & Liu, Z. (1996). Quantitative study on spatial variation of soil erosion in a small watershed in the Loess Hilly Region. *Journal of Soil Erosion and Soil Conservation*, *2*, 1–9 (in Chinese).
- Jiang, C., Zhang, H., Zhang, Z., & Wang, D. (2019). Model-based assessment soil loss by wind and water erosion in China's Loess Plateau: Dynamic change, conservation effectiveness, and strategies for sustainable restoration. *Global and Planetary Change*, *172*, 396–413. <https://doi.org/10.1016/j.gloplacha.2018.11.002>.
- Lal, R. (2001). Soil degradation by erosion. *Land Degradation & Development*, *12*, 519–539. <https://doi.org/10.1002/ldr.472>.
- Lal, R. (2018). Accelerated Soil erosion as a source of atmospheric CO₂. In *Soil and tillage Research*. <https://doi.org/10.1016/j.still.2018.02.001>.
- Li, D., Fan, J., Zhang, X., Xu, X., He, N., Wen, X., et al. (2017a). Hydrolase kinetics to detect temperature-related changes in the rates of soil organic matter decomposition. *European Journal of Soil Biology*, *81*, 108–115. <https://doi.org/10.1016/j.ejsobi.2016.10.004>.
- Li, M., Li, Z., Liu, P., & Yao, W. (2005). Using cesium-137 technique to study the characteristics of different aspect of soil erosion in the wind-water erosion crisscross region on Loess Plateau of China. *Applied Radiation and Isotopes*, *62*, 109–113. <https://doi.org/10.1016/j.apradiso.2004.06.005>.
- Li, Z., Liu, C., Dong, Y., Chang, X., Nie, X., Liu, L., et al. (2017b). Response of soil organic carbon and nitrogen stocks to soil erosion and land use types in the Loess hilly-gully region of China. *Soil and Tillage Research*, *166*, 1–9. <https://doi.org/10.1016/j.still.2016.10.004>.
- Li, Z., Nie, X., He, J., Chang, X., Liu, C., Liu, L., et al. (2017c). Zonal characteristics of sediment-bound organic carbon loss during water erosion: A case study of four typical loess soils in shaanxi province. *Catena*, *156*, 393–400. <https://doi.org/10.1016/j.catena.2017.05.001>.
- Li, J., Okin, G. S., & Epstein, H. E. (2009b). Effects of enhanced wind erosion on surface soil texture and characteristics of windblown sediments. *Journal of Geophysical Research: Biogeosciences*, *114*, G02003. <https://doi.org/10.1029/2008JG000903>.
- Liu, B., Bi, X., & Fu, S. (2010). *Beijing soil loss equation*. Beijing: China Science Publishing & Media Ltd (in Chinese).
- Liu, R., Liu, J., Zhang, Z., Borthwick, A. G. L., Cai, Y., Dong, L., et al. (2018). Risks of airborne pollution accidents in a major conurbation: Case study of Zhangjiakou, a host city for the 2022 winter Olympics. *Stochastic Environmental Research and Risk Assessment*, *32*, 3257–3272. <https://doi.org/10.1007/s00477-018-1590-5>.
- Liu, B., Nearing, M. A., & Risse, L. M. (1994). Slope gradient effects on soil loss for steep slopes. *Transactions of the ASAE*, *37*, 1835–1840.
- Li, F., Zhao, W., Liu, J., & Huang, Z. (2009a). Degraded vegetation and wind erosion influence soil carbon, nitrogen and phosphorus accumulation in sandy grasslands. *Plant and Soil*, *317*, 79–92. <https://doi.org/10.1007/s11104-008-9789-8>.
- Nearing, M. A., Xie, Y., Liu, B., & Ye, Y. (2017). Natural and anthropogenic rates of soil erosion. *International Soil and Water Conservation Research*, *5*, 77–84. <https://doi.org/10.1016/j.iswcr.2017.04.001>.
- Parfitt, R. L., Baisden, W. T., Ross, C. W., Rosser, B. J., Schipper, L. A., & Barry, B. (2013). Influence of erosion and deposition on carbon and nitrogen accumulation in resampled steepland soils under pasture in New Zealand. *Geoderma*, *192*, 154–159. <https://doi.org/10.1016/j.geoderma.2012.08.006>.
- Qi, Y., Liu, J., Shi, H., Hu, Y., & Zhuang, D. (2008). Using 137Cs tracing technique to estimate wind erosion rates in the typical steppe region, northern Mongolian Plateau. *Science Bulletin*, *53*, 1423–1430. <https://doi.org/10.1007/s11434-008-0070-6>.
- Quinton, J. N., Govers, G., Van Oost, K., & Bardgett, R. D. (2010). The impact of agricultural soil erosion on biogeochemical cycling. *Nature Geoscience*, *3*, 311–314. <https://doi.org/10.1038/ngeo838>.
- Renard, K. G., & USA, U. S. A. (Eds.). (1997). *Predicting soil erosion by water: A guide to conservation planning with the revised universal soil loss equation (RUSLE)*. Washington, DC: Agriculture handbook.
- Ruiz-Colmenero, M., Bienes, R., Eldridge, D. J., & Marques, M. J. (2013). Vegetation cover reduces erosion and enhances soil organic carbon in a vineyard in the central Spain. *Catena*, *104*, 153–160. <https://doi.org/10.1016/j.catena.2012.11.007>.
- Shi, P., Yan, P., Yuan, Y., & Nearing, M. A. (2004). Wind erosion research in China: Past, present and future. *Progress in Physical Geography: Earth and Environment*, *28*, 366–386. <https://doi.org/10.1191/0309133304pp416ra>.
- Song, S., Zhang, S., Wang, T., Meng, J., Zhou, Y., & Zhang, H. (2018). Balancing conservation and development in winter olympic construction: Evidence from a multi-scale ecological suitability assessment. *Scientific Reports*, *8*. <https://doi.org/10.1038/s41598-018-32548-2>.
- Su, Z., Li, Y., Zhang, J., Xiong, D., Dong, Y., Zhang, S., et al. (2017). Spatial variation in soil, SOC, and total N redistribution on affected and non-affected slope terraces due to the 8.0 Wenchuan Earthquake in 2008 by using 137Cs technique. *Catena*, *155*, 191–199. <https://doi.org/10.1016/j.catena.2017.03.018>.
- Teng, H., Liang, Z., Chen, S., Liu, Y., Viscarra Rossel, R. A., Chappell, A., et al. (2018). Current and future assessments of soil erosion by water on the Tibetan Plateau based on RUSLE and CMIP5 climate models. *The Science of the Total Environment*, *635*, 673–686. <https://doi.org/10.1016/j.scitotenv.2018.04.146>.
- Tuo, D., Xu, M., & Gao, G. (2018). Relative contributions of wind and water erosion to total soil loss and its effect on soil properties in sloping croplands of the Chinese

- Loess Plateau. *The Science of the Total Environment*, 633, 1032–1040. <https://doi.org/10.1016/j.scitotenv.2018.03.237>.
- Tuo, D., Xu, M., Zhao, Y., & Gao, L. (2015). Interactions between wind and water erosion change sediment yield and particle distribution under simulated conditions. *Journal of Arid Land*, 7, 590–598. <https://doi.org/10.1007/s40333-015-0128-7>.
- Van Pelt, R. S., Hushmurodov, S. X., Baumhardt, R. L., Chappell, A., Nearing, M. A., Polyakov, V. O., et al. (2017). The reduction of partitioned wind and water erosion by conservation agriculture. *Catena*, 148, 160–167. <https://doi.org/10.1016/j.catena.2016.07.004>.
- Visser, S. M., & Sterk, G. (2007). Nutrient dynamics—wind and water erosion at the village scale in the Sahel. *Land Degradation & Development*, 18, 578–588. <https://doi.org/10.1002/ldr.800>.
- Visser, S. M., Sterk, G., & Ribolzi, O. (2004). Techniques for simultaneous quantification of wind and water erosion in semi-arid regions. *Journal of Arid Environments*, 59, 699–717. <https://doi.org/10.1016/j.jaridenv.2004.02.005>.
- Visser, S. M., Stroosnijder, L., & Chardon, W. J. (2005). Nutrient losses by wind and water, measurements and modelling. *Catena*, 63, 1–22. <https://doi.org/10.1016/j.catena.2005.07.003>.
- Wang, Y., Shao, M., Han, X., & Liu, Z. (2015). Spatial variability of soil parameters of the van Genuchten model at a regional scale: Spatial variability of soil parameters of the van Genuchten model. *Clean - Soil, Air, Water*, 43, 271–278. <https://doi.org/10.1002/clen.201300903>.
- Wang, W., Wang, Y., Sun, Q., Zhang, M., Qiang, Y., & Liu, M. (2018a). Spatial variation of saturated hydraulic conductivity of a loess slope in the South Jingyang Plateau, China. *Engineering Geology*, 236, 70–78. <https://doi.org/10.1016/j.enggeo.2017.08.002>.
- Wang, Y., Wu, Y., Lu, R., & Pan, M. (2018c). Application of Empirical Orthogonal Function (EOF) method to detect the spatial grain-size fractionation of aeolian sediment and comparison with other methods in case studies from northwestern China. *Physical Geography*, 39, 216–229. <https://doi.org/10.1080/02723646.2017.1361777>.
- Wang, X., Yoo, K., Mudd, S. M., Weinman, B., Gutknecht, J., & Gabet, E. J. (2018b). Storage and export of soil carbon and mineral surface area along an erosional gradient in the Sierra Nevada, California. *Geoderma*, 321, 151–163. <https://doi.org/10.1016/j.geoderma.2018.02.008>.
- Wei, W., Chen, L., Fu, B., Lü, Y., & Gong, J. (2009). Responses of water erosion to rainfall extremes and vegetation types in a loess semiarid hilly area, NW China. *Hydrological Processes*, 23, 1780–1791. <https://doi.org/10.1002/hyp.7294>.
- Wischmeier, W., & Smith, D. (1978). *Predicting rainfall erosion losses—a guide to conservation planning*. U.S. Department of Agriculture, Agriculture Handbook No.537.
- Wu, Y., Ouyang, W., Hao, Z., Lin, C., Liu, H., & Wang, Y. (2018). Assessment of soil erosion characteristics in response to temperature and precipitation in a freeze-thaw watershed. *Geoderma*, 328, 56–65. <https://doi.org/10.1016/j.geoderma.2018.05.007>.
- Yan, P., Dong, G., Zhang, X., & Zhang, Y. (2000). Preliminary results of the study on wind erosion in the Qinghai-Tibetan Plateau using ¹³⁷Cs technique. *Chinese Science Bulletin*, 45, 1019–1025. <https://doi.org/10.1007/BF02884984>.
- Yan, P., Dong, G., Zhang, X., & Zou, X. (2003). Application of caesium-137 technique on wind erosion in gonghe basin, qinghai province. *Journal of Desert Research*, 23, 268–275 (in Chinese).
- Yan, H., Wang, S., Wang, C., Zhang, G., & Patel, N. (2005). Losses of soil organic carbon under wind erosion in China. *Global Change Biology*, 11, 828–840. <https://doi.org/10.1111/j.1365-2486.2005.00950.x>.
- Yan, Y., Xin, X., Xu, X., Wang, X., Yang, G., Yan, R., et al. (2013). Quantitative effects of wind erosion on the soil texture and soil nutrients under different vegetation coverage in a semiarid steppe of northern China. *Plant and Soil*, 369, 585–598. <https://doi.org/10.1007/s11104-013-1606-3>.
- Yuan, J., Niu, Z., & Wang, C. (2006). Vegetation NPP distribution based on MODIS data and CASA model—a case study of northern Hebei Province. *Chinese Geographical Science*, 16, 334–341. <https://doi.org/10.1007/s11769-006-0334-5>.
- Zhang, G., Chan, K., Oates, A., Heenan, D., & Huang, G. (2007b). Relationship between soil structure and runoff/soil loss after 24 years of conservation tillage. *Soil and Tillage Research*, 92, 122–128. <https://doi.org/10.1016/j.still.2006.01.006>.
- Zhang, H., Fan, J., Cao, W., Harris, W., Li, Y., Chi, W., et al. (2018). Response of wind erosion dynamics to climate change and human activity in Inner Mongolia, China during 1990 to 2015. *The Science of the Total Environment*, 639, 1038–1050. <https://doi.org/10.1016/j.scitotenv.2018.05.082>.
- Zhang, W., & Fu, J. (2003). Rainfall erosivity estimation under different rainfall amount. *Resources Science*, 25(1), 35–42 (in Chinese).
- Zhang, Y., Nearing, M. A., Liu, B. Y., Van Pelt, R. S., Stone, J. J., Wei, H., et al. (2011b). Comparative rates of wind versus water erosion from a small semiarid watershed in southern Arizona, USA. *Aeolian Research*, 3, 197–204. <https://doi.org/10.1016/j.aeolia.2011.03.006>.
- Zhang, C., Yang, S., Pan, X., & Zhang, J. (2011a). Estimation of farmland soil wind erosion using RTK GPS measurements and the ¹³⁷Cs technique: A case study in Kangbao county, Hebei province, northern China. *Soil and Tillage Research*, 112, 140–148. <https://doi.org/10.1016/j.still.2010.12.003>.
- Zhang, J., Zhang, C., Chang, C., Wang, R., & Liu, G. (2017). Comparison of wind erosion based on measurements and SWEEP simulation: A case study in Kangbao county, Hebei province, China. *Soil and Tillage Research*, 165, 169–180. <https://doi.org/10.1016/j.still.2016.08.006>.
- Zhang, C., Zou, X., Yang, P., Dong, Y., Li, S., Wei, X., et al. (2007a). Wind tunnel test and ¹³⁷Cs tracing study on wind erosion of several soils in Tibet. *Soil and Tillage Research*, 94, 269–282. <https://doi.org/10.1016/j.still.2006.08.002>.
- Zhao, J., Yang, Z., & Govers, G. (2019). Soil and water conservation measures reduce soil and water losses in China but not down to background levels: Evidence from erosion plot data. *Geoderma*, 337, 729–741. <https://doi.org/10.1016/j.geoderma.2018.10.023>.
- Zhao, Y., Yan, D., Zhang, Q., Zhan, J., & Hu, H. (2012). Spatial distributions of ¹³⁷Cs in surface soil in jing-jin-ji region, north China. *Journal of Environmental Radioactivity*, 113, 1–7. <https://doi.org/10.1016/j.jenvrad.2012.04.005>.
- Zou, X., Li, J., Cheng, H., Wang, J., Zhang, C., Kang, L., et al. (2018). Spatial variation of topsoil features in soil wind erosion areas of northern China. *Catena*, 167, 429–439. <https://doi.org/10.1016/j.catena.2018.05.022>.



Contents lists available at ScienceDirect

International Soil and Water Conservation Research

journal homepage: www.elsevier.com/locate/iswcr

Original Research Article

Can integrated watershed management reduce soil erosion and improve livelihoods? A study from northern Ethiopia

Kassa Teka^{a, *}, Mulu Haftu^b, Madelene Ostwald^{c, d}, Christel Cederberg^d^a Department of Land Resources Management and Environmental Protection, Mekelle University, Ethiopia^b Wukro St.Mary's Institute, Wukro, Tigray, Ethiopia^c Centre for Climate Science and Policy Research, Department of Thematic Studies/Environmental Change, Linköping University, Sweden^d Department of Space, Earth and Environment, Physical Resource Theory, Chalmers University of Technology, Sweden

ARTICLE INFO

Article history:

Received 7 October 2019

Received in revised form

19 June 2020

Accepted 28 June 2020

Available online 9 July 2020

Keywords:

Soil loss

Crop productivity

Water availability

Feed availability

Household income

ABSTRACT

The study aimed at evaluating the impact of integrated watershed management on reducing soil erosion and changes in the livelihoods of rural farming households in Ethiopia. The changes in soil erosion for the years between 2002 and 2015 were estimated using the Revised Universal Soil Loss Equation model, while the impacts on livelihoods were assessed by household interviews. During the study period, the overall average annual soil loss was halved. Furthermore, crop productivity, water availability (irrigation and domestic) and fodder availability increased by 22, 33 and 10%, respectively, while an increase in household income (by 56%) was observed. Moreover, 72% of the sampled households were able to cover their 12-month annual expenditure demands in 2015, while only 50% of the households were able to cover these demands in 2002. It can be concluded that the implemented integrated watershed management activities seemingly resulted in reduced soil loss, enhanced vegetation cover, and additional household income. This paper also elaborates on the hurdles for integrated watershed management expansion.

© 2020 International Research and Training Center on Erosion and Sedimentation and China Water and Power Press. Production and Hosting by Elsevier B.V. This is an open access article under the CC BY-NC-ND license (<http://creativecommons.org/licenses/by-nc-nd/4.0/>).

1. Introduction

Land degradation has been widely recognized as a major problem that threatens food production around the world (Lambin et al., 2000; Pimentel & Burgess, 2013). Among the major causes of land degradation are unsustainable land use practices and the removal of natural vegetation (Lambin et al., 2000). These changes have important environmental consequences through their impacts on soil and water quality and biodiversity (Lambin et al., 2000; Pimentel & Burgess, 2013; Smith et al., 2013).

Several experiments have demonstrated a rapid decline in soil chemical and physical properties following deforestation and intensive cultivation leading to accelerated soil erosion, a deteriorating soil nutrient status, and declining soil productivity (Iticha et al., 2016). The loss of agricultural land as a result of erosion often results in the transformation of natural ecosystems into new cultivated land and grassland, and the need for additional fertilizer

inputs (Pimentel & Burgess, 2013).

The minimum estimated annual cost of land degradation (excluding downstream effects, such as flooding) in Ethiopia is 3% of the agricultural gross domestic product (World Bank, 2012). Land degradation also leads to increased social problems, such as impoverishment, declining productivity, chronic food insecurity, seasonal malnutrition and famines (Yaro et al., 2015).

In response to the negative impacts of land degradation, the Government of Ethiopia, NGOs and communities have implemented environmental rehabilitation activities, such as soil and water conservation measures, exclosures (no human and livestock interference) and water harvesting structures at the watershed scale, which is called integrated watershed management (IWM) (Gebregziabher et al., 2016; Haregeweyn et al., 2012; Yaebyo et al., 2015). Watershed refers to a sub-drainage area of a major river basin (Gebregziabher et al., 2016), whereas IWM is a continuous adaptive process of managing human activities and ecosystems at the watershed scale (CCME, 2016, p. 27). Hence, until 2014, the total area delineated and treated with integrated watershed management activities in the Tigray region was 12,425,869 ha (BoARD, 2016).

* Corresponding author.

E-mail address: kassateka2012@gmail.com (K. Teka).

The integrated watershed management (IWM) approach, in Tigray (northern Ethiopia), was initiated in 1997 in collaboration with the Irish development co-operation programme (Irish Aid) (Chisholm & Tassew, 2012). The programme had six major objectives (GIZ, 2015, p. 236): (i) improve food and cash crop production for food security, (ii) improve soil and water conservation, soil fertility and land management using appropriate biological and physical measures and agricultural inputs, (iii) improve multiple water supplies for domestic, livestock and irrigation purposes, (iv) increase household incomes by diversifying agricultural and non-agricultural activities, (v) empower communities' sustainable development of local resources, and (vi) integrate community priorities by community-based health education, hygiene and sanitation, and savings, as well as to increase the status of women and girls in the target communities.

Researchers (e.g., Descheemaeker et al., 2006; Gebremichael et al., 2005; Herweg & Ludi, 1999) have evaluated the impact of different integrated watershed management practices (e.g. exclosures and stone bunds) on soil erosion and run-off reduction separately. However, any positive or negative impact at the watershed level is the cumulative effect of all the activities in the watershed (Chiang et al., 2012). In the Tigray highlands, the establishment of exclosures has become an important measure to combat land degradation (Descheemaeker et al., 2006) and is estimated to cause mean soil loss reduction rates between 26 and 123 ton ha⁻¹y⁻¹ as the result of reduced runoff volume and speed. According to Herweg and Ludi (1999), reductions in runoff varied between 10 and 60% due to soil and water conservation measures. Based on measurements on 202 plots, Gebremichael et al. (2005) found that the introduction of stone bunds in Tigray decreased soil erosion by 68%. However, the impact of the IWM implementations on the livelihood of beneficiary rural households had been less documented. Therefore, our aims are to i) map the changes in soil loss and ii) assess the land-based livelihood of households for the years 2002 (before IWM) and 2015 (after IWM).

2. Materials and methods

2.1. Study area

The study was conducted at Gule Watershed, Tigray regional state (Fig. 1). The total watershed area is 1382 ha, with a landscape consisting of rugged hills, high plateaus and valleys. The altitude ranges from 2001 to 2460 m above sea level (m asl). The agroecology of the watershed, based on the traditional classification (Hurni et al., 2016, p. 134), is Woina Dega to 84% (midland, dry-warm, elevation between 1500 and 2300 m asl) and Dega to 16% (highland, dry-cold, elevation between 2301 and 3200 m asl). The climate is semi-arid and characterized by erratic rainfall (a mean annual rainfall of 550 mm) and a mean annual temperature ranging from 17 °C (night) to 23 °C (day) between the years 1992 and 2015 (data obtained from the Ethiopian Meteorological Agency, Mekelle branch). Approximately 86% of the annual precipitation falls in the main rainy season (June to September), while 14% falls in the short rain season (February to May). The mean annual potential and actual evapotranspiration, computed using Thornthwaite soil-water balance model (Dunne & Leopold, 1978, p. 818), were found to be 833 mm and 406 mm, respectively (Negusse et al., 2013).

The watershed consists of Gule Village, which has a human population of 4373 individuals (800 households) (Kilte-Awlaelo District OoARD, 2014). The households earn their living from agricultural activities, mainly crop and animal husbandry. Although rainfed practices dominate, the use of small scale irrigation has grown since the last two decades. The average land holding is less

than 1 ha per family, 0.6 ha (min 0.2, max 1 ha), and is characterized by traditional technology based entirely on animal traction (Kilte-Awlaelo District OoARD, 2014). The major soils are Leptosols (38%), Regosols (42%), Cambisols (12%) and Fluvisols (8%).

2.2. Implemented IWM activities

IWM activities were implemented by the Ethiopian Catholic Church Diocese of Adigrat Wukro St. Mary's College, with technical collaboration with the local government and beneficiaries who reside in the watershed. The project implementation was also supported by the district's Productive Safety Net Program (PSNP) and the annual soil and water conservation campaign. The key activities include i) physical and biological conservation measures in all land use types (Table 1); ii) water harvesting structures (2 percolation ponds, 3 deep trenches, and 3 cemented gabion (wire basket) check dams) on hill sides; iii) integrated soil fertility management activities (plantation of 20500 trees for agroforestry, and compost production) on farm lands; iv) fuel-saving technologies (672 fuel-saving stoves); v) capacity building of development agents, experts and model farmers (on improved soil and water conservation and management); vi) introduction of livestock (6–12 local sheep breeds per household) and chicken (12 chickens per household) for 672 households.

The tree seedlings and cuttings were planted on hillsides, across gullies and on farmers' fields. Approximately 407 ha of land was rehabilitated and treated by the project, benefitting 615 households (77% of the total). Exclosures, rehabilitating degraded lands through closed areas (Descheemaeker et al., 2006), were introduced. Moreover, community bylaws (i.e., regulations devised by communities) were developed to sustain the exclosures, a common strategy in areas where exclosures are introduced (Yami et al., 2013).

During the project period, soil fertility improvement was the central issue, primarily through agroforestry tree plantation (13325 trees on farmlands and 7175 trees on grazing land), compost preparation, and chemical fertilizer distribution and application. The major agroforestry and multi-purpose trees planted in both farm and grazing lands are *Fehiderbia albida*, *Leucaena leucocephala*, *Sesbania sesban* and *Rhamnus prinoides*. Di-ammonium phosphate (100 kg ha⁻¹) and urea (50 kg ha⁻¹) were the synthetic fertilizer types used in most parts of Tigray (FAO, 2002). In addition to agroforestry and multi-purpose tree planting, grass species such as *elephant grass* (*Pennisetum purpureum*), *vetiver grass* (*Chrysopogon zizanioides*), *desho grass* (*Pennisetum pedicellatum*) and *local bamboo* are planted in gullies and grazing lands. To sustain the agroforestry tree plantation and to further strengthen the adaptation of households to climate anomalies, a zero-grazing approach, in which livestock are tethered at the homestead and fed by a cut-and-carry system (Reda, 2014), was introduced.

2.3. Study method

2.3.1. Soil erosion change assessment

For the assessment of soil erosion rates, the Revised Universal Soil Loss Equation (RUSLE) was used for both years (2002 and 2015). The RUSLE assesses the long-term average soil erosion rate per unit area for inter-rill and rill erosion, expressed in ton ha⁻¹y⁻¹ (Wischmeier & Smith, 1978, p. 58). The RUSLE was selected because of its simplicity, but the model has shortcomings since it accounts for rill and inter-rill erosion processes but does not take into account the processes of gully erosion, land sliding and deposition; in fact, no regional scale model considers these processes. Hence, soil erosion by gully, tillage and landslide was not estimated. The RUSLE is a multiplicative model of six factors (eq (1)).

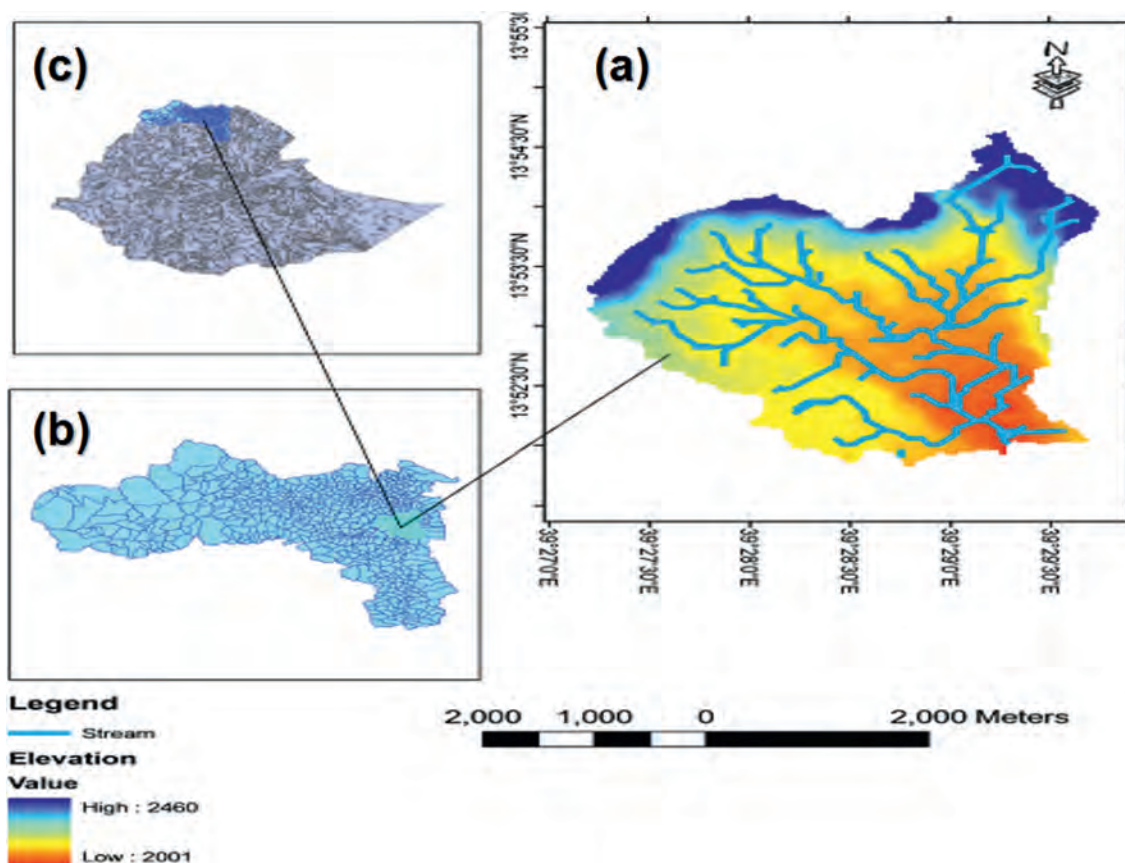


Fig. 1. Location of the Gule Watershed (a) in Tigray (b) and Ethiopia (c) (Source: own map).

Table 1
Implemented soil and water conservation measures.

Physical measures	Unit	Quantity
Gabion check dams	M ³	1564
Loose stone check dams	M ³	11,908
Retention wall	M ³	570
Gully reshaping	M ³	600
Hillside bench terraces	Metre	6394
Bench terraces	Metre	10,931
Tree and cutting seedling plantation	Number	107,270
Percolation pond	M ³	750

Source: own survey (2015)

$$A = R * K * L * S * C * P \quad (1)$$

where A = the average annual soil loss (in ton ha⁻¹y⁻¹).

R = the rainfall and runoff erosivity (in mega joule (MJ) mm⁻¹ha⁻¹hour⁻¹y⁻¹),

K = the soil erodibility factor (in ton hour MJ⁻¹mm⁻¹),

LS = the topographical factor (dimensionless), with L as the slope length factor and S as the slope gradient factor,

C = cover management/land cover factor (dimensionless), and

P = support practices/management factor (dimensionless).

The R factor is assessed if information on the rainfall intensity and its associated kinetic energy is available (Petkovš and Mikoš, 2004). However, due to limited data for the area, the most applicable equation used in northern Ethiopia by Nyssen et al. (2009) (eq (2)) was used.

$$R = 0.562 * Pr - 8.12 \quad (2)$$

Where Pr = the annual precipitation (in mm).

Four meteorological stations (Wukro, Hawzen, Senkata and Hagerselam) from around the watershed were used to calculate the rainfall erosivity factor (R value). The monthly precipitation (1992–2015) was collected from the National Meteorology Agency of Ethiopia (Mekelle Branch). The annual precipitation surface was interpolated using hybrid regression Kriging interpolation, which gives cell-based values for the area. This technique is found to be the optimal interpolation method for complex terrains (Yao et al., 2013).

The K factor that describes the soil erodibility for different soil types (Wischmeier & Smith, 1978, p. 58) (Table 2) was adapted from FAO (1989). The soil reference groups of the study watershed were adapted from Rabia et al. (2013) and developed for the district.

The topographic (LS) factor, which is a combined factor of the slope gradient and slope length (Wischmeier & Smith, 1978, p. 58), was calculated using a raster calculator following equation (3). The values for the slope length and the slope gradient were derived

Table 2
Soil erodibility (K) and Crop factor (C) values used in our RUSLE assessment.

Soil type	K-value	Land use type	C-value	Source
Lithic Leptosols	0.1	Bare soil	0.6	BCEOM (1998)
Vertic Cambisols	0.2	Cropland	0.14	Nyssen et al. (2009)
Eutric Fluvisols	0.15	Bare soil	0.6	BCEOM (998)
Eutric Regosols	0.15	Cropland	0.14	Nyssen et al. (2009)

Source: FAO (1989). Reconnaissance physical land evaluation in Ethiopia

from Aster DEM (Digital Elevation Model), with a pixel resolution of 30×30 m, one of the vital inputs required for soil erosion modelling (Ganasri & Gowda, 2016).

conducted in the months between February and May 2015. Finally, the collected data were analysed using descriptive statistical method.

$$LS = \text{Power}(\text{Flow accumulation} * \text{Cell resolution} / 22.1, 0.4) * \text{Power}(\text{Sin}(\text{slope}_{\text{DEM}} * 0.01745) / 0.09, 1.4) * 1.4 \quad (3)$$

The C-factor value, the ratio of soil loss from an area with a specified cover and management to soil loss from an identical area in a tilled, continuous fallow (Pierce et al., 1984), for each land use type (Table 2) was taken from the works of BCEOM (1998), Eweg et al. (1998) and Nyssen et al. (2009).

The land use types in the years 2002 and 2015 were delineated from TM (Thematic Mapper) and ETM⁺ (Enhanced Thematic Mapper Plus), respectively (pixel resolution 30×30 m). Both images were taken in January after the rainfed crop harvest to avoid confusion between cropland and grassland. The images were enhanced radiometrically and spectrally in ERDAS Imagine 9.3. The different temporal images were cross-referenced with ground truth (102 points) and other ancillary data to make the classification as accurate as possible. An overall land use classification accuracy of 82% was estimated for the year 2015 (Congalton, 1991).

The P factor was assessed on the basis of Table 3 (Nyssen et al., 2008). The activities implemented in the watershed were recorded from a field survey with the help of 102 ground control points and secondary documents.

Finally, by multiplying the different RUSLE-factors described above, the mean annual soil erosion values were determined for each land unit, land use type and slope class for both study years. For a better visual understanding of these quantities, RUSLE values were grouped into five classes of soil erosion risks in accordance with Singh and Phadke (2006) (Table 3).

2.3.2. Livelihood change assessment

The changes in livelihood (water availability, land productivity, and farm and off-farm income) were assessed through semi-structured questionnaires provided to farmers and by the use of secondary sources (reports and CSA, 2008 census documents to cross check the accuracy of the primary data) covering the years 2002 and 2015. As there were no adequate baseline data for the year 2002, an event calendar (a locally known incidences such as the occurrence of extreme drought and the introduction of water harvesting household ponds locally known as 'Horeye' in the area) was developed in consultation with key informants and used in the interviews. This method was found to be an appropriate method in areas where baseline data were absent (e.g., Nyssen et al., 2006; Showers, 1996). The sample size used was 269 households (167 men-headed and 102 women-headed), determined based on the recommendation of Yemane (1967). The interviews were

3. Results

3.1. Erosion assessment results

The present IWM interventions resulted in an overall soil loss reduction for the whole area (1382 ha), with an average loss of 29 ton ha⁻¹y⁻¹ in 2002 and an average loss of 14 ton ha⁻¹y⁻¹ in 2015 (Fig. 2 and Table 4). The area covered by physical land management interventions (mainly stone and soil bunds) almost doubled, increasing from 15% to 29% during the study period. This could be due to the fact that these structures led to reduced slope length and, therefore, most likely reduced erosion, and they increased soil depth and moisture with time (Wischmeier & Smith, 1978, p. 58).

There is also a change in erosion rate as the result of change in land use. The major land use types and their percent area coverage for the year 2002 were grassland (2%), bush land (13%), bare land (23%) and cultivated land (62%), while the major land use types for the year 2015 were grassland (6%), bush land (23%), bare land (7%) and cultivated land (64%) (Fig. 3 and Table 5).

Even though there is a reduction in soil loss for all land use types, the soil loss rate in the watershed is still high (14 tons ha⁻¹y⁻¹). Moreover, soil loss rates show strong variations in the watershed, which is more associated with the variations in topography and soils types. The overall annual soil loss at the watershed in both years varied between 2 tons ha⁻¹y⁻¹ at the foot slope to 57 tons ha⁻¹y⁻¹ at the hill slope (Fig. 3 and Table 4). The watershed is dominated by slopes greater than 5% (76% area), followed by 3–5% (20% area), 1–3% (4% area) and 0–1% (0.6% area). Predominant unstable and shallow soil types, such as Leptosols and Regosols, are found on the steep slopes.

3.2. Livelihood changes assessment results

3.2.1. Changes in irrigation and water development

As part of the IWM intervention, new shallow ground waters have emerged, and the water levels of previously existing ground waters have increased by an average of 1 m. At the low part of the watershed, 14 water supply schemes (9 household ponds and 5 shallow wells) were developed for domestic purposes, and 29 hand-dug wells were developed to irrigate 18.6 ha (Fig. 4). In addition to the irrigated area development, a majority (57%) of the sampled households reported that the distance to water points from the homesteads decreased from an average of 1.5 km in 2002

Table 3
Management (P) factor values and soil loss classes.

Quality of stone and soil bunds ^a	P for non-arable land	P for arable land	Soil loss description ^b	Soil loss range (ton/ha/y) ^a
None	1	0.90	Very slight	0–5
Remains	0.8	0.72	Slight	5–10
Poor	0.6	0.54	Moderate	10–25
Moderate	0.4	0.36	Severe	25–45
Good	0.2	0.18	Very severe	≥45

^a Values & descriptions adapted from Nyssen et al. (2008).

^b From Singh and Phadke (2006).

Table 4
Soil loss changes in the study watershed.

Class of Soil loss	Soil Loss ton/ha/y	2002		2015		Soil loss change	
		Area (ha)	%	Area (ha)	%	ha	%
Very Slight	0–5	82	5.9	227.1	16.4	+145.1	+10.5%
Slight	5–10	425	30.8	395.8	28.6	–29.2	–2.1
Moderate	10–25	488	35.3	393.4	28.5	–94.6	–6.8
Severe	25–45	285	20.6	293.6	21.3	+8.6	+0.7
Very Severe	45–56.87	102.1	7.4	71.5	5.2	–30.6	–2.2
Total		1381.59		1381.6			

Source: own survey (2015)

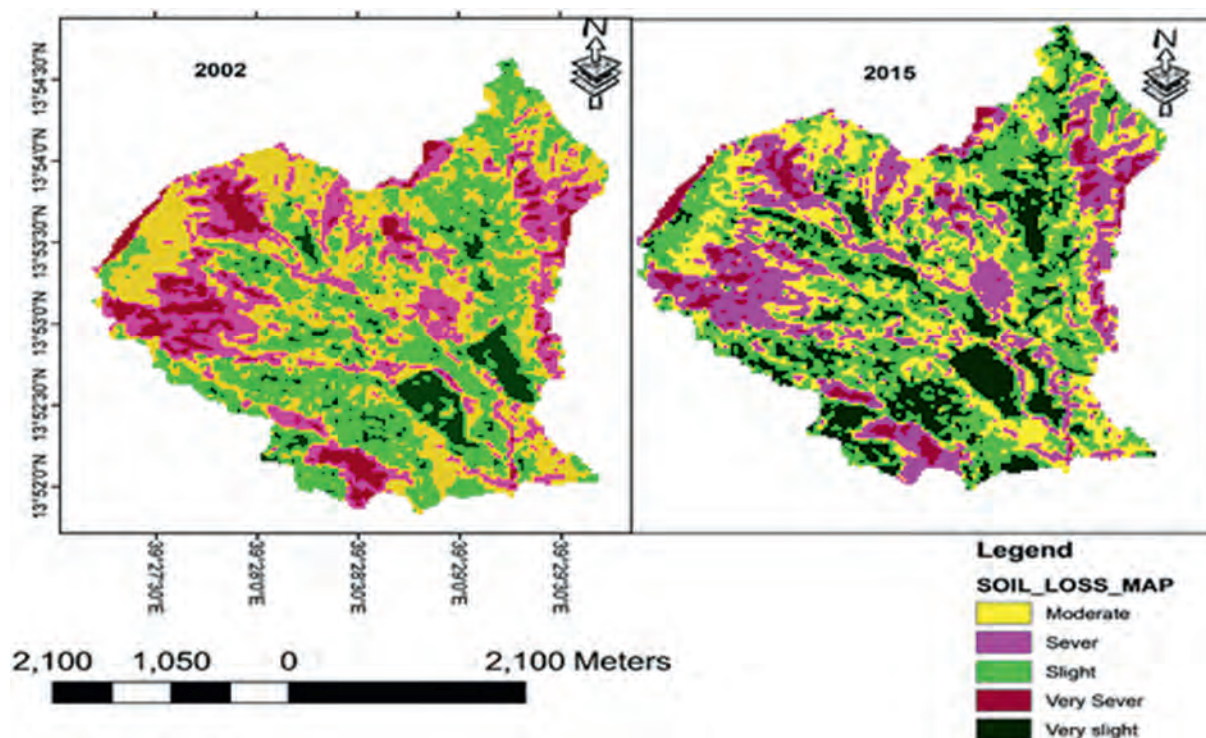


Fig. 2. Soil erosion maps from the RUSLE assessment before and after the IWM introduction (see soil loss rates in Table 4) (Source: own map).

to an average of 1 km in 2015 as new water sources emerged. The domestic water distribution per head also increased from 10 to 25 L per day. Moreover, respondents perceived the water quality and health conditions had improved; the number of households with toilets increased by 188 households, and hand washing facilities were established in 195 households.

3.2.2. Changes in fruit, vegetable and grain crop production

Approximately 47% of the households grew some kind of fruit or vegetable crops in 2015, which did not exist in 2002. Cereal crop productivity also increased in 2015 compared to 2002. The average yield for the dominant crops increased from 1.8 to 2.2 tons ha⁻¹ (Table 6). The yield of *Eragrostis tef*, *Sorghum bicolor* and *Zea mays* increased by 62, 61 and 27%, respectively.

3.2.3. Changes in livestock production

From 2002 to 2015, the availability of animal feed increased by 33% compared to the baseline survey in the area. Milk production from local cows increased from 1.5 to 2.5 L per day. While the number of oxen increased by 4% and the number of bee colonies increased by 8%. Only 7% of the produced honey went to the family for direct consumption, while the remaining amount went to the market.

3.2.4. Changes in household income and expenditures

Crops, livestock and their products and off-farm activities are the main sources of household income in the watershed. The responses of the sampled households indicate that the household income improved by 62% since the IWM interventions. Hence, a majority of the respondents (72%) were able to cover their annual expenditure demands in 2015; in contrast, before the IWM activities, only approximately 50% were able to cover these demands. Furthermore, the capacity of the households to cover school expenses and purchase medicine, farm inputs, farm equipment, clothes, livestock, communication facilities such as radios, and additional food items to diversify their food consumption increased (Table 7). Hence, the number of student dropouts was reduced by 34%, and youth migration was reduced by 47%. The Ethiopian Youth Policy defines youth as to include part of the society who are between 15 and 29 years (Broussard & Tekleselassie, 2012).

4. Discussions

4.1. Erosion assessment

As shown in Fig. 3, the mean annual soil loss rate at the watershed for the year 2002 was within the severe soil loss range

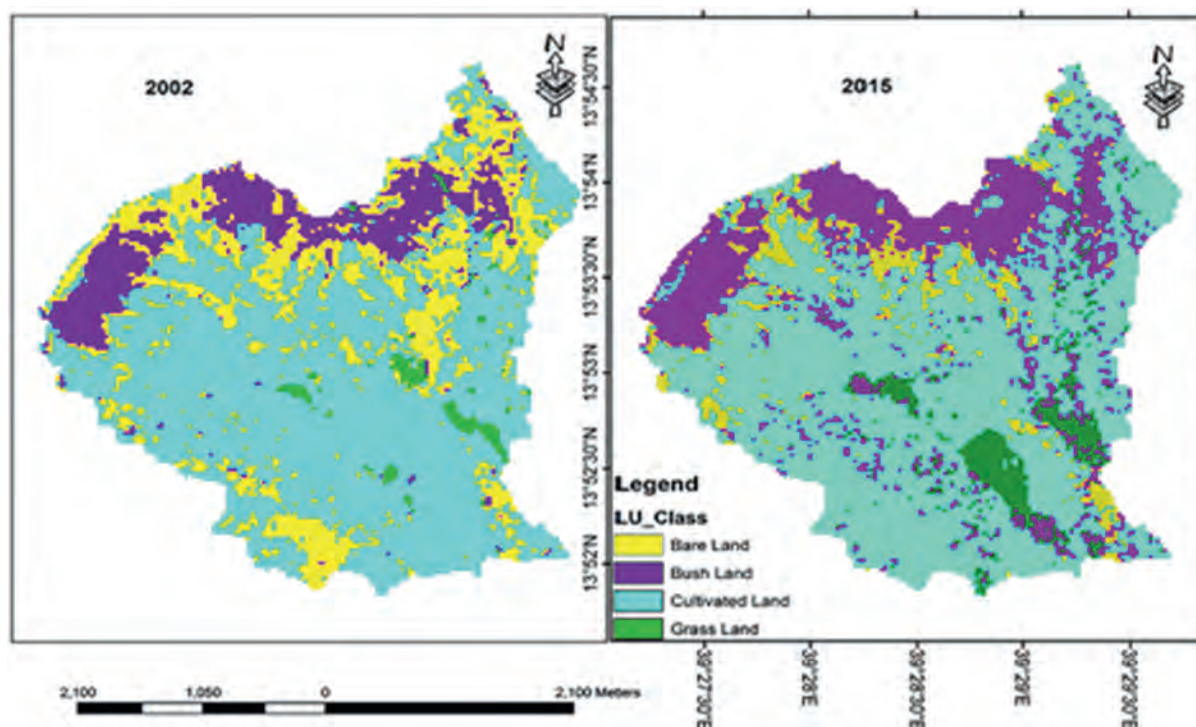


Fig. 3. Land use maps for the years 2002 and 2015 based on Landsat data (see area % in the text) (Source: own map).

Table 5

Soil loss affected by land use.

Land use class	2002		2015	
	Ha	ton/ha/y	ha	ton/ha/y
Grass land	24	4.3	85	3.1
Bush land	182	22.2	312	9.8
Bare land	322	56.8	99	47.4
Cropland	854	20.6	886	12.8
Overall		29		14

Source: own survey (2015)

(25–45 $\text{ton ha}^{-1}\text{y}^{-1}$), while it was reduced to the moderate soil loss range (10–25 $\text{ton ha}^{-1}\text{y}^{-1}$) in the year 2015. These numbers are still high compared to the maximum tolerable soil loss level (18 $\text{ton ha}^{-1}\text{y}^{-1}$) set for Ethiopia (Hurni, 1985) but lower than the findings of Gessesse et al. (2015) for the Modjo watershed and Senti et al. (2014) for the Haramaya Catchment (Ethiopia), where, for both places, a mean annual soil loss rate of 24 $\text{ton ha}^{-1}\text{y}^{-1}$ was found. Soil formation rate, confined to in situ formation, for the highlands of Ethiopia including the study area was estimated to be from 2 to 22 $\text{ton ha}^{-1}\text{y}^{-1}$ (FAO, 1986, p. 354). Another study by Boj6 and Cassells (1995, p. 56) based on soil formation rates estimated by Hurni and using a rule of thumb on soil depth, reported soil formation rates of 3–7 tons per hectare per year, well below the estimated loss rates. However, these values fall within the extreme range (16–300 $\text{tons ha}^{-1}\text{y}^{-1}$) reported by EHRS (1986) in Ethiopia.

The high soil erosion rate in the area is related to the steep slopes and area of bare land on the steep slopes, which contributed to the highest erosion rate, approximately 57 $\text{tons ha}^{-1}\text{y}^{-1}$. The dominance of steeper slopes, which represent 76% of the watershed, implies the existence of a large erosion-prone area. Hence, the limited number of physical structures along the contours led to significant losses of soil (Hurni, 1985; Wischmeier & Smith, 1978, p. 58), which cannot be sufficiently stopped by various land covers (e.g., scrubs).

The erosion reduction is most likely highly related to changes in land use due to the IWM interventions. All land use types showed an increase in area, with the exception of bare land (Fig. 2). The increase in vegetation cover might be due to increased onsite soil depth and soil moisture as a result of the interventions and the enclosures (Teka, 2017). The increase in cultivated land might also be due to the implemented bench terraces. A similar study in Eastern Tigray (Teka et al., 2015) indicated that, on some of the rangelands, there are abandoned to enclosures in which shrubs and bushes are allowed to regenerate. Hence, the increase in vegetation cover at the expense of a reduction in the rangeland area implies reduced erosion (Teka, 2017; Wischmeier & Smith, 1978, p. 58).

The assessed physical soil and water conservation structures (e.g., stone terraces and soil bunds) implemented in each land use type revealed that the area of these structures increased with time, implying reduced erosion (Brhane and Mekonen, 2009; Teka, 2017; Wischmeier & Smith, 1978, p. 58). By 2015, the constructed check dams were filled with sediments, and the degraded gullies had become more productive. An experimental study in the watershed (WAHARA, 2015 unpublished report) showed that surface runoff was reduced by 50%. This is very high compared to the findings of Haregeweyn et al. (2012), who estimated a runoff reduction of 27% for southern Tigray. Suspended sediment measurements in streams during the rainy season (WAHARA, 2015) indicated that sediment concentrations were dramatically reduced from 30 g/L (before the intervention) to less than 5 g/L (after the intervention).

4.2. Livelihood changes assessment

4.2.1. Changes in irrigation and water development

In 2015, the inhabitants experienced favourable results, such as improvements in the groundwater levels. Similarly, a groundwater level increase of approximately 5 m was also reported in Abraha–Atsbaha Watershed, northern Ethiopia (Gebregziabher et al., 2016). Negusse et al. (2013) also reported an approximately 10

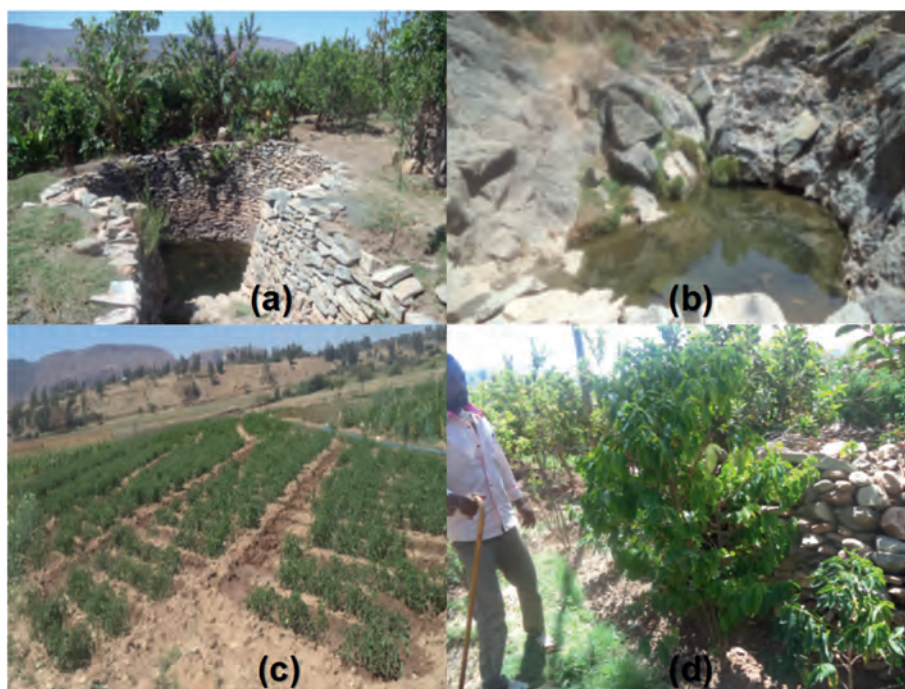


Fig. 4. Shallow irrigation well (a), spring (b), irrigated vegetables (c) and fruits (d) (Source: own map).

Table 6

Change in crop productivity in the study watershed.

Crop type	HH size (n)	Crop productivity (ton ha ⁻¹)		Change (ton ha ⁻¹)
		Before	After	
Wheat (<i>Triticumaestivum</i>)	240	2.1	2.4	0.3
Teff (<i>Eragrostistef</i>)	238	1.4	1.5	0.1
Maize (<i>Zea mays</i>)	168	3.1	4.8	1.7
Barley (<i>Hordeum vulgare</i>)	157	1.7	2.0	0.3
Sorghum (<i>Sorghum bicolor</i>)	168	2.1	2.2	0.1
Beans (<i>Phaseolus vulgaris</i>)	160	1.6	1.7	0.1
Peas (<i>Pisum sativum</i>)	158	1.3	1.5	0.2
Lentils (<i>Lens culinaris</i>)	119	1.2	1.3	0.1
Finger millet (<i>Eleusine coracana</i>)	240	1.7	2.2	0.5
Chick pea (<i>Cicer arietinum</i>)	178	1.7	1.8	0.1
Average	183	1.8	2.2	0.4

HH = household size, n = number; Source: own survey (2015).

Table 7

Number of HHs and their perception on household expenditures before and after the interventions.

Expenditure Item	HH response to improvement after IWM		
	Yes (n)	No (n)	Change (%)
Purchasing capacity of agricultural inputs and equipment	178	91	66
House improvements	121	148	45
Purchasing capacity of medicine or drugs	179	90	67
Purchasing capacity of household equipment	187	82	70
Purchasing capacity of clothes	178	91	66
Purchasing capacity of animals	164	105	61
Purchasing capacity of radios	164	105	61
Purchasing capacity of crops for consumption	161	108	60
Capacity to pay school fees and expenses	202	67	75
Capacity to rent farm land	144	125	54
Savings in banks	165	104	61

HH = household size, n = number, change (%) = proportion of people responded to change; Source: own survey (2015).

times increase in the groundwater level of Abraha–Atsbaha since 1993. According to these authors, the volume of water that percolated down and joined the groundwater increased from 84,029 m³

(which is 1.4% of the mean annual rainfall of the catchment before the intervention) to 652,375 m³ which is 11.1% of the mean annual rainfall of the catchment after the intervention).

The increase in groundwater can be related to the improved soil moisture, run-off and groundwater recharge resulting from IWM interventions (Descheemaeker et al., 2009). Upstream IWM interventions have the potential to alter infiltration into the ground. These interventions can also have an impact on lowering the dry period for wells (Nerkar et al., 2014), leading to an enhanced irrigation capacity of these wells.

The increase in the groundwater level and the emergence of new water sources helped the introduction of irrigation agriculture in the area. The total irrigation area developed during the studied period expanded from zero to 18.6 ha. With irrigation, the farmers were able to produce crops twice a year, which influenced household income. Our findings are in line with earlier reports on the positive impacts of irrigation development in Ethiopia (Gebregziabher et al., 2016; Yaebyo et al., 2015).

The impact of IWM interventions also played a great role in increasing the domestic water supply and water quality, thereby improving health and reducing the distance and time to water points. The distance to water points from homesteads was reduced by approximately 33%, and the per capita water availability increased by 150%. In contrast to the national standard level of service (20 L/head/day) and maximum walking distance of 1 km from the nearest water source (African Development Fund, 2005), the result was found to be higher than the national standard, as the whole population was within a 1 km radius from water and had 25 l/head/day water access. Respondents indicated that this reduced the family workload in general and those of women and children in particular; the saved time is now used for other productive work activities and schooling. Different studies, such as Singh et al. (2010) and Nerkar et al. (2015), have also indicated that women have to walk significantly less to fetch water and the workload of women and children can be reduced by up to 2 h daily in areas where IWM interventions are implemented compared to areas with no intervention.

The increased domestic water availability also influenced hygiene and sanitation practices, which ultimately have an impact on human health. The number of households with toilets increased by 188, and the number of households with hand washing facilities increased by 195, reducing the open-air defecation practice and contamination of water sources. Consequently, respondents perceived the water quality and their health conditions had improved. These results are supported by Nerkar et al. (2014, 2015), that reported a significant decrease in the illness risk of people living near their water source. A study from India confirmed that water sample contamination by *Escherichia coli* was 2.3 times lower in areas with IWM intervention compared to control areas (Nerkar et al., 2014). Other studies, such as Cairncross and Cuff (1987), have linked water access to increased water use for food preparation, thereby influencing the quantity and diversity of diets.

4.2.2. Changes in fruit, vegetable and grain crop production

The implementation of IWM interventions appears to have an influence on the production and choice of food grains, vegetables and fruits. Our results showed that previously degraded areas and gullies have been rehabilitated and reclaimed, allowing farmers to grow fruits, forages, trees and vegetables. Prior to the implementation of IWM activities, cropping systems were purely rainfed, and they were limited to the cultivation of cereal crops and pulses. By 2015, however, crop diversification had occurred on both irrigated and rainfed farms, and farmers had started to produce high-value irrigated crops and fruits for the market.

Studies have indicated that crop diversification not only provides a wider choice in the production of various crops but also minimizes risks and increases profitability, in addition to harnessing the maximum potential of land, water, humans and climate

(Gebregziabher et al., 2016). The improvement was not limited to crop diversity; it also applied to crop productivity. The average crop productivity for the dominant crops increased from 1.8 to 2.2 ton ha⁻¹, by 0.4 ton ha⁻¹ (approximately 22%). The cereal yield in the 2015 harvest year was equivalent to the national average which is 2.3 ton ha⁻¹ (CSA, 2015). This result is also in line with the findings of Yaebyo et al. (2015) that reported a yield increase of 0.7 ton ha⁻¹ (44%); however, it is much lower than the findings of Gebregziabher et al. (2016) that reported yield increase of 1.9 ton ha⁻¹ for similar crops. This indicates that an increase in the availability of water, soil fertility and developmental efforts in IWM interventions might influence and increase the variety and productivity of the cultivated crops.

4.2.3. Changes in livestock production

In most parts of the Tigray region, grazing lands are common property resources. Most of the grazing lands are grazed and trampled the entire year, without any resting period, resulting in the depletion of edible species for livestock and the invasion by less edible species (Hags et al., 1999). In our case, due to overgrazing on most of the pasturelands and to watershed degradation, access to water and animal feed was the most important problem for livestock development prior to the watershed intervention. The stall feeding of livestock was not a common practice in rural Tigray in 2002, before the IWM (Gebremedhin & Swinton, 2003). Animals had to travel long distances, particularly in the dry season, for watering and grazing on communal land. This may negatively influence the productivity of small-holder farmers and animal health and productivity. Following the IWM interventions, however, the availability of animal feed (both green and dry) increased significantly, leading to increased stall feeding. According to Gebremedhin and Swinton (2003), stall feeding can increase the availability of manure and reduce the energy loss of livestock due to the reduced walking time during the search for feed. Furthermore, under IWM interventions, yearly milk production from local cows increased by approximately 67% per head. This value is much higher than the findings of Yaebyo et al. (2015) that reported a 12% increase in the milk yield of local dairy cows after IWM in northern Ethiopia. The change in milk production has a direct impact on greenhouse gas (GHG) emissions. According to Gerber et al. (2011), the emissions of GHGs such as methane and nitrous oxide decrease with increasing productivity. An increase in milk productivity, therefore, offers a pathway to satisfying an increasing demand for milk and is a viable GHG mitigation approach, especially in areas such as the studied watershed, where milk yields are currently below 2000 kg cow⁻¹y⁻¹ (Gerber et al., 2011).

An 8% increase in the number of bee colonies was also observed from 2002 to 2015, and it encouraged 72 landless people and youngsters to become involved in honey bee and colony production. This corresponds with the findings of Yaebyo et al. (2015), who reported a honey bee yield increase of 24%. Moreover, approximately 7% of the produced honey is consumed by the family, which contributes to the family livelihood by providing a highly nutritious food product. This value is, however, smaller than the household consumption (38%) reported for the nation (Ethiopia) (Alemu et al., 2016).

4.2.4. Changes in household income and expenditure

After the IWM intervention in 2015, the household income improved by 62% (cal.13600 birr or 680 USD). These results are twice the findings of Yaebyo et al. (2015) that reported a 31% household income improvement due to the income generating activities of IWM, such as crops, bee-keeping and dairy. Taking the wealth category scale developed by USAID (5600 Ethiopian birr or 280 USD per capita per year), 79% of the irrigation users were in a

higher well-being category, whereas only 34% of non-users were in this category. However, changes in household economy are complex, and it is difficult to ascribe simple causal relationships to a particular intervention.

The increase in income has encouraged households to invest in various activities, which can improve their livelihood. The major investments were in education, health, communication, construction and the purchase of farm tools. This evidence supports the findings of Nerkar et al. (2015) and Gebregziabher et al. (2016), which revealed an improvement in household expenditures on agricultural inputs, house improvements, schooling and medical expenses due to IWM. A study in other parts of Ethiopia (Asayehegn, 2012) also reported that the number of irrigation users who completed nine years of schooling and above was two times higher than that of non-users. This was further supported by the findings of Yeabiyo et al. (2015) in northern Ethiopia, which indicated that the mean education of irrigation users was 3 times higher than that of non-users.

4.3. Hurdles for the scale-up of IWM technologies

The benefits of the IWM approach in addressing the interrelated problems of land degradation, low agricultural productivity and food insecurity are widely recognized by the government and development partners (Tesfaye et al., 2016). Regardless of its benefits, its sustained development and expansion are challenged by various factors. Some of the challenges considered are as follows:

- i) The high investment and maintenance costs of IWM technologies: Tesfaye et al. (2016) estimated the cost of some IWM technologies in three watersheds (Ethiopia) and found that the investment costs of soil bund, stone bund and fanyajuu bund construction were USD 29, 33 and 87 per ha, respectively. Moreover, they estimated a maintenance cost of USD 5.2 ha⁻¹y⁻¹ for soil bunds, USD 1.7 ha⁻¹y⁻¹ for stone bunds and USD 6.1 ha⁻¹y⁻¹ for fanyajuu. These investment and maintenance costs are indeed an obstacle for up-scaling the activities.
- ii) Inadequate community participation: It is still a challenge in some areas to negotiate and convince farmers to participate in IWM. Inadequate community participation in the planning process of many watersheds, which mainly focuses on technical and physical activities with less attention to the economic viability and social acceptability aspects, has led to the reluctance of some farmers. Moreover, the lack of properly integrating introduced practices with indigenous knowledge limits the willingness of farmers to participate and their responsibility for the assets created (Chimdesa, 2016).
- iii) Weak linkages among concerned institutions: In the IWM practice, the level of coordination among researchers, extension centres and educational institutions is relatively poor, which affects the development and transfer of technologies from researchers to local experts and local communities, particularly farmers (Chimdesa, 2016).
- iv) Staff mobility: The frequent restructuring of government institutions causes staff turnover, which leads to the discontinuity of activities and initiatives. These all result in limited up-scaling of successful sustainable environmental management practices in the country.
- v) Dependency on incentives: The food- and cash-for-work programmes are believed to reduce the confidence of farmers to work independently, as they increase dependency (Little, 2006), which in turn affects the sustainability of the programme negatively. Cash and grain payment incentives to compensate the labour of food-insecure rural households are provided with the support of the World Food Program and PSNP for most months during the year. These are believed to affect the sustainability of IWM interventions, though, because i) when the farmers graduate, their willingness to participate and work in IWM decrease; ii) the food-secured households are less involved and are unwilling to participate in a massive amount of work (Chimdesa, 2016).
- vi) Land and tenure security: Even though land certificates are provided to households to create a sense of ownership, this certificate is only awarded to farmlands. Other land uses remain under state ownership, which again creates a limited sense of ownership, and the sustainability issue remains in question (Gorfu, 2016).
- vii) Frequent change in IWM technologies: There are changes in technologies from time to time; for example, bench terracing replaced the existing technologies prior to the impact evaluation. Farmers, therefore, lose confidence in the introduced technologies and their sustainability and effectiveness.
- viii) Farmers' preference for short-term benefits: IWM, by its very nature, is a long-term investment discouraging small-scale, resource-poor farmers from obtaining short-term benefits (Mekonnen & Fekadu, 2015). Since the main occupation and means of livelihood for rural communities is agriculture, farmers have less interest in long-term conservation interventions. Rather, they prefer interventions and watershed technologies with quick returns (Chimdesa, 2016). Farmers living in densely populated areas, with a low per capita land holding, prefer to use communal land to graze and browse their herds. Hence, they are reluctant to apply or implement measures on communal land because they are inclined towards their short-term benefits such as feed for their herds, timber and fuel wood sources (Mekonnen & Fekadu, 2015). These require the provision of farmers with agricultural technologies, such as improved crops, forage, animal breeds and practices, to compensate their short-term interests, which has been the case in many successful watersheds, including the studied watershed. However, this requires additional investments and external support.

5. Conclusions

The results from this study show that integrated watershed management (IWM) offers a promising land resources management and development solutions. It enabled new opportunities linked to crops diversification, land reclamation, fertility improvement, and off-farm activities (e.g. sand mining, cash/food for work).

The IWM activities also increased: 1) knowledge among the population on a variety of topics (natural resources management, agriculture and irrigation techniques & beekeeping); 2) the number of children in school and ability to pay school fees; 3) time-saving for women to collect water and fuel wood; 4) natural resources management interventions in the way of soil and water conservation, resulting in raised water tables and allowed new water sources development. As the result of massive mobilization, groundwater levels have risen, soil erosion has reduced, and people's ability to grow food and gain, and income has improved.

It can be concluded that the model for restoration of degraded land, IWM, sets an achievable example for other African countries. However, the expansion of the technology is challenged by hurdles. To overcome these hurdles, farmer-extension-research-policy integration should be lifted to high level.

Declaration of competing interest

All authors confirmed that there is no conflict of interest and no any ethical issue in relation to this work/paper.

Acknowledgements

The authors would like to thank Wukro St. Mary's Institute and the AgriFoSe2030 program for the technical, financial and logistic support. We also extend our gratitude to the administrators, farmer respondents and development agents of Gule Village for their support in providing information during data collection.

References

- African Development Fund. (2005). *Ethiopia: Rural water supply and sanitation programme. Appraisal report* (p. 73). North, East and South, Onin: Infrastructure Department. www.afdb.org/fileadmin/uploads/afdb/Documents.
- Alemu, A. E., Maertens, M., Deckers, J., Bauer, H., & Mathijs, E. (2016). Impact of supply chain coordination on honey farmers' income in Tigray, Northern Ethiopia. *Agricultural and Food Economics*, 4, 1–22. <https://doi.org/10.1186/s40100-016-0053-x>
- Asayehegn, K. (2012). Irrigation versus rain-fed agriculture: Driving for households' income disparity- A study from central Tigray, Ethiopia. *International Journal of Agricultural Sciences*, 2, 67–74. ISSN-L: 2026-6073 ©2012 International Research Journals.
- BCEOM. (1998). Abbay river basin integrated development master plan, main report. The federal democratic republic of Ethiopia, ministry of water resources: Addis ababa, Ethiopia. www.tandfonline.com.
- BoARD. (2016). *Tigray bureau of agriculture and rural development (TBoARD) annual report. Mekelle, Ethiopia* (p. 33).
- Bojö, J., & Cassells, D. (1995). *Land degradation and rehabilitation in Ethiopia: A reassessment. AFTES working paper No. 17*. World Bank.
- Broussard, N. H., & Tekleselassie, T. G. (2012). Youth unemployment: Ethiopia country study. *International Growth Centre*, 38. Working Paper 12/0592.
- Cairncross, S., & Cuff, J. (1987). Water use and health in Mueda, Mozambique. *Transactions of the Royal Society of Tropical Medicine and Hygiene*, 81, 51–54. [https://doi.org/10.1016/0035-9203\(87\)90280-X](https://doi.org/10.1016/0035-9203(87)90280-X)
- CCME (Canadian Council of Ministers of the Environment). (2016). *Summary of integrated watershed management approaches across Canada*. Canadian Council of Ministers of the Environment. PN 1559, ISBN 978-1-77202-034-2 pdf.
- Chiang, L., Chaubey, I., Hong, N., Lin, Y., & Huang, T. (2012). Implementation of BMP strategies for adaptation to climate change and land use change in a pasture-dominated watershed. *International Journal of Environmental Research and Public Health*, 9, 3654–3684. <https://doi.org/10.3390/ijerph9103654>
- Chimdesa, G. (2016). Historical perspectives and present scenarios of watershed management in Ethiopia. *International Journal of Natural Resource Ecology and Management*, 1, 115–127. <https://doi.org/10.11648/j.ijnrem.20160103.17>
- Chisholm, N., & Tassew, W. (2012). Managing watersheds for resilient livelihoods in Ethiopia. *OECD, development Co-operation report 2012: Lessons in linking sustainability and development*. OECD Publishing. <https://doi.org/10.1787/dcr-2012-15-en>
- Congalton, R. (1991). A review of assessing the accuracy of classifications of remotely sensed data. *Remote Sensing of Environment*, 37, 35–46. [https://doi.org/10.1016/0034-4257\(91\)90048-B](https://doi.org/10.1016/0034-4257(91)90048-B)
- CSA. (2008). Summary and statistical report of the 2007 population and housing census results. Population size by age and sex. Central Statistical Agency of Ethiopia: Addis Ababa, 113 www.scribd.com/doc/28289334/Summary-and-Statistical-Report-of-the-2007.
- Descheemaeker, K., Nyssen, J., Rossi, J., Peosen, J., Haile, M., Moeyesons, J., & Deckers, J. (2006). Sedimentation deposition and pedogenesis in enclosure in the Tigray Highlands, Ethiopia. *Geoderma*, 132, 291–314. <https://doi.org/10.1016/j.geoderma.2005.04.027>
- Descheemaeker, K., Raes, D., Nyssen, J., Poesen, J., Haile, M., & Deckers, J. (2009). Changes in water flows and water productivity upon vegetation regeneration on degraded hill slopes in northern Ethiopia: A water balance modelling exercise. *The Rangeland Journal*, 31, 237–249. <https://doi.org/10.1017/RJ09010>
- Dunne, T., & Leopold, L. B. (1978). *Water in environmental planning*. San Francisco, xviii: W. H. Freeman. ISBN-10: 0716700794, ISBN-13: 978-0716700791.
- Eweg, H. P. A., Van Lammeren, R., Deurloo, H., & Woldu, Z. (1998). Analyzing degradation and rehabilitation for sustainable land management in the highlands of Ethiopia. *Land Degradation & Development*, 9, 529–542. [https://doi.org/10.1002/\(SICI\)1099-145X](https://doi.org/10.1002/(SICI)1099-145X)
- FAO. (1986). *Ethiopian highlands reclamation study: Ethiopia. Final report. Volume I. Report prepared for the government of Ethiopia by the food and agriculture organization of the united nations*. Rome. AG:UTF/ETH/037/ETH.
- FAO. (1989). *Reconnaissance physical land evaluation in Ethiopia. Addis ababa, Ethiopia*.
- FAO. (2002). Global information and early warning system on food and agriculture world food programme special report FAO/WFP crop and food supply assessment mission to Ethiopia. Addis ababa, Ethiopia, 22 www.fao.org/docrep/012/ak336e/ak336e00.htm.
- Ganasri, B. P., & Gowda, R. (2016). Assessment of soil erosion by RUSLE model using remote sensing and GIS - a case study of Nethravathi Basin. *Geoscience Frontiers*, 7, 953–961. <https://doi.org/10.1016/j.gsf.2015.10.007>
- Gebregziabher, G., Abera, D. A., Gebresamuel, G., Giordano, M., & Langan, S. (2016). *An assessment of integrated watershed management in Ethiopia. International water management Institute (IWMI) working paper 170, colombo*. <https://doi.org/10.5337/2016.214>. Sri Lanka.
- Gebremedhin, B., & Swinton, S. M. (2003). Investment in soil conservation in northern Ethiopia: The role of land tenure security and public programs. *Agricultural Economics*, 29, 69–84. <https://doi.org/10.1111/j.1574-0862.2003.tb00148.x>
- GebreMichael, D., Nyssen, J., Peosen, J., Deckers, J., Haile, M., Govers, G., & Moeyesons, J. (2005). Effectiveness of stone bunds in controlling soil erosion on crop land in Tigray high lands, Northern Ethiopia. *Soil Use & Management*, 21, 287–297. <https://doi.org/10.1111/j.1475-2743.2005.tb00401.x>
- Gerber, P., Vellinga, T., Opio, C., & Steinfeld, H. (2011). Productivity gains and greenhouse gas emissions intensity in dairy systems. *Livestock Science*, 139, 100–108. <https://doi.org/10.1016/j.livsci.2011.03.012>
- Gessesse, B., Bewket, W., & Bräuning, A. (2015). Model-based characterization and monitoring of runoff and soil erosion in response to land use/land cover changes in the Modjo watershed, Ethiopia. *Land Degradation & Development*, 26, 711–724. <https://doi.org/10.1002/ldr.2276>
- GIZ. (2015). *GIZ Ethiopia: Lessons and experiences in sustainable land management. GIZ support for Ethiopia's sustainable land management program, addis ababa, Ethiopia*.
- Gorfu, S. A. (2016). *The impact of Ethiopian land certification on land conservation, maintenance and tree planting*. Master's Thesis (p. 36). Norwegian University of Life Science <http://hdl.handle.net/11250/2403898>.
- Hags, F., Pender, J., & Nega, G. (1999). Land degradation in the highlands of Tigray and strategies for sustainable land management. International livestock research Institute socio-economics and policy research working paper 25. Livestock policy analysis project: Addis ababa, 75 <https://cgispace.cgiar.org/bitstream/handle/10568/79424/WP25.pdf?>
- Haregeweyn, N., Berhe, A., Tsunekawa, A., Tsubo, M., & Meshesha, D. T. (2012). Integrated watershed management as an effective approach to curb land degradation: A case study of the enabered watershed in northern Ethiopia. *Environmental Management*, 50, 1219–1233. <https://doi.org/10.1007/s00267-012-9952-0>
- Herweg, K., & Ludi, E. (1999). The performance of selected soil and water conservation measures – case studies from Ethiopia and Eritrea. *Catena*, 36, 99–114. [https://doi.org/10.1016/S0341-8162\(99\)00004-1](https://doi.org/10.1016/S0341-8162(99)00004-1)
- Hurni, H. (1985). Erosion - productivity - conservation systems in Ethiopia. In *Proceedings 4th international conference on soil conservation* (pp. 654–674). Maracay, Venezuela.
- Hurni, H., Berhe, W. A., Chadhokar, P., Daniel, D., Gete, Z., Grunder, M., & Kassaye, G. (2016). *Soil and water conservation in Ethiopia: Guidelines for development agents* (Second revised edition). Bern, Switzerland: Centre for Development and Environment (CDE), University of Bern, with Bern Open Publishing (BOP).
- Iticha, B., Mohammed, M., & Kibret, K. (2016). Impact of deforestation and subsequent cultivation on soil fertility in Komto, Western Ethiopia. *Journal of Soil Science and Environmental Management*, 7, 212–222. <https://doi.org/10.5897/JSEM2016.0578>
- Lambin, E. F., Ronsevell, M. D. A., & Geist, H. J. (2000). Are agricultural land-use models able to predict changes in land-use intensity? *Agriculture*, 82, 321–331. [https://doi.org/10.1016/S0167-8809\(00\)00235-8](https://doi.org/10.1016/S0167-8809(00)00235-8)
- Little, P. D. (2006). Are Ethiopia's farmers dependent on food aid? Basis brief collaborative research support program. Number 43. Pp. 4 http://pdf.usaid.gov/pdf_docs/PNADGG699.pdf.
- Mekonnen, G. T., & Fekadu, A. (2015). Experiences and challenges of integrated watershed management in central zones of southern Ethiopia. *International Journal of Current Research*, 7, 20973–20979. ISSN: 0975-833X.
- Negusse, T., Yazew, E., & Tadesse, N. (2013). Quantification of the impact of integrated soil and water conservation measures on groundwater availability in mendae catchment, Abraha we-atsebaha, eastern Tigray, Ethiopia. *Momona Ethiopian Journal of Science*, 5, 117–136. ISSN:2220-184X.
- Nerker, S. S., Pathak, A., Lundborg, C. S., & Tamhankar, A. J. (2015). Can integrated watershed management contribute to improvement of public health? A cross-sectional study from hilly tribal villages in India. *International Journal of Environmental Research and Public Health*, 12, 2653–2669. <https://doi.org/10.3390/ijerph120302653>
- Nerker, S. S., Tamhankar, A. J., Khedkar, S. U., & Lundborg, C. S. (2014). Quality of water and antibiotic resistance of *Escherichia coli* from water sources of hilly tribal villages with and without integrated watershed management—a one year prospective study. *International Journal of Environmental Research and Public Health*, 11, 6156–6170. <https://doi.org/10.3390/ijerph110606156>
- Nyssen, J., Naudts, J., De Geyndt, K., Mitiku, H., Poesen, J., Moeyesons, J., & Deckers, J. (2008). Soils and land use in the Tigray highlands (northern Ethiopia). *Land Degradation & Development*, 19, 250–274. <https://doi.org/10.1002/ldr.840>
- Nyssen, J., Poesen, J., Haile, M., Moeyerson, J., Deckers, J., & Hurni, H. (2009). Effects of land use and land cover on sheet and rill erosion rates in the Tigray high lands, Ethiopia. *Zeitschrift für Geomorphologie*, 53, 171–197. <https://doi.org/10.1127/0372-8854/2009/0053-0171>

- Nyssen, J., Poesen, J., Veyret-Picot, M., Moeyersons, J., Haile, M., Deckers, J., Dewit, J., Naudts, J., Teka, K., & Govers, G. (2006). Assessment of gully erosion rates through interviews and measurements: A case study from northern Ethiopia. *Earth Surface Processes and Landforms*, 31, 167–185. <https://doi.org/10.1002/esp.1317>
- Petkovišek, G., & Mikos, M. (2004). Estimating the R factor from daily rainfall data in the sub-Mediterranean climate of southwest Slovenia. *Hydrological Sciences Journal*, 49, 869–877. <https://doi.org/10.1623/hysj.49.5.869.55134>
- Pierce, F. J., Dowdy, R. H., Larson, W. E., & Graham, W. A. P. (1984). Soil productivity in the corn belt: An assessment of erosion's long-term effects. *Journal of Soil & Water Conservation*, 39, 131–136. Online ISSN: 1941-3300.
- Pimentel, D., & Burgess, M. (2013). Soil erosion threatens food production. *Agriculture*, 3, 443–463. <https://doi.org/10.3390/agriculture3030443>
- Rabia, A. H., Affi, R. R., Gelaw, A. M., Bianchi, S., Figuredo, H., Huong, T. L., Lopez, A. A., Mandala, S. D., Matta, E., Ronchi, M., Solomon, H. W., Tine, A. K., Youssef, M. S., Gutierrez, M. G., Yusuf, M. M., & Alessandro, V. (2013). Soil mapping and classification: A case study in the Tigray region, Ethiopia. *Journal of Agriculture and Environment for International Development*, 107, 73–99. <https://doi.org/10.12895/jaeid.20131.81>
- Reda, A. H. (2014). Community-based adaptation to climate change: Interconnections between environment, livelihoods and development in abrha we atsba, eastern Tigray, Ethiopia. *African Study Monographs Supplement*, 48, 113–123. http://www.africa.kyoto-u.ac.jp/kiroku/asm_suppl
- Senti, E. T., Tufa, B. B., & Gebrehiwot, K. A. (2014). Soil erosion, sediment yield and conservation practices assessment on Lake Haramaya Catchment. *World Journal of Agricultural Sciences*, 2, 186–193. ISSN 2329-9312.
- Showers, K. (1996). Soil erosion in the kingdom of Lesotho and development of historical environmental impact assessment. *Ecological Applications*, 6, 653–664. <https://doi.org/10.2307/2269399>
- Singh, P., Behera, H., & Singh, A. (2010). Impact and effectiveness of watershed development programmes in India. *Mussorie India Centre Rural Studies*, 29, 1–55. <https://doi.org/10.13140/RG.2.1.2903.0247>
- Singh, R., & Phadke, V. S. (2006). Assessing soil loss by water erosion in Jamni river basin, Bundelkhand region, India, adopting universal soil loss equation using GIS. *Current Science*, 90, 1431–1435.
- Teka, K. (2017). Identification of erosion prone areas at macro-watershed level for regional development planning in northern Ethiopia. *Journal of the Drylands*, 7(1), 598–609.
- Teka, K., Van Rompaey, A., Poesen, J., Van Bruyssel, S., Deckers, J., & Amare, K. (2015). Spatial analysis of land cover changes in eastern Tigray (Ethiopia) from 1965 till 2007: Are there signs of a forest transition? *Land Degradation & Development*, 26, 680–689. <https://doi.org/10.1002/ldr.2275>
- Tesfaye, A., Brouwer, R., vanderZaag, P., & Negatu, W. (2016). Assessing the costs and benefits of improved land management practices in three watershed areas in Ethiopia. *International Soil and Water Conservation Research*, 4, 20–29. <https://doi.org/10.1016/j.iswcr.2016.01.003>
- The Federal Democratic Republic of Ethiopia Central Statistical Agency (CSA). (2015). *Agricultural sample survey 2014/2015 (2007 E.C.). Volume 1 report on area and production of major crops (private peasant holdings, meher season), statistical bulletin* (Vol. 278, p. 125). Addis Ababa.
- Wischmeier, W. H., & Smith, D. D. (1978). *Predicting rainfall erosion losses—a guide to conservation planning. Agriculture Handbook No. 537*. Washington, D.C, U.S.A: U.S Department of Agriculture Science and Education Administration.
- World Bank. (2012). The cost of land degradation in Ethiopia: A review of past studies. <https://openknowledge.worldbank.org/handle/10986/7939?show=full>.
- Yaebiyu, G., Tesfay, Y., & Assefa, D. (2015). Socio-economic impact assessment of integrated watershed management in sheka watershed, Ethiopia. *Journal of Economics and Sustainable Development*, 6, 202–2012. ISSN 2222-1700 (Paper) ISSN 2222-2855 (Online).
- Yami, M., Mekuria, W., & Hauser, M. (2013). The effectiveness of village bylaws in sustainable management of community-managed exclosures in northern Ethiopia. *Sustainability Science*, 8, 73–86. <https://doi.org/10.1007/s11625-012-0176-2>
- Yao, X., Fu, B., Lu, Y., Sun, F., Wang, S., & Liu, M. (2013). Comparison of four spatial interpolation methods for estimating soil moisture in a complex terrain catchment. *PloS One*, 8, Article e54660. <https://doi.org/10.1371/journal.pone.0054660>
- Yaro, M. A., Okon, A. E., & Ukpali, E. O. (2015). Effects of environmental degradation on residence of yakurr local government area of croos river state-Nigeria. *International Journal of Science, Environment and Technology*, 4, 488–500. ISSN 2278-3687 (O), 2277-663X (P).
- Yemane, T. (1967). *Statistics: An introductory analysis* (2nd ed.). New York: Harper and Row.



Contents lists available at ScienceDirect

International Soil and Water Conservation Research

journal homepage: www.elsevier.com/locate/iswcr

Original Research Article

Fingerprinting sediment sources in a typical karst catchment of southwest China

Zhenwei Li ^a, Xianli Xu ^{a,*}, Yaohua Zhang ^{a,b}, Kelin Wang ^a^a Huanjiang Observation and Research Station for Karst Ecosystem, Key Laboratory for Agro-Ecological Processes in Subtropical Region, Institute of Subtropical Agriculture, Chinese Academy of Sciences, Changsha, 410125, China^b University of Chinese Academy of Sciences, Beijing, 100049, China

ARTICLE INFO

Article history:

Received 9 December 2019

Received in revised form

13 May 2020

Accepted 23 June 2020

Available online 28 June 2020

Keywords:

Soil erosion

Sedimentation

Sediment tracing

Earth's critical zone

Ecohydrology

ABSTRACT

Due to the complex hydrogeological conditions in karst regions, it is difficult to measure sediment source contributions at a catchment scale directly. The objective of this study was to quantify the relative contributions of sediment sources and their temporal variability in a karst catchment in southwest China. Karst depressions can trap eroded sediment similar to a dam or reservoir and, thus, are representative and typical test beds for identifying sediment sources in karst regions. Three sediment cores were taken from a karst depression, 58 soil samples from three potential sediment sources were collected, and 18 soil properties were analyzed. The relative contributions of cropland, forestland, and fissure or crack soils were calculated using a multivariate mixing model. The fingerprinting results demonstrated that the cropland was the main sediment source in karst catchment. Specifically, according to the mean sediment contributions of the three deposited sediment cores, the sediment contribution from cropland topsoil was 69.3%, varying from 46.9% to 92.3%, and forestland soil and crack soil accounted for 8.6% and 22.1% of the sediment yield, and varying from 2.8% to 16.5% and 4.8%–36.6%, respectively. This result indicated that great attention should be paid when using only a single core to quantify sediment provenance. Due to the deposited sediment was generally disturbed as cropland in the karst depression, the area that has not been disturbed in recent decades in depression was more appropriate to trace sediment sources in karst catchment. To the best of our knowledge, this study was the first to quantify the contributions of sediment sources in the karst catchment of southwest China. This study provides valuable information and a preliminary reference for applying a composite fingerprinting technique to quantify sediment sources in karst catchments.

© 2020 International Research and Training Center on Erosion and Sedimentation and China Water and Power Press. Production and Hosting by Elsevier B.V. This is an open access article under the CC BY-NC-ND license (<http://creativecommons.org/licenses/by-nc-nd/4.0/>).

1. Introduction

Harmful physical impacts to soils and fertility loss due to accelerated soil erosion by water has occurred through on-site land degradation and also through a conspicuous number of off-site events (e.g., flooding, pollution, sedimentation, siltation and eutrophication of streams, lakes, and reservoirs) (Borrelli et al., 2017; Foley et al., 2005; Wang et al., 2017; Yu et al., 2013). For example, each year about ten million hectares of cropland was lost, which reduced the cropland available for food production (Pimentel, 2006). To solve this issue, specification and delivery of

appropriate management solutions require a full understanding of the sediment problem at the catchment scale and a focus upon the key sources involved (Collins et al., 2010; Nearing et al., 2017; Nosrati et al., 2018). Therefore, it is of paramount importance to determine the sources of sediment to effectively facilitate control of soil erosion and to manage catchments effectively.

In recent decades, the sediment fingerprinting technique has provided a direct, successful, and effective approach to trace sources of sediments from river stretches to catchment scale (Collins et al., 2017; Collins & Walling, 2004; Laceby et al., 2017; Owens et al., 2016; Walling, 2013). This method is based on linking the physical or geochemical properties of the sediment to their corresponding sediment sources within a catchment (Lamba et al., 2015a; Walling et al., 2008; Zhang et al., 2016). Fingerprinting techniques have evolved from single-property fingerprints to

* Corresponding author.

E-mail addresses: lizhenwei337@isa.ac.cn (Z. Li), xianlixu@isa.ac.cn (X. Xu), 442967467@qq.com (Y. Zhang), kelin@isa.ac.cn (K. Wang).

multi-property composite fingerprints, because a single tracer does not fulfill all the requirements to identify the sediment sources at a large scale (e.g., catchment) (Collins & Walling, 2002; Stevens & Quinton, 2008; Walling, 2005; Zhang et al., 2017). A variety of fingerprinting properties, such as physical and chemical characteristics of soils, metals, magnetic susceptibility, stable isotopes, radionuclides, and biomarkers have been used to quantify sediment sources (Blake et al., 2012; Chen et al., 2016; Collins & Walling, 2002; Fang, 2015; Walling et al., 2008; Zhang & Liu, 2016; Zhao et al., 2017). The Kruskal-Wallis H test was used to select fingerprint properties that significantly differed between sediment sources, followed by discriminant function analysis (DFA) to identify the minimum number of fingerprint properties that represented the largest proportion of variance (Zhao et al., 2017; Zhou et al., 2016). As a most widely used model, the mixing model was then used to calculate the contributions of each sediment sources (Huang et al., 2019; Zhang et al., 2017). Generally, the sampling methods, tracer selection, source discrimination, and mixing models can yield uncertainty estimations in the identification of source contributions (Lacey et al., 2017; Zhang et al., 2016). Recently, identification of sediment sources has become a central topic in soil erosion research and has been conducted in Australia, Brazil, Korea, Spain, UK, USA, the Chinese Loess Plateau, and the Northeast and Southeast regions of China (Fang, 2015; Jin et al., 2013; Lin et al., 2015; Palazón et al., 2015b; Walling et al., 2008; Wilkinson et al., 2013; Zhang et al., 2016; Zhao et al., 2017). This issue, however, has received little attention in karst regions of southwest China, which are experiencing severe soil erosion due to their special geological conditions, unfavorable land use practices, and lower rate of soil formation.

Karst landscapes cover 7%–12% of the Earth's continental area, and southwest China is one of the largest contiguous karst areas in the world (Dai et al., 2017; Hartmann et al., 2015). This region is characterized by shallow surface soil, high infiltration capacity, and complex topography due to special geologic conditions (Jiang et al., 2014; Li et al., 2017). A complex karst landform includes a porous rock matrix, fissures, fractures, cracks, and a network of solution conduits embedded in karst aquifers, which can be described as a double-porosity (matrix as opposed to conduits) hydraulic media (Li et al., 2016; Martin et al., 2016). In this region, carbonate rocks are highly soluble and do not produce much soil, thus, the soil erosion rate is far greater than the soil formation rate (Peng & Wang, 2012). It requires 2500–7500 years to form 1 cm of soil by dissolving a 25 cm thickness of pure carbonate rock (Jiang et al., 2014). Hence, it is essential to determine soil erosion rates and sediment sources to develop strategic plans for the sustainable management of karst catchments.

Peak-cluster depressions are widespread and numerous, and they are a unique and intriguing geomorphologic pattern in the karst areas of southwest China (Jiang et al., 2014; Li et al., 2019). They have similar dimensions with overlapping steep hills and ridges that surround a flat center (Fig. 1) (Li et al., 2016). Although one or more sinkholes exist at the bottom of the depressions, the eroded soils from the surface and subsurface can generally fill in the sinkholes and block the drainage outlets in karst depressions. As a consequence, karst depressions are frequently inundated after rainstorms, and almost all the eroded sediment is deposited in the bottom of the depression (Bai et al., 2010). That is, the deposited sediments in karst depressions may record information about changes in the surroundings (Jiang et al., 2014). Therefore, the depression is a representative and typical test bed for identifying sediment sources in karst regions. The surface and subsurface of a karst system leads to the loss of soil resources at the surface (cropland, forestland, grassland) and subsurface (fissures or cracks) (Jiang et al., 2014; Peng & Wang, 2012). Nevertheless, the relative contribution of the



Fig. 1. Typical landscape of peak-cluster depressions in the karst region of southwest China.

potential sediment sources in karst catchments is still not clear. Furthermore, sediment sources and sinks are highly variable in time because of variations in precipitation and vegetation cover (Fang, 2015; Jin et al., 2013; Lamba et al., 2015). Few studies have been conducted to identify long-term changes in sediment sources in these depressions and, for karst areas of southwest China, even general studies of sediment sources are very rare.

Thus, the objective of this study was to quantify the relative contributions of sources to the sediment deposited in the depression and their temporal variability in a karst catchment in southwest China. As far as we know, this is the first study to apportion contributions of sediment sources in karst catchments in southwest China, and the results would be especially helpful for selecting appropriate measures to reduce soil erosion and sediment yield.

2. Study area

This study was conducted in the Guzhou catchment ($24^{\circ}53'–24^{\circ}56'$ N, $107^{\circ}55'–107^{\circ}58'$ E) of Huanjiang Observation and Research Station, located in the Huanjiang County of northwest Guangxi province, southwest China (Fig. 2). The catchment has a total area of 1.87 km^2 , and the altitude ranges from 375 m to 816 m. The local climate is subtropical monsoonal, with a mean annual air temperature of $18.5 \text{ }^{\circ}\text{C}$ and a mean annual precipitation of 1389 mm. Guzhou catchment is a typical karst, peak-cluster depression landscape, which is characterized by a flat depression at the center that is surrounded by steep hillslopes. About 70% of the hillslopes have a gradient $>25^{\circ}$. The calcareous soils initiated from limestone contain few rock fragments and have a mean depth of 100 cm in the depression and about 10–30 cm on hillslopes. Bare rocks are exposed on most of the steep hillslopes, and the soils can only be observed in fissures and cracks. The depression has an area of 0.17 km^2 and is mostly covered by cropland, grassland, and forestland and the hillslopes are mainly covered by secondary forestland, shrub land, and grassland. The lower part of the hillslope is less steep and has been cultivated. To control soil erosion, the project 'Grain for Green' was implemented to convert steep croplands ($>15^{\circ}$) to green land in 1999. During the wet season, water logging generally occurs in the depression due to the poor drainage capacity of the depression. For example, the Guzhou depression was flooded $>10 \text{ d}$ after a rainfall in June 2016 (Fig. 3). It is feasible to trace sediment sources, because almost all sediments were deposited in the depression.

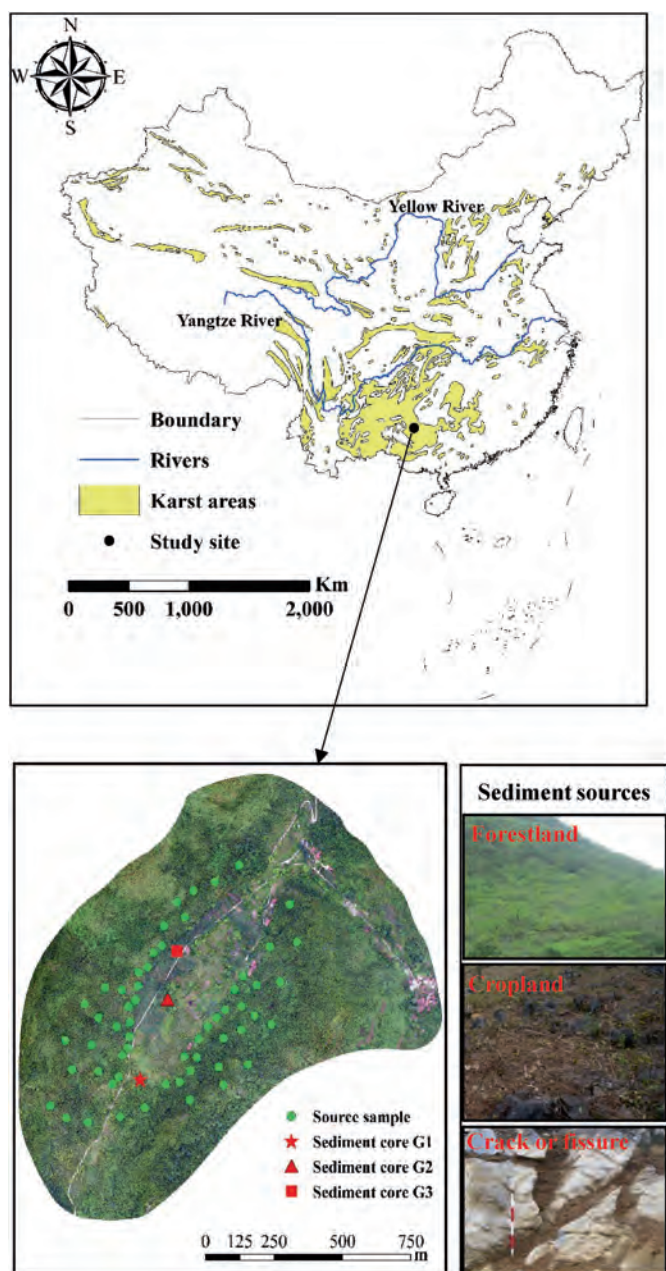


Fig. 2. Locations of the study area, the sampling sites, and landscapes of the three sediment sources.

3. Materials and methods

3.1. Sample collection

Sample collection included the deposited sediment cores in the flat depression and representative samples of sediment source materials in the steep hillslopes (Fig. 2). The sediment deposit cores G1, G2, and G3 were recovered from the Guzhou karst depression in August 2016. These three sediment cores were extracted by manual excavation to depths of 70 cm. Cores G1 and G2 were extracted from the *Zenia insignis* field and a bamboo field, respectively. These two cores were taken at depth increments of 1 cm. The bamboo field had not been disturbed manually for about 100 years, but the field from which core G2 was collected was cultivated initially and converted subsequently to *Zenia insignis* in 2002. Core G3 was

collected from cropland (corn) and the soil was relatively homogeneous at the plough depth (0–20 cm). Thus, for core G3, the soil depth increments were about 5 cm and 1 cm in the 0–20 cm and 20–70 cm soil layers, respectively. In total, 70, 70, and 54 sediment samples were extracted from cores G1, G2, and G3, respectively.

The forestland, cropland, and fissure or crack soils in the hillslopes were identified as potential sediment sources in the catchment (Fig. 2). The vegetation coverage was very high in forestland, but there was high rock coverage in the cropland (Fig. 2). At each sampling site of forest land or cropland, at least 10 sub-samples were collected from the top 2 cm of the topsoil and then combined to form a representative composite source sample. For the crack soil, the freshly-eroded scars were selected as the sampling points and the sampling location was >30 cm below the ground surface to avoid topsoil. Altogether, 47 surface soil samples were taken for the study area, with 31 from forestland and 16 from cropland, and 11 samples were taken from the crack soil where soil erosion was active.

3.2. Analysis of soil samples

All the deposited sediments and samples from soil sources were air-dried and passed through a 2-mm sieve for further analysis. Distribution of soil particle size was measured using a Mastersizer 2000 (Malvern Instruments, Malvern, England) with three replicates for each sample, and then distribution curves of grain size were constructed. Thus, the different soil grain sizes (i.e., $D_{10} \dots D_{90}$) of the samples were calculated. Soil magnetic susceptibility was measured using a Bartington magnetic susceptibility meter (MS2 Oxfordshire, UK) with an MS2B sensor at both low (470 Hz) and high (4700 Hz) frequencies. The low-frequency (χ_{lf}) and high-frequency (χ_{hf}) susceptibilities were measured. Then, the percentage of frequency-dependent, magnetic susceptibility ($\chi_{fd}\%$) was calculated by equation $\chi_{fd}\% = (\chi_{lf} - \chi_{hf}) / \chi_{lf} \times 100$. The soil samples were passed through a 0.25-mm sieve to measure soil organic carbon (SOC), total nitrogen (TN), and total phosphorus (TP). SOC was determined using the potassium dichromate colorimetric method. TN was determined according to the Kjeldahl method using a flow injection apparatus. TP was determined using an ultraviolet spectrophotometer (Lambda 25) based on the Mo–Sb colorimetric method.

3.3. Selection of composite fingerprints

We used the composite fingerprint method to trace sediment sources. Specifically, a Kruskal-Wallis H test and the multivariate discriminate function analysis (DFA) were applied to select composite fingerprints (Collins & Walling, 2007; Zhao et al., 2017). First, the power of individual properties to discriminate between sediment sources was examined using the Kruskal-Wallis H test, and properties with $P > 0.05$ were excluded (Collins & Walling, 2002). Then, based on the results of the Kruskal-Wallis H test, DFA was used to examine the ability of the tracer properties to confirm the existence of inter-category contrast and to assess the discriminatory power of those tracer properties, which determined the optimal group (Palazón et al., 2015a; Wilkinson et al., 2013). By minimizing Wilks' lambda, DFA can select an optimum composite fingerprint with the minimum number of tracer properties that supply the greatest discrimination between the analyzed source materials (Chen et al., 2016; Collins & Walling, 2002). The lambda value close to zero as the variability within source categories was reduced relative to the variability between categories based on the removal or entry of tracer properties from the analysis (Collins et al., 2010; Zhou et al., 2016). Results of the DFA were used to test the proportion of samples that was classified accurately into the correct source groups.

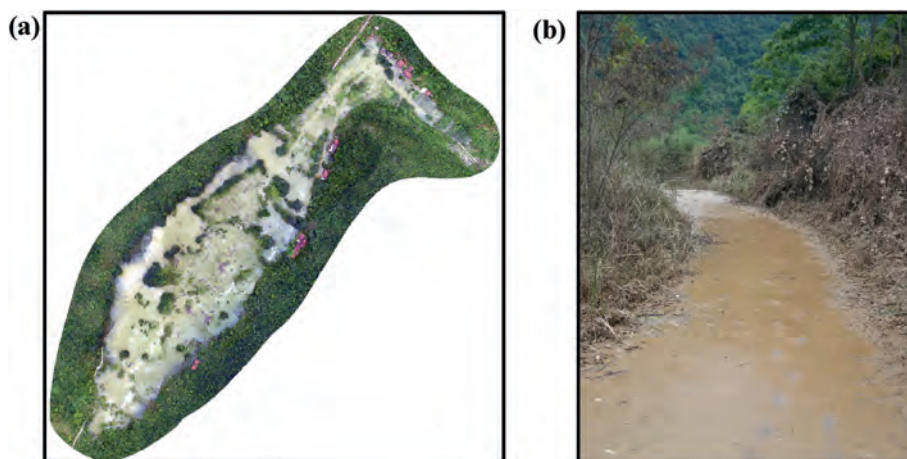


Fig. 3. (a) Aerial photography of the flooded Guzhou karst depression, and (b) the deposited sediment after the flood.

3.4. Contribution of sediment sources to deposition

The percentage of the contribution of each potential source to sediment deposition for each soil depth of the sediment cores in the depression was quantified by using a multivariate mixing model (Walling, 2005; Walling et al., 2015). This model minimizes the sum of the squares of the relative errors (*RDs*) as:

$$RDs = \sum_{i=1}^m \left\{ \left[C_i - \left(\sum_{s=1}^n P_s S_{Si} \right) \right] / C_i \right\} \quad (1)$$

where m is the number of fingerprint properties selected in the optimal combination of fingerprinting properties, C_i is the concentration of fingerprint property i in the sediment, n is the number of sources, P_s is the proportional contribution from the source, and S_{Si} is the concentration of fingerprint property i in source s . This model was constrained by the following two equations (Collins et al., 1997; Palazón et al., 2015):

$$\sum_{s=1}^n P_s \times S_{Si} = C_i \quad (2)$$

$$\sum_{s=1}^n P_s = 1 \quad (0 \leq P_s \leq 1) \quad (3)$$

If the *RDs* are minimal, the proportion of the contribution of each potential sediment source can be determined. To assess model performance and optimization results, a goodness-of-fit (*GOF*) metric is used commonly (Collins et al., 2010; Lin et al., 2015; Zhang & Liu, 2016; Zhao et al., 2017):

$$GOF = 1 - \left\{ \sum_{i=1}^m \left(\left| C_i - \sum_{s=1}^n P_s S_{Si} \right| / C_i \right) \right\} / m \quad (4)$$

Generally, the mixing model was considered satisfactory to explain the contribution of sediment sources when the *GOF* value was >0.8 (Motha et al., 2003; Zhang et al., 2017; Zhou et al., 2016).

4. Results

4.1. Selection of potential sources

For the three sediment sources, cropland generally had high clay content and low sand content, and forestland exhibited the reverse.

Forestland had the largest magnetic susceptibility, followed by cropland and crack soil. Furthermore, SOC, TN, and TP in forestland was greater than that in cropland and crack soil. Interestingly, the coefficient of variation of each of the 18 tracer properties for sediment sources was greater than that of deposited sediment (Table 1).

Of the tracer properties, 14 individual properties (i.e., clay, silt, sand, D_{10} , D_{20} , D_{30} , D_{40} , D_{50} , D_{60} , D_{70} , D_{80} , D_{90} , SOC, and TN) passed the Kruskal-Wallis H test, which yielded test statistics in excess of the critical value, and H values ranged from 10.55 to 38.86 (Table 1). DFA analysis was conducted on these properties to obtain the optimum combination of properties for discriminating sediment sources. Four properties (i.e., χ_{lf} , χ_{hf} , χ_{fd} , and TP) were not significant at $P < 0.05$ and, thus, failed to pass the Kruskal-Wallis H test. Therefore, 14 tracer properties passed Kruskal-Wallis H test and could undergo a DFA analysis to obtain the optimum combination of the properties for discriminating sediment sources.

4.2. Discrimination of sediment sources

The optimum composite fingerprinting consisted of four tracer properties (clay, silt, D_{60} , and D_{70}), and it correctly distinguished 89.5% of the source type samples (Table 2). Clay content was the principal fingerprint factor, which had the highest predictive power of 73.5%. The classification accuracies were different between the three source types. Specifically, 90.0%, 88.2%, and 100% of the forestland, cropland, and crack soil samples, respectively, were classified correctly.

The depth distributions of clay, silt, D_{60} , and D_{70} for cores G1, G2, and G3 showed that cores G1 and G2 were similar, and they were different from G3 (Fig. 4). There were no significant vertical variations in the clay content of G1 and G2, but comparatively high values at depths of 47–49 cm and 67–70 cm were observed in core G3. Within the profile, the silt content was almost evenly distributed in all three cores. D_{60} and D_{70} decreased slightly with soil depth in G1 and G2, but no obvious variation was found in G3.

4.3. Mixing model: sediment source apportionment

The mean *GOF* values for the sediment samples collected in cores G1, G2, and G3 were estimated to be 91.7%, 95.3%, and 87.7%, respectively, which implied that the multivariate mixing model provided an acceptable discrimination for the fingerprint factors in the sediment samples (Table 3). The mean relative contributions of cropland, forestland, and crack soil to depression sediments were 69.3%, 8.6%, and 22.1%, respectively. That is, cropland was the main

Table 1

Descriptive statistics of tracer properties in potential sediment sources and deposited sediments in karst depressions in southwest China, and the results of the Kruskal-Wallis *H* test for datasets of source type fingerprint properties.

Tracers	Unit	Forestland		Cropland		Crack soil		Deposited sediment		<i>H</i> value	<i>P</i> value
		Mean	CV	Mean	CV	Mean	CV	Mean	CV		
Clay	%	10.80	33.50	23.40	14.21	14.72	15.37	22.65	6.73	33.41	<0.01*
Silt	%	68.07	11.56	70.47	5.70	76.30	4.87	72.29	5.78	10.55	<0.01*
Sand	%	21.12	35.48	6.13	28.81	8.98	26.49	5.06	2.72	37.57	<0.01*
D ₁₀	μm	3.17	137.80	0.81	14.62	1.34	21.11	0.92	0.28	33.73	<0.01*
D ₂₀	μm	5.26	93.45	1.65	17.10	2.84	16.86	1.89	0.67	33.53	<0.01*
D ₃₀	μm	7.58	70.68	2.79	14.15	4.39	15.03	3.16	1.04	35.20	<0.01*
D ₄₀	μm	10.56	54.76	4.12	11.28	6.24	13.98	4.73	1.53	36.58	<0.01*
D ₅₀	μm	14.82	43.33	5.84	9.46	8.65	12.79	6.95	2.07	37.95	<0.01*
D ₆₀	μm	21.60	39.96	8.25	8.24	11.97	11.78	9.93	2.91	38.59	<0.01*
D ₇₀	μm	34.98	55.70	11.95	8.32	16.90	11.73	14.21	3.94	38.86	<0.01*
D ₈₀	μm	61.98	69.48	18.34	11.93	25.35	13.92	20.90	5.53	38.26	<0.01*
D ₉₀	μm	118.06	51.89	33.88	21.64	47.17	22.22	34.00	9.24	37.11	<0.01*
χ _{lf}	10 ⁻⁸ m ³ kg ⁻¹	85.36	109.05	61.88	39.55	54.97	86.06	41.06	33.32	2.89	0.24
χ _{hf}	10 ⁻⁸ m ³ kg ⁻¹	78.06	108.25	56.86	39.01	49.97	85.31	31.53	33.97	2.98	0.23
χ _{fd}	%	8.46	10.07	7.89	16.08	8.88	8.52	8.00	1.79	3.81	0.15
SOC	g kg ⁻¹	24.26	31.07	14.69	28.67	18.74	27.38	8.42	4.96	15.91	<0.01*
TN	g kg ⁻¹	3.70	122.58	1.85	29.87	2.56	27.59	0.90	0.61	12.79	<0.01*
TP	g kg ⁻¹	1.15	46.98	1.04	18.00	1.25	26.05	0.67	0.13	2.21	0.33

The grain size D_i was determined from the grain size distribution curves; χ_{lf}, χ_{hf}, and χ_{fd} refers to the low-frequency, high-frequency, and frequency-dependent magnetic susceptibilities, respectively; CV refers to the coefficient of variation. *Significant at a level of 0.05.

Table 2

Optimal composite fingerprints to determine individual sediment source types.

Steps	Tracer property	Wilks' lambda	Classified correctly based on a single tracer property (%)	Cumulative classified correctly (%)
1	Clay	0.249	73.5	73.5
2	Silt	0.163	50	80.7
3	D ₆₀	0.112	64.7	84.3
4	D ₇₀	0.057	63.2	89.5

source of sediments, but forestland contributed only a small proportion to the total sediment. Interestingly, the relative contribution of each source type was variable in the three sediment cores. Specifically, compared to the mean of the total samples, the mixing model predicted greater soil loss from forestland and crack soil and lower soil loss from cropland in G2. The relative contribution of cropland was greater in G3, while forestland and crack soil contributed less.

For core G1, cropland was the principal sediment source for the layers of 11–30 cm and 46–70 cm, which ranged from 63% to 100%, but there was a great deal of soil loss from forestland and crack soil in the 0–10 cm and 30–45 cm soil layers (Fig. 5). For core G2, the deposited sediments from the crack soil was relatively lower than that from cropland, especially for the layers that were 25–50 cm and 58–67 cm deep. Approximately all of the sediment originated from cropland, and forestland and crack soil contributed relatively small amounts of sediment to core G3. On average, significant differences were observed among forestland, cropland, and crack soil (Fig. 6). Generally, surface soil in sediments came from forestland and cropland. Hence, the estimated proportions of contributed sediment from surface and crack soils were 77.9% and 22.1%, respectively.

5. Discussion

In karst regions, the deposited sediment in depressions generally originates from surface hillslopes and crack (fissures) soils (Jiang et al., 2014; Dai et al., 2017). The composite fingerprinting method indicated that the dominant sediment source type was cropland, while forestland contributed relatively small amounts of sediment (Table 3, Figs. 5, Fig. 6). This result was consistent with

previous studies that sediment from cropland was much greater than that from forestland (Collins & Walling, 2007; Lamba et al., 2015; Zhang et al., 2017; Zhou et al., 2016). Tillage operations, such as planting, ploughing, weeding, and harvesting, had a significant effect on soil erosion and, thus, cropland was the most easily eroded land use (Zhang et al., 2010, 2015; Shi et al., 2012; Wang et al., 2018). Forests reduce soil erosion by intercepting rainfall, enhancing infiltration, transpiring soil water, increasing land surface roughness, and adding organic matter to improve soil structure (Duan et al., 2016; Muzylo et al., 2009; Wei et al., 2007).

It is important to note that crack soil contributed approximately 22% of the total sediment (Table 3, Figs. 5, and Fig. 6). The transported path for subsoil was different between karst and non-karst areas. In karst regions, fissures, cracks, fractures, and a network of solution conduits embedded in karst aquifers made the hydrogeological conditions very complex (Hartmann et al., 2015; Martin et al., 2016). Rainfall drained quickly into soil-epikarst systems through fissures and cracks, and this hindered surface runoff (Jiang et al., 2014; Li et al., 2017). That is, there is generally no surface river or gully in the peak-cluster depression landscape. Previous studies also showed that soil in the fissures or cracks is eroded by water and transported eventually through an extensive network of conduits to the karst depression (Bai et al., 2010; Peng & Wang, 2012). In non-karst areas, subsoil originates primarily from gullies or stream banks (Chen et al., 2016; Zhang et al., 2016). The gully process is mostly triggered or accelerated by a combination of inappropriate cultivation and extreme rainfall events (Zhang et al., 2017). Once gullies are formed, they continue to generate sediment long after the initiating causes have ceased (Valentin et al., 2005). A high gully density often causes severe soil erosion, and many studies have indicated that gullies or stream banks were important

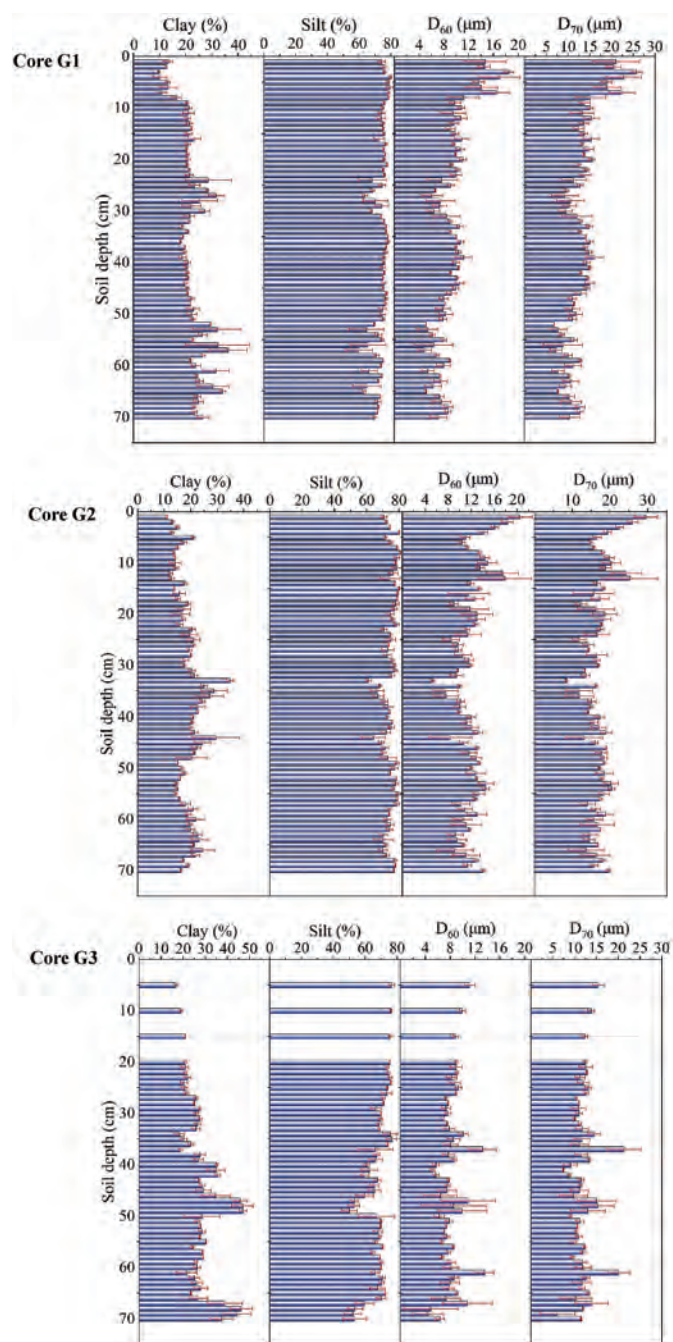


Fig. 4. Profiles of clay content, silt content, D_{60} , and D_{70} of the (a) Core G1, (b) Core G2, and (c) Core G3 that were collected from a karst depression in southwest China. Error bars indicate standard deviation.

sources of sediment (Fang, 2015; Jin et al., 2013; Lamba et al., 2015; Palazón et al., 2015; Zhang & Liu, 2016). However, the percentage of sediments from subsoil was lower than that in non-karst areas. The complex hydrogeological conditions may be responsible for this difference. Actually, the networks of fissures or cracks can increase roughness, which increases water ponding, decreases runoff volume, and decreases flow velocity. Moreover, part of total flow shear stress was dissipated by the wall of fissures or cracks and, therefore, this stress no longer contributed to erosion of soil particles.

It is also worth noting that the contributions of the sediment sources between the three sediment cores were very different

Table 3

Descriptive statistics of sediment source contributions in the three cores.

	No.	Index	Minimum	Maximum	Mean	SD	CV
Core G1	70	Forestland (%)	0.0	67.5	5.2	11.8	228.6
		Cropland (%)	0.0	100.0	72.9	30.9	42.5
		Crack soil (%)	0.0	85.9	20.5	24.0	116.8
Core G2	70	Forestland (%)	0.0	79.1	16.5	16.1	97.7
		Cropland (%)	0.0	100.0	46.9	34.0	72.4
		Crack soil (%)	0.0	90.9	36.6	33.0	90.0
Core G3	54	Forestland (%)	0.0	59.4	2.8	9.4	329.1
		Cropland (%)	26.6	100.0	92.3	15.8	17.1
		Crack soil (%)	0.0	69.5	4.8	13.3	276.9

SD refers to the standard deviation; CV refers to the coefficient of variation.

(Table 3; Fig. 5). Similar results were also observed in the previous studies (Huang et al., 2019; Zhang et al., 2017; Zhou et al., 2016). The core G1 were collected from the undisturbed forestland in karst depression, while the other two sediment cores were extracted from the disturbed land. Hence, the different land utilization types in the karst depression may greatly influence the sediment source contributions. This indicated that caution is needed when using only a single core to provide results for a depression. Actually, the sediment contributions derived from core G1 may be relatively reasonable since the deposited sediment in dam or reservoir was also undisturbed in non-karst areas. In core G1, the eroded sediment from cropland decreased at the topsoil, but that from forestland increased. This temporal changes in sediment sources were probably influenced by the soil conservation practices such as the 'Grain for Green' project. Compared with forestland, the area of the cropland was relatively smaller.

In this study, clay content, silt content, D_{60} , and D_{70} created the optimum composite fingerprint, which correctly distinguished 89.5% of the source type samples (Table 2). This result indicated that the particle size distribution exerted a substantial influence on the selection of optimum fingerprint factors (Krein et al., 2003). The eroding sediment is enriched in clay and silt-sized particles relative to the original soil in the commencement of the erosion event and gradually becomes coarser over time, and at final steady state, its composition becomes very similar to that of the original soil (Asadi et al., 2011; Shi et al., 2012). However, erosion events with low stream power generally resulted in selective removal of fine particles since the flow was insufficient ability to transport large detached particles. The presence of a dual hydrological structure in the karst region dissipated a large part of total shear stress that can be used for soil detachment and generally increased the threshold of the surface runoff generation mechanism. As a result, the large soil loss was mainly created by heavy rainfall storms (Peng and Wang, 2012). This indicated that only clay and silt content were selectively transported to the depression in some rainfall events. Furthermore, the clay and silt particles were very different between the three sediment sources and the cropland topsoil was much more erodible than the other two sources. Therefore, the characteristics of sediment sorting provide an opportunity to fingerprint sediment sources in karst regions. Kurashige and Fusejima (1997) also showed that the distributions of grain size were commonly different between multiple sediment sources and, thus, could be used as a sediment tracer. It is important to highlight that the fallout radionuclide was not used in this study to determine relative contributions of surface and subsurface erosion to deposited sediment. Surface soil was exposed to fallout, and the fine particles can absorb radionuclides readily, but subsurface soil usually received little or no fallout and exhibited little or zero radioactivity (Zhang, 2014; Zhang et al., 2016). Undoubtedly, the contrasting radioactivity between surface and subsurface soils made the fallout radionuclides ideal tracers to discriminate overland erosion from

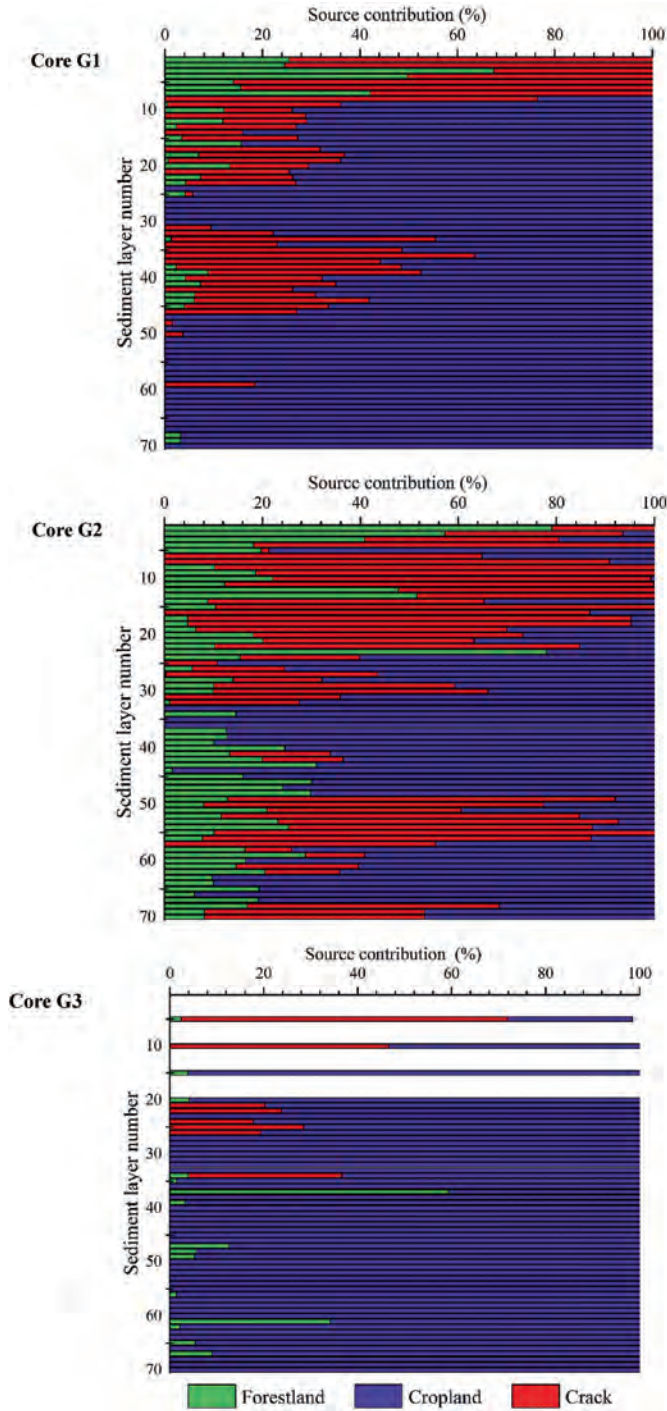


Fig. 5. Profiles of sediment source contributions of the (a) Core G1, (b) Core G2, and (c) Core G3.

subsurface erosion (Palazón et al., 2015). Fallout radionuclides, however, decrease in concentration due to the natural decay process. Therefore, fallout radionuclides were not suitable for discriminating the sediment sources from the assigned sediment, which had been deposited for a long time (e.g., several decades). Yet, fallout radionuclides are still an effective sediment source tracer to quantify the relative contribution of potential sources of deposited sediment over a short period or for sediments suspended in rivers.

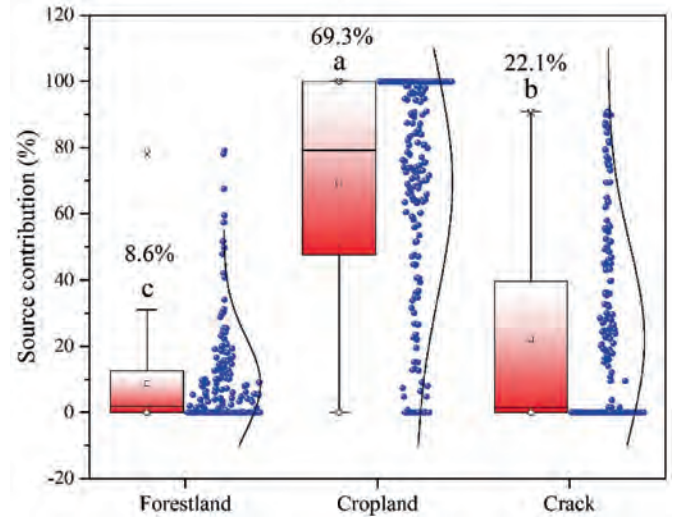


Fig. 6. Comparison of sediment source contributions among forestland, cropland, and crack soil. The curved line to the right of each box is the distribution curve. Different letters indicate significant differences at $P < 0.05$.

The current study represents an initial undertaking aimed at discriminating the sediment sources from a karst depression. We believe this is the first study to quantify the contribution of sediment sources in a karst catchment in southwest China. However, some potential limitations should be taken into account when interpreting the findings of this study. First, the contributions from vertical sediment sources of the three sediment cores were very different (Fig. 5). This was due to the distinct sediment sources and geomorphology of the depression, but also due to the sorting of different particles. Fang et al. (2015) and Lamba et al. (2015a) also found that the sediment sources and sinks were highly variable in time and space. Both the spatial and temporal variation in sediment sources and deposited sediments were the most important uncertainty for predicting sediment sources (Zhang et al., 2016). Actually, eroded sediments may not have been deposited homogeneously in the karst depression, which resulted in great variability in the sedimentation profile (Zhao et al., 2017). To improve identification of the sediment sources of the deposited sediment, more cores should be drilled within the catchment, as D’Haen et al. (2013) suggested. This would be an effective method, although it is time consuming and expensive.

Furthermore, use of the multivariate mixing model may also be an important source of uncertainty in the source contributions (Zhao et al., 2017). It is uncertain whether the use of the mean concentrations of tracers represented the true values for sediment sources in the mixing model to identify those sources accurately (Lamba et al., 2015b). Thus, more attention should be paid to this uncertainty in future studies (Moore & Semmens, 2010; Zhang et al., 2016). Additionally, sediment tracers may be unique to a specific catchment and, hence, a general approach used in previous studies was to select many tracer properties to best apportion deposited sediment to different potential sources (Lamba et al., 2015; Walling, 2013). For example, Collins et al. (2010) used a combination of heavy metals, actinides, and lanthanides (47 soil properties in all) to confirm that tracers, which included a range of different constituents, provided the most powerful discrimination of sediment source types in the catchment. Chen et al. (2016) selected 27 biomarker properties and 45 geochemical properties to discriminate fully the sediment sources from a small catchment in the Loess Plateau. To overcome this limitation, further studies are necessary that choose as many tracer properties as possible to better identify sediment sources.

6. Conclusions

Southwest China is one of the largest contiguous karst areas in the world and is experiencing severe soil erosion due to its special geological conditions. However, the contributions of different sediment sources are still not quantified in this region, which hinders the targeting of best management practices. This study used a composite fingerprinting technique to investigate the main sources of deposited sediment and their relative contributions in a typical karst depression in southwest China. Clay content, silt content, D_{60} , and D_{70} were the optimum tracers that correctly distinguished 89.5% of the source samples, which indicated that particle size distribution had a significant effect on the selection of optimum fingerprint factors in karst regions. It is important to note that cropland contributed approximately 69.3% of the total sediment, and the remaining sediment yield was from crack soil (22.1%) and forestland (8.6%). Thus, comprehensive soil conservation measures are required to control soil erosion for cropland due to its high sediment contribution. This study provides an indirect method to quantify sediment source contributions in karst depressions. Uncertainty in the sediment source partitioning, however, always exists. The contributions of the sediment sources to sediment yield among the three sediment cores were very different, implying that attention should be paid when using only one single core to trace sediment sources. The sediment contributions derived from undisturbed sediment (core G1) may be relatively appropriate since the deposited sediment in a dam or reservoir was also undisturbed in non-karst areas. Further studies are needed to evaluate uncertainties that may be caused by the selection of potential source types, the multivariate mixing model, or the locations of the sampling points.

Declaration of competing interest

The authors declare that they have no known competing financial interests or personal relationships that could have appeared to influence the work reported in this paper.

Acknowledgments

This study was supported by the State Key Program of National Natural Science Foundation of China (41730748), National Natural Science Foundation of China (41601299; 41977073; 41671287), Youth Innovation Promotion Association of CAS (2020359), CAS Interdisciplinary Innovation Team, and the Youth Innovation Team Project of ISA, CAS (2017QNCXTD_XXL).

References

- Bai, X. Y., Zhang, X. B., Chen, H., & He, Y. B. (2010). Using Cs-137 fingerprinting technique to estimate sediment deposition and erosion rates from Yongkang depression in the karst region of Southwest China. *Land Degradation & Development*, 21, 474–479.
- Blake, W. H., Ficken, K. J., Taylor, P., Russell, M. A., & Walling, D. E. (2012). Tracing crop-specific sediment sources in agricultural catchments. *Geomorphology*, 139, 322–329.
- Borrelli, P., Robinson, D. A., Fleischer, L. R., Lugato, E., Ballabio, C., Alewell, C., Meusburger, K., Modugno, S., Schütt, B., & Ferro, V. (2017). An assessment of the global impact of 21st century land use change on soil erosion. *Nature Communications*, 8, 1–13.
- Chen, F., Fang, N., & Shi, Z. (2016). Using biomarkers as fingerprint properties to identify sediment sources in a small catchment. *The Science of the Total Environment*, 557–558, 123–133.
- Collins, A. L., Foster, I. D. L., Gellis, A. C., Porto, P., & Horowitz, A. J. (2017). Sediment source fingerprinting for informing catchment management: Methodological approaches, problems and uncertainty. *Journal of Environmental Management*, 408, 5461–5471.
- Collins, A. L., & Walling, D. E. (2002). Selecting fingerprint properties for discriminating potential suspended sediment sources in river basins. *Journal of Hydrology*, 261, 218–244.
- Collins, A. L., & Walling, D. E. (2004). Documenting catchment suspended sediment sources: Problems, approaches and prospects. *Progress in Physical Geography*, 28, 159–164.
- Collins, A. L., & Walling, D. E. (2007). Sources of fine sediment recovered from the channel bed of lowland groundwater-fed catchments in the UK. *Geomorphology*, 88, 120–138.
- Collins, A. L., Walling, D. E., & Leeks, G. (1997). Source type ascription for fluvial suspended sediment based on a quantitative composite fingerprinting technique. *Catena*, 29, 1–27.
- Collins, A. L., Walling, D. E., Webb, L., & King, P. (2010). Apportioning catchment scale sediment sources using a modified composite fingerprinting technique incorporating property weightings and prior information. *Geoderma*, 155, 249–261.
- Collins, A. L., Zhang, Y., Walling, D. E., Grenfell, S. E., & Smith, P. (2010). Tracing sediment loss from eroding farm tracks using a geochemical fingerprinting procedure combining local and genetic algorithm optimisation. *The Science of the Total Environment*, 408, 5461–5471.
- D'Haen, K., Verstraeten, G., Duser, B., Degryse, P., Haex, J., & Waelkens, M. (2013). Unravelling changing sediment sources in a Mediterranean mountain catchment: A Bayesian fingerprinting approach. *Hydrological Processes*, 27, 896–910.
- Dai, Q., Peng, X., & Yang, Z. (2017). Runoff and erosion processes on bare slopes in the karst rocky desertification area. *Catena*, 152, 218–226.
- Duan, L., Huang, M., & Zhang, L. (2016). Differences in hydrological responses for different vegetation types on a steep slope on the Loess Plateau, China. *Journal of Hydrology*, 537, 356–366.
- Fang, H. (2015). Temporal variations of sediment source from a reservoir catchment in the black soil region, Northeast China. *Soil and Tillage Research*, 153, 59–65.
- Foley, J. A., Defries, R., Asner, G. P., Barford, C., Bonan, G., Carpenter, S. R., Chapin, F. S., Coe, M. T., Daily, G. C., & Gibbs, H. K. (2005). Global consequences of land use. *Science*, 309, 570–574.
- Hartmann, A., Goldscheider, N., Wagener, T., Lange, J., & Weiler, M. (2015). Karst water resources in a changing world: Review of hydrological modeling approaches. *Reviews of Geophysics*, 52, 218–242.
- Huang, D., Du, P., Wang, J., Wei, X., Liu, B., & Xu, J. (2019). Using reservoir deposits to quantify the source contributions to the sediment yield in the Black Soil Region, Northeast China, based on the fingerprinting technique. *Geomorphology*, 339, 1–18.
- Jiang, Z., Lian, Y., & Qin, X. (2014). Rocky desertification in southwest China: Impacts, causes, and restoration. *Earth-Science Reviews*, 132, 1–12.
- Jin, K. K., Onda, Y., Yang, D. Y., & Min, S. K. (2013). Temporal variations of reservoir sediment sources in a small mountainous catchment in Korea. *Earth Surface Processes and Landforms*, 38, 1380–1392.
- Krein, A., Petticrew, E., & Udelhoven, T. (2003). The use of fine sediment fractal dimensions and colour to determine sediment sources in a small watershed. *Catena*, 53, 165–179.
- Kurashige, Y., & Fusejima, Y. (1997). Source identification of suspended sediment from grain-size distributions: I. Application of nonparametric statistical tests. *Catena*, 31, 39–52.
- Lacey, J. P., Evrard, O., Smith, H. G., Blake, W. H., Olley, J. M., Minella, J., & Owens, P. N. (2017). The challenges and opportunities of addressing particle size effects in sediment source fingerprinting: A review. *Earth-Science Reviews*, 169, 85–103.
- Lamba, J., Karthikeyan, K. G., & Thompson, A. M. (2015a). Apportionment of suspended sediment sources in an agricultural watershed using sediment fingerprinting. *Geoderma*, 239–240, 25–33.
- Lamba, J., Karthikeyan, K. G., & Thompson, A. M. (2015b). Using radiometric fingerprinting and phosphorus to elucidate sediment transport dynamics in an agricultural watershed. *Journal of Soils and Sediments*, 29, 2681–2693.
- Lin, J., Huang, Y., Wang, M. K., Jiang, F., Zhang, X., & Ge, H. (2015). Assessing the sources of sediment transported in gully systems using a fingerprinting approach: An example from South-east China. *Catena*, 129, 9–17.
- Li, Z., Xu, X., Liu, M., Li, X., Zhang, R., Wang, K., & Xu, C. (2017). State-space prediction of spring discharge in a karst catchment in southwest China. *Journal of Hydrology*, 549, 264–276.
- Li, Z., Xu, X., Xu, C., Liu, M., Wang, K., & Yi, R. (2017). Monthly sediment discharge changes and estimates in a typical karst catchment of southwest China. *Journal of Hydrology*, 555, 95–107.
- Li, Z., Xu, X., Yu, B., Xu, C., Liu, M., & Wang, K. (2016). Quantifying the impacts of climate and human activities on water and sediment discharge in a karst region of southwest China. *Journal of Hydrology*, 542, 836–849.
- Li, Z., Xu, X., Zhang, Y., Wang, K., & Zeng, P. (2019). Reconstructing recent changes in sediment yields from a typical karst watershed in southwest China. *Agriculture, Ecosystems & Environment*, 269, 62–70.
- Martin, J. B., Kurz, M. J., & Khadka, M. B. (2016). Climate control of decadal-scale increases in apparent ages of eogenetic karst spring water. *Journal of Hydrology*, 540, 988–1001.
- Moore, J. W., & Semmens, B. X. (2010). Incorporating uncertainty and prior information into stable isotope mixing models. *Ecology Letters*, 11, 470–480.
- Motha, J. A., Wallbrink, P. J., Hairsine, P. B., & Grayson, R. B. (2003). Determining the sources of suspended sediment in a forested catchment in southeastern Australia. *Water Resources Research*, 39, 53–62.
- Muzylo, A., Llorens, P., Valente, F., Keizer, J. J., Domingo, F., & Gash, J. H. C. (2009). A review of rainfall interception modelling. *Journal of Hydrology*, 370, 191–206.
- Nearing, M. A., Xie, Y., Liu, B. Y., & Ye, Y. (2017). Natural and anthropogenic rates of soil erosion. *International Soil and Water Conservation Research*, 5, 77–84.

- Nosrati, K., Collins, A. L., & Madankan, M. (2018). Fingerprinting sub-basin spatial sediment sources using different multivariate statistical techniques and the Modified MixSIR model. *Catena*, *164*, 32–43.
- Owens, P. N., Blake, W. H., Gaspar, L., Gateuille, D., Koiter, A. J., Lobb, D. A., Petticrew, E. L., Reiffarth, D. G., Smith, H. G., & Woodward, J. C. (2016). Fingerprinting and tracing the sources of soils and sediments: Earth and ocean science, geoarchaeological, forensic, and human health applications. *Earth-Science Reviews*, *162*, 1–23.
- Palazón, L., Gaspar, L., Latorre, B., Blake, W. H., & Navas, A. (2015a). Identifying sediment sources by applying a fingerprinting mixing model in a Pyrenean drainage catchment. *Journal of Soils and Sediments*, *15*, 2067–2085.
- Palazón, L., Latorre, B., Gaspar, L., Blake, W. H., Smith, H. G., & Navas, A. (2015b). Comparing catchment sediment fingerprinting procedures using an auto-evaluation approach with virtual sample mixtures. *The Science of the Total Environment*, *532*, 456–466.
- Peng, T., & Wang, S. J. (2012). Effects of land use, land cover and rainfall regimes on the surface runoff and soil loss on karst slopes in southwest China. *Catena*, *90*, 53–62.
- Pimentel, D. (2006). Soil erosion: A food and environmental threat. *Environment, Development and Sustainability*, *8*, 119–137.
- Shi, Z. H., Ai, L., Fang, N. F., & Zhu, H. D. (2012). Modeling the impacts of integrated small watershed management on soil erosion and sediment delivery: A case study in the three Gorges area, China. *Journal of Hydrology*, *438–439*, 156–167.
- Stevens, C. J., & Quinton, J. N. (2008). Investigating source areas of eroded sediments transported in concentrated overland flow using rare earth element tracers. *Catena*, *74*, 31–36.
- Valentin, C., Poesen, J., & Li, Y. (2005). Gully erosion: Impacts, factors and control. *Catena*, *63*, 132–153.
- Walling, D. E. (2005). Tracing suspended sediment sources in catchments and river systems. *The Science of the Total Environment*, *344*, 159–184.
- Walling, D. E. (2013). The evolution of sediment source fingerprinting investigations in fluvial systems. *Journal of Soils and Sediments*, *13*, 1658–1675.
- Walling, D. E., Collins, A. L., & Stroud, R. W. (2008). Tracing suspended sediment and particulate phosphorus sources in catchments. *Journal of Hydrology*, *350*, 274–289.
- Walling, D. E., Owens, P. N., & Leeks, G. J. L. (2015). Fingerprinting suspended sediment sources in the catchment of the River Ouse, Yorkshire, UK. *Hydrological Processes*, *13*, 955–975.
- Wang, S., Fu, B., Piao, S., Lü, Y., Ciais, P., Feng, X., & Wang, Y. (2017). Reduced sediment transport in the Yellow River due to anthropogenic changes. *Nature Geoscience*, *9*, 38–41.
- Wang, B., Zhang, G. H., Yang, Y. F., Li, P. P., & Liu, J. X. (2018). The effects of varied soil properties induced by natural grassland succession on the process of soil detachment. *Catena*, *166*, 192–199.
- Wei, W., Chen, L., Fu, B., Huang, Z., Wu, D., & Gui, L. (2007). The effect of land uses and rainfall regimes on runoff and soil erosion in the semi-arid loess hilly area, China. *Journal of Hydrology*, *335*, 247–258.
- Wilkinson, S. N., Hancock, G. J., Bartley, R., Hawdon, A. A., & Keen, R. J. (2013). Using sediment tracing to assess processes and spatial patterns of erosion in grazed rangelands, Burdekin River basin, Australia. *Agriculture, Ecosystems & Environment*, *180*, 90–102.
- Yu, X. X., Wang, H. N., Xin, Z. B., & Lv, X. Z. (2013). Effect of forest on sediment yield in North China. *International Soil and Water Conservation Research*, *1*, 58–84.
- Zhang, X. C. (2014). New insights on using fallout radionuclides to estimate soil redistribution rates. *Soil Science Society of America Journal*, *79*, 1–8.
- Zhang, X. C., & Liu, B. L. (2016). Using multiple composite fingerprints to quantify fine sediment source contributions: A new direction. *Geoderma*, *268*, 108–118.
- Zhang, X. C., Liu, B. L., Liu, B., & Zhang, G. H. (2016). Quantifying sediment provenance using multiple composite fingerprints in a small watershed in Oklahoma. *Journal of Environmental Quality*, *45*, 1296–1302.
- Zhang, G. H., Tang, M. K., & Zhang, X. C. (2010). Temporal variation in soil detachment under different land uses in the Loess Plateau of China. *Earth Surface Processes and Landforms*, *34*, 1302–1309.
- Zhang, J., Yang, M., Zhang, F., Zhang, W., Zhao, T., & Li, Y. (2017). Fingerprinting sediment sources after an extreme rainstorm event in a small catchment on the Loess Plateau, China. *Land Degradation & Development*, *28*, 2527–2539.
- Zhang, X. C., Zhang, G. H., Garbrecht, J. D., & Steiner, J. L. (2015). Dating sediment in a fast sedimentation reservoir using Cesium-137 and Lead-210. *Soil Science Society of America Journal*, *79*, 948–956.
- Zhang, X. C., Zhang, G. H., Liu, B. L., & Liu, B. (2016). Using cesium-137 to quantify sediment source contribution and uncertainty in a small watershed. *Catena*, *140*, 116–124.
- Zhao, G., Mu, X., Han, M., An, Z., Gao, P., Sun, W., & Xu, W. (2017). Sediment yield and sources in dam-controlled watersheds on the northern Loess Plateau. *Catena*, *149*, 110–119.
- Zhou, H., Chang, W., & Zhang, L. (2016). Sediment sources in a small agricultural catchment: A composite fingerprinting approach based on the selection of potential sources. *Geomorphology*, *266*, 11–19.



Contents lists available at ScienceDirect

International Soil and Water Conservation Research

journal homepage: www.elsevier.com/locate/iswcr

Original Research Article

Cadmium speciation as influenced by soil water content and zinc and the studies of kinetic modeling in two soils textural classes

Farzad Rassaei^{a,*}, Mehran Hoodaji^a, Seyed Ali Abtahi^b^a Department of Soil Science, Isfahan (Khorasgan) Branch, Islamic Azad University, Isfahan, Iran^b Department of Soil Science, Shiraz University, Shiraz, Iran

ARTICLE INFO

Article history:

Received 20 July 2019

Received in revised form

24 April 2020

Accepted 15 May 2020

Available online 30 May 2020

Keywords:

Cadmium

Chemical forms

Field capacity

Flooding condition

Kinetic model

Sequential technique

Soil water content

Zinc

ABSTRACT

Background and aims: Since few studies have existed in the literature about the effect of zinc (Zn) on cadmium (Cd) chemical forms in soils. Therefore, this study has been performed to determine the impact of Zn on cadmium Cd chemical forms in two soil textural classes in Fars province-Iran at two soil water content (SWC) (flooded soil water content (FSWC) and field capacity soil water content (FCSWC)) and study the kinetic modeling of Cd.

Methods and materials: Variables were three levels of Cd (0, 30 and 60 mg kg⁻¹ of soil as CdSO₄·8H₂O), three levels of Zn (0, 5 and 10 mg kg⁻¹ of soil as Zn-EDTA) three level Incubation times (2, 4 and eight weeks), two soil textural classes (clay and sandy clay loam) and two SWC. The randomized completed block design (RCBD) was used for this experiment. The Tessier sequential extraction method was used to determine the Cd concentration in (WsEx), (Fe-MnOx), (Car), (Om) and (Res) chemical forms.

Results: In the FSWC, Zn reduced the Cd concentration in Fe-MnOx, Car and Om forms and increased the WsEx but had no significant effect on the Res form. Changes in the Cd chemical forms under the influence of Zn in both soils followed a similar trend. In the FCSWC, Zn reduced the Cd concentration Car and Om forms and increased the Cd concentration in the Fe-MnOx and WsEx forms while had no significant effect on Res form in the sandy clay loam soil. In the clay soil adding Zn reduced the Cd concentration in Car and Om fractions and increased the Fe-MnOx and Res forms while has no significant effect on WsEx form. The competitive transport and adsorption Interactions between these two ions caused the changing in the Cd concentration in its chemical forms. Zn reduces the Cd concentration in the forms which are easily released into the soil solution from where they can be absorbed by plants. The power function kinetic mode is the best fitted model which can describe the Cd adsorption in our soil samples. The clay and organic compounds control the Cd adsorption in soils. The higher rate of Cd adsorption in almost all shaking times shows that Cd has more ability to occupy the adsorption sites in soils.

© 2020 International Research and Training Center on Erosion and Sedimentation and China Water and Power Press. Production and Hosting by Elsevier B.V. This is an open access article under the CC BY-NC-ND license (<http://creativecommons.org/licenses/by-nc-nd/4.0/>).

1. Introduction

The heavy metal pollution of soils has become widely environmental problem (Tóth, Hermann, Szatmári, & Pásztor, 2016) and raises our concern about the food chain safety and human health (Duan, Lee, Liu, Chen, & Hu, 2016; Wu & Sun, 2016). Cd is considered as a toxic element among the heavy metals (Wu et al., 2016). Cd is a non-essential element which can take up by plants and enter our food chain (Adriano, 1986).

Changes in soil water content have a significant effect on soil redox potential (Eh) and heavy metals solubility (Kashem & Singh, 2001). Highly reduced condition in soil reduces the Cd solubility due to the formation of Cd Sulphide (De Livera, McLaughlin, Hettiarachchi, Kirby, & Beak, 2011; Rassaei, Hoodaji, & Abtahi, 2019; Zheng, Zheng, & Chen, 2013). Insoluble Fe³⁺ and Mn⁴⁺ hydroxides in aerobic soils provide sorption surface for Cd and other metals' ions (Gray, McLaren, Roberts, & Condon, 1999; Hindersmann & Mansfeldt, 2014; Loganathan, Vigneswaran, Kandasamy, & Naidu, 2012; McLaren & Cameron, 1996, p. 340). At flooded soil due to drop of Eh Mn⁴⁺ and Fe³⁺ become reduced to their more soluble oxidized forms Mn²⁺ and Fe²⁺ (Hindersmann &

* Corresponding author.

E-mail address: Farzad.rassaei20@gmail.com (F. Rassaei).

Abbreviation explanation

WsEx	Water Soluble and Exchangeable
Car	Carbonate
Fe-MnOx	Iron–Magnesium Oxides
Om	Organic matter
Res	Residual

Mansfeldt, 2014; McLaren & Cameron, 1996, p. 340). Dissolution of Mn and Fe hydrous oxides releases the co-sorbed metal ions into soil solution and increasing metal absorption by plants. Flooded condition reduces soil pH in alkaline soils. Ferric ions will act as electron receptors while organic matter will act as an electron donor (Sahrawat, 2012). Due to limited diffusion in the water layer above the flooded soils, CO₂ is retained in soils and with formation of carbonic acid decreases soil pH. Formation of CO₂ can reduce soil pH and therefore increases the solubility of heavy metals (Yoshida & Tanaka, 1969).

Cd and Zn have similar chemical characteristics; they both are maintained in soil's exchangeable sites as a divalent ion (Robert et al., 2003). Hewitt (1966) resulted elements with the similar chemical-physical properties could act as antagonistic. Both Zn and Cd are in group II of the periodic table and usually are together in the ores and compete for ligands (Aravind & Prasad, 2005). The flooded condition has positive impacts on Zn availability (Ponnamperuma, 1972). Zn dynamic in the soil depends on pH, clay content and organic matter. Fe–Mn (hydr) and Al oxides, organic matter and clays provide sorption surfaces for Zn. Mn²⁺ and Fe²⁺ compete with Zn²⁺ for sorption sites on the organic matter (Hafeez, Khanif, & Saleem, 2013). Jamali, Ghaderian, & Karimi, 2014 resulted Cd toxicity in the shoot of *M. flavida* was declined by using Zn as a treatment. They concluded that the competition between Cd and Zn led to a decline in Zn and Cd uptake. It has been reported that Zn (ZnSO₄) has both antagonistic (Abdel-Sabour, Mortvedt, & Kelose, 1988) and synergistic impact on Cd uptake by plants (Williams & David, 1976). Applying a large quantity of Zn fertilizer reduced Cd uptake in soybean (Haghir, 1974).

Zn can be used in order to reduce the harmful effects of Cd concentration in grain of wheat grown in Cd contaminated soil (Sarwar et al., 2015). Zn is an essential nutrition while Cd is a poisonous heavy metal and a non-essential element. It can be possible that the toxic effects of Cd can be declined by Zn (Rassaei, Hoodaji, & Abtahi, 2019; Hart, Welch, Norvell, & Kochian, 2002). These hypotheses lead to the successful examination of soil extractable Cd concentration differences over time. This paper was therefore performed to examine the effect of Zn and short-term periods of soil water content on soil Cd chemical forms in two soil textural classes in Fars-Iran. Improving our knowledge of the effect of Zn and SWC on soil Cd chemical forms may provide greater insight into appropriate strategies to better manage Cd accumulation in soils.

Kinetic models describe the adsorption, precipitation and exchange process of heavy metals in soils (Singh & Pandeya, 1998). Kinetic model of heavy metals usually shows a sharp step in the first hours which is related to soil surface adsorption of heavy metals. The second step is slow adsorption rate which is related to chemical sorption or diffusion of heavy metals in soils (Jalali & Khanlari, 2008). Soil properties like OM, pH, Clay content and OM will affect the sorption behavior of heavy metals can be affected by soil's factors like organic matter, pH, Clay content, CEC and CCE (Diatta and Kocalkowski; 1998; McBride, 1989). Exponential and elovich models are the most general models which can describe the

sorption of Zn in the calcareous soils (Reyhanitabar, Ardalan, Karimian, Savaghebi, & Gilkes, 2011) in addition to diffusion and second order equations (Ma & Liu, 1997). The adsorption mechanism is important to determine the solubility of Cd and Zn in the soil solution (Hanafi & Salwa, 1998).

The objectives of this paper are to (1) examine the effect of Zn on Cd chemical forms due to their similar properties; (2) examine the effect of soil water content on Cd and Zn interaction; (3) study the kinetics of Cd (4) examine the effect of soil characteristics on the kinetics model of Cd.

2. Materials and methods

2.1. Study area

Sarvestan is located in 80 km south of Shiraz, Fars-Iran by the name of Sarvestan plain, between latitude 29° 11' to 29° 25' N and longitude 52° 45' to 53° 25' E. This region covers an area of 95000 ha. The climate conditions are different in temperature (i.e. mean monthly max. Temperature is 6.30–29.50) and rainfall occurs mostly in November to May (346 mm on average). Soil moisture and temperature regimes are classified as xeric and thermic (Mahmudi, 1997).

Kamfirouz is located in 110 km north west of Shiraz, Fars-Iran by the name of Kamfirouz Plain, between latitude 30° 25' to 30° 10' N and longitude 52° 20' to 52° 10' E along the eastern and western sides of the Chour river and north of Dorodzan dam in Fars-Iran. This area is 11300 ha. The minimum and maximum rainfall is 370 and 800 mm respectively and the mean precipitation is 580 mm. The soil in this region is mostly calcareous (carbonate). Kamfirouz is known as the rice production in Fars-Iran.

2.2. Soil

2.2.1. Sample collection

Two kinds of soil samples (top soil, a depth of 0–25 cm) were collected from Sarvistan series and Kamfirouz series of Fars province, Iran for this study. The soils reference groups identified using the FAO-WRB system (IUSS Working Group WRB, 2015) as Calcic Luvisols (LK) (World Reference Base for Soil Resources, 2014).

2.2.2. Sample preparation

Soil samples had passed through a 2 mm sieve. They were then oven-dried at 105 ± 0.5 °C until constant weight, cooled and stored until analysis (Allen, Grinshaw, Parkinson, & Qjuarmby, 1974, p. 565).

2.2.3. Sample analysis

Soil texture was measured by the hydrometer method (Gee & Bauder, 1986), pH in the 1:1 suspension of soil and distilled water (Richards, 1969), electrical conductivity (EC) in the 1:1 suspension extract of soil and distilled water (Gupta, 2000), organic carbon by the method of Walkley and Black (Nelson & Sommers, 1982), calcium carbonate equivalent (CCE) by the method of neutralizing with hydrochloric acid (Richards, 1969) and available Mn, Fe, Zn, Cu, and Cd extracted with the 0.005M DTPA solution (Lindsay & Norvell, 1978) were calculated (Table 1).

2.3. Preparation of Cd–Zn test at FSWC

The variables were three levels of Zn (0, 5 and 10 mg kg⁻¹), three levels of Cd (0, 30 and 60 mg kg⁻¹) and three incubation time levels (2, 4 and eight weeks). This research was performed in a randomized completed block design (RCBD) with two replications. The incubation experiment was performed in the plastic beakers. Each

Table 1
Selected chemical properties of soils used.

Properties	Amount	
	Kamfiroz series	Sarvestan series
Sand (%)	51.8	12
Silt (%)	25.5	34.8
Clay (%)	22.7	53.2
Texture	Sandy clay loam	Clay
Om (%) ^a	3.4	2.61
CCE (%) ^b	52.3	34.1
CEC (Cmol kg ⁻¹) ^c	8.34	30.31
EC (dS. m ⁻¹) ^d	0.74	0.76
pH(1:1)	7.92	7.38
Fe(mg/kg)	3.3	4.4
Mn(mg/kg)	5.4	8.7
Zn(mg/kg)	0.33	0.51
Cu(mg/kg)	0.93	1.42
Cd(mg/kg)	nd	nd

^e- ND: None Detectable.

^a - Organic matter.

^b - Calcium carbonate equivalent.

^c - Cation exchange capacity.

^d - Electrical conductivity.

beaker (equal to 0.5 kg soil) was treated with three Zn levels from source of EDTA zinc salt (Zn-EDTA, Merck Co. Germany) three Cd levels from source of cadmium sulphate (CdSO₄. 8H₂O, Merck Co. Germany). The beakers were kept in an incubator at 25 °C in the flooded condition. For FSWC condition, the deionized water was added to the beakers to make a 5 cm of water layer over the soil samples. The pots were covered by porous plastic to stop the rapid evaporation.

Table 2
Summary of sequential extraction method provided by Tessier et al. (1979) to determine the chemical forms of cadmium.

Row	Chemical forms	Time(h)	Temperature(°c)	Soil(g)/Solution Volume(ml)	Used solution
1	Water soluble and Exchangeable WsEx.	1	25	16	MgCl2 (1 mol/l), pH = 7
2	Carbonate Car.	5	25	16	NaOAc (1 mol/l), pH = 5
3	Iron and Manganese Oxides Fe-MnOx.	6	96	16	NH2OH·HCl(0.04 mol/l) in HOAc (%25 v: v), pH = 2
4	Organic Mater OM.	5.5	85	16	3 ml HNO3 (0.02 mol/l), 8 ml H2O2 (%30), pH = 2, 5 ml NH4OAc (3.2 mol/l)/HNO3 (%20 v in v)
5	Residual Res.	2	130	16	(3:1 v/v) HCl:HNO3

Table 3
ANOVA table between Cd chemical forms and Zn salt in clay soil at the FSWC.

Cd chemical forms		Sum of Squares	df	Mean Square	F	Sig.
WsEx * Zinc	Between Groups	373.442	2	186.721	3.494	.042
	Within Groups	1763.403	33	53.436		
	Total	2136.845	35			
Car * Zinc	Between Groups	13.428	2	6.714	3.574	.039
	Within Groups	61.988	33	1.878		
	Total	75.416	35			
Fe-Mnox * Zinc	Between Groups	41.861	2	20.930	3.536	.041
	Within Groups	195.321	33	5.919		
	Total	237.181	35			
Om* Zinc	Between Groups	1.383	2	.692	4.422	.020
	Within Groups	5.162	33	.156		
	Total	6.546	35			
Res* Zinc	Between Groups	17.294	2	8.647	.123	.885
	Within Groups	2318.423	33	70.255		
	Total	2335.717	35			

2.4. Preparation of Cd–Zn test at FCSWC

The variables were three levels of Zn (0, 5 and 10 mg kg⁻¹), three levels of Cd (0, 30 and 60 mg kg⁻¹). The incubation experiment was performed in plastic beakers. The study was RCBD with two replications. Each beaker (equal to 0.5 kg soil) was treated with three levels of Cd from cadmium sulphate source (Merck Co. Germany) and three levels of Zn from source of EDTA zinc salt (Zn-EDTA, Merck Co. Germany). The beakers were placed alternatively in FC (33 kPa) conditions (By weighing the beakers on the first day and comparing their weight in the following days with the initial weight). The beakers were covered with the porous plastic membrane and placed in an incubator at the constant temperature (25 °C) to prevent the fast evaporation while the air can pass through.

2.5. Preparation for studies of kinetic modeling

Two-gram samples of soil were added in 100 mL polypropylene centrifuge tubes, then 30 mL 0.01M CaCl₂ containing 800 mg L⁻¹ Cd as CdSO₄ was added to each centrifuge tubes in two replications. Centrifuge tubes were shaken for 1, 10, 30, 60, 120, 450, 840 and 1440 min at 25 °C and then centrifuged at 3000 rpm. The filtered supernatants were analyzed for Cd by an atomic absorption spectrophotometer (Shimadzo AA-670). We determined the sorbed metals by soils by Eq. (1) and seven kinetics models were used to demonstrate the adsorption pattern of Cd and Zn in soil samples from Eq. (2) to Eq. (8):

$$M = \frac{(C_i - C_f)V}{W} \quad (1)$$

Table 4
ANOVA table between Cd chemical forms and Zn salt in sandy clay loam soil at the FSWC.

Cd chemical forms		Sum of Squares	df	Mean Square	F	Sig.
WsEx* Zinc	Between Groups	373.293	2	186.646	3.754	.034
	Within Groups	1640.594	33	49.715		
	Total	2013.886	35			
Car* Zinc	Between Groups	13.720	2	6.860	3.701	.035
	Within Groups	61.160	33	1.853		
	Total	74.881	35			
Fe-Mnox* Zinc	Between Groups	42.174	2	21.087	4.687	.016
	Within Groups	148.463	33	4.499		
	Total	190.637	35			
Om* Zinc	Between Groups	1.481	2	.741	4.897	.014
	Within Groups	4.991	33	.151		
	Total	6.472	35			
Res* Zinc	Between Groups	25.759	2	12.879	.216	.807
	Within Groups	1972.063	33	59.759		
	Total	1997.822	35			

- Zero-order ($q_t = q_0 - k_0t$) (2) Third-order ($1/q_t^2 = 1/q_0^2 - k_3t$) (7)
- First-order ($\ln q_t = \ln q_0 - k_1t$) (3) Elovich ($q_t = 1/p_s \ln a_s p_s - 1/p_s \ln t$) (8)
- Second-order ($1/q_t = 1/q_0 - k_2t$) (4) Where M is the amount of metal adsorbed (mg kg^{-1}), C_i is the initial metal concentration (mg L^{-1}), C_f is the metal concentration after every shaking times (mg L^{-1}), V is the solution volume and W is the weight of air dried soil samples. k_p is diffusion rate constant [$(\text{mg kg}^{-1})^{-0.5}$], k_0 is zero-order rate constant ($\text{mg kg}^{-1}\text{s}^{-1}$), k_1 is first-order
- Power function ($q_t = a t^b$) (5)
- Parabolic diffusion ($q_t = q_0 - k_p t^{0.5}$) (6)

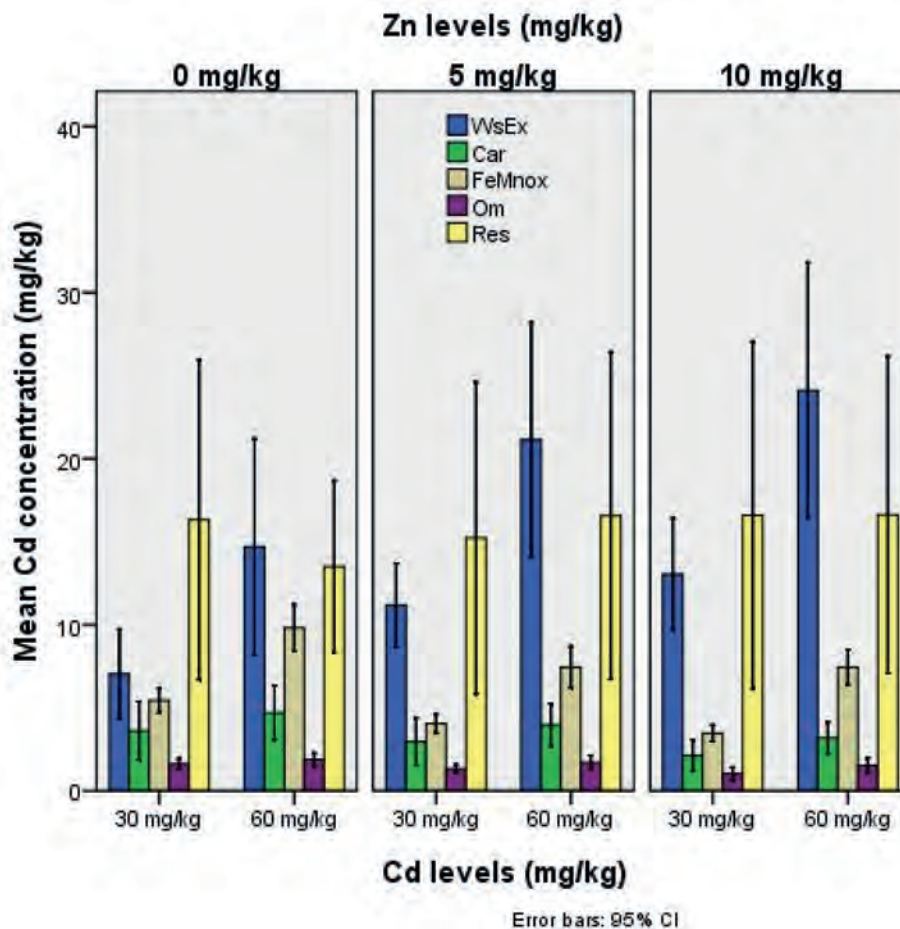


Fig. 1. Effect of Zn on Cd chemical forms in clay soil at the FSWC.

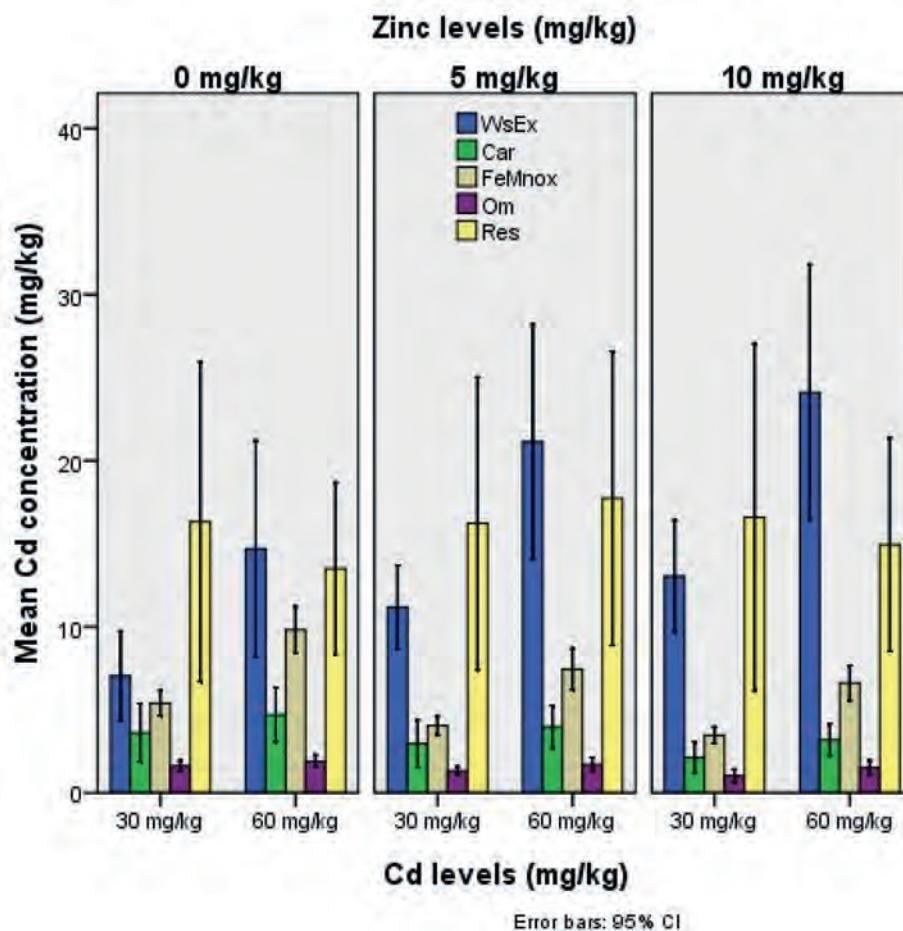


Fig. 2. Effect of Zn on Cd chemical forms in sandy clay loam soil at the FSWC.

Table 5

Correlation between Cd chemical forms (mg/kg soil) and Zn levels in clay and sandy clay loam soil in the FSWC.

Soil	Zn		WsEx	Car	Fe-MnOx	Om	Res
Sandy Clay Loam	Zn	Pearson Correlation	.421 ^b	-.428 ^a	-.455 ^a	-.478 ^a	.047
		Sig. (2-tailed)	.011	.009	.005	.003	.786
		N	36	36	36	36	36
Clay	Zn	Pearson Correlation	.431 ^a	-.421 ^b	-.378 ^b	-.460 ^a	.086
		Sig. (2-tailed)	.009	.010	.023	.005	.619
		N	36	36	36	36	36

^a Correlation is significant at the 0.01 level (2-tailed).

^b Correlation is significant at the 0.05 level (2-tailed).

Table 6

ANOVA table between Cd chemical forms and Zn salt in clay soil at the FCSWC.

Cd chemical forms		Sum of Squares	df	Mean Square	F	Sig.
WsEx * Zinc	Between Groups	18.770	2	9.385	.130	.879
	Within Groups	2384.909	33	72.270		
	Total	2403.679	35			
Car * Zinc	Between Groups	16.745	2	8.373	4.683	.016
	Within Groups	58.996	33	1.788		
	Total	75.741	35			
Fe-Mnox * Zinc	Between Groups	42.695	2	21.348	3.695	.036
	Within Groups	190.649	33	5.777		
	Total	233.344	35			
Om* Zinc	Between Groups	1.532	2	.766	5.091	.012
	Within Groups	4.966	33	.150		
	Total	6.498	35			
Res* Zinc	Between Groups	367.701	2	183.851	3.398	.046
	Within Groups	1785.723	33	54.113		
	Total	2153.425	35			

Table 7
ANOVA table between Cd chemical forms and Zn salt in sandy clay loam soil at the FCSWC.

Cd chemical forms		Sum of Squares	df	Mean Square	F	Sig.
WsEx * Zinc	Between Groups	358.632	2	179.316	3.624	.038
	Within Groups	1632.669	33	49.475		
	Total	1991.301	35			
Car * Zinc	Between Groups	15.944	2	7.972	4.436	.020
	Within Groups	59.308	33	1.797		
	Total	75.252	35			
Fe-Mnox * Zinc	Between Groups	42.695	2	21.348	3.692	.036
	Within Groups	190.789	33	5.781		
	Total	233.484	35			
Om* Zinc	Between Groups	1.481	2	.741	4.897	.014
	Within Groups	4.991	33	.151		
	Total	6.472	35			
Res* Zinc	Between Groups	211.525	2	105.762	1.591	.219
	Within Groups	2193.190	33	66.460		
	Total	2404.715	35			

rate constant (s^{-1}), k_2 is second-order rate constant $[(mg\ kg^{-1})^{-1}]$, k_3 is third-order rate constant $[(mg\ kg^{-1})^{-2}\ min^{-2}]$, b_s is adsorption constant $[(mg\ kg^{-1})^{-1}]$, q_t and q_0 are the amount of soil adsorbed ($mg\ kg^{-1}$) after t (s) time of examination and at $t = 0$, respectively. a is initial adsorption rate constant ($mg\ kg^{-1}s^{-1}$), a_s is initial adsorption rate ($mg\ kg^{-1}s^{-1}$), b is adsorption rate coefficient $[(mg\ kg^{-1})^{-1}]$.

2.6. Sequential method

The Tessier, Campbell, and Bisson (1979) sequential extraction method was used to calculate the Cd concentration in the water

soluble-exchangeable (WsEx), Iron-manganese oxide (Fe-MnOx), Carbonate (Car), organic matter (Om) and residual (Res) chemical forms after 2, 4 and eight weeks of incubation time Table 2. Extractions were put in 100 ml centrifuge tubes. Between each consecutive extraction, the supernatant was centrifuged for 30 min at 4000 r/min and then purified. The total cadmium concentration in soils were determined by digesting 0.5 g soil samples (oven dry weight) with $HNO_3_HF_HClO_4$ mixture accompanied by elemental analysis, the concentrations of Cd in all solutions were studied by an atomic absorption spectrophotometer (Shimadzu-AA 670).

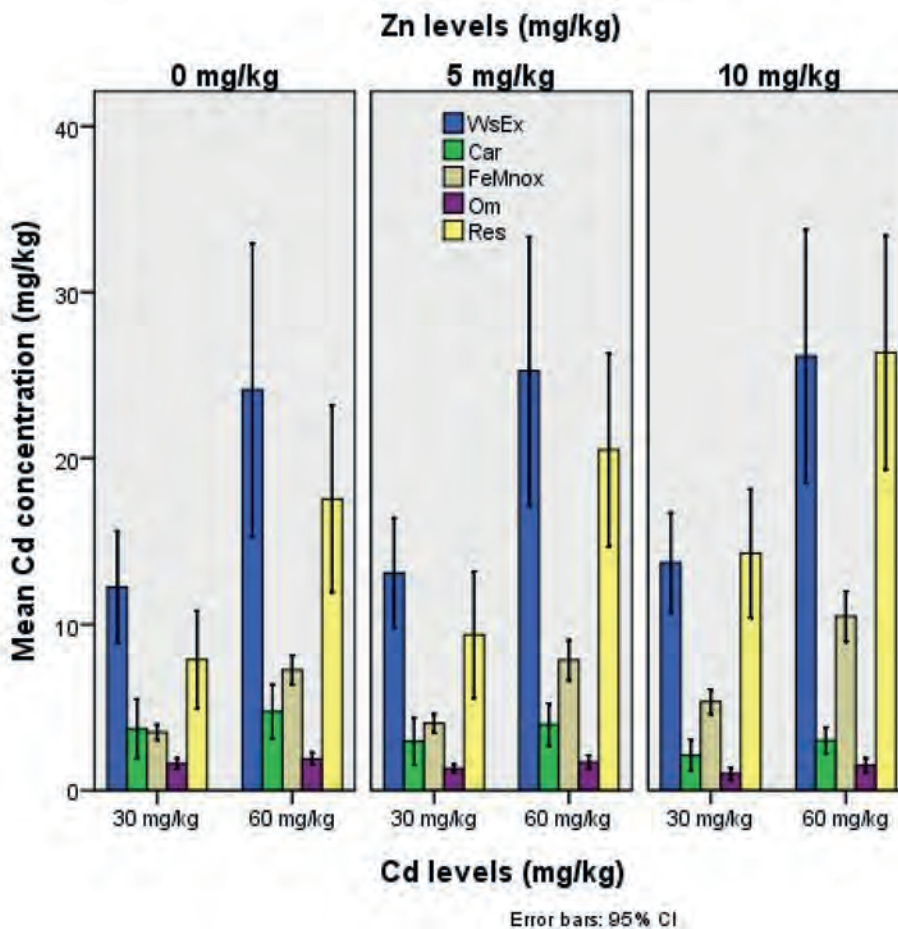


Fig. 3. Effect of Zn on Cd chemical forms in clay soil at the FCSWC.

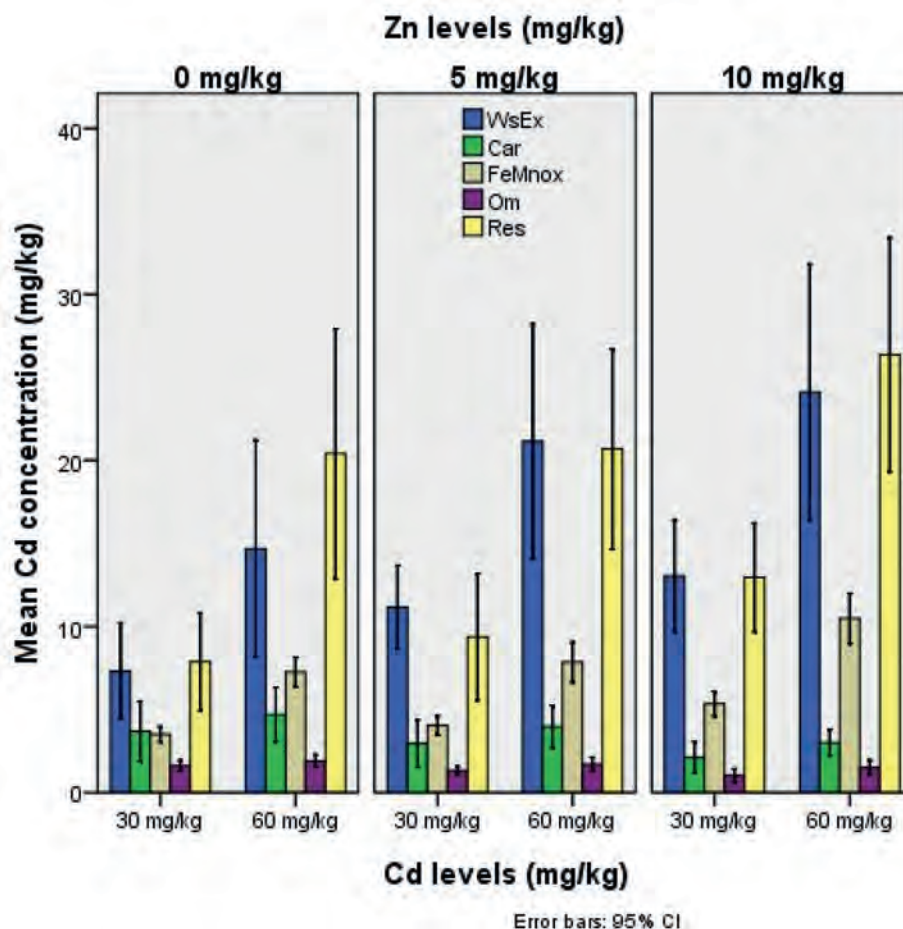


Fig. 4. Effect of Zn on Cd chemical forms in sandy clay loam soil at the FCSWC.

3. Data analysis

Statistical analysis was performed with SPSS Version 16.0 statistical software package (IBM, USA). Data were demonstrated as means \pm standard deviation (SD). Differentiations between groups were performed with analysis of non-parametric test. A value of $P < 0.05$ was regarded statistically significant. The Duncan's multiple range tests used to decide statistical significance of the effects due to treatments and their interaction.

4. Result and discussion

4.1. Effect of Zn on Cd chemical forms in the FSWC

The ANOVA table between Cd chemical forms and Zn indicated that adding Zn to the soil samples has significant effect on Cd concentration in its chemical forms in two soils textural classes (Tables 3 and 4). Zn reduced the Cd concentration in the Fe-MnOxide, Car and Om chemical forms while increased the Cd concentration in the WsEx and had no effect on Res chemical form (Figs. 1 and 2). The effect of Zn on reducing the Cd concentration on the Om form in the sandy clay loam soil ($p = 0.014$) is more significant than the clay soil ($p = 0.020$). Changes in the Cd concentration in the chemical forms as influenced by Zn followed a similar trend in both textural soils which suggests that soil properties do

not have a significant effect on this interaction (Table 5). We could not find the definite reason for these changes in the literature, but the competition between the Zn and Cd should be the reason due to their chemical similarities. Cd and Zn are both similar in ionic structures and electro negativities but they are also different in ionic radius ($\text{Cd}^{2+} = 0.097 \text{ nm}$, $\text{Zn}^{2+} = 0.074 \text{ nm}$). Their similarities and their differences may cause competition between these two ions on their sorption in the soil or absorption by the plants. The reduction of Cd concentration in Car, Fe-MnOx and Om chemical forms caused by Zn could be resulted from the competitive transport and adsorption interaction between them. Zn has a more tendency to form a chemical bond and to create a more stable complex with the carbonate group, iron and manganese hydroxides and organic matter agents. Zn reduces Cd uptake in soybean (Haghiri, 1974). The definition of hard and soft acids and bases could explain the strength of metal complexes. Based on this definition, cations and ligands are Lewis acids and Lewis bases respectively. Metal cation and ligand are acting as electron acceptor and donor in a complex (Pearson (1973)). The bonds between hard bases and hard acids are strong while the bonds made between hard-soft or soft-hard acids and bases are weak. Cd^{+2} is a soft Lewis acid but Zn^{+2} is a borderline Lewis acid (between hard and soft) while carbonates and organic matters are hard Lewis base. Hence, the complexes between Zn^{+2} and carbonate and organic compounds are stronger than Cd^{+2} complexes.

Table 8

Correlation between Cd chemical forms (mg/kg soil) and Zn levels in clay and sandy clay loam soil in the FCSWC.

Soil			WsEx	Car	Fe-MnOx	Om	Res
Sandy Clay Loam	Zn	Pearson Correlation	.415 ^b	-.460 ^a	.407 ^b	-.478 ^a	.276
		Sig. (2-tailed)	.012	.005	.014	.003	.103
		N	36	36	36	36	36
Clay	Zn	Pearson Correlation	.088	-.470 ^a	.407 ^b	-.485 ^a	.402 ^b
		Sig. (2-tailed)	.609	.004	.014	.003	.015
		N	36	36	36	36	36

^a Correlation is significant at the 0.01 level (2-tailed).^b Correlation is significant at the 0.05 level (2-tailed).**Table 9**Coefficients of determination (R²) and standard errors (SE) for Cd kinetics models.

Kinetic model	R ²	Range	SE	Range
Zero order	0.58	0.35–0.75	512	254–717
First order	0.56	0.34–0.71	0.08	0.04–0.1
Second order	0.53	0.33–0.68	1.2 × 10 ⁻⁵	8 × 10 ⁻⁶ – 2 × 10 ⁻⁵
Third order	0.50	0.31–0.64	3.8 × 10 ⁻⁹	2 × 10 ⁻⁹ – 5 × 10 ⁻⁹
Parabolic diffusion	0.75	0.55–0.88	391	179–597
Power function	0.89	0.84–0.95	0.04	0.02–0.06
Elovich	0.88	0.82–0.95	266	124–460

Table 10

Correlation between adsorbed Cd and soil properties.

	pH	EC	OM	Clay	Silt	Sand	CEC	CCE
Cd-1	-0.92**	-0.23	0.89**	0.76*	-0.55	-0.05	0.89**	-0.88**
Cd-15	-0.86**	-0.05	0.95**	0.80**	-0.54	-0.14	0.87**	-0.90**
Cd-30	-0.81**	-0.06	0.95**	0.75*	-0.50	-0.14	0.81**	-0.92**
Cd-60	-0.83**	-0.12	0.94**	0.79**	-0.54	-0.12	0.88**	-0.92**
Cd-120	-0.87**	-0.14	0.91**	0.84**	-0.64*	0.002	0.92**	-0.88**
Cd-450	-0.83**	-0.19	0.88**	0.81**	-0.62	0.002	0.87**	-0.90**
Cd-840	-0.76*	-0.11	0.87**	0.83**	-0.61	-0.05	0.86**	-0.88**
Cd-1440	-0.75*	-0.22	0.80**	0.76*	-0.63*	0.10	0.79**	-0.82**

* And ** are Significant at 0.05 and 0.01, respectively.

4.2. Effect of Zn on Cd chemical forms in the FCSWC

Based on the ANOVA table using Zn into the soil samples has significant effect on Cd concentration in two textural soils (Tables 6 and 7). The mean of data analysis showed that adding Zn has significant effect on almost all Cd chemical forms in both soils textural classes. Zn reduced the Cd concentration in the Car and Om forms and increased the Fe-MnOx and Res fractions but has no effect on WsEx ($P = 0.879$) form. Zn decreased the Cd concentration in the Car and Om forms and increased the WsEx and Fe-MnOx forms but has no effect on Res form in sandy clay loam soil (Figs. 3 and 4). Soil properties have significant effects on the influence of Zn in soil samples at the FC water content. Correlation between Zn and Car, Fe-MnOx, Om and Res forms in the clay soil were higher than the sandy clay loam soil (Table 8). Mazumdar, Das, and Patra (2006) resulted that adding Zn to the Cd-contaminated soil reduced the Cd concentration in the available forms. They also stated that reducing Cd concentration by Zn and incubation time is more significant than using Zn alone. It has been suggested that the competition between these two ions for adsorbing at the soil surface reduces the adsorption and accumulation of Cd in the plants (Misra, Sarkunan, Das, & Nayar, 1990; Oliver, Wilhelm, McFarlan, Tiller, & Cozens, 1997; Petruzzelli, 1996). Chakravarty and Srivastava (1997) reported that the interaction of Zn and Cd can overcome the toxicity of Cd and reduce its toxicity.

4.3. Adsorption kinetic

The Cd adsorption rate at the first hours of the study was rapid and then became slower. The power function kinetic model (Eq.

(5)) was the best model due to higher coefficient determination ($R^2 = 0.89$) and less standard error ($SE = 0.04$) (Table 9). The adsorption patterns of heavy metals identify in two fast and slow steps. The fast step is related to surface sorption of on soil components and the slow step is due to the chemical sorption into soil components with a stronger chemical bond (Jalali & Khanlari, 2008). The correlation between Cd adsorption and shaking periods were significantly negative with CCE and soil pH and positive with Om, clay and CEC which means the soils with high CCE and pH has low Cd adsorption rate (Table 10). The Om, clay and CEC increase the Cd adsorption rate due to providing sorption sites for ions. Shaheen (2009) resulted that the main soil components which can affect the Cd adsorption are Om, clay content and CCE.

5. Conclusion

Zn reduced the Cd concentration in the Fe-MnOxide, Car and Om forms in both soil samples and increased the Cd concentration in the WsEx while had no effect on Res form which shows that soil characteristics do not have significant effect on the influence of Zn in the FSWC. In the FCSWC, Zn reduced the Cd concentration in the Car and Om forms and increased the Fe-MnOx and Res forms while has no effect on WsEx form in the clay soil. In the sandy clay loam soil, Zn declined the Cd concentration in the Car and Om fractions and increased the Fe-MnOx and WsEx forms while had no effect on Res form. This means soil properties affected the Cd concentration in the Cd chemical fractions in this SWC. The Cd adsorption rate was sharp at the first hours of the study and then became slower. The best fitted model for Cd kinetic model was the power function. The negative correlation with Cd adsorption and pH and CCE showed that this two soil factors reduces Cd adsorption rate.

Availability of data and materials

The datasets during and/or analyzed during the current study available from the corresponding author on reasonable request.

Funding

There is no funding regarding this manuscript.

Authors' contributions

Farzad Rassaei: design of the work, the acquisition, analysis, interpretation of data, writing the manuscript, revised the manuscript.

Mehran Hoodaji: design of the work, analysis, interpretation of data, revised the manuscript.

Seyed Ali Abtahi: interpretation of data, revised the manuscript.

Declaration of competing interest

The authors declare that they have no conflict of interest.

Acknowledgement

I would like to express my appreciation to my family (Dr. Farhang Rassaei, Mahdokht Massoud, Dr. Liza Rassaei, Dr. Farshad Rassaei, Farhad and Janet Rassaei) who provided me the possibility to complete this paper.

References

- Abdel-Sabour, M., Mortvedt, J., & Kelose, J. (1988). Cadmium-zinc interaction in plants and extractable cadmium and zinc fractions in soil. *Soil Science*, *145*, 424–431.
- Adriano, D. C. (1986). *Trace elements in the terrestrial environment*. New York: Springer.
- Allen, S. E., Grimshaw, H. M., Parkinson, J. A., & Quarmby, C. (1974). *Chemical methods for analyzing ecological materials*. London: Oxford Blackwell Scientific Publications.
- Aravind, P., & Prasad, M. N. V. (2005). Cadmium–zinc interactions in a hydroponic system using ceratophyllum demersum L.: Adaptive ecophysiology, biochemistry and molecular toxicology. *Brazilian Journal of Plant Physiology*, *17*, 3–20.
- Chakravarty, B., & Srivastava, S. (1997). Effect of cadmium and zinc interaction on metal uptake and regeneration of tolerant plants in linseed Agriculture. *Ecosystems & Environment*, *61*, 45–50.
- De Livera, J., McLaughlin, M. J., Hettiarachchi, G. M., Kirby, J. K., & Beak, D. G. (2011). Cadmium solubility in paddy soils: Effects of soil oxidation, metal sulfides and competitive ions. *The Science of the Total Environment*, *409*, 1489–1497.
- Diatta, J., & Kocalkowski, W. (1998). Adsorption of zinc in some selected soils. *Polish Journal of Environmental Studies*, *7*, 195–200.
- Duan, Q., Lee, J., Liu, Y., Chen, H., & Hu, H. (2016). Distribution of heavy metal pollution in surface soil samples in China: A graphical review. *Bulletin of Environmental Contamination and Toxicology*, *97*(3), 303–309.
- Gee, G. W., & Bauder, J. W. (1986). Particle-size analysis. In A. Klute (Ed.), *Methods of soil analysis. Part 1. Physical and mineralogical methods* (2nd ed.). Madison, WI: ASA, SSSA.
- Gray, C. W., McLaren, R. G., Roberts, A. H. C., & Condron, L. M. (1999). Solubility, sorption and desorption of native and added cadmium in relation to properties of soils in New Zealand. *European Journal of Soil Science*, *50*, 127–137.
- Gupta, P. K. (2000). *Soil, plant, water and fertilizer analysis*. New Delhi, India: Agrobios.
- Hafeez, B., Khanif, Y., & Saleem, M. (2013). Role of zinc in plant nutrition—a review. *American Journal of Experimental Agriculture*, *3*, 374–391.
- Haghiri, F. (1974). Plant uptake of cadmium as influenced by cation exchange capacity, organic matter, zinc, and soil temperature. *Journal of Environmental Quality*, *3*, 180–182.
- Hanafi, M. M., & Salwa, H. (1998). Cadmium and zinc in acid tropical soils: Influence of humic acid addition on soil properties and their adsorption. *Communications in Soil Science and Plant Analysis*, *29*, 1933–1947.
- Hart, J. J., Welch, R. M., Norvell, W. A., & Kochian, L. V. (2002). Transport interactions between cadmium and zinc in roots of bread and durum wheat seedlings. *Physiologia Plantarum*, *116*, 73–78.
- Hewitt, E. J. (1966). *Sand and water culture methods used in the study of plant nutrition*. C.A.B. England: Farnham Royal.
- Hindersmann, I., & Mansfeldt, T. (2014). Trace element solubility in a multimetal contaminated soil as affected by redox conditions. *Water, Air, & Soil Pollution*, *225*, 1–20.
- Jalali, M., & Khanlari, Z. V. (2008). Effect of Aging process on the fractionation of heavy metals in some calcareous soils of Iran. *Geoderma*, *143*, 26–40.
- Jamali, N., Ghaderian, S. M., & Karimi, N. (2014). Effects of cadmium and zinc on growth and metal accumulation of *Mathiola flavidia* boiss. *Environmental Engineering and Management Journal*, *12*(13), 2937–2944.
- Kashem, M. A., & Singh, B. R. (2001). Metal availability in contaminated soils: I. Effects of flooding and organic matter on changes in Eh, pH and solubility of Cd, Ni and Zn. *Nutrient Cycling in Agroecosystems*, *61*, 247–255.
- Lindsay, W. L., & Norvell, W. A. (1978). Development of a DTPA soil test for zinc, iron, manganese and copper. *Soil Science Society of America Journal*, *42*, 421–428.
- Loganathan, P., Vigneswaran, S., Kandasamy, J., & Naidu, R. (2012). Cadmium sorption and desorption in soils: A review. *Critical Reviews in Environmental Science and Technology*, *42*, 489–533.
- Mahmudi, sh (1997). Properties and management of gypsiferous soils. In *Soil and water institute of Iran. Magazing of gypsiferous soil*.
- Ma, Y. B., & Liu, J. F. (1997). Adsorption kinetics of zinc in a calcareous soil as affected by pH and temperature. *Communications in Soil Science and Plant Analysis*, *28*, 1117–1126.
- Mazumdar, M., Das, S. S., & Patra, S. K. (2006). Remediation of soil cadmium toxicity Using Cd-Zn interaction for sustainable agriculture. In *18th world Congr. Soil Sci. July 9-15, - Philadelphia, Pennsylvania, USA*.
- McBride, M. B. (1989). Reactions controlling heavy metal solubility in soils. *Advances in Soil Science*, *10*, 1–56.
- McLaren, R. G., & Cameron, K. C. (1996). *Soil science: Sustainable production and environmental protection* (2nd ed.). Auckland, New Zealand: Oxford University Press.
- Misra, A. K., Sarkunan, V., Das, M., & Nayar, P. K. (1990). Transformation of added heavy metals in soils under flooded condition. *Journal of the Indian Society of Soil Science*, *38*, 416–418.
- Nelson, D. W., & Sommers, L. E. (1982). Total carbon, organic carbon and organic matter. In A. L. Page, et al. (Eds.), *Methods of soil analysis* (pp. 539–579). Madison, WI: ASA, SSSA.
- Oliver, D. P., Wilhem, N. S., McFarlan, J. D., Tiller, K. G., & Cozens, G. D. (1997). Effect of soil and foliar applications of zinc on Cd concentration in wheat grain. *Australian Journal of Experimental Agriculture*, *37*, 103–107.
- Pearson, R. G. (1973). *Hard and soft acids and bases*. Stroudsburg, PA: Dowden, Hutchinson & Ross.
- Petruzzelli, G. (1996). Heavy metals in compost and their effect on soil quality. p. 213-223. In M. Bertodi etal (Ed.), *The science of composting* (1st ed.). Glasgow. UK: Blakie Academic and Professional. part 1.
- Ponnamperuma, F. N. (1972). The chemistry of submerged soils. In N. C. Brady (Ed.), *Advances in Agronomy* (Vol. 24, pp. 29–96). New York and London: Academic Press, Inc.
- Rassaei, F., Hoodaji, M., & Abtahi, S. A. (2019). Cadmium chemical forms in two calcareous soils treated with different levels of incubation time and moisture regimes. *Journal of Environmental Protection*, *10*(4), 500–513.
- Rassaei, F., Hoodaji, M., & Abtahi, S. A. (2019). Zinc and incubation time effect on cadmium chemical fractions in two types of calcareous soil. *Agrochimica*, *63*(4), 337–349.
- Reyhaniatabar, A., Ardalan, M. M., Karimian, N., Savaghebi, G. R., & Gilkes, R. J. (2011). Kinetics of zinc sorption by some calcareous soils of Iran. *Journal of Agricultural Science and Technology*, *13*, 263–272.
- Richards, L. A. (1969). Diagnosis and improvement of saline and alkali soils. In *US Salinity Laboratory Staff. Agricultural Handbook* (Vol. 60)USA: USDA.
- Robert, D. R., Ford, R. G., & Sparks, D. L. (2003). Kinetics and mechanisms of Zn complexation on metal oxides using EXAFS spectroscopy. *Journal of Colloid and Interface Science*, *263*, 364–376.
- Sahrawat, K. L. (2012). Soil fertility in flooded and non-flooded irrigated rice systems. *Archives of Agronomy and Soil Science*, *58*, 423–436.
- Sarwar, N., Ishaq, W., Farid, G., Shaheen, M. R., Imran, M., Geng, M., et al. (2015). Zinc-cadmium interactions: Impact on wheat physiology and mineral acquisition. *Ecotoxicology and Environmental Safety*, *122*, 528–536.
- Shaheen, S. M. (2009). Sorption and lability of cadmium and lead in different soils from Egypt and Greece. *Geoderma*, *153*, 61–68.
- Singh, A. K., & Pandeya, S. B. (1998). Sorption and release of cadmium-fulvic acid complexes in sludge treated soils. *Bioresource Technology*, *66*, 119–127.
- Tessier, A., Campbell, P. G. C., & Bisson, M. (1979). Sequential extraction procedure for the specification of particular trace elements. *Analytical Chemistry*, *51*, 844–851.
- Tóth, G., Hermann, T., Szatmári, G., & Pásztor, L. (2016). Maps of heavy metals in the soils of the European Union and proposed priority areas for detailed assessment. *The Science of the Total Environment*, *565*, 1054–1062.
- Williams, C., & David, D. (1976). The accumulation in soil of cadmium residues from phosphate fertilizer and their effect on the cadmium content of plants. *Soil Science*, *121*, 86–93.
- World Reference Base for Soil Resources. (2014). International soil classification system for naming soils and creating legends for soil maps. In *World soil Resources Reports* (Vol. 106)Rome: FAO. update 2015.
- Wu, J., & Sun, Z. (2016). Evaluation of shallow groundwater contamination and associated human health risk in an alluvial plain impacted by agricultural and industrial activities, Mid-west China. *Exposure Health*, *8*(3), 311–329.
- Wu, Z., Wang, F., Liu, S., Du, Y., Li, F., Du, R., et al. (2016). Comparative responses to silicon and selenium in relation to cadmium uptake, compartmentation in roots, and xylem transport in flowering Chinese cabbage (*Brassica campestris* L. ssp. *chinensis* var. *utilis*) under cadmium stress. *Environmental and Experimental Botany*, *131*, 173–180.
- Yoshida, S., & Tanaka, A. (1969). Zinc deficiency of the rice plant in calcareous soils. *Soil Science & Plant Nutrition*, *15*, 75–80.
- Zheng, S., Zheng, X., & Chen, C. (2013). Transformation of metal speciation in purple soil as affected by water logging. *International Journal of Environmental Science and Technology*, *10*, 351–358.



Contents lists available at ScienceDirect

International Soil and Water Conservation Research

journal homepage: www.elsevier.com/locate/iswcr

Original Research Article

Spatiotemporal changes in terrestrial water storage in the Beijing-Tianjin Sandstorm Source Region from GRACE satellites

Yingjun Pang^{a, b, *}, Bo Wu^{a, b}, Yanping Cao^c, Xiaohong Jia^{a, b}^a Institute of Desertification Studies, Chinese Academy of Forestry, Beijing, 100091, China^b Key Laboratory of Desert Ecosystem and Global Change, State Administration of Forestry and Grassland, Beijing, 100091, China^c The College of Environment and Planning of Henan University, Kaifeng, 475004, Henan, China

ARTICLE INFO

Article history:

Received 18 October 2019

Received in revised form

13 June 2020

Accepted 16 June 2020

Available online 9 July 2020

Keywords:

Terrestrial water storage

Beijing-Tianjin Sandstorm Source Region

Groundwater

LULC

ABSTRACT

The Sandstorm Source Control Project in and around the Beijing-Tianjin region was one of the most important ecological projects in China. Terrestrial water storage (TWS) has important impacts on the ecological construction, agriculture, industry, and resident's lives. Based on the Gravity Recovery and Climate Experiment (GRACE) data, meteorological and Moderate Resolution Imaging Spectroradiometer (MODIS) data, etc., this paper analyzed spatiotemporal characteristics of TWS, groundwater storage, and precipitation, and explored the influencing factors of regional TWS combined with land use and land cover (LULC), social and economic data. The most important results were as follows: (1) From 2003 to 2016, TWS in the Beijing-Tianjin Sandstorm Source Region showed a decreasing trend with a rate of 3.14 mm yr⁻¹. (2) The TWS decline was caused mainly by groundwater overexploitation, but not precipitation variation. (3) Spatiotemporal variations of TWS were related to LULC. The area with the most serious decrease of TWS was mainly located in the southwestern part of the region, where farmland percentage and population density were greater. (4) Reducing the percent of farmland and tree planting, and adding the shrub and grass planting, could be a viable choice for the Beijing-Tianjin Sandstorm Source Control Project. These results provide a scientific basis for regional water resource and ecological management.

© 2020 International Research and Training Center on Erosion and Sedimentation and China Water and Power Press. Production and Hosting by Elsevier B.V. This is an open access article under the CC BY-NC-ND license (<http://creativecommons.org/licenses/by-nc-nd/4.0/>).

1. Introduction

Terrestrial water storage (TWS), as a vital component of hydrological and biogeochemical cycles, influences ecological security and the distribution of human settlements. However, TWS is affected by climate change, drought and heavy rainfall, increasing water use, land use, and agricultural activity (Wang et al., 2015). TWS variation in large arid areas is generally hard to detect due to a lack of effective monitoring methods, especially in remote regions. However, the Gravity Recovery and Climate Experiment (GRACE) mission was designed to track changes in the Earth's gravity field. GRACE observations have enabled the detection of small changes in the Earth's gravity field associated with variations in TWS (Xie et al., 2016). Previous work has validated that GRACE data are applicable

for areas larger than approximately 200,000 km². Therefore, GRACE satellites have provided a new approach for monitoring TWS (including groundwater storage, surface water storage, soil moisture storage, snow water equivalent storage and biological water storage) over large areas on multiple time scales. GRACE data have been successfully used to explore regional-scale TWS variabilities across the world, such as in Illinois (Swenson et al., 2006), the Amazon Basin (Xavier et al., 2012), Africa (Anyah et al., 2018), Australia (Xie et al., 2016), India (Bhanja et al., 2017), the Yangtze River Basin (Sun et al., 2018), the Three-River Source Region of the Tibetan Plateau (Xu et al., 2018), and Northwest China (Cao et al., 2018; Xie et al., 2018). The ability of GRACE to monitor TWS is significant because no global networks of observations exist with the temporal and spatial resolution necessary to adequately characterize the water balance at regional to continental scales (Swenson et al., 2006).

To improve the ecological and environmental conditions of Beijing, Tianjin, and the surrounding areas and mitigate wind-blown sand hazards, the Chinese government launched an

* Corresponding author. Institute of Desertification Studies, Chinese Academy of Forestry, Beijing, 100091, China.

E-mail address: pangyingjun@caf.ac.cn (Y. Pang).

ecological construction project in 2000 with great strategic significance, which was named the “Beijing-Tianjin Sandstorm Source Control Project”. The Beijing-Tianjin Sandstorm Source Region was defined as the construction scope of the Beijing-Tianjin Sandstorm Source Control Project. The project aims to prevent the expansion of desertification and improve the ecological environment through engineering measures such as the protection of existing vegetation, enclosure and afforestation, aerial sowing for afforestation, artificial afforestation, returning farmland to forests, grassland management, and small watershed comprehensive management (Gao, 2008). Water resources are indispensable to ecological projects, especially to biological projects. To date, research has mainly focused on land degradation (Yang et al., 2015), vegetation growth (Yang et al., 2015), and engineering benefits (Gao, 2008). Numerous studies have analyzed TWS and groundwater storage depletion surrounding the Beijing-Tianjin Sandstorm Source Region, such as in the North China Plain (Feng et al., 2013; Yin et al., 2018), the Hai River Basin (Shen et al., 2015), the West Liaohe River Basin, and Northern China (Yin et al., 2017). The results showed that the groundwater depletion in this region was very serious and led to serious problems, such as land subsidence (Gong et al., 2018; Guo et al., 2015). Moiwo and Tao (2014) suggested that changes in surface water storage in the Hai River Basin are mainly driven by land use and related water demands, which are largely human factors. However, less attention has been paid to the impacts of LULC on changes in the TWS in the Beijing-Tianjin Sandstorm Source Region.

Thus, this study aims (1) to investigate the characteristics of spatiotemporal changes in the TWS, soil moisture storage, snow water equivalent storage, groundwater storage, precipitation, temperature, and normalized difference vegetation index (NDVI) in the Beijing-Tianjin Sandstorm Source Region based on the GRACE data, Global Land Data Assimilation System (GLDAS) data, and meteorological and Moderate Resolution Imaging Spectroradiometer (MODIS) data and (2) to explore the influencing factors of regional TWS combined with land use and land cover (LULC), social and economic data. These results provide a scientific basis for regional water resource and ecological management.

2. Materials and methods

2.1. Study area

The scope of this study is the range of the second phase of the Beijing-Tianjin Sandstorm Source Control Project. The region (105.20°–120.98°E, 36.82°–46.78°N) mainly involves six provinces: Beijing, Tianjin, Hebei, Inner Mongolia, Shanxi, and Shaanxi. The total area of the region is 710,500 km². The area of desertified land is 226,900 km², accounting for 31.9% of the whole study region (Fig. 1). There are two climate belts and five climate zones in the project area, including the warm temperate semi-humid zone, temperate semi-humid zone, temperate semi-arid zone, temperate arid zone and temperate extreme arid zone (Yang et al., 2015). The annual precipitation ranges from 144 to 607 mm (Fig. 2). The study region extends across four river basins, including the Songhua and Liaohe River Basin, Yellow River Basin, Haihe River Basin, and Northwestern River Basins; the major rivers are the Yellow River, Yongding River, Luan River, and West Liaohe River. The topography includes plains, plateaus, and mountains. Grassland is the main land use type in the project area and is mainly located in the northern area.

2.2. TWS from GRACE

The GRACE satellites launched by NASA and the German

Aerospace Centre on March 17, 2002, were designed to exploit the changes in mass at the Earth's surface (Tapley et al., 2004). The two satellites operate in a low-Earth orbit (450 km above the Earth), with a distance of 220 km between them (Chen et al., 2014). Over the land, the main components of changes in mass are caused by the movement of water. Thus, the GRACE-derived gravitational variations can be inverted to provide global estimates of vertical changes in TWS, including groundwater storage, soil moisture storage, surface water storage, snow water equivalent storage and biological water storage (Long et al., 2016). To date, GRACE-derived TWS changes have been widely applied in various kinds of ecohydrological studies, including in China (Xu et al., 2018; Zhu et al., 2018).

Previous studies showed that the GRACE mascon solutions, which reduce information leakage through increased signal amplitudes, are preferred over other GRACE solutions (Save et al., 2016; Scanlon et al., 2016). The GRACE mascon products from the Center for Space Research (CSR) at the University of Texas have been widely used in previous studies (Sun et al., 2018; Zhong et al., 2018). The spatiotemporal patterns of GRACE CSR mascon solutions are consistent with the solutions from the Jet Propulsion Laboratory (JPL), USA (Save et al., 2016; Scanlon et al., 2016). In this study, we used the GRACE CSR RL05 mascon solutions, which were downloaded from the website <http://www2.csr.utexas.edu/grace>. GRACE CSR RL05 mascon solutions are represented on a 0.5° lon-lat grid and are derived purely from GRACE CSR RL05 spherical harmonics solutions. These monthly GRACE anomalies are relative to the 2004–2009 time-mean baseline, which has been pre-processed to remove signals from the atmosphere and oceans.

2.3. Soil moisture and snow water equivalent data

GLDAS consists of four land surface models, namely, Noah, the Community Land Model (CLM), Mosaic, and the Variable Infiltration Capacity (VIC). Tiwari et al. (2009) compared the modelled groundwater storage anomalies from four hydrological models in GLDAS and concluded that the use of these different models would not noticeably affect estimations of groundwater storage. The soil moisture storage and snow water equivalent storage data in this study are from the GLDAS Noah model. GLDAS is a robust simulation system that integrates a large quantity of in situ ground data and satellite-based observational data products and is executed globally at high resolutions, with spatial resolutions of both 0.25° and 1° (Rodell et al., 2004). Here, we used the 0.25° data from 2013 to 2016 from the Noah model. The temporal resolution of the GLDAS products is one month, which is achieved through temporally averaging the 3-hourly products. GLDAS can provide various continuous, high-resolution estimates of land surface states and fluxes, such as soil moisture storage, soil temperature, latent heat flux, and sensible heat flux. For more details about GLDAS, readers are referred to Rodell et al. (2004). The Noah model is a standalone, 1D column model that can be executed in either coupled or uncoupled mode. The four soil layers of the Noah model are 0–10 cm, 10–40 cm, 40–100 cm and 100–200 cm. The GLDAS Noah model products have been widely applied in a range of studies (Bi et al., 2016; Chen et al., 2013).

2.4. Groundwater data

Based on the *China Water Resources Bulletin* issued by the Ministry of Water Resources of the People's Republic of China (<http://www.mwr.gov.cn/sj/tjgb/szygb/>), the average change in surface water reservoir storage in the study region was approximately 0.11 mm yr⁻¹ in the six river basins in Northern China (Songhuajiang River Basin, Liao River Basin, Haihe River Basin, Yellow

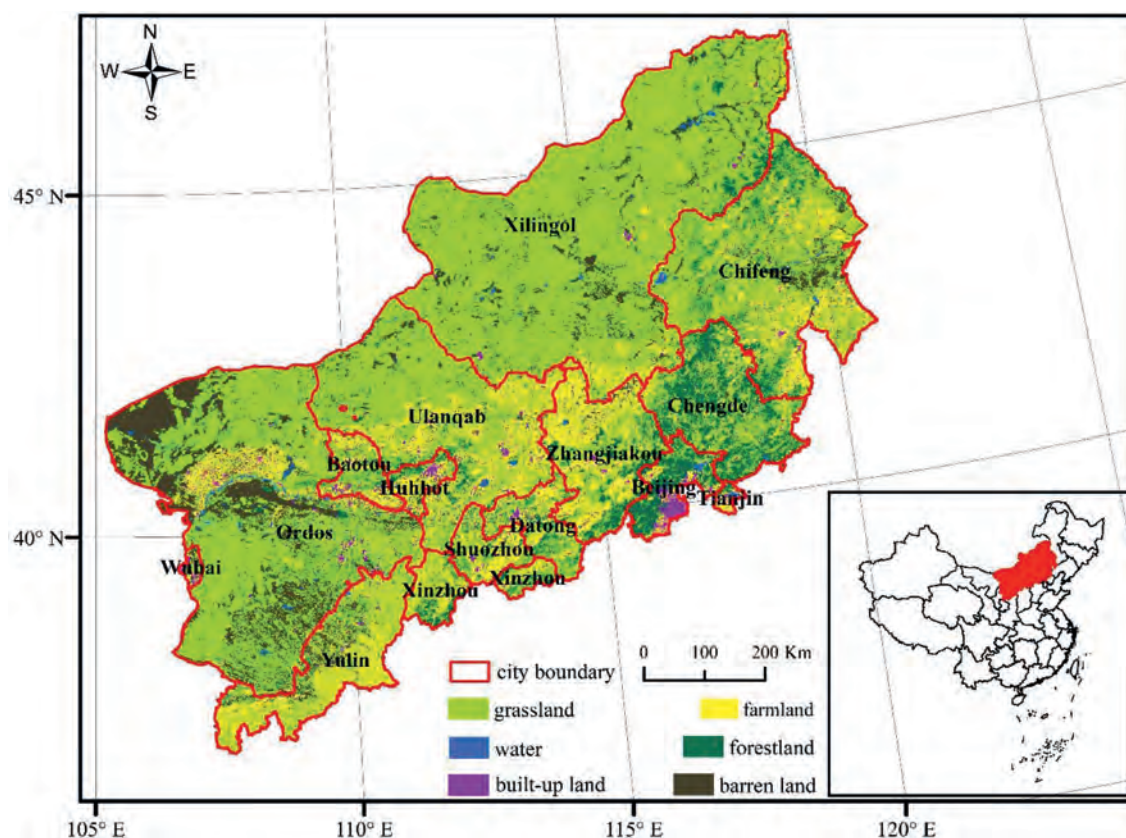


Fig. 1. General location of the study area (LULC in 2015).

River Basin, Huai River Basin and Northwestern River Basins) from 2003 to 2016. The surface water variability in the study region is small and can be neglected (Feng et al., 2013; Yin et al., 2017). Therefore, groundwater storage, soil moisture storage, and snow water equivalent storage are the only significant contributors to the TWS variability in this study region.

The groundwater storage anomalies (GWSA) can be calculated from the water balance equation (Jin & Feng, 2013). The following equation was used to calculate the GWSA across the Beijing-Tianjin Sandstorm Source Region:

$$GWSA = TWSA - SMSA - SWESA \quad (1)$$

where TWSA represents the GRACE-derived terrestrial water storage anomalies, SMSA represents the soil moisture storage anomalies, and SWESA represents the snow water equivalent storage anomalies.

The in situ groundwater level data from 2005 to 2016 were from the *Groundwater Level Yearbook* published by the China Institute of Geo-Environmental Monitoring. The groundwater observation wells that were missing more than four months of data were not taken into account. There were 29 groundwater observation wells in the study region (Fig. 2), and their monthly data were collected to verify the accuracy of the GWSA calculated using Equation (1).

2.5. Meteorological data

There are 111 national meteorological stations around the Beijing-Tianjin Sandstorm Source Region. The monthly precipitation and temperature data from 2003 to 2016 were obtained from China Meteorological Data Service Center (<http://data.cma.cn>). The

monthly precipitation and temperature data from 111 sites were interpolated by the kriging method with a spatial resolution of $0.25^\circ \times 0.25^\circ$ and then extracted by masking the Beijing-Tianjin Sandstorm Source Region vector boundary.

2.6. NDVI data

The NDVI index was used to characterize changes in vegetation. The MODIS NDVI products (MOD13C2, Collection 6) from 2003 to 2016 were downloaded from the online data pool at NASA's Level-1 and Atmosphere Archive and Distribution System Distributed Active Archive Center (<https://ladsweb.modaps.eosdis.nasa.gov/>). Global MOD13C2 data are provided every month as a gridded level-3 product projected on a 0.05° geographic climate modelling grid. Cloud pixels and "fill value pixels" were masked out using the MODIS data quality flags based on the quality assessment flags provided in the MOD13C2 product. Based on the monthly NDVI, the annual NDVI values for each 0.05° grid cell were calculated using the maximum-value composites method.

2.7. LULC, water supply and consumption, and population data

The LULC and population distribution data were downloaded from the Resource and Environment Data Cloud Platform (<http://www.resdc.cn>). The LULC data from 2000, 2005, 2010 and 2015 were used. The production of LULC data was based on the Landsat TM/ETM/OLI remote-sensing images. The spatial resolution of the LULC data was 1 km.

The water supply and consumption data from 2013 to 2016 were collected from the *China Statistical Yearbook* compiled by the National Bureau of Statistics of China.

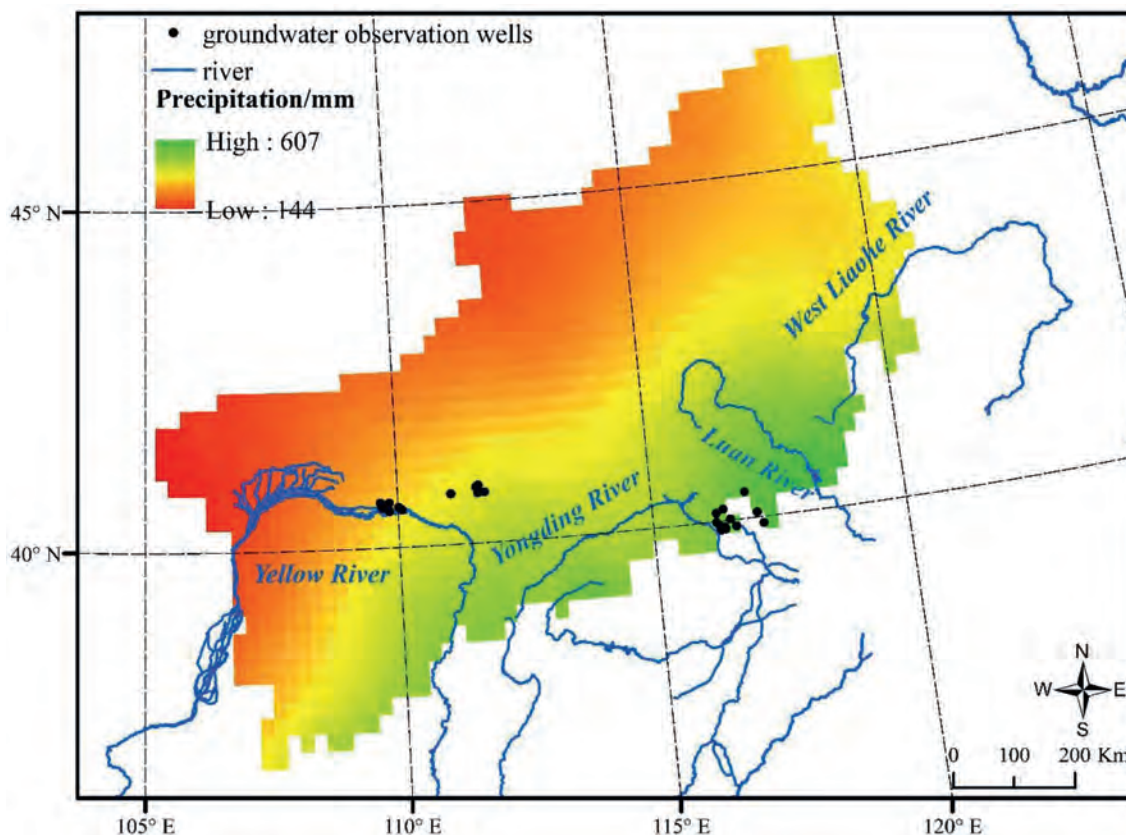


Fig. 2. The annual precipitation pattern of the study area from 2003 to 2016 and a schematic diagram of rivers and groundwater observation wells.

The production of the spatial distribution dataset of the population considered many factors, such as the land use type, night light brightness, and residential density, which were closely related to the population, and used the multifactor weight distribution method. The population data in 2015 with a 1 km spatial resolution were used.

2.8. Change trend analysis method

To analyse the temporal characteristics of hydrological factors and the NDVI, the one-way linear regression analysis method was applied to calculate the change trends. The formula of the change rates is shown as follows.

$$\theta_{\text{slope}} = \frac{n \times \sum_{i=1}^n (i \times Y_i) - \sum_{i=1}^n i \times \sum_{i=1}^n Y_i}{n \times \sum_{i=1}^n i^2 - \left(\sum_{i=1}^n i \right)^2} \quad (2)$$

where θ_{slope} is the change rate, n is the number of years, i is the year (year = 2003–2016), and Y is the hydrological factors and NDVI. If $\theta_{\text{slope}} > 0$, the variables increased during the study period; otherwise, the variables decreased when $\theta_{\text{slope}} < 0$.

3. Results

3.1. Monthly distributions of the hydrological factors and vegetation

Fig. 3 shows the monthly distributions of GRACE TWSA, GLDAS SMSA, GLDAS SWESA, GWSA (obtained by subtracting the GLDAS SMSA and SWESA estimates from GRACE TWSA), precipitation,

temperature, and NDVI during 2003–2016 in the Beijing–Tianjin Sandstorm Source Region. The TWSA showed a bimodal curve, with two peak values of 3.93 mm (in March) and 6.68 mm (in August) and two trough values of -2.29 mm (in June) and -4.89 mm (in October). December and January to March were nongrowing seasons, and plant water demand was very low, which may be the reason for the first annual TWS peak (in March), although the precipitation was low. The second annual TWS peak (in August) could be attributed to precipitation. The SMSA showed a unimodal curve, with lower values during January and June, ranging from -4.39 mm to -1.89 mm, increasing values from June to August, with a peak value of 5.74 mm, and then decreasing values. The fluctuation amplitude of the SWESA was lower. The value of the SWESA ranged from -0.80 to 0.64 mm from April to October and ranged from 0.35 mm to 1.59 mm in the other months. The amount of snow water equivalent storage was less than that of soil moisture storage and groundwater storage. However, snow cover is an important factor in the interaction between the global atmospheric cycle and the matter cycle on the Earth's surface. There was less rainfall in spring in the study area, and ice/snow meltwater was the main supplementary source of water for rivers and lakes. Snow cover has important potential impacts on vegetation (especially grass) reversion, growth and final yields. The GWSA variation was similar to that of the GRACE TWSA and showed a bimodal curve, with two peak values of 7.37 mm (in March) and 1.99 mm (in August) and two trough values of 0.03 mm (in June) and -8.07 mm (in October). The maximum value of the GWSA was in March, but the maximum value of the TWSA was in August. The precipitation showed a unimodal curve and was mainly concentrated from May to September, accounting for 83.98% of the total annual precipitation, and the peak of the monthly precipitation was 79.98 mm in July. The temperature showed a similar trend to that of

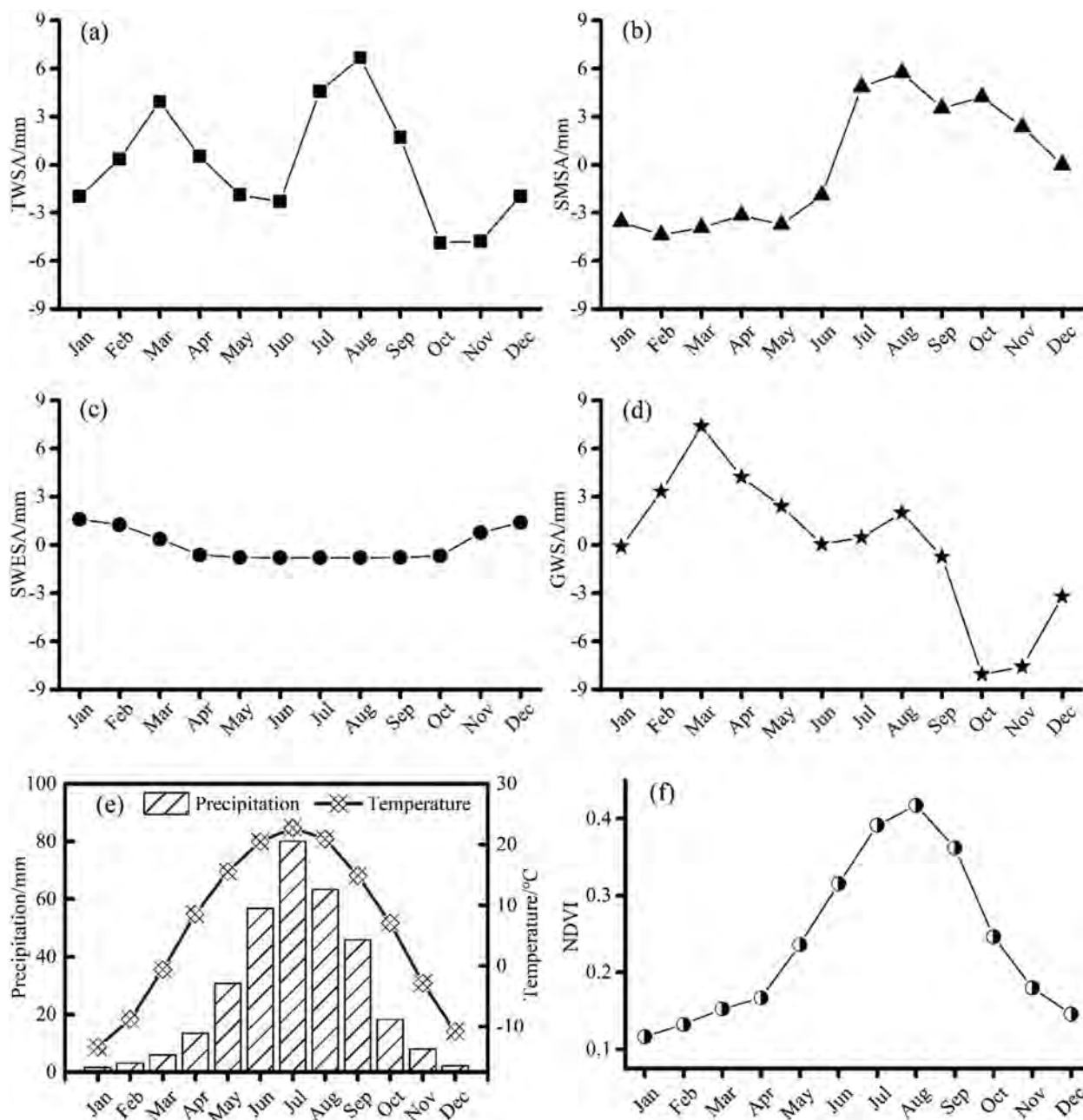


Fig. 3. Monthly distributions of the hydrological factors and NDVI.

the precipitation, with positive values from April to October and negative values during the other months. Furthermore, the maximum and minimum values were 22.70 °C (in July) and -13.37 °C (in January), respectively. The curve of variation in the NDVI was similar to those of the precipitation, temperature and SMSA. The maximum NDVI value was 0.42, which occurred in August.

3.2. Interannual variation in the hydrological factors and vegetation

The time series of the GRACE TWSA, GLDAS SMSA, GLDAS SWESA, GWSA (obtained by subtracting the GLDAS SMSA and SWESA estimates from the GRACE TWSA), precipitation, temperature, and NDVI from 2003 to 2016 in the Beijing-Tianjin Sandstorm

Source Region showed distinct annual fluctuations (Fig. 4). The TWSA decreased rapidly at a rate of 3.14 mm yr⁻¹. The SMSA and SWESA increased slightly. The SWESA reached a maximum in 2010, which was mainly attributed to the snowfall being very high in 2010 (Wang & Zhou, 2018). The GWSA decreased rapidly at a rate of 3.04 mm yr⁻¹. The annual precipitation increased slightly with fluctuations from 2003 to 2016, and the rate of increase was 4.60 mm yr⁻¹. The NDVI increased noticeably at a rate of 0.0017 yr⁻¹.

3.3. Spatiotemporal variations of the hydrological factors and vegetation

By applying a linear regression model, we calculated the annual change slopes of all the hydrological factors and NDVI at each pixel

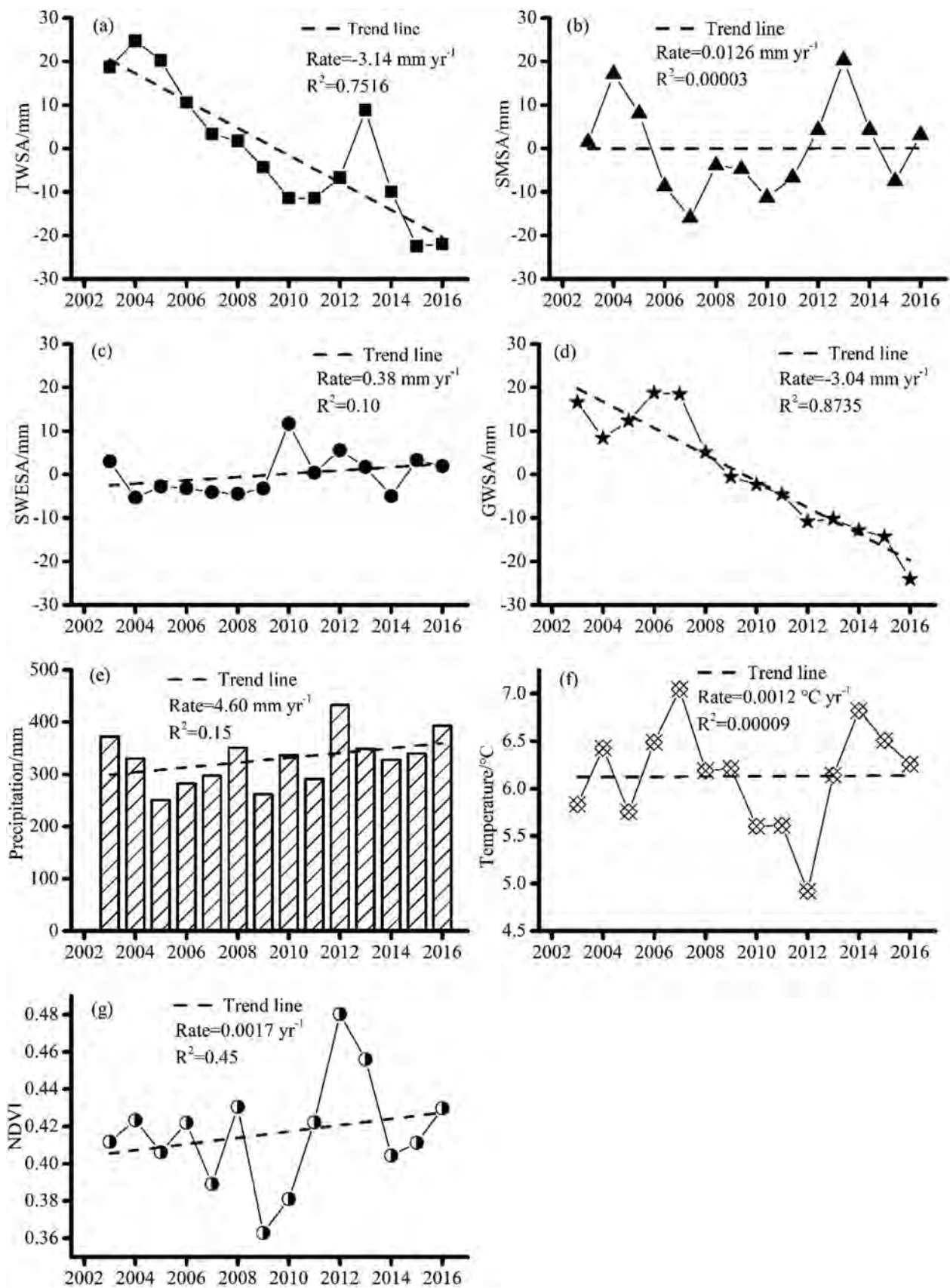


Fig. 4. Interannual variation in the hydrological factors and NDVI.

from 2003 to 2016. As shown in Fig. 5, the GRACE TWS in the study area mainly decreased, and the rates of decrease became higher from north to south. The area with the most serious decrease of TWS was mainly located in the southwestern part of the region. The soil moisture storage increased in most parts of the study area, and the area that decreased was mainly scattered in the central part. The snow water equivalent storage decreased in the southwestern part of the study area and increased in the northeastern part. The pixel variation in groundwater storage in the study area (Fig. 5(d)), which was calculated by Equation (1), was similar to the GRACE TWS and mainly showed a decreasing trend. The area with the most serious decrease in groundwater storage was also located in the southwestern part. The precipitation mainly showed an increasing trend. The temperature increased in the southwestern and central parts of the study area and decreased in the northeastern part. As seen, the spatial distribution of the GRACE TWS trend was not consistent with that of the precipitation. The NDVI mainly increased, and a significant increase occurred in the southwestern part. There were some scattered areas where the NDVI showed a slight decrease in the northern part.

4. Discussion

4.1. Contribution of groundwater overexploitation to the TWS decline

As an integrative TWS research method, the GRACE results have been validated according to multisource data, such as finer satellite observations, modelling data, and in situ data. The monthly TWSA and precipitation values were both high during July and September. The annual TWSA increased from 2011 to 2013, and the precipitation increased from 2010 to 2012. As shown above, all the precipitation variation had impacts on the TWSA. The monthly TWSA increased from October to March, when the precipitation values were low. The annual TWSA decreased distinctly, whereas the precipitation increased slightly from 2003 to 2016. The correlation coefficient between the annual TWSA and precipitation was -0.28 (Table 1). As shown above, the TWS decline in the Beijing-Tianjin Sandstorm Source Region was not caused by precipitation variation.

The correlation between the annual TWSA and GRACE-derived GWSA by Equation (1) was extremely significant, and the correlation coefficient reached 0.77. The correlations between the annual TWSA and SMSA, and the annual TWSA and SWESA were lower, at 0.44 and -0.41 , respectively. The annual and monthly GWSA derived from GRACE and TWSA had similar trends. The TWSA decreased at a rate of 3.14 mm yr^{-1} , and the GRACE-derived GWSA decreased at a rate of 3.04 mm yr^{-1} from 2003 to 2016. Therefore, the groundwater storage decrease was the main reason for the TWS decline. The GWSA data derived from GRACE in the grid locations of the 29 groundwater well sites (Fig. 2) were extracted and compared with the in situ groundwater level observation results. The groundwater level changes based on the monitoring groundwater wells had similar trends to that of the groundwater storage variations derived from GRACE (Fig. 6 and Fig. 7). The in situ groundwater level also dropped markedly. These results were consistent with results obtained in North China (Ebead et al., 2017), on the North China Plain (Su et al., 2011), and in the West Liaohe River Basin (Zhong et al., 2018).

Since the groundwater monitoring network in this study area still needs to be improved and the groundwater data have not been fully publicly shared, the measured groundwater data in this paper are limited, and the distribution of the groundwater observation wells is uneven. We cannot accurately obtain the groundwater level changes over the entire study area based on measured groundwater well data and cannot assess the accuracy of the groundwater

inversion results for the entire study area. We extracted inversion raster data of groundwater storage derived from GRACE in the grid locations of the 29 groundwater well sites and compared them with measured groundwater well point data. However, the spatial scales of the two types of data are different. The two results were consistent and may indicate that the groundwater inversion results are good to some extent. However, the comparison between the inversion and measured results of groundwater has certain limitations, and the measurement data of groundwater cannot fully verify the groundwater inversion results in the whole study region, especially in the area lacking measured groundwater level data. Previous studies have shown that the groundwater inversion method based on GRACE data is fast, effective, and widely applied (Feng et al., 2018; Rodell et al., 2009; Yeh et al., 2006). With the successful launch of the GRACE follow-on satellite in May 2018, the GRACE data will play more significant roles in water resource monitoring, especially in groundwater monitoring.

The water supply constituents of the six provinces (Beijing, Tianjin, Hebei, Inner Mongolia, Shanxi, and Shaanxi) involved in the Beijing-Tianjin Sandstorm Source Control Project from 2003 to 2016 are shown in Fig. 8. The groundwater supply accounted for 57.86% of the total water supply. The average depth to the groundwater table was approximately 6.34 m in the Song-Liao Plain, 7.43 m in the Huang-Huai-Hai Plain, and 12.33 m in the Huhehaote-Baotou Plain based on groundwater datasets collected from *Monthly Report of Groundwater Dynamics* issued by the Ministry of Water Resources of the People's Republic of China (<http://www.mwr.gov.cn/sj/tjgb/dxsdtyb/>). The high-intensity utilization of regional groundwater was the main reason for the continuous decline in groundwater levels. Groundwater overexploitation is a global issue that has been reported in India (Asoka et al., 2017; Pathak & Dodamani, 2019; Rodell et al., 2009), Australia (Chen et al., 2016), California's Central Valley (Famiglietti et al., 2011), and the Middle East (Joodaki, 2014). Groundwater decline can trigger adverse environmental effects, such as groundwater quality degradation, land subsidence (Saber et al., 2018), and saltwater intrusion (Dim & Chikita, 2004).

4.2. Impacts of LULC on TWS

The water consumption constituents of the six provinces (Beijing, Tianjin, Hebei, Inner Mongolia, Shanxi, and Shaanxi) from 2003 to 2016 are shown in Fig. 9. Agriculture was a significant source of water use in this region. Agricultural water use (including farm irrigation, forest and fruit tree irrigation, grass irrigation, and water for fishponds and poultry) accounted for 68.55%, and industrial water use, domestic water use and ecological water use accounted for 13.72%, 13.94% and 3.79%, respectively. Irrigated agriculture is the main source of water withdrawals, accounting for approximately 70% of all the world's freshwater withdrawals (Rodell et al., 2018; Rosegrant et al., 2010).

The area with the most serious decrease of TWS was mainly located in the southwestern part, where the farmland percentage was higher (Figs. 1 and 5(a)). Fig. 10 shows the distribution of the population density. The population density was also higher where the TWS decreased. The higher the population density is, the greater the water demand, especially for providing water to sustain resident's lives. In addition, industry is often located in densely populated areas and requires plenty of water. Therefore, the TWS decrease is significantly related to human activities.

The impacts of LULC on regional water resource quantity and quality were significant (Elmahdy & Mohamed, 2016; Wang et al., 2017). Based on the TWS slope, six regions were identified (Fig. 11): Region A, where the TWS decreased by -11.77 to -7.84 mm yr^{-1} ; Region B, where the TWS decreased by -7.84

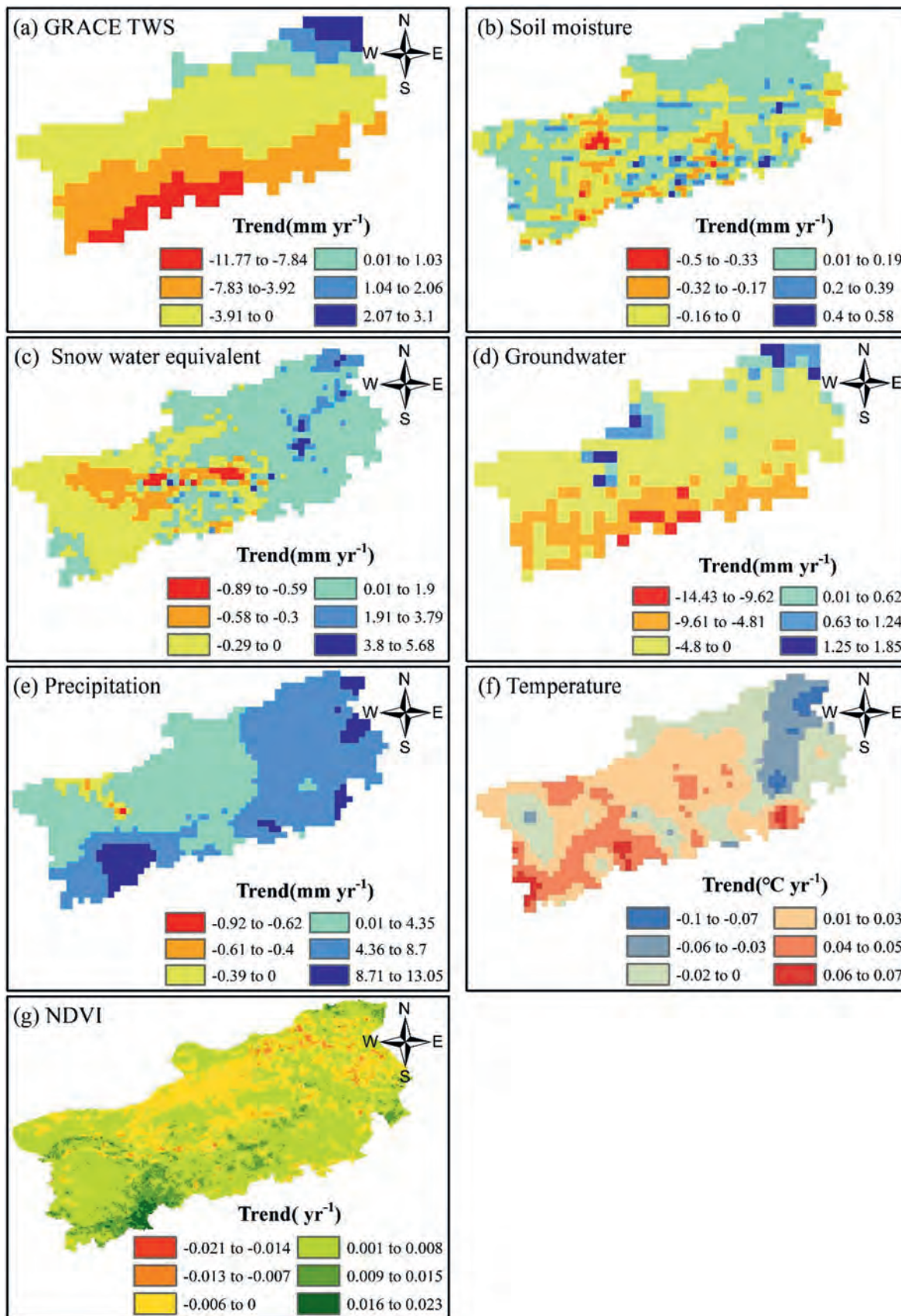


Fig. 5. Spatiotemporal variations of the hydrological factors and NDVI.

Table 1
Relationships among annual hydrological variables in the Beijing-Tianjin Sandstorm Source Region.

	TWSA	SMSA	SWESA	GWSA	Precipitation
TWSA	1.00				
SMSA	0.44	1.00			
SWESA	-0.41	-0.15	1.00		
GWSA	0.77**	-0.23	-0.37	1.00	
Precipitation	-0.28	0.25	0.49	-0.49	1.00

*95% confidence level.

**99% confidence level.

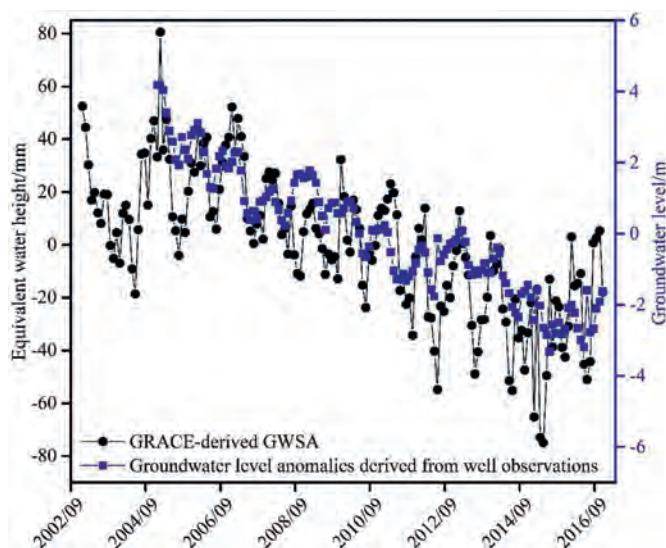


Fig. 6. Groundwater storage variations derived from GRACE in the grid locations of the 29 groundwater well sites and groundwater level changes derived from well observations.

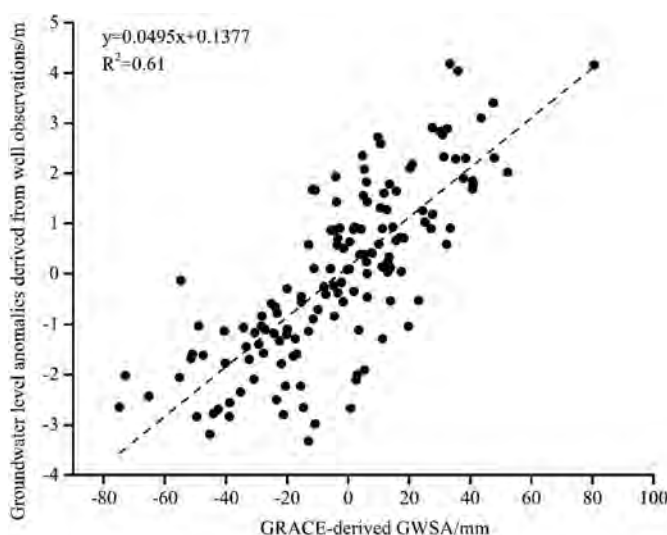


Fig. 7. The relation between the groundwater storage variations derived from GRACE in the grid locations of the 29 groundwater well sites and groundwater level changes derived from well observations during 2005 and 2016.

to -3.92 mm yr^{-1} ; Region C, where the TWS decreased by -3.92 to 0 mm yr^{-1} ; Region D, where the TWS increased by 0 – 1.03 mm yr^{-1} ; Region E, where the TWS increased by 1.01 – 2.06 mm yr^{-1} ; and Region F, where the TWS increased by 2.06 – 3.10 mm yr^{-1} . In

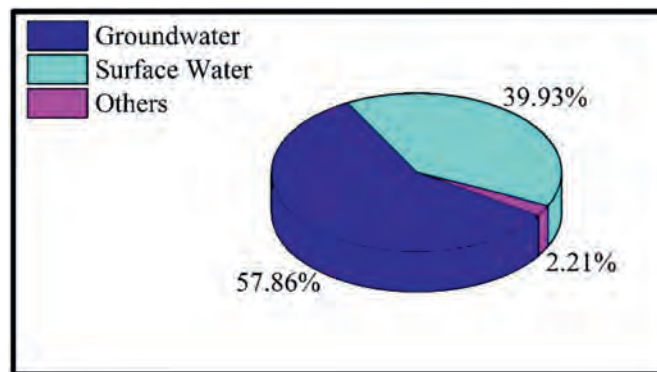


Fig. 8. Regional water supply constituents from 2003 to 2016.

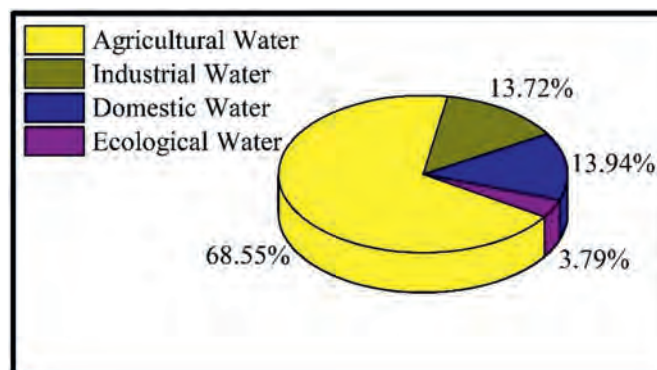


Fig. 9. Regional water consumption from 2003 to 2016.

general, the percentage of farmland was higher where the TWS decreased (Fig. 12). The percentage of farmland was 39.41–40.55% where the TWS decreased by -11.77 to -7.84 mm yr^{-1} , 23.79–24.34% where the TWS decreased by -7.84 to -3.92 mm yr^{-1} , 12.85–12.96% where the TWS decreased by -3.92 to 0 mm yr^{-1} , and 0.48–4.15% where the TWS increased. The percentage of forestland was 12.85–18.76% where the TWS decreased by -11.77 to -7.84 and -7.84 to -3.92 mm yr^{-1} , and was 0.25–5.56% in the other regions. The percentage of grassland was lower where the TWS decreased and higher where the TWS increased. The percentage of grassland was 38.57–41.32% where the TWS decreased by -11.77 to -7.84 and -7.84 to -3.92 mm yr^{-1} , 64.41–64.81% where the TWS decreased by -3.92 to 0 mm yr^{-1} , and 77.26–85.00% where the TWS increased. The percentages of water area and built-up land varied slightly with the TWS slope. Therefore, farmland water consumption contributed greatly to the decrease in TWS (Prabhakar & Tiwari, 2015). Forestland also needs abundant water. Zhang et al. (2018) indicated that increasing human-planted vegetation significantly increased the water loss over the Badain Jaran Desert, China. The increasing built-up land would result in a high demand for water and affect the variation in groundwater levels, but the proportion of built-up land in the study region was low.

4.3. The implications of TWS decline for the Beijing-Tianjin Sandstorm Source Control Project

Until 2017, the cumulative area of governance had reached $147,083 \text{ km}^2$ since the start of the Beijing-Tianjin Sandstorm Source Control Project in 2000, including $109,643 \text{ km}^2$ of forestry project, $25,211 \text{ km}^2$ of grassland management, and $12,229 \text{ km}^2$ of small

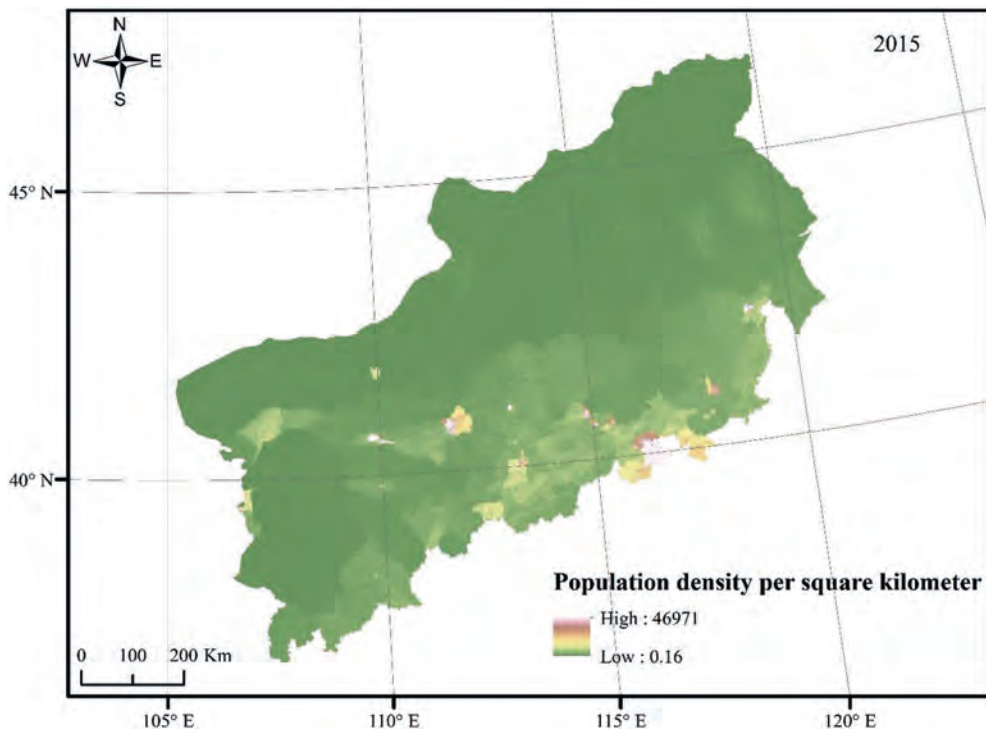


Fig. 10. The distribution of the population density.

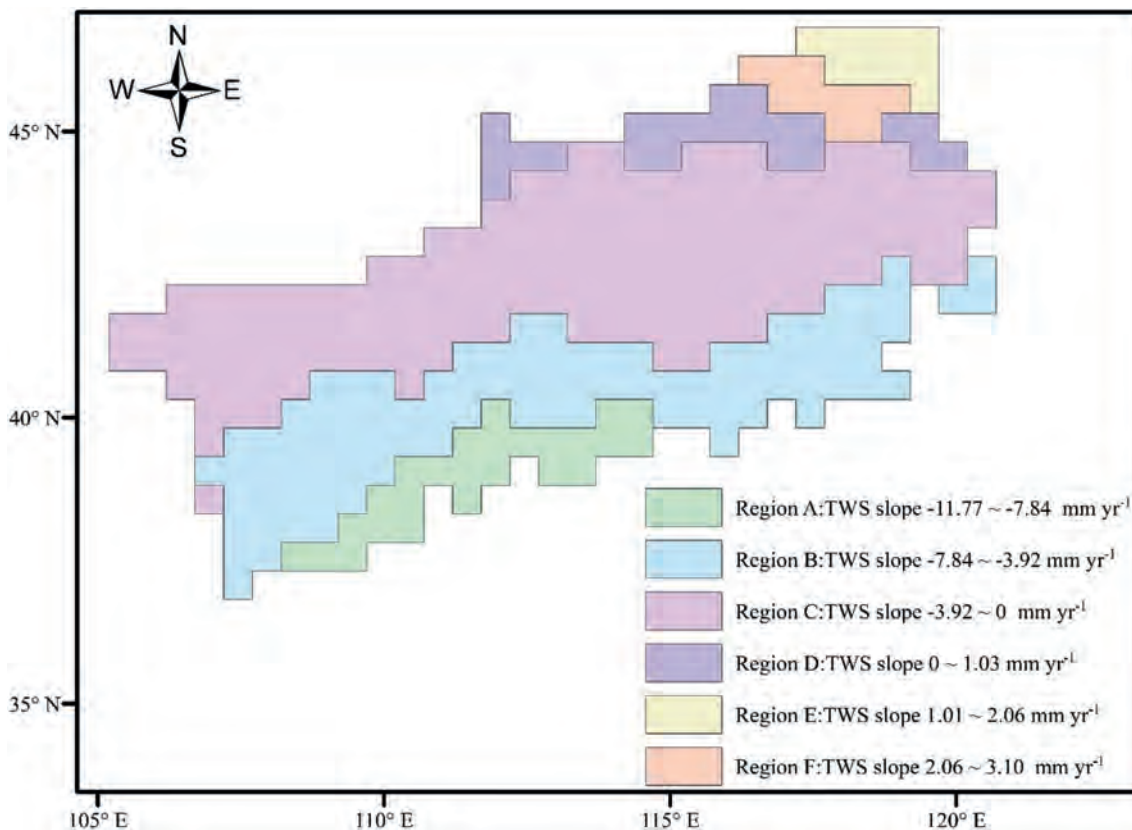


Fig. 11. Six regions divided by the TWS slope.

watershed management (National Forestry and Grassland Administration, 2017). The forestry project mainly included

40,792 km² of artificial afforestation, 10,998 km² of afforestation by aerial seeding, and 31,733 km² of enclosure for afforestation.

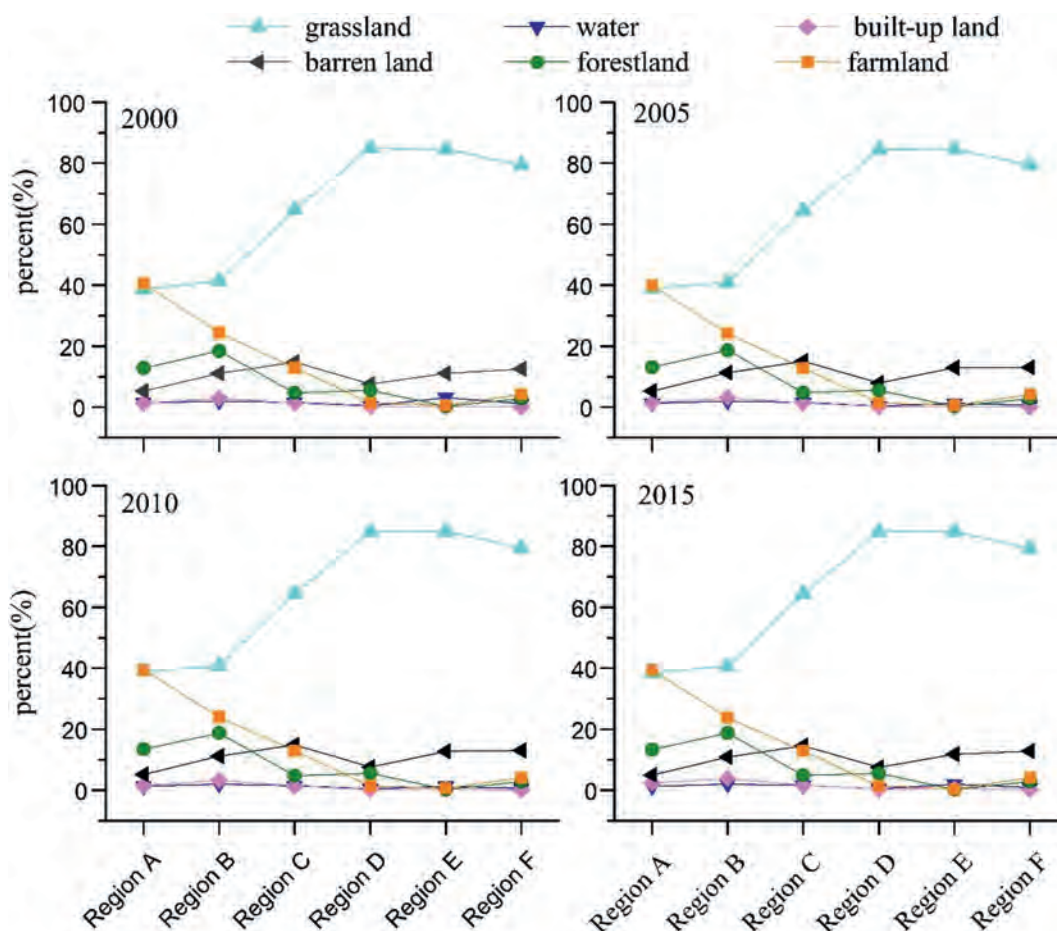


Fig. 12. The LULC in different regions based on the TWS slope.

Although the project plays an important role in mitigating wind-blown sand hazards and reducing soil and water erosion, it also consumes a large quantity of water resources.

The regional TWS decline is not conducive to the sustainable implementation of the Beijing-Tianjin Sandstorm Source Control Project. According to the above results, reducing the percent of farmland and tree planting, and adding the shrub and grass planting would alleviate the consumption of water resources, and provide a viable choice for the Beijing-Tianjin Sandstorm Source Control Project.

5. Conclusions

In this study, the characteristics of spatiotemporal changes in the TWS, soil moisture storage, snow water equivalent storage, groundwater storage, precipitation, temperature, and NDVI in the Beijing-Tianjin Sandstorm Source Region during the period of 2003–2016 were analyzed, and the influencing factors of regional TWS were also explored. The main conclusions are as follows:

- (1) The monthly TWSA and GWSA derived from GRACE showed a bimodal curve, with two peak values in March and August. The monthly SMSA, precipitation, temperature, and NDVI showed unimodal curves. The peak values of the monthly SMSA and NDVI occurred in August, while the peak values of the monthly precipitation and temperature occurred in July.
- (2) From 2003 to 2016, the TWS in the Beijing-Tianjin Sandstorm Source Region showed a decreasing trend with a rate

of -3.14 mm yr^{-1} . However, the annual precipitation increased at a rate of 4.60 mm yr^{-1} . The TWS decline was not caused by the precipitation variation.

- (3) The SMSA and SWESA increased slightly. The GRACE-derived GWSA decreased rapidly at a rate of 3.04 mm yr^{-1} . Groundwater overexploitation was the main reason for the decline of regional TWS.
- (4) The implementation effect of the Beijing-Tianjin Sandstorm Source Control Project region was obvious. The NDVI noticeably increased at the rate of 0.0017 yr^{-1} from 2003 to 2016.
- (5) LULC played an important role in the TWS variation. Spatiotemporal changes in the TWS related to LULC. The area with the most serious decrease of TWS was mainly located in the southwestern part of the region, where farmland percentage and population density were greater.
- (6) Reducing the percent of farmland and tree planting, and adding the shrub and grass planting, could be a viable choice for the Beijing-Tianjin Sandstorm Source Control Project to not only improve the ecological environment but also reduce the regional water consumption.

Declaration of competing interest

We declare that we have no financial and personal relationships with other people or organizations that can inappropriately influence our work, there is no professional or other personal interest of any nature or kind in any product, service and/or company that

could be construed as influencing the position presented in, or the review of, the manuscript entitled, “Spatiotemporal changes in terrestrial water storage in the Beijing-Tianjin Sandstorm Source Region from GRACE satellites”.

Acknowledgements

This work was supported by the National Key Research and Development Program of China (Grant No. 2016YFC0500801 and 2016YFC0500804), the National Natural Science Foundation of China (Grant Nos. 41701010 and 410701503), and the Fundamental Research Funds for the Central Non-profit Research Institution of Chinese Academy of Forestry (Grant No. CAFYBB2019MA009). We are grateful for the insightful comments from the anonymous reviewers and editors during the review phase of this article.

References

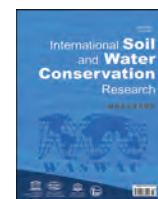
- Anyah, R. O., Forootan, E., Awange, J., & Khaki, M. (2018). Understanding linkages between global climate indices and terrestrial water storage changes over Africa using GRACE products. *The Science of the Total Environment*, 635, 1405–1416.
- Asoka, A., Gleeson, T., Wada, Y., & Mishra, V. (2017). Relative contribution of monsoon precipitation and pumping to changes in groundwater storage in India. *Nature Geoscience*, 10(2), 109–117.
- Bhanja, S., Rodell, M., Li, B., Saha, D., & Mukherjee, A. (2017). Spatio-temporal variability of groundwater storage in India. *Journal of Hydrology*, 544, 428–437.
- Bi, H., Ma, J., Zheng, W., & Zeng, J. (2016). Comparison of soil moisture in GLDAS model simulations and in-situ observations over the Tibetan Plateau. *J. Geophys. Res. Atmos.*, 121(6), 1–2.
- Cao, Y., Nan, Z., Cheng, G., & Ling, Z. (2018). Hydrological variability in the arid region of northwest China from 2002 to 2013. *Adv. Meteorol.*, (1), 1–13, 2018.
- Chen, J., Jin, L. I., Zhang, Z., & Shengnan, N. I. (2014). Long-term groundwater variations in Northwest India from satellite gravity measurements. *Global and Planetary Change*, 116(1), 130–138.
- Chen, J. L., Wilson, C. R., Tapley, B. D., Scanlon, B., & Güntner, A. (2016). Long-term groundwater storage change in Victoria, Australia from satellite gravity and in situ observations. *Global and Planetary Change*, 139, 56–65.
- Chen, Y., Yang, K., Qin, J., Long, Z., Tang, W., & Han, M. (2013). Evaluation of AMSR-E retrievals and GLDAS simulations against observations of a soil moisture network on the central Tibetan plateau. *J. Geophys. Res. Atmos.*, 118(10), 4466–4475.
- Dim, J. R., & Chikita, K. A. (2004). Impact of groundwater level decrease and sea level fluctuations on potential saltwater intrusion in the subsurface coastal area of west hokkaido, Japan. In *Proceedings of international symposium on "dawn of a new natural history - integration of geoscience and biodiversity studies"* (pp. 165–174). Hokkaido: Graduate School of Science, Hokkaido University.
- Ebead, B., Ahmed, M., Niu, Z., & Huang, N. (2017). Quantifying the anthropogenic impact on groundwater resources of North China using Gravity Recovery and Climate Experiment data and land surface models. *Journal of Applied Remote Sensing*, 11(2), Article 026029.
- Elmahdy, S. I., & Mohamed, M. M. (2016). Land use/land cover change impact on groundwater quantity and quality: A case study of Ajman emirate, the United Arab Emirates, using remote sensing and GIS. *Arabian J. Geosci.*, 9(19), 722.
- Famiglietti, J. S., Lo, M., Ho, S. L., Bethune, J., & Rodell, M. (2011). Satellites measure recent rates of groundwater depletion in California's Central Valley. *Geophysical Research Letters*, 38(3), L03403–L03406.
- Feng, W., Shum, C., Zhong, M., & Pan, Y. (2018). Groundwater storage changes in China from satellite gravity: An overview. *Remote Sensing*, 10(5), 674.
- Feng, W., Zhong, M., Lemoine, J.-M., Biancale, R., Hsu, H.-T., & Xia, J. (2013). Evaluation of groundwater depletion in North China using the Gravity Recovery and Climate Experiment (GRACE) data and ground-based measurements. *Water Resources Research*, 49(4), 2110–2118.
- Gao, S. Y. (2008). *Benefits of beijing-tianjin sand source Control engineering*. Beijing: Science Press (in Chinese).
- Gong, H., Pan, Y., Zheng, L., Li, X., Zhu, L., Zhang, C., & Zhou, C. (2018). Long-term groundwater storage changes and land subsidence development in the North China Plain (1971–2015). *Hydrogeology Journal*, 26(5), 1417–1427.
- Guo, H., Zhang, Z., Cheng, G., Li, W., Li, T., & Jiao, J. (2015). Groundwater-derived land subsidence in the north China plain. *Environ. Earth Sci.*, 74(2), 1415–1427.
- Jin, S., & Feng, G. (2013). Large-scale variations of global groundwater from satellite gravimetry and hydrological models, 2002–2012. *Global and Planetary Change*, 106(3), 20–30.
- Joodaki, G. (2014). Estimating the human contribution to groundwater depletion in the Middle East, from GRACE data, land surface models, and well observations. *Water Resources Research*, 50(3), 2679–2692.
- Long, D., Chen, X., Scanlon, B. R., Wada, Y., Hong, Y., Singh, V. P., & Yang, W. (2016). Have GRACE satellites overestimated groundwater depletion in the Northwest India Aquifer? *Scientific Reports*, 6(1), 24398.
- Moiwo, J. P., & Tao, F. (2014). Evidence of land-use controlled water storage depletion in Hai River basin, north China. *Water Resources Management*, 28(13), 4733–4746.
- National Forestry and Grassland Administration. (2017). *2017 China Forestry and Grassland Development Report*. Beijing: China Forestry Press (in Chinese).
- Pathak, A. A., & Dodamani, B. M. (2019). Trend analysis of groundwater levels and assessment of regional groundwater drought: Ghataprabha river basin, India. *Natural Resources Research*, 28(3), 631–643.
- Prabhakar, A., & Tiwari, H. (2015). Land use and land cover effect on groundwater storage. *Model. Earth Syst. Environ.*, 1(45), 1–12.
- Rodell, M., Famiglietti, J. S., Wiese, D. N., Reager, J. T., Beaudoing, H. K., Landerer, F. W., & Lo, M. H. (2018). Emerging trends in global freshwater availability. *Nature*, 557(7707), 651–659.
- Rodell, M., Houser, P. R., Jambor, U. e. a., Gottschalk, J., Mitchell, K., Meng, C., & Bosilovich, M. (2004). The global land data assimilation system. *Bulletin of the American Meteorological Society*, 85(3), 381–394.
- Rodell, M., Velicogna, I., & Famiglietti, J. S. (2009). Satellite-based estimates of groundwater depletion in India. *Nature*, 460(7258), 999–1002.
- Rosegrant, M. W., Ringler, C., & Zhu, T. (2010). Water for agriculture: Maintaining food security under growing scarcity. *Annual Review of Environment and Resources*, 34(34), 205–222.
- Saber, M., Abdel-Fattah, M., Kantoush, S., & Sumi, T. (2018). Implications of land subsidence due to groundwater over-pumping: Monitoring methodology using GRACE data. *Int. J. GEOMATE*, 14(41), 52–59.
- Save, H., Bettadpur, S., & Tapley, B. D. (2016). High-resolution CSR GRACE RL05 mascons. *Journal of Geophysical Research: Solid Earth*, 121(10), 7547–7569.
- Scanlon, B. R., Zhang, Z., Save, H., Wiese, D. N., & Chen, J. (2016). Global evaluation of new GRACE mascon products for hydrologic applications. *Water Resources Research*, 52, 9412–9429.
- Shen, H., Leblanc, M., Tweed, S., & Liu, W. (2015). Groundwater depletion in the Hai River basin, China, from in situ and GRACE observations. *Hydrological Sciences Journal*, 60(4), 671–687.
- Sun, Z., Zhu, X., Pan, Y., Zhang, J., & Liu, X. (2018). Drought evaluation using the GRACE terrestrial water storage deficit over the Yangtze River Basin, China. *The Science of the Total Environment*, 634, 727–738.
- Su, X. L., Ping, J. S., & Ye, Q. X. (2011). Terrestrial water variations in the North China Plain revealed by the GRACE mission. *Science China Earth Sciences*, 54(12), 1965–1970.
- Swenson, S., Yeh, P. J. F., Wahr, J., & Famiglietti, J. (2006). A comparison of terrestrial water storage variations from GRACE with in situ measurements from Illinois. *Geophysical Research Letters*, 33(16), 627–642.
- Tapley, B. D., Srinivas, B., Ries, J. C., Thompson, P. F., & Watkins, M. M. (2004). GRACE measurements of mass variability in the Earth system. *Science*, 305(5683), 503–505.
- Tiwari, V. M., Wahr, J., & Swenson, S. C. (2009). Dwindling groundwater resources in northern India, from satellite gravity observations. *Geophysical Research Letters*, 36(18), 184–201.
- Wang, F., Ge, Q., Yu, Q., Wang, H., & Xu, X. (2017). Impacts of land-use and land-cover changes on river runoff in Yellow River basin for period of 1956–2012. *Chinese Geographical Science*, 27(1), 13–24.
- Wang, H., Xiang, L., Jia, L., Wu, P., Steffen, H., Jiang, L., & Shen, Q. (2015). Water storage changes in North America retrieved from GRACE gravity and GPS data. *Geodesy & Geodynamics*, 6(4), 267–273.
- Wang, Z., & Zhou, H. (2018). Large-scale atmospheric circulations and water vapor transport influencing interannual variations of intense snowfalls in northern China. *Chinese Journal of Geophysics*, 61(7), 2654–2666.
- Xavier, L., Becker, M., Cazenave, A., Longuevergne, L., Llovel, W., & Rotunno Filho, O. C. (2012). Interannual variability in water storage over 2003–2008 in the Amazon Basin from GRACE space gravimetry, in situ river level and precipitation data. *Remote Sensing of Environment*, 114(8), 1629–1637.
- Xie, Y., Huang, S., Liu, S., Leng, G., Peng, J., Huang, Q., & Li, P. (2018). GRACE-based terrestrial water storage in northwest China: Changes and causes. *Remote Sensing*, 10, 1163.
- Xie, Z., Huete, A., Restrepo-Coupe, N., Ma, X., Devadas, R., & Caprarelli, G. (2016). Spatial partitioning and temporal evolution of Australia's total water storage under extreme hydroclimatic impacts. *Remote Sensing of Environment*, 183(C), 43–52.
- Xu, M., Kang, S., Chen, X., Wu, H., Wang, X., & Su, Z. (2018). Detection of hydrological variations and their impacts on vegetation from multiple satellite observations in the Three-River Source Region of the Tibetan Plateau. *The Science of the Total Environment*, 639, 1220–1232.
- Yang, X. C., Xu, B., Jin, Y. X., Qin, Z. H., Ma, H. L., Li, J. Y., & Zhu, X. H. (2015). Remote sensing monitoring of grassland vegetation growth in the Beijing-Tianjin sandstorm source project area from 2000 to 2010. *Ecological Indicators*, 51(51), 244–251.
- Yeh, P. J. F., Swenson, S. C., Famiglietti, J. S., & Rodell, M. (2006). Remote sensing of groundwater storage changes in Illinois using the Gravity Recovery and Climate Experiment (GRACE). *Water Resources Research*, 42(12), W12203.
- Yin, W., Hu, L., & Jiao, J. J. (2017). Evaluation of groundwater storage variations in northern China using GRACE data. *Geofluids*, 1–13, 2017.

- Yin, W., Hu, L., Zhang, M., Wang, J., & Han, S.-C. (2018). Statistical downscaling of GRACE-derived groundwater storage using ET data in the north China plain. *Journal of Geophysical Research: Atmosphere*, *123*(11), 5973–5987.
- Zhang, X., Wang, N. A., Xie, Z., Ma, X., & Huete, A. (2018). Water loss due to increasing planted vegetation over the Badain Jaran Desert, China. *Remote Sensing*, *10*(1), 134.
- Zhong, Y., Min, Z., Feng, W., Zhang, Z., Shen, Y., & Wu, D. (2018). Groundwater depletion in the West Liaohe River basin, China and its implications revealed by GRACE and in situ measurements. *Remote Sensing*, *10*(4), 493.
- Zhu, B., Xie, X., & Kang, Z. (2018). Water storage and vegetation changes in response to the 2009/10 drought over North China. *Hydrology Research*, *49*(5), Article nh2018087.



Contents lists available at ScienceDirect

International Soil and Water Conservation Research

journal homepage: www.elsevier.com/locate/iswcr

Original Research Article

Double mulching improves soil properties and productivity of maize-based cropping system in eastern Indian Himalayas



Bidyapati Ngangom^{a, b, c}, Anup Das^{a, d, *}, Rattan Lal^e, Ramkrushna Gandhiji Idapuganti^{a, f}, Jayanta Layek^a, Savita Basavaraj^{a, g}, Subhash Babu^{a, h}, Gulab Singh Yadav^d, Probir Kumar Ghoshⁱ

^a ICAR Research Complex for NEH Region, Umiam, Meghalaya, India

^b Krishi Vigyan Kendra-ICAR Research Complex for NEH Region, Arunachal Pradesh Centre, Basar, Arunachal Pradesh, India

^c College of Post Graduate Studies, Central Agricultural University, Umiam, Meghalaya, India

^d ICAR Research Complex for NEH Region, Tripura Centre, Lembucherra, Tripura, India

^e Carbon Management and Sequestration Centre, Ohio State University, USA

^f ICAR- Central Institute for Cotton Research, Nagpur, Maharashtra, India

^g ICAR-KrishiVigyan Kendra, Indi, University of Agricultural Sciences, Dharwad, India

^h ICAR-Indian Agricultural Research Institute, New Delhi, India

ⁱ ICAR- National Institute of Biotic Stress Management, Raipur, Chhattisgarh, India

ARTICLE INFO

Article history:

Received 20 May 2020

Received in revised form

2 July 2020

Accepted 7 July 2020

Available online 14 July 2020

Keywords:

Cropping systems

Rainfed agriculture

Residual soil moisture

Soil properties

Water productivity

ABSTRACT

A field experiment was conducted for two consecutive years at North Eastern Indian Himalayan region to assess the effect of soil moisture conservation measures on soil and water productivity of different rainfed maize (*Zea mays* L.) - based cropping sequences. Results revealed that double mulching with *in-situ* maize stover mulch (MSM) + fresh biomass of white hoary pea (WHP-*Tephrosia candida*) and MSM + fresh biomass of ragweed (RW- *Ambrosia artemisiifolia*) improved soil moisture content (SMC) and leaf relative water content of crops during dry season. The soil organic carbon (SOC) content and stocks under MSM + WHP and MSM + RW mulches were significantly higher than that under no mulch at 0–15 cm depth. The soil microbial biomass carbon and dehydrogenase activity were maximum under MSM + WHP/RW. The highest system productivity was obtained from maize-French bean (Pole type-PT) sequence under MSM + RW followed by MSM + WHP. The water productivity was the highest under MSM + WHP. While SOC content was the highest under maize-French bean (PT), the maximum plant available nitrogen and phosphorus were obtained under maize-black gram sequence. Thus, double mulching technology involving MSM and RW (available in plenty) is a viable option for improving soil, crop and water productivity under rainfed hill ecosystems of eastern Indian Himalayas.

© 2020 International Research and Training Center on Erosion and Sedimentation and China Water and Power Press. Production and Hosting by Elsevier B.V. This is an open access article under the CC BY-NC-ND license (<http://creativecommons.org/licenses/by-nc-nd/4.0/>).

1. Introduction

Achieving environmental sustainability concurrently with food and nutritional security is a major challenge before the researchers and policymakers more specifically in hill and mountain eco-regions of the globe (Babu et al., 2020). Low crop and water productivity and declining soil properties like soil fertility, water holding properties, soil organic carbon (SOC) content and a

widening cycle of inadequate food production-food insecurity-poverty-resource degradation are the major challenges of hill agriculture (Pratap, 2011). The SOC plays a key role in determining soil fertility, environmental sustainability and crop productivity (Ladha et al., 2016). An organic carbon rich soil is likely to have high water holding capacity, aggregate stability and above all nutrient supplying capacity to the crops. Thus, SOC is an important indicator of sustaining agricultural productivity and ecosystems. Persistent depletion of carbon (C) in Indian soils including those in Himalayan region due to improper agriculture management have been a great concern for sustaining agriculture and achieving sustainable development goal (Lal, 2015). Further, decline in soil properties in

* Corresponding author. ICAR Research Complex for NEH Region, Tripura Centre, Lembucherra, Agartala, Tripura, India.
E-mail address: anup.das2@icar.gov.in (A. Das).

terms of low nutrient availability, poor soil physical, and biological properties owing to non-adoption of best management practices and conservation measures contributes to unsustainability in hill agriculture (Das et al., 2020).

Maize (*Zea mays* L.) is the most versatile crop and has variety of uses like food, feed, fodder and in recent past as source of bio-fuel. Because of its low water requirement (500 mm) and high production potential, maize is the crop of choice in rainfed areas especially in hill ecosystems (Rakshit et al., 2017). Being an exhaustive crop, continuous cultivation of maize as monocrop has several consequences like degrading soil fertility, decline in SOC, low productivity and income (Zingore, 2011). The North-Eastern Region (NER) has total geographical area of 26.23 million ha (M ha) and receives a plenty of rainfall (>2000 mm annual rainfall). However, there is a large loss of water through runoff, percolation and evaporation. Thus, only a small amount of rainfall received is retained as green water for crop production system (Kuotsu et al., 2014). After harvesting of summer season crops, lack of sufficient soil moisture limits the cultivation of winter season crops. Thus, about 66% of the cultivated area remains fallow during the winter season mainly because of scanty rainfall during the post-monsoon season (about 20% of total annual rainfall) and the lack of infrastructure and measures to harvest and utilize the bountiful rains during the monsoon season (Ghosh et al., 2010). Soil moisture depletes rapidly under upland conditions with the cessation of rainfall leading to poor establishment and growth of winter-season crops. Thus, identification of resource efficient winter/post rainy crops for a sustainable maize based cropping system would contribute to multiple objectives of food and nutritional security, resource conservation and climate resilience. Mulching by crop residues, weed biomass and hedge-plant biomass protects soil against erosion and recycles plant nutrients upon decomposition. Improvement in soil moisture content (SMC) by mulching has been widely reported in the region (Kuotsu et al., 2014). However, in most cases, mulching is not cost-effective and non-availability of mulch biomass locally is another important constraint to its widespread adoption (Sharma, Singh, Dhyani, & Dube, 2010a, 2010b).

In rainfed hill ecosystems, after the maize harvest, soil surface remains largely bare resulting in rapid drying and depletion of residual moisture leading to poor germination of winter season crops (Sharma & Acharya, 2000). Thus, conservation of soil moisture offers an opportunity for stabilising and increasing yields of winter season crops in rainfed areas. In the NER, maize stover is not used as fodder for animals, and is either burnt or removed from the field. Favorable climatic conditions (i.e., high rainfall, humidity, moderate temperature) leads to a high vegetative growth of shrubs and weed biomass. Rag weed (RW) (*Ambrosia artemisiifolia*) is an obnoxious weed which grows in abundance in wastelands, roadsides, farm fences and is often difficult to control. The use of weed biomass (shrubs) such as boneset (*Eupatorium adhenophorum*), RW etc. as mulching material for soil and moisture conservation for crop production has been reported (Das et al., 2017; Sharma & Acharya, 2000). However, response of a wide range of short duration and deep rooted winter crops to such mulching measures is not known. Usefulness of leguminous hedgerow species like *Tephrosia candida* (WHP-white hoary pea), *Crotalaria tetragonoloba*, *Gliricidia* sp. and others for soil and water conservation, weed management and soil fertility build up through leaf mulching, root binding, N-fixation in summer and rainy season crops have also been reported earlier (Laxminarayan et al., 2006; Xu et al., 2012). Double mulching approaches of *in-situ* retention of maize stover along with external application of mulches like weed biomass (RW) or biomass from leguminous shrubs (WHP) may create an effective ground cover and conserve soil moisture and improve soil properties compared with those under *in-situ* retention of maize stover alone.

Monocropping with low above and below ground diversity actually promotes the process of soil organic matter (SOM) decomposition and subsequent loss of C from the soils (Yadav et al., 2019). Thus, utilizing maize fallow areas for growing a suitable winter crop in a sequence may generate additional biomass in addition to increases C sequestration potential and achieving food security (Nath et al., 2019). After maize harvest, cultivation of short duration crops with residual moisture along with effective conservation measures would enhance cropping intensity and water productivity. It is widely accepted that legumes play a vital role in having beneficial food secure systems, and rotations involving legumes diversify crop production systems and improve fertility of soils. French bean (*Phaseolus vulgaris* L.), black gram (*Vigna mungo*), rapeseed (*Brassica campestris* L) etc. are important short duration crops, and may be suitable for agro-climate of the NER. However, their suitability needs to be tested under a system approach. Moreover, French bean is an important, grain legume grown for their tender pods as vegetable as well as mature dry seed (red kidney beans) in the eastern region of the India (Prasad et al., 1995). Generally, it is cultivated for vegetable purposes round the year except during the winter season (October–January) in foothills as well as in the mid altitude in all the NER states. Rapeseed is mostly grown as a rainfed crop on residual soil moisture, moderately tolerant to soil acidity and can fairly tolerate drought (Das et al., 2010). Rapeseed has a low water requirement (240–400 mm), and it fits well within rainfed cropping systems (Saha et al., 2009). Black gram (*Vigna mungo* Viridis) is an important short duration pulse crop grown in cropping system as mixed crop, catch crop, sequential crop besides growing as sole crop under residual soil moisture after the harvest of maize, rice and other crops. The SOC accumulation is largely affected by a wide range of soil and climatic conditions, tillage systems and soil disturbances, residue management, cropping system and many others (Lal, 2018). Legumes may be the best option to make agricultural system sustainable by enhancing soil fertility, SOC storage, making balanced diet and protein rich feed for livestock (Shrestha et al., 2008). Thus, French bean, black gram and rapeseed were grown as test crops in the present study after maize to identify efficient cropping system for enhancing crop and water productivity. Conservation and management of rainwater *in-situ* and its efficient use may help in improving agricultural productivity, soil quality and SOC while protecting environmental quality on sloping lands of the eastern Himalayas. Hence, present study was undertaken with the objectives to identify efficient maize-based cropping sequence and soil moisture conservation measures for enhancing soil fertility, crop and water productivity in the eastern Himalayan region of India. The hypothesis tested was that residue mulching would improve soil properties, conserve residual soil moisture which facilitates the inclusion of short duration deep rooted winter crop in maize fallow, while enhancing crop and water productivity and improving SOC stocks.

2. Materials and methods

2.1. Experimental site

The field experiment was conducted at the upland Agronomy field of Indian Council of Agricultural Research (ICAR) Research Complex for North Eastern Hill Region, Umiam, Meghalaya, India. The experimental site is located at 25°41' N latitude and 91°54' E longitude with an altitude of 980 m above mean sea level (Fig. 1). The total rainfall received during the cropping period was 2053 mm in 2012–13 and 1966 mm in 2013–14, where the highest rainfall was received in the month of August (440 mm) in 2012 and June (407 mm) in 2013 and no rain in December in both the years (Fig. 2). The average rainfall received at experimental site during

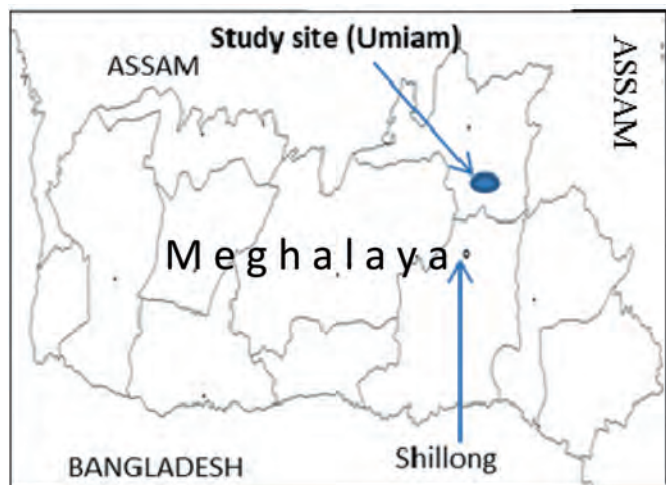


Fig. 1. Map of Meghalaya state of north eastern Himalayan region of India showing experimental site.

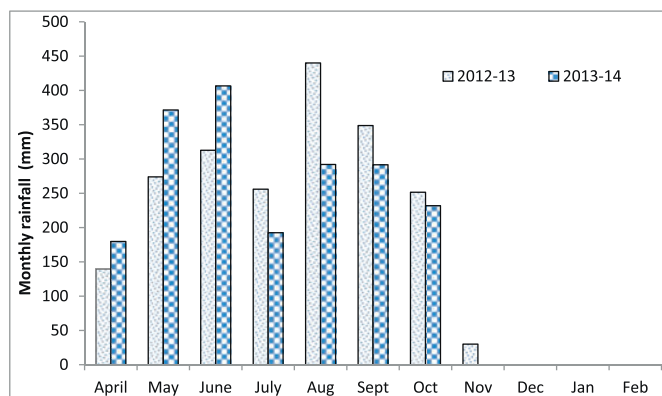


Fig. 2. Rainfall received during the cropping seasons in 2012–13 & 2013–14.

the *kharif* season (maize) was 1073 mm and during the winter (*rabi*) season was 660 mm. The average evaporation recorded during the entire period was about 637 mm, of which was the highest recorded during April (108 mm) and the lowest during December (47 mm). The mean maximum temperature was recorded during May (29.5 °C) and the minimum in December (20.9 °C). Wind speed was less variable and ranged from 1 to 3 km h⁻¹. Average relative humidity was 85% in the mornings and 67% in the afternoons. Soil of the experimental site was a well-drained silty clay loam and classified as *Typic Paleudalf* (Sarkar et al., 2017). The soil of the site was acidic in reaction, high in SOC, low in available phosphorus (P) and medium in nitrogen (N) and potassium (K) (Table 1).

2.2. Treatment details

Five maize-based cropping sequences tested were: S₁: maize – fallow, S₂: maize – rapeseed, S₃: maize – French bean (BT-bush type), S₄: maize – French bean (PT-pole type) and S₅: maize – black gram. These sequences were laid out as main plots. The four moisture conservation measures laid out as sub-plots were: M₀– no mulch (residue removal), M₁– *in-situ* maize stover mulch (MSM), M₂– *in-situ* MSM + RW fresh biomass 10 Mg ha⁻¹ and M₃– *in-situ* MSM + WHP fresh biomass 10 Mg ha⁻¹. All treatments were replicated thrice and laid out in a split plot design. The fresh biomass of RW and WHP were collected from nearby areas (i.e., road sides, wastelands, farm fences

Table 1
Initial soil parameters of the experimental field.

Soil parameters	0–15 cm	15–30 cm
Soil pH	5.24	5.29
Organic carbon (g kg ⁻¹)	15.7	14.0
Available nitrogen (kg ha ⁻¹)	228.3	205.6
Available phosphorus (kg ha ⁻¹)	6.29	5.95
Available potassium (kg ha ⁻¹)	238.4	212.6
Bulk density (Mg m ⁻³)	1.27	1.26

etc.) of the experimental farm. The upper tender portions of these plants were retained, discarding the woody lower portion of stems which decompose slowly. The fresh biomass was weighed and applied as mulch in between the rows of standing maize 20 days before the harvest of maize as per the treatment. The moisture content in RW and WHP was 81% and 77%, respectively. Systemic herbicide roundup (N-phosphonomethyl, glycine, active ingredient glyphosate) 41% SL at the rate of 1.0 kg active ingredient (*a.i.*) per ha was applied to control weeds after the harvest of maize (before cutting the stalks). The winter season crops were grown following a no-till (NT) system. After the harvest of maize, furrows were opened in between two maize rows using a manual furrow opener by pushing the mulch on the side of maize rows to sow the seeds of winter crops. Both fertilizers and seeds were placed in the furrows and covered with soil, and the mulch materials were adjusted to cover the surface. The winter season crops of French bean (BT and PT) and black gram were sown during last week of August. After the seedling emergence, the maize stover was cut and spread all over the field on top of the mulch to cover the soil surface. Therefore, there were two layers of mulch *i.e.* MSM and RW/WHP mulch to cover the soil surface. Rapeseed was also sown in between the rows of maize by pushing the mulch aside. The mulch was adjusted back between the rows to properly cover the soil surface on the same day and immediately after sowing. Two manual weedings were given [20 and 40 days after sowing (DAS)] for all winter season crops, except in the rapeseed for which weeding was done on 25 and 50 DAS, and the weed biomass was retained along with MSM *in-situ* for moisture conservation. The details of cultural practices followed are outlined in Table 2.

2.3. Soil sampling and analysis

The SMC was measured gravimetrically (at 0–15 cm, 15–30 cm and 30–45 cm depths) at 15– days' interval from sowing of winter season crops up to the harvest. Soil bulk density was determined by the core method (Blake & Hartge, 1986) after harvest of winter crops. The core was 6.4 cm long and 4.9 cm in diameter. Water holding capacity (WHC) was measured at 0–15 and 15–30 cm (Jalota et al., 1998, pp. 65–67) after the harvest of winter crop.

Soil samples were collected before (0–15 cm) and after (0–15 and 15–30 cm) the experimentation following standard procedure for analyzing physico-chemical and biological properties. The SOC concentration was determined by Walkley and Black method (Nelson & Sommers, 2005) and soil pH by the glass electrode method (Kalra, 1995). Soil available nitrogen (N) was determined by alkaline potassium permanganate method (Subbiah & Asija, 1956), P by Bray and Kurtz No. 1 method (Olsen & Sommers, 1982) and K by ammonium acetate method (Knudsen et al., 1982). Soil microbial biomass carbon (SMBC) was estimated by the chloroform fumigation method (Brookes & Joergensen, 2006). SMBC was calculated as the difference between fumigated and non-fumigated samples and divided by the K₂SO₄ efficiency factor (KE_C = 0.38) (Vance et al., 1987) and expressed as μg g⁻¹ soil. Dehydrogenase activity (DHA) in soil was determined by Triphenylformazan (TPF) reduction method as per the procedure described by Casida et al. (1964).

Table 2
Input used and cultural practices followed in the experiment.

Particulars	Maize (<i>Zea mays</i> L.)	Rapeseed (<i>Brassica campestris</i> L.)	French bean (bush) [<i>Phaseolus vulgaris</i> L.]	French bean (pole) [<i>Phaseolus vulgaris</i> L.]	Black gram (<i>Vignamungo Viridis</i> L.)
Variety	DA-61A	TS-46	Arkaanoop	Naga local	PD-4
Tillage	Minimum tillage	No-till	No-till	No-till	No-till
Date of sowing	1st week of May	Last week of Oct.	Last week of August	Last week of August	Last week of August
Spacing (cm)	60 × 20	30 × 5	30 × 15	30 × 15	30 × 10
FYM	5 Mg ha ⁻¹	–	–	–	–
Fertilizer doses (N:P ₂ O ₅ :K ₂ O kg ha ⁻¹)	60:60:40	60:60:40	50:60:40	50:60:40	20:60:40
Gap filling (DAS)	10	10	8	8	12
Hand weeding (DAS)	25	25	20	20	20
	45	50	40	40	40
Top dressing of N (DAS)	30	30	–	–	–
Herbicide application for sowing winter crops	–	Glyphosate 41 % SL 1.0 kg a.i./ha	Glyphosate 41 % SL 1.0 kg a.i./ha	Glyphosate 41 % SL 1.0 kg a.i./ha	Glyphosate 41 % SL 1.0 kg a.i./ha
Date of harvesting	2nd week of August	Last week of Dec.	2 nd week of Nov.	Last week of Nov.	1st week of Dec.

N-nitrogen; DAS- days after sowing; FYM-farmyard manure.

Total SOC stock (Mg ha⁻¹) for 0–15 cm and 15–30 cm depth was computed by using the following equation (Srinivasarao et al., 2012):

$$\text{SOC stock (Mg ha}^{-1}\text{)} = 10^4 \text{ m}^2 \text{ ha}^{-1} \times \text{SOC concentration (\%)} \times 10^{-2} \times \text{Bulk density (Mg m}^{-3}\text{)} \times \text{depth (m)} \quad (1)$$

2.4. Crop yields and maize equivalent yield

At maturity, yields were recorded from the net plot area (4 × 3.5 m) and reported at 14% grain moisture content. Yields of all crops were converted to maize equivalent yield (MEY) to facilitate comparison among treatments as follows:

$$\text{MEY} = \text{Yield of winter crops (kg ha}^{-1}\text{)} \times \text{price of winter crops (\$ kg}^{-1}\text{)} / \text{price of maize (\$ kg}^{-1}\text{)} \quad (2)$$

2.5. Leaf relative water content (LRWC)

Samples of 5 leaves were obtained and the fresh weight recorded. Fresh leaves were then transferred into beakers filled with water for 18–24 h. After 24 h, the leaves were removed, the turgid weight recorded, and dried in an oven at 65 ± 1 °C. Once dried, leaves were weighed. The leaf water content was computed by deducting the dry weight (DW) of samples from that of the fresh weight (FW). Water content at saturation was computed by deducting DW from turgid weight (TW). The LRWC was calculated by using Eq (3) (Weatherly, 1950):

$$\text{LRWC (\%)} = \frac{\text{FW} - \text{DW}}{\text{TW} - \text{DW}} \times 100 \quad (3)$$

2.6. Water use efficiency (WUE)

The WUE was calculated by using Eq (4) (Sarkar & Singh, 2007):

$$\text{WUE (\%)} = \frac{\text{Seed yield (kg ha}^{-1}\text{)}}{\text{Evapo - transpiration (ET)} \times \text{Kc}} \quad (4)$$

where, seed yield is the grain or economic yield of crops in kg ha⁻¹. Crop water requirement (ETc) in millimeter was evaluated by pan evaporation and the crop coefficient method (Balasubramanian & Palaniappan, 2007).

2.7. Land use efficiency (LUE)

The LUE was calculated by dividing total duration of crops in a cropping system by 365 days (Eq (5)):

$$\text{LUE (\%)} = \frac{\text{Duration of maize} + \text{Duration of rabi crop}}{365 \text{ (days)}} \times 100 \quad (5)$$

2.8. Water productivity (WP)

The WP was calculated by using Eq. (6) (kg m⁻³) (Hashim et al., 2012):

$$\text{WP} = \frac{\text{Yield of maize} + \text{rabi crop (kg ha}^{-1}\text{)}}{\text{Rainfall received (maize} + \text{rabi crop) (mm)}} \times 10000 \text{ m}^2 \quad (6)$$

2.9. Production efficiency (PE)

The PE was calculated by using Eq. (7) (Tomar & Tiwari, 1990):

$$\text{Production efficiency} = \frac{\text{Total production of a system (kg ha}^{-1}\text{)}}{\text{Duration of the system}} \quad (7)$$

2.10. Soil moisture content and stock

The SMC was determined by the gravimetric method (Jalota et al., 1998, pp. 65–67) using Eq (8):

$$\text{SMC}(\%) = \frac{\text{Weight of fresh soil} - \text{Weight of oven dried soil}}{\text{Weight of oven dried soil}} \times 100 \quad (8)$$

Soil moisture stock (SMS) was computed at the flowering stages in all the crops. It was calculated by using Eq9 and expressed in cm per 45 cm:

$$\text{SMS (cm)} = \frac{\text{Soil moisture content (\%)}}{100} \times \text{soil bulk density } (\rho_b) \times \text{Depth (cm)} \quad (9)$$

Where soil ρ_b is in g cm^{-3} for the specific depth, and then summed for 3 depths.

2.11. Statistical analysis

The two year pooled data i.e., average of two years were statistically analysed for Analysis of Variance (Gomez & Gomez, 1984, p. 324). The difference between the treatment means were tested with Least Significant difference (LSD) value at 5% level of probability ($p = 0.05$). Interaction between treatments were presented and discussed whenever found significant.

3. Results

3.1. Leaf relative water content (LRWC)

Prominent effect of moisture conservation measures was observed on LRWC at 60 DAS in all crops which were significantly higher under *in-situ* MSM + WHP mulch over no mulch control (Table 3). The LRWC under *in-situ* MSM + WHP mulch and *in-situ* MSM + RW mulch were at par with each other in all the crops and at all phenological stages. The increase in average LRWC under *in-situ* MSM + WHP mulch over no mulch at 60 DAS in rapeseed, French bean (BT), French bean (PT) and black gram were 19, 21, 17 and 7%, respectively. Among winter season crops, black gram under MSM + WHP recorded the maximum LRWC at 60 DAS (78.5%). The LRWC increased from 30 to 60 DAS in all crops except in rapeseed. The lowest LRWC was observed in no mulch control for all crops. In general, LRWC in 2013-14 was slightly lower than those recorded in 2012-13.

Table 3

Effect of mulching treatments on leaf relative water content (%) of winter season crops at 60 days after sowing (two year average data).

Mulching measures	Rapeseed	Black gram	French bean (Bush)	French bean (Pole)
Treatment				
No mulch	61.9	73.3	63.0	64.4
MSM	66.2	75.8	67.8	69.2
MSM + RW	68.5	77.0	73.1	73.0
MSM + WHP	73.6	78.5	76.1	75.7
SE(m) ±	1.11	0.69	1.30	1.09
LSD (P = 0.05)	3.83	2.34	4.51	3.74

MSM- maize stalk mulch, RW-Ragweed, WHP- White hoary pea, SE (m)± - Standard error of mean, LSD- Least Significant Difference.

3.2. Soil moisture content and soil moisture stock (SMS)

Among the cropping systems, soil under maize-French bean (PT) system contained higher moisture from seeding up to 45 DAS. From 60 DAS to harvest, plots of maize-black gram had higher SMC followed by that of maize-French bean (PT) as compared to that in plots of other systems (Fig. 3). The lowest SMC at harvest was recorded in plots under maize-rapeseed cropping system.

The maximum SMC was observed under *in-situ* MSM + WHP mulch at all growth stages, and it was similar to that under *in-situ* MSM + RW mulch. The lowest SMC was measured under no mulch control treatment. The maximum SMS (Table 4) was recorded un-

der plots of maize- French bean (BT) system, which was significantly more than that of maize-rapeseed system. The SMS was 24% more in plots under maize- French bean (BT) system than that under maize-rapeseed system. Soil moisture conservation measures had a significant influence on SMS at the flowering stage. The highest SMS was observed with the retention of *in-situ* MSM + WHP mulch which was 11% higher than that under the no mulch control. The SMS did not vary statistically in plots under *in-situ* MSM + WHP, *in-situ* MSM + RW and *in-situ* MSM, however, it was significantly more than that under non-mulched control plot.

3.3. Water use efficiency (WUE) and water productivity (WP)

Significant effect of mulching was observed on WUE of all winter season crops (Fig. 4). The highest WUE was recorded under *in-situ* MSM + WHP mulch followed by that under *in-situ* MSM + RW mulch treatment in all crops. Relative increase in pooled WUE in black gram, French bean (PT), French bean (BT) and rapeseed, under *in-situ* MSM + WHP mulch than that under no-mulch was 76.9, 55.6, 45.9, and 36.5%, respectively.

The WP was significantly influenced by mulch treatments in all cropping sequences (Fig. 5). The highest pooled WP was recorded in the maize-rapeseed sequence followed by that under maize-black gram for all mulch treatments. Significantly higher WP was obtained with maize-rapeseed sequence under *in-situ* MSM + WHP mulch relative to no-mulch. The WP of maize-rapeseed system under *in-situ* MSM + WHP mulch was 7% higher than that under no mulch. Similarly, WP obtained under *in-situ* MSM + WHP mulch and *in-situ* MSM + RW mulch was significantly more than that under no-mulch.

Since WUE and WP values observed between two years were statistically similar with slightly smaller values in 2013-14 than 2012-13, thus, only two years average data presented.

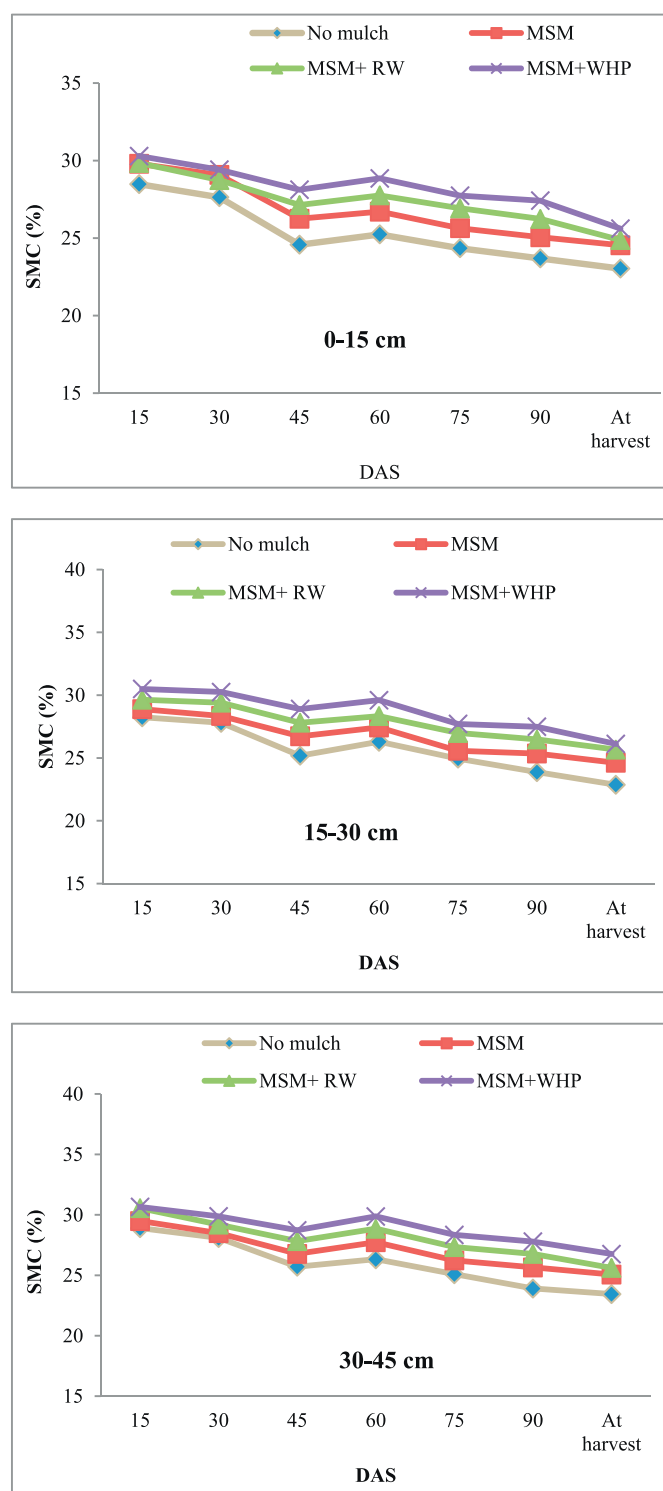


Fig. 3. Effect of mulching treatments on soil moisture content at different depth at 15 days interval from sowing to harvest of winter season crops (2013–14).

3.4. Bulk density and water holding capacity

Significant effects of cropping systems and soil moisture conservation measures were observed on bulk density of soil (Table 4). Soils under maize-black gram system had the lowest bulk density followed by that under maize-rapeseed system. Soil bulk density increased with increase in soil depth across the cropping systems.

Soil moisture conservation measures did not affect soil bulk density at all the depths (Table 4). Despite the lack of statistical differences, soils under residue removal at all depths had relatively higher bulk density while the minimum was observed under MSM + WHP/RW.

Significant effects of cropping systems and soil moisture conservation measures were observed on WHC (Table 4). The maximum WHC was observed in soils under maize-black gram system followed that under maize-French bean (PT) while lowest under maize-fallow system. Soil moisture conservation measures also affected WHC significantly at all the depths. Soils under residue removal at all depths had the lowest WHC while the maximum WHC was observed under MSM + WHP/RW.

3.5. Soil organic carbon

The SOC content was the highest in plots under maize-French bean (PT) system followed by that under maize-black gram system in 0–15 cm (Table 5). The SOC content in plots under maize-French bean (PT) was 10.7% higher than that of plots under maize-fallow system.

The SOC content under MSM + WHP mulch was significantly higher relative to no mulch at 0–15 cm. The SOC content under MSM + RW mulch (1.75 and 1.66% at 0–15 and 15–30 cm, respectively) remained at par with that for MSM + WHP. *In-situ* MSM alone could increase SOC by 5.7 and 7% over no mulching in 0–15 and 15–30 cm soil layer, respectively after 2 cropping cycles.

3.6. Soil available nitrogen (N)

After two cropping cycles, the amount of plant available N varied significantly under different cropping systems and soil moisture conservation measures (Table 5). Soil under maize-black gram system had the highest available N in 0–15 cm layer as compared to those under other cropping systems. The soil available N under maize-black gram system was 13% higher than that under maize-fallow systems. However, soil available N in 15–30 cm layer was the maximum under maize-French bean (BT) which was 10.6% higher than that under maize-fallow system.

Residue mulching had significant impact on soil available N after two cropping cycle. The highest soil available N was observed under MSM + WHP followed by MSM + RW mulch. *In-situ* retention of MSM could enhance soil available N by 5% and 2.8% over no mulch after two cropping cycle.

3.7. Soil available phosphorus (P)

Soil available P was significantly influenced by cropping systems and soil moisture conservation measures (Table 5). The highest available P was observed in soils under maize-black gram system followed by that under maize-French bean (PT) at 0–15 cm and maize-rapeseed system at 15–30 cm depths. Soils under maize-black gram and maize-French bean systems had 33.3 and 27.8% higher available P after two cropping cycles compared to that under maize-fallow system at 0–15 cm depth. Among the soil moisture conservation measures, higher soil available P was observed under MSM + WHP mulch followed by that under MSM + RW mulch in both the depths. The available P under MSM + WHP and MSM + RW were 39.5 and 40.3% higher at 0–15 cm and 33.9 and 24.7% higher at 15–30 cm soil depths, respectively relative to no mulch.

3.8. Soil available potassium (K)

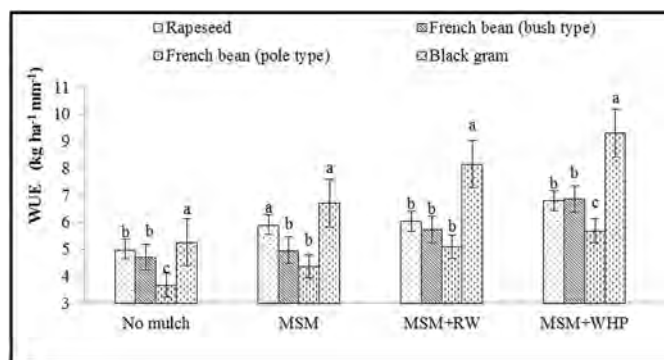
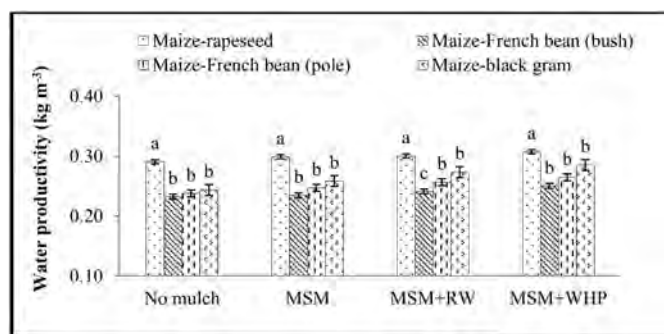
Significant effect of cropping systems and soil moisture conservation measures were observed on soil available K (Table 5). Soil

Table 4

Effect of cropping systems and mulching treatments on soil physical properties and soil moisture stock (after 2 cropping cycle).

Treatments	WHC (%)		Bulk density (Mg m^{-3})		^a Soil moisture stock ($\text{cm } 45 \text{ cm}^{-1}$)
	A	B	A	B	
Cropping systems					
Maize – Fallow	68.88	66.79	1.27	1.32	18.0
Maize – Rapeseed	71.92	70.18	1.25	1.31	16.6
Maize – French bean (BT)	71.63	69.88	1.26	1.26	19.6
Maize – French bean (PT)	73.12	69.16	1.26	1.29	18.2
Maize – Blackgram	74.65	71.6	1.24	1.28	18.1
SE (m)±	1.08	1.21	0.01	0.04	0.35
LSD (P = 0.05)	3.49	3.92	0.03	0.14	1.12
Mulching measures					
No mulch	68.06	66.11	1.27	1.35	17.1
In-situ Maize stover mulch (MSM)	71.53	68.29	1.25	1.34	17.9
MSM + Ambrosia	73.78	70.21	1.25	1.33	18.4
MSM + Tephrosia	75.29	72.33	1.25	1.33	19.0
SE(m)±	1.33	1.277	0.01	0.13	0.27
LSD(p = 0.05)	4.26	4.15	NS	NS	0.87

BT-bush type, PT-pole type, A-0 to 15 cm, B-15 to 30 cm, WHC- Water holding capacity, NS- non-significant, SE(m)± - Standard error of mean, LSD- Least Significant Difference.

^a Estimated at flowering stage of winter season crops (2013–14).**Fig. 4.** Water use efficiency of winter seasoncrops under different mulching treatments (average of 2 years).**Fig. 5.** Water productivity of different cropping sequences affected by mulching treatments (average of two year).

available K was the highest in plots under maize-French bean (PT) system followed by that under maize-French bean (BT) cropping system. Among the mulching measures, MSM + *Tephrosia* mulch had the highest soil available K as compared to that under other soil moisture conservation measures.

3.9. Soil biological properties

In the present study, a significant influence of cropping systems and soil moisture conservation measures was observed on DHA at 0–15 cm depth (Table 6). Significantly higher DHA was recorded in

soils under maize-French bean (PT) system followed by that under maize-French bean (BT) system. The DHA concentrations under maize-French bean (PT) and maize-French bean (BT) were higher by 57% and 40.8% than that in soil under maize-fallow system, respectively. The DHA concentration under maize-rapeseed system was non-significantly higher than that under maize-fallow system. Higher DHA was recorded under MSM + WHP mulch followed by MSM + RW mulch as compared to that for the no mulch control. The DHA concentration under MSM + WHP and MSM + RW mulches were 39.5 and 24.9% higher than that under no mulch after two cropping cycles. Soils under *in-situ* MSM also had significantly higher DHA than that under no mulch.

Relatively higher SMBC was observed in soil under maize-French bean (PT) system followed by that under maize-black gram system. Among the mulching measures, SMBC was the highest in soil under MSM + WHP mulch followed by that under MSM + RW mulch, which were 16.3 and 13.7% higher than that under no mulch, respectively. *In-situ* MSM also had significantly higher SMBC than that under no mulch (Table 6).

3.10. Soil organic carbon stock

Among the cropping sequences, Maize – French bean (PT) sequence had significantly higher SOC stock than those under maize – fallow system in 0–15 cm. However, SOC stocks under all the cropping sequences remained at par with each other except maize-fallow sequence. Maize – French bean (PT) and maize – French bean (BT) had 11.1 and 9.4% higher SOC stock than maize-fallow system at 0–15 cm after 2 cropping cycles. The SOC stock under MSM + WHP/RW was significantly higher than no-mulch at 0–15 cm after 2 cropping cycles (Table 6).

3.11. Productivity of winter season crops and maize equivalent yield (MEY)

Mulching measures had a significant impact on seed and stover yields of all cropping sequences (Table 7). In comparison with the no mulch control, increase in pooled seed yield by mulching with MSM + WHP was 37, 59, 51 and 72% for rapeseed, French bean (BT), French bean (pole type) and black gram, respectively (Table 7). The productivity of all the winter crops during two years of the study were statistically similar with slightly lower yields in second year. Thus, only average yield data of two years are presented.

Table 5

Effect of cropping systems and mulching measures on soil chemical properties at harvest of winter crops (after 2 cropping cycle).

Treatments	SOC (g kg ⁻¹)		N (kg ha ⁻¹)		P (kg ha ⁻¹)		K (kg ha ⁻¹)	
	A	B	A	B	A	B	A	B
Cropping systems								
Maize–Fallow	15.8	14.8	240.0	213.3	12.6	9.0	251.7	218.2
Maize–Rapeseed	16.9	15.3	261.3	217.3	15.5	11.7	277.4	235.0
Maize–French bean (BT)	17.3	16.7	266.4	236.0	15.3	11.3	282.5	221.9
Maize–French bean (PT)	17.5	16.6	264.2	232.3	16.1	11.1	285.6	225.9
Maize–Blackgram	17.3	16.3	271.3	233.6	16.8	11.6	256.4	219.3
SE(m)±	0.21	0.74	4.15	6.38	0.58	0.39	2.67	7.11
LSD (P = 0.05)	0.73	NS	13.46	NS	1.88	1.28	8.71	NS
Mulching measures								
No mulch	15.9	14.3	242.4	217.1	12.4	9.7	254.7	214.1
<i>In-situ</i> Maize stover mulch (MSM)	16.8	15.3	254.5	223.1	14.3	10.2	272.0	219.7
MSM + <i>Ambrosia</i>	17.5	16.3	266.6	231.3	16.6	12.1	271.9	228.3
MSM + <i>Tephrosia</i>	17.7	16.5	275.2	238.3	17.3	13.6	286.1	236.1
SE(m)±	0.23	0.4	1.21	1.05	0.51	0.18	1.73	1.08
LSD(p = 0.05)	0.76	01.3	3.92	3.44	1.65	0.58	5.59	3.48

BT-bush type, PT-pole type, SOC- Soil organic carbon, A-0 to 15 cm, B-15 to 30 cm, SE (m)± -Standard error of mean, CD(P = 0.05)- Critical difference, N - Nitrogen, P - Phosphorus, K- Potassium in kg ha⁻¹, NS - non-significant.

Table 6

Effect of cropping systems and mulching measures on biological properties and soil organic carbon stocks at harvest of winter crops (0–15 cm) (After 2 cropping cycle).

Treatments	SMBC (μg g ⁻¹ soil)		DHA (μg TPF hr ⁻¹ g ⁻¹)		Soil organic carbon stock (Mg ha ⁻¹)	
	A	B	A	B	A	B
Cropping systems						
Maize – Fallow	237.2		27.7		20.24	19.37
Maize – Rapeseed	251.3		31.1		20.81	19.67
Maize – French bean (BT)	259.6		39.0		21.19	21.00
Maize – French bean (PT)	263.6		43.5		21.67	20.68
Maize – Black gram	261.7		36.3		20.97	19.24
SE(m)±	4.53		1.3		0.26	0.77
LSD (P = 0.05)	NS		4.37		0.84	NS
Mulching measures						
No mulch	232.0		27.41		20.23	18.90
<i>In-situ</i> Maize stover mulch (MSM)	244.3		31.72		20.82	19.81
MSM + <i>Ambrosia</i>	263.7		34.23		21.18	20.56
MSM + <i>Tephrosia</i>	269.8		38.23		21.68	20.70
SE(m)±	2.89		1.10		0.24	0.68
LSD(p = 0.05)	9.33		3.57		0.77	NS

BT-bush type, PT-pole type, A-0 to 15 cm, B-15 to 30 cm, SMBC-soil microbial biomass carbon, DHA dehydrogenase activity, TPF - Triphenylformazan, NS- non-significant, SE(m)± - Standard error of mean, LSD- Least Significant Difference.

Table 7Effect of soil moisture conservation measures on seed and stover productivity (Mg ha⁻¹) of winter crops (two year average data).

Treatment	Rapeseed		Black gram		French bean (Bush)		French bean (Pole type)	
	Seed	Stover	Seed	Stover	Seed	Stover	Seed	Stover
No mulch	0.60	1.37	0.94	1.22	0.61	1.13	0.85	1.16
MSM	0.70	1.63	1.17	1.52	0.69	1.20	0.97	1.30
MSM + RW	0.72	1.79	1.43	1.74	0.80	1.30	1.15	1.40
MSM + WHP	0.82	1.97	1.62	1.90	0.94	1.43	1.28	1.52
SE(m) ±	0.03	0.04	0.05	0.04	0.02	0.04	0.04	0.06
LSD (P = 0.05)	0.10	0.14	0.15	0.15	0.10	0.14	0.14	0.19

MSM- maize stalk mulch, RW-Ragweed, WHP- White hoary pea, SE(m)± - Standard error of mean, LSD- Least Significant Difference.

3.11.1. Rapeseed

Significant effects of mulching treatments were observed on seed and stover yields of rapeseed. MSM + WHP had significantly higher rapeseed yield than those under MSM only and no-mulch. *In-situ* MSM also had significantly higher rapeseed seed yield than that of no-mulch control. The seed yields under MSM + WHP and MSM + RW were at par with each other. Increase in pooled yields of seed and stover under *in-situ* MSM + WHP mulch than no-mulch was 37 and 47.7%, respectively.

3.11.2. French bean

Seed and stover yields of French bean (PT and BT) was significantly higher under *in-situ* MSM + WHP mulch followed by that under *in-situ* MSM + RW mulch and the least under no-mulch control. In comparison with the no mulch control, the *in-situ* MSM + WHP increased the average seed yield of French bean by 54.1% for BT and 56.1% for the PT, respectively.

3.11.3. Black gram

There was a significant impact of mulch treatments on black

Table 8
Interaction effect of treatments on system maize equivalent yield (Mg ha^{-1}) (two year average data).

Cropping sequences/Mulching measures	Maize–fallow	Maize –rapeseed	Maize–French bean (bush type)	Maize–French bean (Pole type)	Maize–Black gram	Mean
No mulch	3.22	4.44	6.42	7.42	5.73	5.44
MSM	3.27	4.68	6.73	8.14	6.41	5.84
MSM + RW	3.29	4.73	7.31	9.01	7.10	6.29
MSM + WHP	3.31	4.92	8.05	9.68	7.61	6.71
Mean	3.27	4.69	7.13	8.56	6.71	
	SE(m) \pm			LSD (P = 0.05)		
Cropping sequences (CS)	0.0615			0.21		
Mulch type (MT)	0.051			0.1585		
For MT at same or different level of CS	0.1075			0.3165		
For CS at same or different level of MT	0.116			0.3475		

MSM- maize stalk mulch, RW-Ragweed, WHP- White hoary pea, SE(m) \pm - Standard error of mean, LSD- Least Significant Difference.

gram productivity. The highest seed yield was recorded under *in-situ* MSM + WHP mulch (1.7 Mg ha^{-1}) followed by that under *in-situ* MSM + RW mulch and the least under no mulch control. The average seed yield of black gram increased by 72.3, 52.1 and 24.4% under *in-situ* MSM + WHP, MSM + RW and MSM mulch than no mulch, respectively.

The interaction effect of cropping systems and soil moisture conservation measures indicated that the highest MEY (Table 8) was recorded for the maize-French bean (PT) cropping sequence under *in-situ* MSM + WHP mulch followed by that under *in-situ* MSM + RW mulch. The average MEYs for the maize-French bean (PT) system under *in-situ* MSM + WHP and MSM + RW mulches were 218% and 202% higher than that recorded with maize-rapeseed cropping sequence under no mulch. Similarly, the MEYs obtained with maize –French bean (BT), maize-black gram and maize –rapeseed systems under MSM + WHP mulch were 150, 136 and 52.8%, respectively higher than that recorded with maize-fallow under no-mulch, respectively.

3.11.4. Land use efficiency (LUE) and production efficiency (PE)

Maize-black gram (56.4%) had the highest LUE followed by that under maize-rapeseed, maize- French bean (pole type) and maize-French bean (bush type) sequence (data not presented). Maize-fallow system had the lowest LUE. Relative increase in pooled LUE in maize-black gram, maize-rapeseed, maize-French bean (PT), and maize-French bean (BT) cropping sequences were by 92, 85, 84, and 70% compared with maize-fallow cropping sequences, respectively.

The effect of mulch types on PE was significant in all cropping sequences (Table 9) and it was the highest under *in-situ* MSM + WHP mulch. In terms of the cropping sequences, the highest PE was obtained for the maize-black gram sequence under *in-situ* MSM + WHP mulch. This was followed by that under maize-French bean (PT) under *in-situ* MSM + WHP mulch. .

4. Discussions

It has been established that the cropping sequences, type of crops, residue management and mulching measures influence the

soil physico-chemical and biological environment and crop performance. In the present study, diverse cropping systems and moisture conservation measures had a variable effect on soil properties, crop and water productivity. Total annual rainfall was little higher in first year than second year, similarly, winter rain in second year of the study was less than first year (Fig. 2). As a result, plant water content and productivity of winter crops in second year were non-significantly lower than first year.

4.1. Leaf relative water content

Relatively higher LRWC content under retention of maize stover mulch along with WHP or RW might be due to higher amount of soil moisture reserves, and lower drought stress. Improvement in soil properties like WHC, IR might have contributed in enhancing soil moisture reserve and subsequent alleviation of drought stress. Higher plant water status with mulch than without mulch has been reported in other crops (Gupta & Gupta, 1986). Because of lower SMC and SMS under no mulch control, the leaves experienced soil moisture stress earlier than roots, and developed lower LRWC (Unyayar et al., 2004).

4.2. Soil moisture and water holding capacity

Spreading and broad leaves nature of black gram which cover the ground effectively and reduce exposure of soil surface to the sun and evaporation might have attributed to relatively higher SMC in soil under maize-black gram system. A high SMC due to close canopy and good ground coverage was also reported in other crops (Obalum et al., 2010).

The SMC and WHC were significantly higher in soil under diverse mulching measures than those under no-mulch. Relatively higher SMC and WHC under retention of maize stover mulch along with RW or WHP might be due to even distribution of crop residues on the soil surface which decreased losses by surface runoff and evaporation (Kuotsu et al., 2014). The mulch materials reduced evaporation loss of water and conserved moisture in the soil profile. It insulates the soil, moderates soil temperature and reduces soil

Table 9
Effect of soil moisture conservation measures on production efficiency (kg ha^{-1}) of winter crops (two year average data).

Treatment	Maize–Rapeseed	Maize–French bean (Bush)	Maize–French bean (Pole)	Maize–Black gram
No mulch	19.6	21.5	21.2	20.69
MSM	20.1	21.9	21.8	21.84
MSM + RW	20.2	22.5	22.7	23.08
MSM + WHP	20.7	23.3	23.4	23.98
SE(m) \pm	0.15	0.35	0.20	0.21
LSD (P = 0.05)	0.53	1.22	0.71	0.74

MSM- maize stalk mulch, RW-Ragweed, WHP- White hoary pea, SE(m) \pm - Standard error of mean, LSD- Least Significant Difference.

evaporation (Rathore et al., 1998). Higher SMC in soil under mulch than no-mulch plots at all soil depths have been reported by Pervaiz et al. (2009). Use of plant residues as mulch cover or any biomass application improves available water capacity (AWC) (Bhagat & Verma, 1991), increases water infiltration rate (Acharya et al., 1988), reduces evaporation and modifies water retention capacity (Yang et al., 2003) and decreases soil bulk density (Khaleel et al., 1981). Relatively higher SMS under mulching is attributed to higher water infiltrability of the soil surface and reduction in soil evaporation (Salau et al., 1992; Das et al., 2015). The time and amount of mulch application and the rainfall pattern greatly effects rainwater conservation (Sharma & Acharya, 2000). Mulching in standing crop of maize with its saturated soil profile has been reported as the most suitable for conserving moisture for succeeding crop. This conserved soil moisture is highly precious for field preparation, sowing and establishment of succeeding winter crops under rainfed conditions (Sharma & Acharya, 2000).

4.3. Water use efficiency and productivity

The higher WUE of the crops in mulched plot was because of enhanced productivity. Mulching also maintained high plant-available water and the WUE increased as a result of soil water being used for crop growth rather than for evaporation (Das et al., 2017). Among all crops, black gram under *in-situ* MSM + WHP mulch recorded the highest WUE probably because of higher yield and longer growth duration of black gram than that of other crops. The increase in yield is indicative of the efficiency of soil management practices to improve AWC and WUE. For example, NT combined with crop residues mulch also improves soil physical quality and increases crop yield because of a higher WUE (Das et al., 2017; Wang, 2006, p. 187). Increased crop productivity and efficient utilization of limited soil moisture due to mulching contributed to enhance WP (Das et al., 2015).

4.4. Soil organic carbon content and stocks

Inclusion of more number of crops in a cropping sequence and protection of soil aggregates with mulching or other conservation practices increase SOC content and stocks (Yadav et al., 2019). This trend might be attributed to a higher SOC content and stocks in maize-based cropping system with inclusion of black gram, rapeseed and French bean than that of prevailing maize fallow system. In addition, the higher SOC content under maize-black gram system might be due to the presence of higher soil moisture content that increased the microbial population and hastened the decomposition of crop residues leading to building up of organic carbon in soil (Timsina, 2018). In the present study, different cropping systems have different biomass production, and that brought different quantities and qualities of C into the soil and affected soil carbon conservation and stocks. Soil bulk density was also affected by different sequences and SMC measures. Higher SOC in soils under maize - legume system has been also reported from other part of India (Tiwari et al., 2000) as well as the world (Adiku et al., 2008; Yousefi et al., 2008). Crop rotation effects SOC and nutrients from agroecosystem and improves soil fertility, N contents and nutrient use efficiency (Acosta-Martinez et al., 2008). Inclusion of legume in cropping systems is reported to be more efficient in increasing SOC than that under cereals (Meena et al., 2015), and that higher plant biomasses often lead to more SOC sequestration (Somnro & de Benito, 2010).

Decomposition of surface applied plant-based mulches leads to the formation of micro-aggregates and subsequently macro-aggregates (Zheng et al., 2018) and buildup of SOM (Ramesh et al., 2019), which might be attributed to the higher SOC under

MSM along with WHP/RW in the present study. The same reason was also responsible for higher SOC stocks under these treatments. An increase in SOC concentration of soil following incorporation of crop residues has been previously reported (Meena et al., 2015). The increase in SOC content under NT with mulching might have resulted from incorporation of OM rich crop residues and plant biomass (Khurshid et al., 2006; Sharma et al., 2010a, 2010b).

4.5. Available N, P and K in soil

Cropping systems with legumes as component crop enhance soil available N substantially over non-legume crop rapeseed and maize-fallow system (Das et al., 2018). This trend might be ascribed to biological N fixing ability of leguminous crop that left varying amount of N in soil leading to increase in soil available N (Jat et al., 2011).

In the present study, all the residue mulching measures had a positive effect on soil available N at both the soil layers. However, MSM + HWP /RW had higher available N than that under other measures. This trend could be ascribed to addition of some nutrient from WHP/RW biomass on mineralization. Significant improvement in fertility status due to addition of leaf biomass from hedge row species has been reported from eastern Himalayas (Laxminarayan et al., 2006). Sharma et al. (2010a, 2010b) indicated that the direct effects of live mulching on maize might be less pronounced but the residual effects on the following crops are larger due to enhanced moisture content and nutrient supply. The increase in the soil available N in both the depth might be ascribed to the addition of mineral N that may decrease the C: N ratio of organic mulches. The enhanced conservation of moisture in the soil profile due to mulching results in greater available N (Sharma et al., 2010a, 2010b). Further, earlier studies indicated that legumes increase soil N either because of fixed N or sparing effect since their demand for N is less than cereals (<https://www.ncbi.nlm.nih.gov/pmc/articles/PMC6561941/-CR23>(Peoples et al., 2013).

The higher available P under maize-black gram system than that under other systems was attributed to growing of leguminous crops like black gram or French bean that increased SOC content and in turn improved the soil available P (Roldan et al., 2003). Available P was higher in the surface soil layer where there was high content of SOC which helps to convert immobile P into labile P.

Addition of OM on decomposition of mulching materials and favorable microclimate due to mulching promotes soil microbial activities (Yang et al., 2003). The higher available P under mulching could be ascribed to reduction in the fixation of water soluble P (Sinkevicienė et al., 2009) and increased mineralization of organic P due to microbial action (Ni, Song, Zhang, Yang, & Wang, 2016) and thus, enhanced availability of P.

Higher available K in soil under diverse mulching treatments might be due to high amount of biomass maintained at the surface as mulching material, comprising both maize stover and WHP/RW mulch. This increase in soil available K under soil moisture conservation measures could be attributed to decomposition of mulching material and subsequent addition of K in the soil (Mina et al., 2008; Prasad et al., 2010).

4.6. Soil biological activities

Cropping sequence influences soil biological activities through kind and quantity of crop residue food source the system provide and their impact on soil physico-chemical properties (Liebig et al., 2006). Higher DHA under French bean and black gram systems might be due to their leguminous nature and subsequent improvement in soil properties which favors soil microbial activities (Roldan et al., 2003). The higher DHA under MSM + WHP

mulch may be due to decomposition of maize stover and weed biomass where residues of maize had higher C:N ratio which remained in surface for longer duration leading to moisture conservation and WHP being a legume had lower C:N ratio and easily decomposed by microbes (Abera et al., 2013). Mina et al. (2008) also reported that higher organic matter due to residue addition and increased carbohydrate content acted as an energy sources for microbes and resulted in increase of DHA.

Improvement in soil biological activities like SMBC due to inclusion of leguminous crops in cropping system (Patel et al., 2015) and adoption of NT with residue retention (Saha et al., 2009) has been indicated by earlier researchers. Adoption of NT and surface accumulation of crop residues offers the best opportunity to sequester SOC and increase soil microbial biomass (Salinas-Garcia et al., 2002). The increase in SMBC and soil respiration can be attributed to the incorporation of easily degradable mulch material which stimulates microbial activity (Tejada & Gonzalez, 2006).

4.7. Crop productivity

The higher seed yield of crops under combined use of maize stover mulch and RW/WHP is attributed to enhancement in SMC and SMS as well as nutrient supplying capacity of the soil (Campbell & Zentner, 1997), which in turn improved seed yield (Das et al., 2017). Crop residues recycle nutrients upon decomposition which improve soil physico-chemical and biological properties and enhance growth and yield parameters of dry season crops (Das et al., 2017). Increase in seed yield under *in-situ* MSM + WHP mulch was attributed to addition of some nutrients after the decomposition of the leguminous WHP which decomposes within 45 days after the application (Kuotsu et al., 2014). The *in-situ* retention of previous maize crops residues and addition of RW/HHP mulch under NT systems reduce moisture loss and improves soil hydrological environment which enable better crop growth and productivity (Saha & Ghosh, 2010).

The retention of maize stover and WHP/RW mulch enhances nutrient availability (Liu et al., 2002), conserves water in the root zone; increases root proliferation, and crop yield (Das et al., 2017). Equivalent yield is an indicator to assess the capacity of the system to outperform the existing system on a time scale. The higher MEY under maize-French bean (PT) system and *in-situ* MSM + WHP may be attributed to higher seed yield and its higher market price relative to other crops.

4.8. Land use efficiency and production efficiency

Different maize based cropping system enhanced LUE by 70–92% relative to maize-fallow system. Higher LUE with black gram and rapeseed than that of French bean may be attributed to longer duration of black gram and rapeseed than French bean and thus, to an efficient utilization of land resources. The higher LUE indicates that mulch farming can prolong the cropping duration of a land within a calendar year. The PE of a system is influenced by the growing duration over which the land is occupied for a specific cropping sequence (Das et al., 2008) and the productivity of the component crops in the system. Relatively shorter duration of black gram and French bean along with reasonably good productivity led to the higher PE than other sequences.

5. Conclusions

The study proven the hypothesis that residue mulching improve soil properties, conserve residual soil moisture and enhance crop and water productivity of maize based systems. The data presented herein supports the following conclusions:

- Maize-French bean (pole type)/black gram systems had higher SOC content and stocks, available N, P and K, SMBC and DHA than those of other systems
- Maize-French bean (pole type) cropping system produced maximum MEY.
- Double mulching technology comprising *in-situ* MSM along with WHP or RW mulch helped to improve soil properties, SOC stocks, conserved soil moisture and increased productivity.
- The WUE was the highest in maize-black gram under *in-situ* MSM + WHP mulch followed by that under *in-situ* MSM + RW mulch. However, WP was the highest in maize-rapeseed cropping system under *in-situ* MSM + WHP mulch.
- The WP was significantly higher for the *in-situ* MSM + WHP, which was at par with the *in-situ* MSM + RW but was higher than those under *in-situ* MSM or no mulch treatments.

Thus, double mulching comprising *in-situ* retention of maize stover along with RW mulch (considering its plentiful availability) is a recommendable option for conserving soil moisture and enhancing soil and crop productivity and SOC stocks in maize-based sequences under rainfed hill ecosystem of Eastern Himalayas, India and other similar agro-ecoregions.

Declaration of competing interest

Declare that authors doesn't have any conflict of interests.

Acknowledgement

The authors are thankful to the Director, ICAR Research Complex for NEH region, Umiam, Meghalaya and Dean, College of Post Graduate Studies, Central Agricultural University, Umiam, Meghalaya, India for providing various supports in conducting the research.

References

- Abera, G., Wolde-meskel, E., & Bakken, L. R. (2013). Effect of organic residue amendments and soil moisture on N mineralization, maize (*Zea mays* L.) dry biomass and nutrient concentration. *Archives of Agronomy and Soil Science*, 59(9), 1263–1277. <https://doi.org/10.1080/03650340.2012.722623>
- Acharya, C. L., Bisnoi, S. K., & Yaduvanshi, H. S. (1988). Effect of long-term application of fertilizers and organic and inorganic amendments under continuous cropping on soil physical and chemical properties in an Alfisol. *Indian Journal of Agricultural Sciences*, 58, 509–516.
- Acosta-Martinez, V., Rowland, D., Sorensen, R. B., & Yeater, K. M. (2008). Microbial community structure and functionality under peanut-based cropping systems in a sandy soil. *Biology and Fertility of Soils*, 44, 681–692.
- Adiku, S. G. K., Narh, S., Jones, J. W., Laryea, K. B., & Bowuona, G. N. (2008). Short term effect of crop rotation, residue management and soil water on carbon mineralization in a tropical cropping systems. *Plant Science*, 311, 29–38.
- Babu, S., Mohapatra, K. P., Das, A., Yadav, G. S., Tahasildar, M., Singh, R., Panwar, A. S., Yadav, V., & Chandra, P. (2020). Designing energy-efficient, economically sustainable and environmentally safe cropping system for the rainfed maize–fallow land of the Eastern Himalayas. *The Science of the Total Environment*, 722, 137874. <https://doi.org/10.1016/j.scitotenv.2020.137874>
- Balasubramanian, P., & Palaniappan, S. P. (2007). *Principles of Agronomy* (pp. 268–270). Agrobios India.
- Bhagat, R. M., & Verma, T. S. (1991). Impact of rice straw management on soil physical properties and wheat yield. *Soil Science*, 152, 108–115.
- Blake, G. R., & Hartge, K. H. (1986). Bulk density. In A. Klute (Ed.), *Methods of soil analysis, Part 1, ASA monograph No. 9* (pp. 363–376). Madison).
- Brookes, P. C., & Joergensen, R. G. (2006). Microbial biomass measurements by fumigation extractant. In J. Bloem, D. W. Hopkins, & A. Benedetti (Eds.), *Microbiological methods for assessing soil quality* (pp. 77–83). Oxfordshire, UK: CABI publishing.
- Campbell, C. A., & Zentner, R. P. (1997). Crop production and soil organic matter in long-term crop rotations in the semi-arid northern Great Plains of Canada. In E. A. Paul, E. T. Elliott, K. Paustian, & C. V. Cole (Eds.), *Soil organic matter in temperate agroecosystems* (Vols. 317–334). Boca Raton, FL: CRC Press.
- Casida, L. E., Jr., Klein, D. A., & Sautoro, T. (1964). Soil dehydrogenase activity. *Soil Science*, 98, 371–376.
- Das, A., Ghosh, P. K., Lal, R., Saha, R., & Ngachan, S. V. (2017). Soil quality effect of

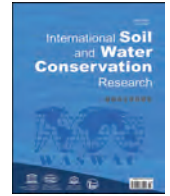
- conservation practices in maize – rapeseed cropping system in eastern Himalaya. *Land Degradation & Development*, 28, 1862–1874. <https://doi.org/10.1002/ldr.2325>
- Das, A., Ghosh, P. K., Verma, M. R., Munda, G. C., Ngachan, S. V., & Mandal, D. (2015). Tillage and residue mulching effect on productivity of maize (*Zea mays*) – toria (*Brassica campestris*) cropping system in fragile Ecosystem of northeast Indian Himalayas. *Experimental Agriculture*, 51(1), 107–125.
- Das, A., Layek, J., Ramkrushna, G. I., Basavaraj, S., Lal, R., Krishnappa, R., Yadav, G. S., & Babu, S. (2020). Conservation tillage and residue management improves soil properties under upland rice–rapeseed system in subtropical eastern Himalayas. *Land Degradation & Development*. <https://doi.org/10.1002/ldr.3568>
- Das, A., Lyngdoh, D., Ghosh, P. K., Lal, R., Layek, J., & Ramkrushna, G. I. (2018). Tillage and cropping sequence effect on physico-chemical and biological properties of soil in Eastern Himalayas, India. *Soil Till Research*, 180, 182–193.
- Das, A., Patel, D. P., Munda, G. C., & Ghosh, P. K. (2010). Effect of organic and inorganic sources of nutrients on yield, nutrient uptake and soil fertility of maize (*Zea mays*)—mustard (*Brassica campestris*) cropping system. *Indian Journal of Agricultural Sciences*, 80(1), 85–88.
- Das, A., Patel, D. P., Munda, G. C., Hazarika, U. K., & Bordoloi, J. (2008). Nutrient recycling potential in rice – vegetable cropping sequences under in-situ residue management at mid-altitude subtropical Meghalaya. *Nutrient cycle Agro-Ecosyst*, 82(3), 251–258.
- Ghosh, P. K., Das, A., Saha, R., Kharkrang, E., Tripathi, A. K., Munda, G. C., & Ngachan, S. V. (2010). Conservation agriculture towards achieving food security in North East India. *Current Science*, 99(7), 915–921.
- Gomez, K. A., & Gomez, A. A. (1984). *Statistical procedures for Agricultural research* (2nd ed.). New York: Int. Rice Res Inst Los Banos Philippines. John Willy and Sons.
- Gupta, J. P., & Gupta, G. K. (1986). Effect of tillage and mulching on soil environment and cowpea seedling growth under arid conditions. *Soil Till Research*, 7, 233–240.
- Hashim, M. A. A., Siam, N., Al-Dosari, A., Asl-Gaadi, K. A., Patil, V. C., Tola, E. H. M., Rangaswamy, M., & Samdani, M. S. (2012). Determination of water requirement and crop water productivity of crops grown in the Makkah region of Saudi Arabia. *Australia Journal of Basic Application Science*, 6(9), 196–206.
- Jalota, S. K., Khera, R., & Ghuma, B. S. (1998). *Method in soil physics*. New Delhi: Narosa publishing House.
- Jat, H. S., Meena, L. R., Roopchand, C. S., & Sharma, S. C. (2011). Relatively efficiency of different cropping sequences in a farmers participatory research in semi-arid agro-ecosystem of Rajasthan. *Indian Journal of Agronomy*, 56(4), 321–327.
- Kalra, Y. P. (1995). Determination of pH of soils by different methods: Collaborative study. *JAOAC International*, 78, 310–321.
- Khaleel, R., Reddy, K. R., & Overcash, M. R. (1981). Changes in soil physical properties due to organic waste application, a review. *Journal of Environmental Quality*, 10, 133–141.
- Khurshid, K., Iqbal, M., Arif, S., & Nawaz, A. (2006). Effect of tillage and mulch on soil physical properties and growth of maize. *International Journal of Agriculture and Biology*, 8, 593–596.
- Knudsen, D., Peterson, G. A., & Pratt, P. F. (1982). Lithium, sodium, and potassium. In A. L. Page, R. H. Miller, & D. R. Keeney (Eds.), *Methods of soil analysis, part 2: Chemical and microbiological properties*. Wisconsin, USA: American Society of Agronomy.
- Kuotsu, K., Das, A., Lal, R., Munda, G. C., Ghosh, P. K., & Ngachan, S. V. (2014). Land forming and tillage effects on soil properties and productivity of rainfed groundnut (*Arachis hypogaea* L.) – rapeseed (*Brassica campestris* L.) cropping system in North eastern India. *Soil Till Research*, 142, 15–24.
- Ladha, J. K., Rao, A. N., Raman, A. K., Padre, A. T., Dobermann, A., Gathala, M., Kumar, V., Saharawat, Y., Sharma, S., Piepho, H. P., & Alam, M. M. (2016). Agronomic improvements can make future cereal systems in South Asia far more productive and result in a lower environmental footprint. *Global Change Biology*, 22(3), 1054–1074.
- Lal, R. (2015). Sequestering carbon and increasing productivity by conservation agriculture. *Journal of Soil and Water Conservation*, 70(3), 55A–62A.
- Lal, R. (2018). Digging deeper: A holistic perspective of factors affecting soil organic carbon sequestration in agroecosystems. *Global Change Biology*, 24(8), 3285–3301.
- Laxminarayana, K., Bhatt, B. P., & Rai, T. (2006). Soil fertility build up through hedgerow intercropping in integrated farming system: A case study. In B. P. Bhatt, & K. M. Bujarbaruah (Eds.), *Agroforestry in north east India: Opportunities and challenges* (pp. 479–490). Umiam, Meghalaya, India: ICAR Research Complex for NEH Region.
- Liebig, M., Carpenter-Boggs, L., Johnson, J. M. F., Wright, S., & Barbour, N. (2006). Cropping system effects on soil biological characteristics in the Great Plains. *Renewable Agriculture and Food Systems*, 21(1), 36–48.
- Liu, J., Xu, S. A., Zhou, G. Y., & Lu, H. H. (2002). Effects of transplanting multi-cropping spring maize with plastic film mulching on the ecological effect, plant growth and grain yield. *Journal of Hubei Agriculture Coll*, 2, 100–102.
- Meena, J. R., Behera, U. K., & Chakraborty, D. (2015). Tillage and residue management effect on soil properties, crop performance and energy relations in green gram (*Vigna radiata* L.) under maize-based cropping systems. *International Soil and Water Conservation Research*, 3(4), 261–272.
- Mina, B. L., Saha, S., Kumar, N., Srivastava, A. K., & Gupta, H. S. (2008). Changes in soil nutrient content and enzymatic activity under conventional and zero tillage practice in an Indian sandy clay loam soil. *Nutrient Cycling in Agroecosystems*, 82, 273–381.
- Nath, C. P., Hazra, K. K., Kumar, N., Praharaj, C. S., Singh, S. S., Singh, U., & Singh, N. P. (2019). Including grain legume in rice–wheat cropping system improves soil organic carbon pools over time. *Ecological Engineering*, 129, 144–153.
- Nelson, D. W., & Sommers, L. E. (2005). Total carbon, organic carbon and Organic Matter. In D. L. Sparks (Ed.), *Analysis of soil and plants chemical methods*. SSSA book series: 5 soil science society of America in. USA: American Society of Agronomy, Inc. Wisconsin.
- Ni, X., Song, W., Zhang, H., Yang, X., & Wang, L. (2016). Effects of mulching on soil properties and growth of tea olive (*Osmanthus fragrans*). *PLoS One*, 11(8), Article e0158228. <https://doi.org/10.1371/journal.pone.0158228>
- Obalum, S. E., Igwe, C. A., & Obi, M. E. (2010). Moisture dynamics in selected layers of a coarse-textured mineral soil as induced by tillage-mulch practices under sorghum and soybean at Nsukka, Southern Nigeria. *Research Journal of Soil and Water Management*, 1(2), 45–60.
- Olsen, S. R., & Sommers, L. E. (1982). Phosphorus. In A. L. Page, R. H. Miller, & D. R. Keeney (Eds.), *Methods of soil analysis, Part 2: Chemical and microbiological properties Agronomy monograph 9*. Madison, Wisconsin, USA: ASA and SSSA.
- Patel, D. P., Das, A., Kumar, M., Munda, G. C., Ngachan, S. V., Ramkrushna, G. I., Layek, J., pongla, N., Buragohain, J., & Somireddy, U. (2015). Continuous application of organic amendments enhance soil health, produce quality and system productivity of vegetable based cropping systems at subtropical eastern Himalayas. *Experimental Agriculture*, 51(1), 85–106. <https://doi.org/10.1017/S0014479714000167>
- Peoples, M. B., Brockwell, J., Hunt, J. R., Swan, A. D., Watson, L., Hayes, R. C., Li, G. D., Hackney, B., Nuttall, J. G., Davies, S. L., & Fillery, I. R. P. (2013). Factors affecting the potential contributions of N 2 fixation by legumes in Australian pasture systems. *Crop & Pasture Science*, 63, 759–786.
- Pervaiz, M. A., Iqbal, M., Shahzad, K., & Hussain, A.-U. I. (2009). Effect of mulch on soil physical properties and N P K concentration in maize (*Zea mays*) shoots under two tillage system. *International Journal of Agriculture and Biology*, 11(2), 119–124.
- Prasad, R. K., Kumar, V., Prasad, B., & Singh, A. P. (2010). Long term effect of crop residue and Zn fertilizer on crop yield uptake and fertility build up under rice-wheat in Calciorthents. *Journal of the Indian Society of Soil Science*, 58(2), 205–211.
- Pratap, T. (2011). Hill agriculture: Challenges and opportunities. *Indian Journal of Agril Economics*, 66(1), 33–52.
- Rakshit, S., Chikkappa, K. G., Jat, S. L., Dhillon, B. S., & Singh, N. N. (2017). Scaling-up of proven technology for maize improvement through participatory approach in India. In P. R. Pandey, & K. B. Koirala (Eds.), *Best practices of maize production technology in South Asia* (pp. 36–60). Dhaka: SAARC Agriculture Centre.
- Ramesh, T., Bolan, N. S., Kirkham, M. B., Wijesekara, H., Kanchikerimath, M., SrinivasaRao, C., Sandeep, S., Rinklebe, J., SikOk, Y., Choudhury, B. U., Wang, H., Tang, C., Wang, X., Song, Z., & Freeman, O. W., II (2019). Soil organic carbon dynamics: Impact of land use changes and management practices: A review. *Advances in Agronomy*, 156, 1–107.
- Rathore, A. L., Pal, A. R., & Sahu, K. K. (1998). Tillage and mulching effects on water use, root growth and yield of rainfed mustard and chickpea grown after lowland rice. *Journal of the Science of Food and Agriculture*, 78, 149–161.
- Roldan, A., Caravaca, F., Hernandez, M. T., Garcia, C., Sanchez-Breto, C., Velasquez, M., & Tiscareno, M. (2003). No tillage, crop residue additions and legumes cover cropping effect on soil quality Characteristic under maize in Patzcuara watershed (Mexico). *Soil Till Research*, 72, 65–73.
- Saha, R., & Ghosh, P. K. (2010). Effect of land configuration on water economy, crop yield and profitability under rice (*Oryza sativa*) -based cropping systems in north-east India. *Indian Journal of Agricultural Sciences*, 80(1), 16–20.
- Saha, R., Ghosh, P. K., & Das, A. (2009). Soil water dynamics and yield as influenced by residue and tillage management in maize (*Zea mays*) - mustard (*Brassica campestris*) cropping system. *Indian Journal of Agricultural Sciences*, 79(5), 340–345.
- Salau, O. A., Opara-Nadi, O. A., & Swennen, R. (1992). Effects of mulching on soil properties, growth and yield of plantain on a tropical ultisol in southeastern Nigeria. *Soil Research*, 23, 73–93, 73.
- Salinas-García, J. R., Velazquez-García, J.dej., Gallardo-Valdez, M., Díaz-Mederos, P., Caballero-Hernández, F., Tapia-Vargas, L. M., & Rosales-Robles, E. (2002). Tillage effects on microbial biomass and nutrient distribution in soils under rain-fed corn production in central western, Mexico. *Soil Till Research*, 66(2), 143–152.
- Sarkar, D., Meitei, C. B., Das, A., Ghosh, P. K., & Mandal, B. (2017). Changes in soil organic carbon pools in a long-term trial with perennial fodder crops in acid soils of northeast India. *Grass and Forage Science*. <https://doi.org/10.1111/gfs.12311>
- Sarkar, S., & Singh, S. R. (2007). Interactive effect of tillage depth and mulch on soil temperature, productivity and water use pattern of rainfed barley (*Hordium vulgare* L.). *Soil Till Research*, 92(1–2), 79–86.
- Sharma, P. K., & Acharya, C. L. (2000). Carry-over effect of residual soil moisture with mulching and conservation tillage practices for sowing of rainfed wheat (*Triticum aestivum* L.) in north-west India. *Soil Till Research*, 57, 43–52.
- Sharma, A. R., Singh, R., Dhyani, S. K., & Dube, R. K. (2010a). Moisture conservation and nitrogen recycling through legume mulching in rainfed maize (*Zea mays*)–wheat (*Triticum aestivum*) cropping system. *Nutrient Cycling in Agroecosystems*, 87, 187–197.
- Sharma, A. R., Singh, R., Dhyani, S. K., & Dube, R. K. (2010b). Effect of live mulching with annual legumes on performance of maize (*Zea mays*) and residual effect on following wheat (*Triticum aestivum*). *Indian Journal of Agronomy*, 55(3), 177–184.

- Shrestha, G., Subedi, M., & Bhatt, a G. D. (2008). Sustainability of maize based cropping pattern in the mid-hills of Nepal. In *Conference on international Research on food security, natural resource management and rural development, tropentag 2008*. University of Hohenheim. October 7-9, 2008 file:///C:/Users/user/Downloads/Sustainability_of_Maize_Based_Cropping_Pattern_in_.pdf. (Accessed 9 January 2020).
- Sinkevičienė, A., Jodaugienė, D., Pupalienė, R., & Urbonienė, M. (2009). The influence of organic mulches on soil properties and crop yield. *Agronomy Research*, 7(Special issue 1), 485–491.
- Sombrero, A., & de Benito, A. (2010). Carbon accumulation in soil. Ten-year study of conservation tillage and crop rotation in a semi-arid area of Castile-Leon, Spain. *Soil Till Research*, 107, 64–70.
- Srinivasarao, C., Venkateswarlu, B., Lal, R., Singh, A. K., Kundu, S., Vittal, K. P. R., Balaguravaiah, G., Vijay, M., Babu, S., Chary, G. R., Prasadbabu, M. B. B., & Reddy, T. Y. (2012). Soil carbon sequestration and agronomic productivity of an Alfisol for a groundnut-based system in a semiarid environment in southern India. *European Journal of Agronomy*, 43, 40–48.
- Subbiah, B. V., & Asija, G. L. (1956). A rapid procedure for determination of available nitrogen in soils. *Current Science*, 25, 259–260.
- Tejada, M., & Gonzalez, J. L. (2006). Crushed cotton gin compost on soil biological properties and rice yield. *European Journal of Agronomy*, 25, 22–29.
- Timsina, J. (2018). Can organic sources of nutrients increase crop yields to meet global food demand? *Agron*, 8, 214. <https://doi.org/10.3390/agronomy810021>
- Tiwari, V. N., Tiwari, K. N., & Upadhyay, R. M. (2000). Effect of crop residue and biogas slurry incorporation in wheat on yield and soil fertility. *Journal of the Indian Society of Soil Science*, 48, 515–520.
- Tomar, S. S., & Tiwari, A. S. (1990). Production potential and economics of different crop sequences. *Indian Journal of Agronomy*, 35(1, 2), 30–35.
- Unyayar, S., Keles, Y., & Unal, E. (2004). Proline and ABA levels in two sunflower genotypes subjected to water stress. *Bulgarian Journal of Plant Physiology*, 30(3–4), 34–47.
- Vance, E. D., Brookes, P. C., & Jenkinson, D. S. (1987). Microbial biomass measurements in forest soils: The use of the chloroform fumigation incubation method in strongly arid soils. *Soil Biology and Biochemistry*, 19, 697–702.
- Wang, X. (2006). *Conservation tillage and nutrient management in dryland farming in China*. Doctorate thesis. The Netherlands, English and Dutch summaries: Wageningen University.
- Weatherly, P. E. (1950). Studies on water relation of the cotton plant I the field measurement of water deficit in leaves. *New Physiology*, 49, 91–97.
- Xu, Q. X., Wang, T. W., Cai, C. F., Li, Z. X., & Shi, H. (2012). Effects of soil conservation on soil properties of citrus orchards in the Three Gorges Area, China. *Land Degradation & Development*, 23(1), 34–42.
- Yadav, G. S., Das, A., Lal, R., Babu, S., Datta, M., Meena, R. S., Patil, S. B., & Singh, R. (2019). Impact of no-till and mulching on soil carbon sequestration under rice (*Oryza sativa* L.)-rapeseed (*Brassica campestris* L. var. rapeseed) cropping system in hilly agro-ecosystem of the Eastern Himalayas, India. *Agriculture, Ecosystems & Environment*, 275, 81–92.
- Yang, Y. J., Dungan, R. S., Ibekwe, A. M., Valenzuela-Solano, C., Crohn, D. M., & Crowley, D. E. (2003). Effect of organic mulches on soil bacterial communities one year after application. *Biology and Fertility of Soils*, 38(5), 273–281.
- Yousefi, M., Hajabbasi, M., & Shariatmadari, H. (2008). Cropping system effects on carbohydrate content and water-stable aggregates in a calcareous soil of Central Iran. *Soil Till Research*, 101, 57–61.
- Zheng, H., Liu, W., Zheng, J., Luo, Y., Li, R., Wang, H., & Qi, H. (2018). Effect of long-term tillage on soil aggregates and aggregate-associated carbon in black soil of Northeast China. *PLoS One*, 13(6), Article e0199523. <https://doi.org/10.1371/journal.pone.0199523>
- Zingore, S. (2011). Maize productivity and response to fertilizer use as affected by soil fertility variability, manure application, and cropping system. *Better Crops*, 95(1), 4–6.



Contents lists available at ScienceDirect

International Soil and Water Conservation Research

journal homepage: www.elsevier.com/locate/iswcr

Original Research Article

Unsupervised learning approach in defining the similarity of catchments: Hydrological response unit based *k-means* clustering, a demonstration on Western Black Sea Region of Turkey



Ersin Aytaç

Zonguldak Bülent Ecevit University, Department of Environmental Engineering, 67100, Zonguldak, Turkey

ARTICLE INFO

Article history:

Received 17 March 2020

Received in revised form

11 May 2020

Accepted 11 May 2020

Available online 14 May 2020

Keywords:

HRU

K-means clustering

Multidimensional scaling

Orange

Silhouette score

QSWAT+

ABSTRACT

This study investigated the similarity of the catchments with the *k-means* clustering method by using the hydrological response unit (HRU) images of 33 catchments located in the Western Black Sea Region of Turkey. HRUs are the unit cells in hydrological models and these units are important because the same HRUs have the same hydrological behavior regarding weather inputs and water runoff. Catchments that reside inside a cluster will have high hydrological similarity, the catchments of two separate clusters would be dissimilar to each other. With the help of the clustered catchments, an elimination process can be conducted that can save time and effort in basin selection for future hydrological studies. In the study, the basic process sequence was carried out in 5 steps. These steps were creating HRUs, assigning a color to HRUs, creating HRU images, image embedding, and *k-means* clustering respectively. Silhouette and multidimensional scaling plots were sketched to visually examine the quality of intra-cluster distributions. Considering the silhouette score values, the optimum number of clusters was determined as 8, and the clustered catchments were illustrated on the study area.

© 2020 International Research and Training Center on Erosion and Sedimentation and China Water and Power Press. Production and Hosting by Elsevier B.V. This is an open access article under the CC BY-NC-ND license (<http://creativecommons.org/licenses/by-nc-nd/4.0/>).

1. Introduction

The past decade witnessed the excessive use of machine learning (ML) in many areas (Lee, Yoo, Kim, Lee, & Hong, 2019). ML attempts to extract patterns from large datasets, commonly in the form of an algorithm and tries to predict an outcome (Doupe, Faghmous, & Basu, 2019). The commonly used learning methods are supervised and unsupervised approaches. Supervised learning algorithms can be neural networks, support vector machines and logistic regression (Ramos-Lima, Waikamp, Antonelli-Salgado, Passos, & Freitas, 2020). Some unsupervised methods are t-SNE, hierarchical clustering and *k-means* clustering. Cluster analysis aims to group similar objects into different clusters and can be used for identifying patterns to provide foresight about the basic structure of data (Govender & Sivakumar, 2020). Clustering methods are divided into two groups, flat (non-hierarchical) clustering and hierarchical clustering (Jafarzadegan, Safi-Esfahani, & Beheshti, 2019). In flat clustering, the similarity between a pair of objects is defined by their distance, which can be measured like Euclidean

distance and the partition divides the data into *k* groups (Govender & Sivakumar, 2020). Clustering approaches create distinct groups in which entities from the same group have similar properties, whereas entities from different groups have dissimilar properties. These methods aim to find out patterns in a dataset or to explore the dataset (Kim, Kim, & Cho, 2020; Renjith, Sreekumar, & Jathavedan, 2020). Clustering is not a classification approach, and the most important feature that distinguishes clustering from classification is that the clustering method does not have any pre-determined labeled data (Lipor & Balzano, 2020). The fact that the clustering process does not have any prior knowledge about the data indicates that this method is not suitable for calibration or validation (Khendek & Gotzhein, 2019; Lipor & Balzano, 2020). Clustering emphasizes homogeneity rather than separation (Christian, Marina, Fionn, & Roberto, 2015).

The *k-means* method which is a flat clustering technique is used since the 1950s and stands out as the most common clustering method (Lucke & Forster, 2019; Wang, Chen, Shang, & Wu, 2019). This algorithm clusters the data set into *k* sets and minimizes the sum of the distances between each point and the nearest centroid. The main advantages of this method over other unsupervised

E-mail address: ersin.aytac@beun.edu.tr.

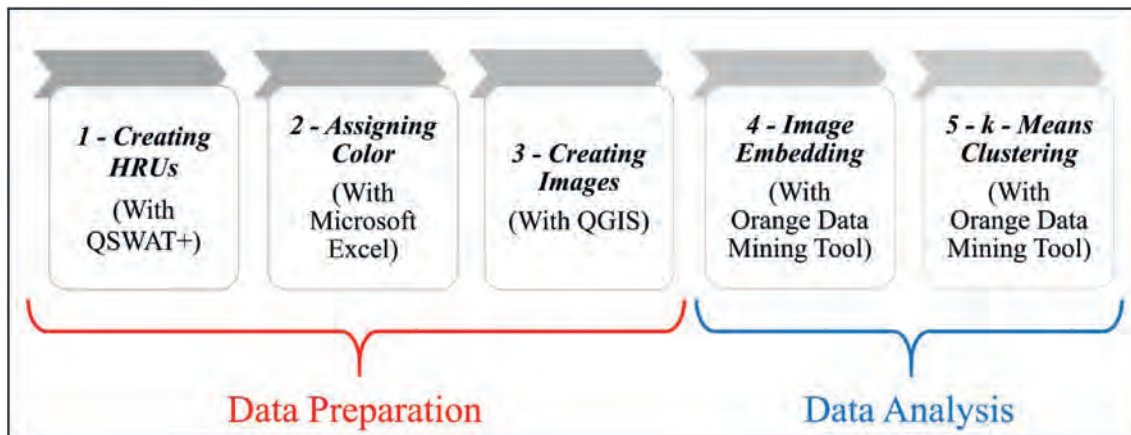


Fig. 1. Basic process sequence.

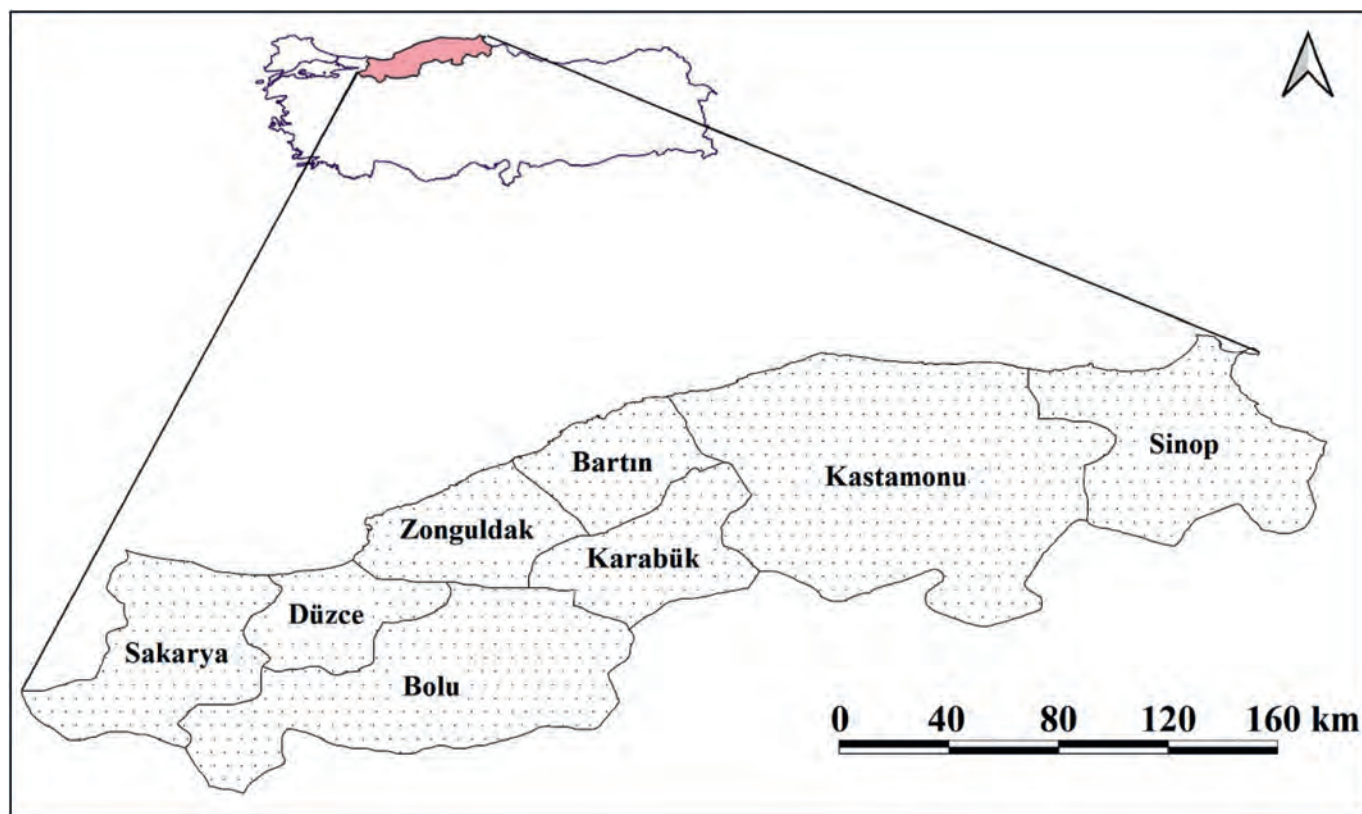


Fig. 2. Study area.

Table 1
Input data for model setup.

Map Type	Description	Source
DEM	30 m resolution, TIFF file format	EROS Archive - Shuttle Radar Topography Mission (SRTM), Downloaded from United States Geological Survey (USGS) Earth Explorer data portal (USGS, 2019).
Land Use/Land Cover map	100 m resolution, TIFF file format	Coordination of Information on the Environment (CORINE) Land Cover (CLC) 2018 map (CORINE, 2019).
Soil map	1 km resolution, TIFF file format	Food and Agricultural Organization (FAO), Harmonized World Soil Database map v 1.2 (FAO, 2019).

clustering methods are low complexity, fast computation, ability to process large data sets, and adjustable cluster membership (Govender & Sivakumar, 2020).

The use of the *k-means* clustering is a common approach in transferring of information from gauged catchments to ungauged ones in hydrology (Tongal & Sivakumar, 2017). Sharghi, Nourani,

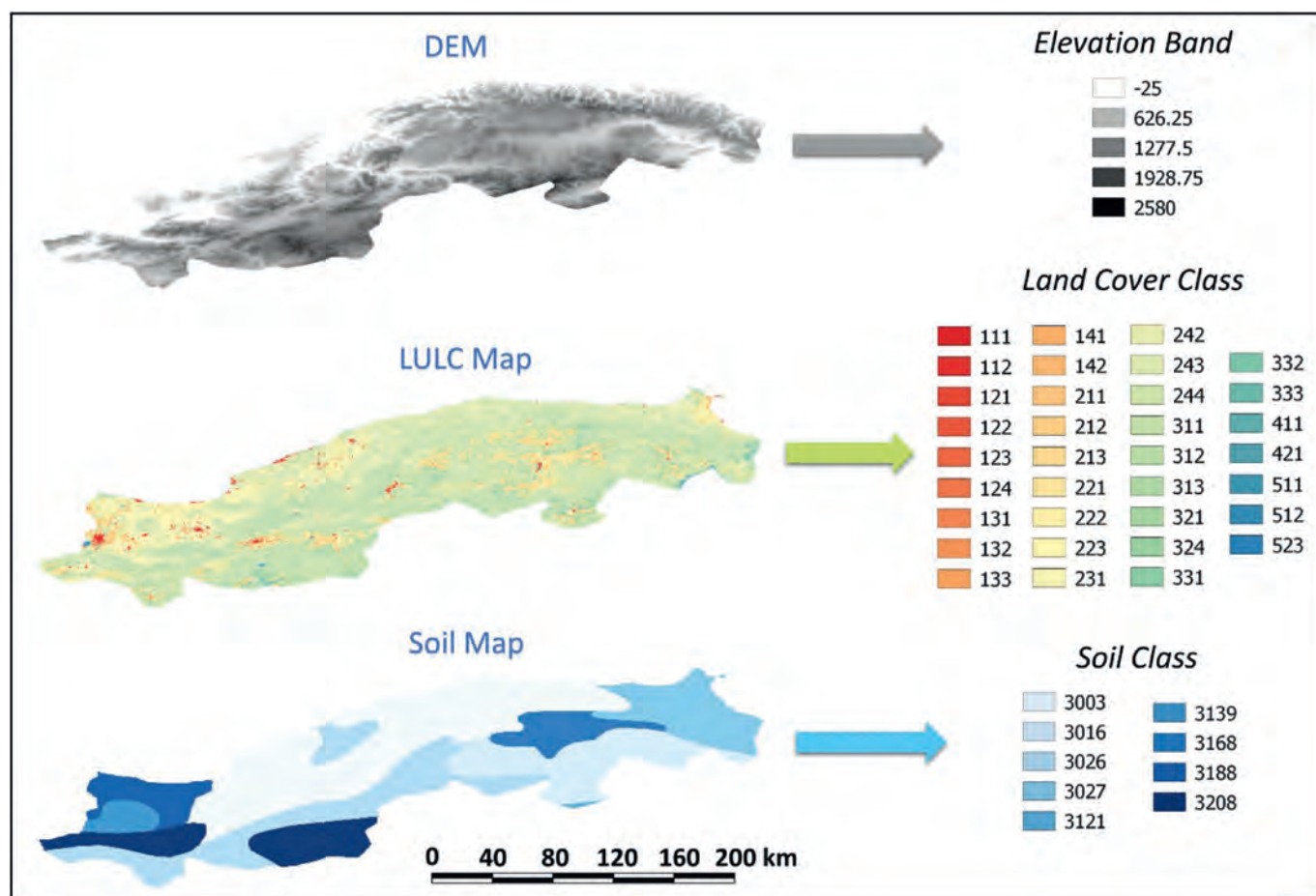


Fig. 3. DEM, LULC and Soil maps of the study area.

Soleimani, and Sadikoglu (2018) used a *k-means* algorithm in hydro-climatological catchment regionalization. Wu, Huang, Xu, and Xi (2015) utilized *k-means* clustering for real-time flood forecasting in basins. Isik and Singh (2008) tried to obtain homogeneous regions and compute streamflow at desired ungauged sites in their study using several approaches that also included the *k-means* method. Li et al. (2018) studied hydrological regionalization based on available hydrological information for runoff prediction. Latt, Wittenberg, and Urban (2015) used *k-means* algorithm to estimate flood for ungauged catchments. Rao and Srinivas (2006) conducted a study for the regionalization of watersheds using hybrid-cluster analysis.

Soil and Water Assessment Tool (SWAT) is a semi-distributed, process-based, continuous basin model that combines both quantity and quality of hydrological processes in a catchment (Arnold, Srinivasan, Muttiah, & Williams, 1998; Gungor & Goncu, 2013). SWAT was used for various agricultural practices, flash flood prediction, to investigate the impacts of climate change to river watershed and predicting nutrient loads in catchments (Arabi, Frankenberger, Enge, & Arnold, 2008; Bauwe, Eckhardt, & Lennartz, 2019; Cerkasova, Umgieser, & Erturk, 2018; Jodar-Abellan, Valdes-Abellan, Pla, & Gomariz-Castillo, 2019). After almost 30 years of use of SWAT, a new generation dubbed as SWAT+ was recently been released with new coding features. SWAT+ was designed as more flexible for users to develop future applications (Yen et al., 2019).

SWAT and also SWAT + primarily creates sub-basins and these sub-basins further divided into Hydrological Response Units

(HRUs) (Lotz, Opp, & He, 2018). HRUs are the smallest units that can be thought of as the cells of the SWAT model (Bhatta, Shrestha, Shrestha, & Talchabhadel, 2019). SWAT + needs a land use/land cover (LULC) map, a soil map and slope values of the terrain to create hydrological response units. A digital elevation model (DEM) is usable to effectuate a terrain slope map (Pai, Saraswat, & Srinivasan, 2012). Then the model combines land cover, soil, and slope of the area to create different types of HRUs (Bhatta et al., 2019).

Hydrological Response Units are elementary units that are characterized by a certain assembly of physical properties of an area (Flugel, 1997). HRUs have unique flow routing, soil and land use properties, and characteristics derived from intersecting polygon layers representing information such as geology, soil type, sub-basins and land use (Sanzana et al., 2013). These small monads are created to reduce the computational units/time in hydrological modeling, to increase the application of modeling in large basins and significantly affect the hydrological processes in a catchment (Khan et al., 2016; Sanzana et al., 2013). HRUs can be developed to reflect fields and other important landscape characteristics. These units are controlling the hydrological dynamics of the landscapes (Flugel, 1995). The same HRUs have the same hydrological behavior regarding weather inputs and water runoff (Ahmed, 2020; Karvonen, Koivusalo, Jauhainen, Palko, & Weppling, 1999). Creating HRUs in a catchment has the following advantages: Simulation of hydrological budget, plant growth, erosion, pesticide dynamics, agricultural management and nutrient cycle can be performed. Water, nutrient, and sediment flow from HRUs to

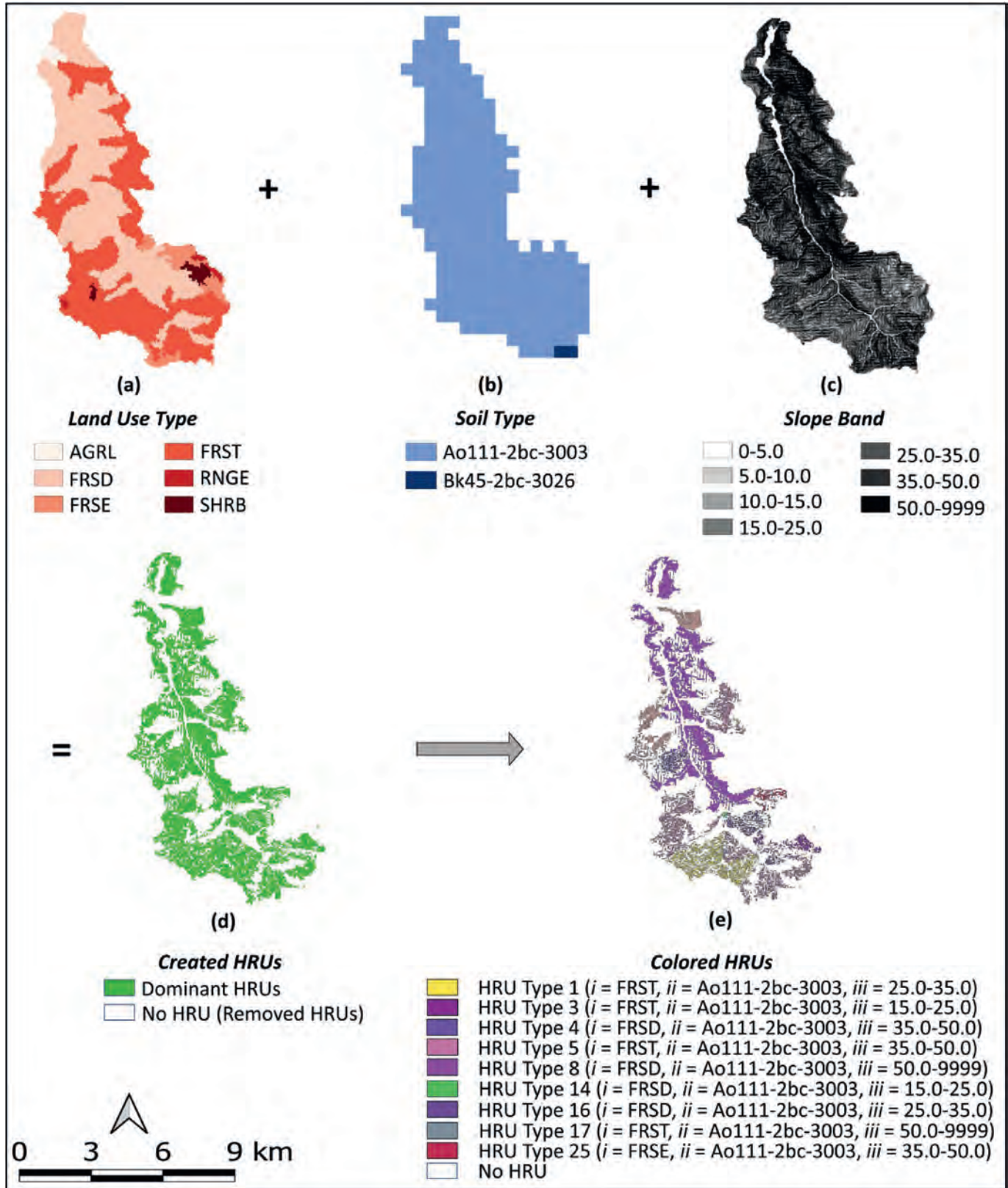


Fig. 4. HRU image creation process of Incebacaklar catchment (a) LULC map, (b) Soil map, (c) Slope Band, (d) Dominant HRUs generated by QSWAT+ and (e) Colored unique HRUs (*i* = Land use type, *ii* = Soil type, *iii* = Slope band).

Table 2
Silhouette scores of different *k* values.

Number of Clusters (<i>k</i>)	Silhouette Score
2	0.117
3	0.139
4	0.137
5	0.148
6	0.163
7	0.154
8	0.168
9	0.161
10	0.122

streams can be controlled daily (Sheshukov, Douglas-Mankin, Sinathamby, & Daggupati, 2016). HRUs represent the geomorphological features of the hydrological processes. HRUs can be used as elementary units to evaluate debris flow risk (Zou, Cui, He, Lei, & Li, 2019). Outputs from HRUs are collected and directed to the sub-basin stream for routing through the stream network to the outlet of the catchments (Aliyari et al., 2019).

This study offers a procedure to define the similarity of catchments depending on their HRU images using image embedding and *k-means* clustering with a demonstration on the Western Black Sea Region of Turkey. The process was carried out in 5 steps as shown in Fig. 1. The first 3 steps are data (image) preparation and the last 2 steps are data analysis. The most important point to consider in this method is that it is not a classification process, and the obtained clusters are not aligned to an order based on the predetermined hydrological properties of the catchments. This method aims to narrow down relations as well as learn novel information from hidden patterns and tries to find whether there is some relationship between the basins.

2. Materials and methods

2.1. Study area

The catchments used in the study are located in the Western Black Sea Region of Turkey between 40° 5' 39" – 42° 5' 13" N, 29° 54' 29" – 35° 29' 13" E coordinates and covers Sakarya, Düzce, Bolu, Zonguldak Bartın, Karabük, Kastamonu and Sinop provinces. The total area of the field is 43,797 km². 33 catchments were created for the study. Names of the catchments were assigned either by the name of the stream in the watershed or by the name of the settlement located in the watershed. The study area can be seen in Fig. 2.

2.2. Data preparation

The data preparation process was carried out with creating HRUs of the catchments, assigning a color to HRUs and generating the images of HRUs respectively. QSWAT+, MS Excel and QGIS software were used in the process.

2.2.1. Creating HRUs

The process was started with QSWAT+ (QGIS interface for SWAT+) model which was only used to delineate HRU's and obtained results were not associated with the model. Soil and Water Assessment Tool was used worldwide to handle complex catchment management (Qi, Zhang, & Cosh, 2019). This model can perform the movement of water, nutrient, sediment, and pesticide by dividing the watershed into sub-basins and further to HRUs (Aliyari et al., 2019). For HRU creation, the model requires a DEM, LULC and soil map. Unique combinations of these maps generate

HRUs (Mengistu, van Rensburg, & Woyessa, 2019). Some information about the input data to set up the model is listed in Table 1 and also the LULC, soil map and DEM of the study area can be seen in Fig. 3.

The creation of HRUs was conducted separately for each catchment and the following were applied to each of them. In the first place, the channel threshold and the stream threshold values were selected as 2 km² and 20 km² respectively and the slope bands were selected as < 5, 5–10, 10–15, 15–25, 25–35, 35–50 and > 50. Then a standard filtering procedure was conducted. Some HRUs that are insignificant (very small and has a minor effect on catchment hydrology) can be removed to simplify the model. QSWAT + either leaves the selection of HRU filtering to the user in which the users can exclude HRUs by their considerations or does the filtering automatically. In hydrological studies carried out with SWAT, users usually worked with a single catchment and a threshold value for HRU filtering was chosen according to the location or the size of the basin and also depending on researcher preference (Azimi et al., 2020; Guo et al., 2019; Himanshu, Pandey, Yadav, & Gupta, 2019; Kling et al., 2014). Since this study covers 33 different catchments with areas ranging between 30.6 – 332.4 km², different threshold values were not applied to each basin. To evaluate all the watersheds in the same dimension, the Dominant HRU option was chosen. Dominant HRU selects the largest of the potential HRUs in each landscape unit and decides this land use, soil and slope range chosen for the whole landscape unit (Dile, Srinivasan, & George, 2018). With this option hydrological properties of the catchments were represented by their dominant HRUs. This filtering process also reduced the combination of land-use type/soil type/slope band (HRU types) by removing insignificant HRU types. Depending on the unique combination of land-use type/soil type/slope band, 33 catchments may have multiple HRUs and HRU types contained within them. Additionally, a comma-separated values (.csv) file of the HRU shapefiles of catchments were exported to be used in the assigning color section.

2.2.2. Assigning color

Since different catchments may contain the same type of HRU, a color assignment was conducted to represent the same HRU types with the same color. For this purpose, an MS Excel macro was coded. The macro first imported.csv files created in section 2.2. Then duplicated combinations of land use type/soil type/slope band were removed. 254 unique combinations were identified in whole catchments after removing the duplicates (which corresponds to 254 unique HRUs). Subsequently, random unique colors were assigned to unique HRU types. Finally, the colorization of 254 HRUs was executed using QGIS rule-based symbology.

2.2.3. Creating images

Image files to be used in image embedding were created with the QGIS print layout option. All HRU images were generated with the same features of 500 × 500 mm in height and width, resolution of 500 dpi, coordinate reference system (CRS) of ESPG: 32636 – WGS 84/UTM zone 36N, the scale of 1/50000 and TIFF file format. The illustration of the HRU image creation process with Incebaçklar catchment example can be seen in Fig. 4.

2.3. Data analysis

Orange (University of Ljubljana, 2019a) data mining tool was used for data analysis. Orange is an open-source machine learning and data mining software that is coded in Python language. The University of Ljubljana, Bioinformatics Laboratory of the Faculty of Computer and Information Science developed the program (Naik & Samant, 2016). It was firstly coded in 1997 by Janez Demšar and

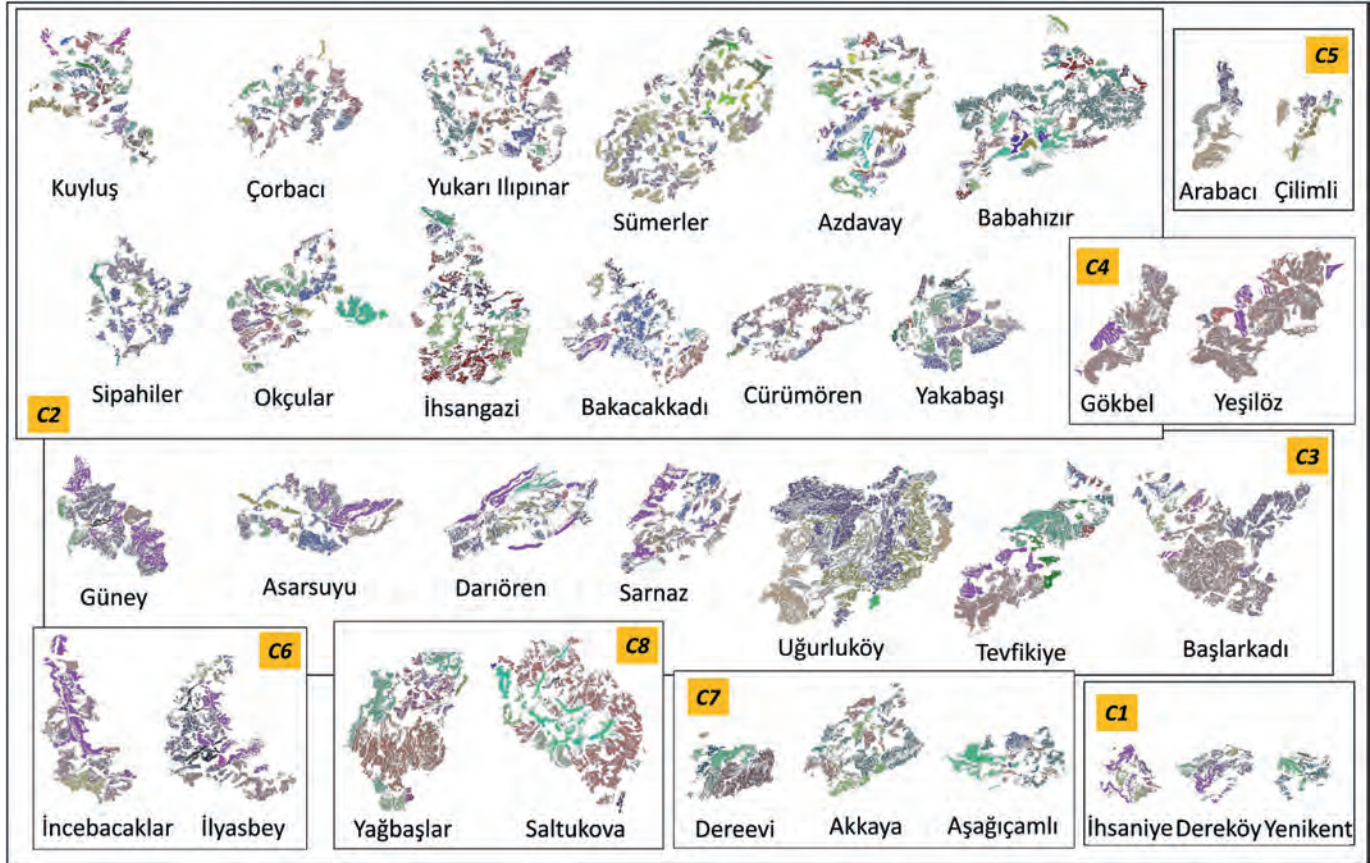


Fig. 5. Clustered HRU images of catchments.

Blaž Zupan. Scientifically Orange was used for implementing new computational approaches in molecular biology and bioinformatics as well as a testing platform for new machine learning algorithms for over 20 years (Demšar & Zupan, 2013). The main branches of the program are data management and preprocessing, classification, regression, association, ensembles, clustering, evaluation and projections (Demšar et al., 2013). This tool has a graphical user interface (visual programming). The graphical user interface is made of widgets. These widgets communicate through channels, and a particular set of connected widgets is called a schema (Demšar, Zupan, Leban, & Curk, 2004). The schema used in this study was for importing images, image embedding, *k-means* clustering, silhouette plot, and multidimensional scaling.

2.3.1. Image embedding

HRU images were imported to Orange canvas with the import images widget. Then the imported images linked to the image embedding widget. Embedded images were analyzed by Google's InceptionV3 image analyzing deep network. In image embedding, images were represented with vectors (Huang, Zhang, Li, Zhao, & He, 2018). The image embedding process can be explained with the Restricted Boltzmann Machine (RBM). By RBM which is a two-layer network, images can be modeled with reduced dimensionality. There are two units of images; the visible units (v) that correspond to the pixels and hidden units (h) that can be recognized by feature detectors. The joint configuration energy of the visible and hidden units can be expressed with Equation (1):

$$E(v, h) = \sum_{i \in \text{pixels}} b_i v_i - \sum_{j \in \text{features}} b_j h_j - \sum_{i, j} v_i h_j w_{ij} \quad (1)$$

where; v_i and h_j are the binary states of pixel i and feature j , b_i and b_j are their biases, and w_{ij} is the weight between them (Hinton & Salakhutdinov, 2006).

A typical image analyzing deep network identifies the curved layers that define the structural properties of images, combines these curved layers and tries to find interactions between them (Godec et al., 2019). InceptionV3 is Google's deep neural network for image recognition. It is trained on the ImageNet data and an image is represented with 2048 features after the embedding process (Godec et al., 2019; University of Ljubljana, 2019b). Some properties of InceptionV3 are, it uses 12 million operations and 42 layers, it has two 3x3 convolution filter size, efficient grid size reduction and it has 1 auxiliary classifier (Jahandad, Kamardin, Amir Sjarif, & Mohamed, 2019). Based on denser networks, InceptionV3 uses much less computation than the best-published results. It is cutting the top-5 (top-1) error by 25% (14%) relative. InceptionV3 uses at least five times fewer parameters and it is six times cheaper (Szegedy, Vanhoucke, Ioffe, Shlens, & Wojna, 2016). The images separated into their vector forms with InceptionV3 were then sent to the *k-means* clustering widget.

2.3.2. K-means clustering, silhouette plot, and multidimensional scaling

HRU images of catchments that were represented with 2048 features in vector form by InceptionV3 clustered with *k-means* clustering widget in Orange. The *k-means* clustering process works

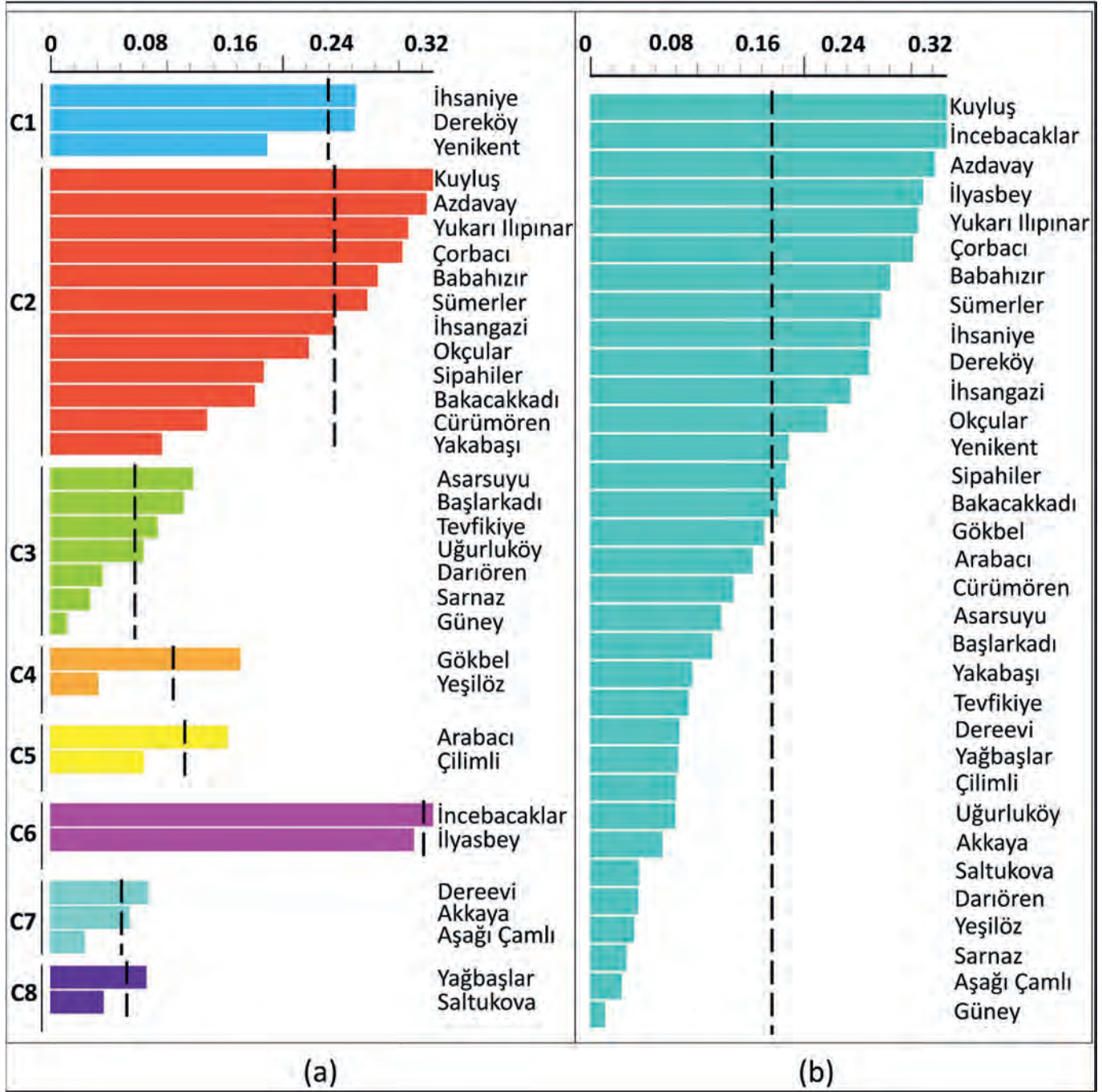


Fig. 6. (a) Silhouette plot by cluster, (b) Silhouette plot for the entire dataset (the average scores are represented by a dashed line).

as follows. In the first step, the researcher selects the number of clusters that he/she wants to identify in the data set. This is the k value in the k -means expression and the selection of k is done arbitrarily. Subsequently, k centroids are distributed randomly into the data set. In the next step, the distance between the first data and centroids are measured. In this study Euclidean distance was used for distance measurement. The Euclidean distance corresponds to the distance between p and q vectors with i dimensions and is calculated by Equation (2):

$$d(p, q) = \sqrt{\sum_{i=1}^i (p_i - q_i)^2} \quad (2)$$

where, p_i and q_i , corresponds the i^{th} dimension of vectors p and q (Mesquita, Gomes, Souza, & Nobre, 2017).

The similarity between the data and the centroid is defined by their distances. Then the first data is assigned to the nearest centroid. The same process is done for the second data and so on and so forth. After all the data is assigned to a centroid, the average

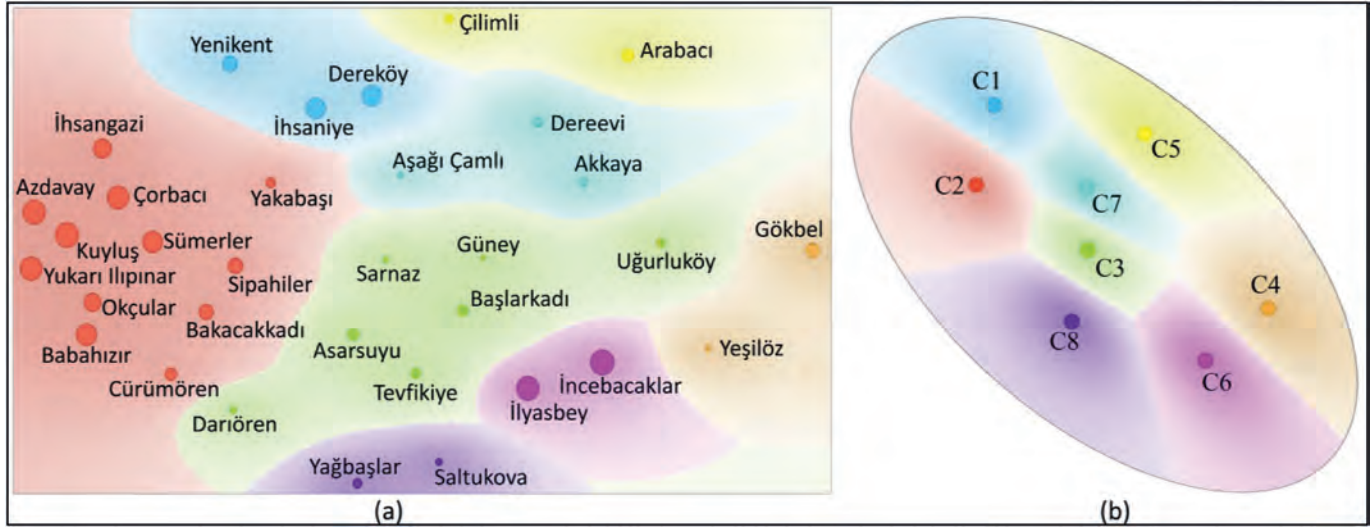


Fig. 7. (a) MDS of clustered catchments and (b) MDS of the cluster centroids.

Table 3
Average intra-cluster silhouette scores.

	Cluster							
	1	2	3	4	5	6	7	8
Average Intra-Cluster Silhouette Score	0.2378	0.2428	0.0723	0.1028	0.1172	0.3250	0.0607	0.0641

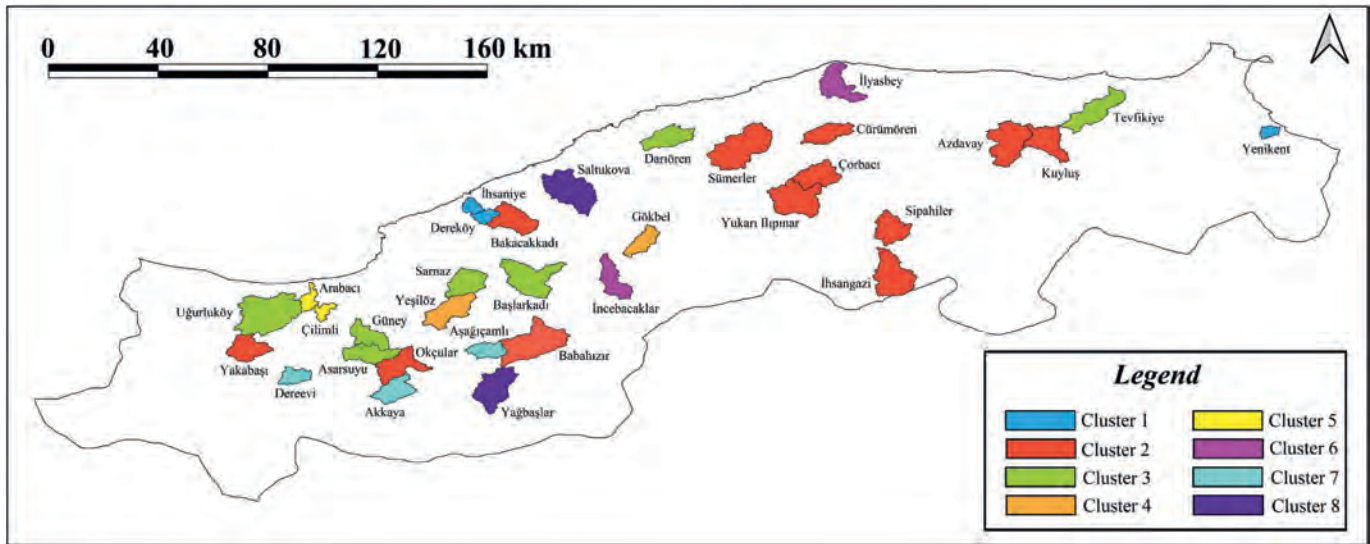


Fig. 8. Clustered catchments on the study area.

of each cluster is calculated. These average values are now new centroids of the clusters, and the assignment of data to new centroids is repeated. This process is continued since the clustering did not change at all during the last iteration (Franti & Sieranoja, 2019; Govender & Sivakumar, 2020). The main purpose of the *k-means* clustering process is to optimize the function in Equation (3):

$$J = \sum_{j=1}^k \sum_{i \in C_j} x_i - c_j^2 \tag{3}$$

where; J criterion function, x_i is the i^{th} observation, c_j is the j^{th} cluster center, C_j is the object set of the j^{th} cluster, k is the number of clusters. The *k-means* belongs to the family of clustering algorithms which requires the desired number of clusters to be determined in advance by the researcher (Govender & Sivakumar, 2020). However, choosing a different number of clusters produces different results, so it is necessary to find the appropriate k value (Tian, Li, Zeng, Evans, & Zhang, 2019). The silhouette score is an important statistical method to evaluate or verify selected k (Anitha & Patil, 2019; Arima, Hakamada, Okamoto, & Hanai, 2008). The silhouette score analyzes the distances of each data point to its cluster and

neighboring clusters (Rousseeuw, 1987). The silhouette score $s(i)$ of a data (x_i) can be calculated as in Equation (4):

$$s(i) = \frac{b(i) - w(i)}{\max\{b(i), w(i)\}} \quad \text{with} \quad b(i) = \min_k \{B(i, k)\} \quad (4)$$

where; $w(i)$ is the average distance from the i^{th} point to the other points in its cluster, and $B(i, k)$ is the average distance from the i^{th} point to points in another cluster k (Lleti, Ortiz, Sarabia, & Sanchez, 2004).

Another form of expression Equation (4) given in Equation (5):

$$s(i) = \begin{cases} 1 - \frac{b(i)}{w(i)} & \text{if } b(i) < w(i) \\ 0 & \text{if } b(i) = w(i) \\ \frac{w(i)}{b(i)} - 1 & \text{if } b(i) > w(i) \end{cases} \quad (5)$$

As can be understood from Equation (5), the silhouette value is in between $-1 \leq s(i) \leq 1$ (Rousseeuw, 1987). The silhouette scores ($\bar{s}(k)$) of each cluster can be calculated using the intra-cluster silhouette values of data instances as in Equation (6):

$$\bar{s}(k) = \frac{\sum_{i=1}^m s(i)}{m} \quad (6)$$

where; m is the number of data in the cluster. The value of $\bar{s}(k)$ varies from -1 to 1 , just like $s(i)$. These values indicate a bad clustering when it is close to -1 , and a perfect clustering is performed if it's close to 1 (Lleti et al., 2004).

For more detailed interpretation of the clusters created depending on the selected k value, silhouette plot and multidimensional scaling (MDS) plot was prepared with Orange. The silhouette plot specifies how similar an object is to its cluster. The silhouette score indicates that the data instance is close to the centroid of its cluster when this value is close to 1 , while a score close to 0 shows that the samples are outliers and a value of -1 indicates that the observations may be assigned to the wrong cluster (Deliu, Sperrin, Belgrave, & Custovic, 2016; University of Ljubljana, 2019c). Multidimensional scaling exposes the similarity of data instances and enables them to observe multidimensional data on spatial maps (Atalay & Yore, 2020; Machado & Mehdi-pour, 2019). The idea behind MDS is to represented similar data with close points. Suppose we have a data set with N data instances in a W dimensional space and a distance. MDS tries to represents this data in a Q dimensional space, where $Q < W$ by using a fitness function. The MDS algorithm first determines a dissimilarity matrix $D = [d_{ij}]$, where, i and j are the distances from $1, \dots, N$, and d_{ij} stands for the dissimilarity between i and j . The obtained dissimilarity matrix is now the reference of the computational information. The algorithm does iterations to optimize the fitness function. In this way MDS produces another dissimilarity matrix $E = [e_{ij}]$, in Q dimensional space with distances e_{ij} . Often, for the fitness function the raw stress (RS) is adopted as in Equation (7):

$$RS = \sum_{i=2}^N \sum_{j=1}^{i-1} [d_{ij} - f(e_{ij})]^2 \quad (7)$$

where, $f(\cdot)$ is a kind of function. (Machado & Lopes, 2019):

3. Results and discussions

Because the k -means clustering is a method in which the user arbitrarily determines the k value, k was chosen in between 2 to 10

to find out the optimum k value with silhouette scores. The resulting silhouette scores are shown in Table 2.

Table 2 indicated that the silhouette scores for different k values are close. In such cases, the choice of k could be difficult. Choosing a low k will lead to a large within dissimilarities (heterogeneous clusters) and hence will result to large average dissimilarity of i to all other objects of its cluster (Rousseeuw, 1987). A decrease in silhouette score was observed in high k values. In the study, to create more homogeneous clusters and to achieve higher intra-cluster catchment similarities, k was chosen as 8, which also had the highest silhouette score with a value of 0.168. This score also pointed out that clustering was performed with above-average success. HRU images of the basins divided into 8 clusters are shown in Fig. 5.

To comprehend the created clusters more deeply, silhouette and MDS plots of the data set was drawn by Orange to visually evaluate the consistency and quality of the cluster. The silhouette plots by cluster and for the entire dataset can be seen in Fig. 6. MDS plots of clustered catchments and cluster centroids shown in Fig. 7.

The silhouette plot is given in Fig. 6(a) specifies the distances of intra-cluster data from their cluster centers. The silhouette scores of İncebacaklar and İlyasbey catchments in cluster 6, were 0.3361 and 0.3140 respectively. On the other hand, in cluster 8 which includes Yağbaşlar and Saltukova catchments, the silhouette scores were determined as 0.0834 and 0.0457, respectively. When these two clusters are compared, the basins in the sixth cluster are closer to their centroids than the basins in the eighth cluster. In other words, the catchments in cluster 6 are more similar to each other than the catchments in cluster 8. This situation is also expressed with the MDS plot in Fig. 7(a). In the MDS plot, each cluster was expressed with a color and the catchments were specified with circles. The distances of the watersheds to their cluster centroids were denoted by the size of the circles. The larger the size of the circle, the closer the data to its cluster centroid. Besides in Fig. 7(a), the similarities of the clusters to each other was defined as whether the clusters are neighboring or separated. For example, the first cluster, which was denoted with blue, is more similar to fifth, seventh and second clusters, which were denoted by yellow, cyan and red respectively, compared to the sixth cluster, which is specified in pink. Fig. 6(a) pointed out that the two basins that are in the same cluster and are most similar to each other were İhsaniye and Dereköy in the 1st cluster with a 0.0011 silhouette score gap. The two catchments that are in the same cluster and are the least similar to each other were Kuyluş and Yakabaşı in cluster 2 with a 0.2427 score distinction.

The catchment with the lowest intra-cluster silhouette score is considered as the outlier of that cluster. Fig. 6(b) ranks the silhouette scores from highest to lowest without clustering. With a silhouette value of 0.0144, the Güney basin stands out as the outlier of its cluster when compared to data instances. Aşağıçamlı and Sarnaz catchments, with silhouette values of 0.0291 and 0.0340 respectively followed Güney watershed as being an outlier. The first 5 catchments that were closest to their cluster centroids are the Kuyluş, İncebacaklar, Azdavay, İlyasbey and Yukarı İlipınar catchments with values of 0.3399, 0.3361, 0.3274, 0.3140 and 0.3111 respectively.

The average of the intra-cluster silhouette scores gives important information about the distribution of the data. Table 3 shows the average intra-cluster silhouette scores.

The average intra-cluster silhouette score values shed light on the similarities of the watershed. The closer the average silhouette score to 1 , the more similar the data in the cluster. As can be seen in Table 3, the highest score was calculated for cluster 6, which means that the watersheds in cluster 6 are the most similar. Just the opposite, cluster 7 with an average silhouette score of 0.0607 contains the most unfamiliar catchments. The illustration of

clustered catchments on the study area can be seen in Fig. 8.

When Fig. 8 is examined, the first noticeable case is that the adjacent basins were more likely to be located in the same cluster. Arabacı – Çilimli, İhsaniye – Dereköy and Güney – Asarsuyu basin can be the examples of this kind of basin pairs. However, some catchments were located in the same cluster and also have more than 270 km distance between them was observed like Yakabaşı – Kuyluş, İhsaniye – Yenikent and Uğurluköy – Tevfikiye.

4. Conclusions

Unsupervised learning approaches stand out as practical methods for determining meaningful patterns in data sets. This study was conducted to obtain information about the similarities of catchments using the *k-means* clustering technique, with the help of QSWAT+, MS Office, Orange, and QGIS software.

HRU images of 33 catchments located in the Western Black Sea Region of Turkey were clustered. *k* values ranging from 2 to 10 were examined and the optimum number of clusters was found to be 8 clusters with a silhouette score of 0.168. Besides, the intra-cluster similarities of basins were investigated with the silhouette plot. By using the MDS plot, multidimensional data were illustrated in two-dimensional space. Depending on the silhouette and the MDS plot, the catchment closest to the center of its cluster was determined as Kuyluş. The two most similar basins found to be İhsaniye and Dereköy. Güney, Aşağı Çamlı, and Sarnaz catchments were turned out to be the outliers of their clusters.

In *k-means* clustering, two clusters can be considered as disjoint; catchments reside inside a cluster will have high hydrological similarity, the catchments of two separate clusters would be dissimilar to each other. It can be considered that two basins in the same cluster will show higher hydrological similarity when the silhouette score is close to 1 and the score gap is low. In a basin, HRUs control hydrological dynamics and basins with similar HRU patterns have the same hydrological behavior regarding weather inputs and water runoff. The method presented in this study can be considered as an elimination process. With the result obtained from this study, researchers may transfer preliminary information from gauged catchments to ungauged ones. By transferring information between catchments time, labor and money losses can be prevented by reducing the number of basins to be selected for the future hydrological application. However, hydrological modeling and measurement of the selected watershed still need to be carried out even if there is a high similarity with a high silhouette score to the compared watershed because the clustering method does not have any prior knowledge of hydrological inputs like weather inputs and outputs or water run-off of the catchments. For this reason, no calibration or validation process can be conducted between catchments. The validation or assessment of results with unsupervised methods are often difficult to ascertain due to its inherent inexactness. Although this study covers basins in a restricted area for demonstration purposes, the boundaries of the implementation of the method can be extended to include countries or continents. The methods and results of this study are good indicators of the usability of the SWAT + model for different applications besides hydrological modeling.

Declaration of competing interest

No conflicts of interest.

References

Ahmed, K. (2020). *Decision support methods for assessing flood risk and vulnerability*. Hershey, PA, USA: IGI Global.

- Aliyari, F., Bailey, R. T., Tasdighi, A., Dozier, A., Arabi, M., & Zeiler, K. (2019). Coupled SWAT-MODFLOW model for large-scale mixed agro-urban river basins. *Environmental Modelling & Software*, 115, 200–210. <https://doi.org/10.1016/j.envsoft.2019.02.014>.
- Anitha, P., & Patil, M. M. (2019). RFM model for customer purchase behavior using K-Means algorithm. *Journal of King Saud University - Computer and Information Sciences*. <https://doi.org/10.1016/j.jksuci.2019.12.011>.
- Arabi, M., Frankenberger, J. R., Enge, B. A., & Arnold, J. G. (2008). Representation of agricultural conservation practices with SWAT. *Hydrological Processes*, 22(16), 3042–3055. <https://doi.org/10.1002/hyp.6890>.
- Arima, C., Hakamada, K., Okamoto, M., & Hanai, T. (2008). Modified fuzzy gap statistic for estimating preferable number of clusters in fuzzy k-means clustering. *Journal of Bioscience and Bioengineering*, 105(3), 273–281. <https://doi.org/10.1263/jbb.105.273>.
- Arnold, J. G., Srinivasan, R., Muttiah, R. S., & Williams, J. R. (1998). Large area hydrologic modeling and assessment - Part 1: Model development. *Journal of the American Water Resources Association*, 34(1), 73–89. <https://doi.org/10.1111/j.1752-1688.1998.tb05961.x>.
- Atalay, N. B., & Yore, S. (2020). Pitch distribution, melodic contour or both? Modeling makam schema with multidimensional scaling and self-organizing maps. *New Ideas in Psychology*, 56. <https://doi.org/10.1016/j.newideapsych.2019.06.002>. UNSP 100746.
- Azimi, S., Dariane, A. B., Modanesi, S., Bauer-Marschallinger, B., Bindlish, R., Wagner, W., et al. (2020). Assimilation of sentinel 1 and SMAP – based satellite soil moisture retrievals into SWAT hydrological model: The impact of satellite revisit time and product spatial resolution on flood simulations in small basins. *Journal of Hydrology*, 581, 124367. <https://doi.org/10.1016/j.jhydrol.2019.124367>.
- Bauwe, A., Eckhardt, K. U., & Lennartz, B. (2019). Predicting dissolved reactive phosphorus in tile-drained catchments using a modified SWAT model. *Ecohydrology and Hydrobiology*, 19(2), 198–209. <https://doi.org/10.1016/j.ecohyd.2019.03.003>.
- Bhatta, B., Shrestha, S., Shrestha, P. K., & Talchabhadel, R. (2019). Evaluation and application of a SWAT model to assess the climate change impact on the hydrology of the Himalayan River Basin. *Catena*, 181. <https://doi.org/10.1016/j.catena.2019.104082>. UNSP 104082.
- Cerkasova, N., Umgieser, G., & Erturk, A. (2018). Development of a hydrology and water quality model for a large transboundary river watershed to investigate the impacts of climate change - a SWAT application. *Ecological Engineering*, 124, 99–115. <https://doi.org/10.1016/j.ecoleng.2018.09.025>.
- Christian, H., Marina, M., Fionn, M., & Roberto, R. (2015). Clustering strategy and method selection. In *Handbook of cluster Analysis*. CRC Press.
- Corine (Coordination of Information on the Environment). (2019, May 15). Land cover. Retrieved from <https://land.copernicus.eu/pan-european/corine-land-cover/clc2018?tab=download>.
- Deliu, M., Sperrin, M., Belgrave, D., & Custovic, A. (2016). Identification of asthma subtypes using clustering methodologies. *Pulmonary Therapy*, 2(1), 19–41. <https://doi.org/10.1007/s41030-016-0017-z>.
- Demšar, J., Tomaz, C., Erjavec, A., Gorup, C., Hocevar, T., Milutinovic, M., et al. (2013). Orange: Data mining toolbox in Python. *Journal of Machine Learning Research*, 14, 2349–2353.
- Demšar, J., & Zupan, B. (2013). Orange: Data mining fruitful and fun - a historical perspective. *Informatica*, 37, 55–60.
- Demšar, J., Zupan, B., Leban, G., & Curk, T. (2004). *Orange: From experimental machine learning to interactive data mining* (Berlin, Heidelberg).
- Dile, Y., Srinivasan, R., & George, C. (2018). QGIS interface for SWAT (QSWAT). In *Setup for robit watershed, lake tana basin* (pp. 20–21).
- Doupe, P., Faghmous, J., & Basu, S. (2019). Machine learning for health services researchers. *Value in Health*, 22(7), 808–815. <https://doi.org/10.1016/j.jval.2019.02.012>.
- FAO (Food and Agriculture Organization of the United Nations). (2019, May 16). Harmonized world soil database v 1.2. Retrieved from <http://www.fao.org/soils-portal/soil-survey/soil-maps-and-databases/harmonized-world-soil-database-v12/en/>.
- Flugel, W. A. (1995). Delineating hydrological response units by geographical information-system Analyses for regional hydrological modeling using prms/mms in the drainage-basin of the river broel, Germany. *Hydrological Processes*, 9(3–4), 423–436. <https://doi.org/10.1002/hyp.3360090313>.
- Flugel, W. A. (1997). Combining GIS with regional hydrological modelling using hydrological response units (HRUs): An application from Germany. *Mathematics and Computers in Simulation*, 43(3–6), 297–304. [https://doi.org/10.1016/S0378-4754\(97\)00013-X](https://doi.org/10.1016/S0378-4754(97)00013-X).
- Franti, P., & Sieranoja, S. (2019). How much can k-means be improved by using better initialization and repeats? *Pattern Recognition*, 93, 95–112. <https://doi.org/10.1016/j.patcog.2019.04.014>.
- Godec, P., Pancur, M., Ilenic, N., Copar, A., Strazar, M., Erjavec, A., ... Zupan, B. (2019). Democratized image analytics by visual programming through integration of deep models and small-scale machine learning. *Nature Communications*, 10. <https://doi.org/10.1038/s41467-019-12397-x>. ARTN 4551.
- Govender, P., & Sivakumar, V. (2020). Application of k-means and hierarchical clustering techniques for analysis of air pollution: A review (1980–2019). *Atmospheric Pollution Research*, 11(1), 40–56. <https://doi.org/10.1016/j.apr.2019.09.009>.
- Gungor, O., & Goncu, S. (2013). Application of the soil and water assessment tool model on the Lower Porsuk Stream Watershed. *Hydrological Processes*, 27(3), 453–466. <https://doi.org/10.1002/hyp.9228>.

- Guo, T., Engel, B. A., Shao, G., Arnold, J. G., Srinivasan, R., & Kiniry, J. R. (2019). Development and improvement of the simulation of woody bioenergy crops in the Soil and Water Assessment Tool (SWAT). *Environmental Modelling & Software*, 122, 104295. <https://doi.org/10.1016/j.envsoft.2018.08.030>.
- Himanshu, S. K., Pandey, A., Yadav, B., & Gupta, A. (2019). Evaluation of best management practices for sediment and nutrient loss control using SWAT model. *Soil and Tillage Research*, 192, 42–58. <https://doi.org/10.1016/j.still.2019.04.016>.
- Hinton, G. E., & Salakhutdinov, R. R. (2006). Reducing the dimensionality of data with neural networks. *Science*, 313(5786), 504–507. <https://doi.org/10.1126/science.1127647>.
- Huang, F. R., Zhang, X. M., Li, Z. J., Zhao, Z. H., & He, Y. Y. (2018). From content to links: Social image embedding with deep multimodal model. *Knowledge-Based Systems*, 160, 251–264. <https://doi.org/10.1016/j.knsys.2018.07.020>.
- Isik, S., & Singh, V. P. (2008). Hydrologic regionalization of watersheds in Turkey. *Journal of Hydrologic Engineering*, 13(9), 824–834. [https://doi.org/10.1061/\(ASCE\)1084-0699\(2008\)13:9\(824\)](https://doi.org/10.1061/(ASCE)1084-0699(2008)13:9(824)).
- Jafarzadegan, M., Safi-Esfahani, F., & Beheshti, Z. (2019). Combining hierarchical clustering approaches using the PCA method. *Expert Systems with Applications*, 137, 1–10. <https://doi.org/10.1016/j.eswa.2019.06.064>.
- Jahandad, S. M. S., Kamardin, K., Amir Sjarif, N. N., & Mohamed, N. (2019). Offline signature verification using deep learning convolutional neural network (CNN) architectures GoogLeNet inception-v1 and inception-v3. *Procedia Computer Science*, 161, 475–483. <https://doi.org/10.1016/j.procs.2019.11.147>.
- Jodar-Abellan, A., Valdes-Abellan, J., Pla, C., & Gomariz-Castillo, F. (2019). Impact of land use changes on flash flood prediction using a sub-daily SWAT model in five Mediterranean ungauged watersheds (SE Spain). *The Science of the Total Environment*, 657, 1578–1591. <https://doi.org/10.1016/j.scitotenv.2018.12.034>.
- Karvonen, T., Koivusalo, H., Jauhainen, M., Palko, J., & Wepling, K. (1999). A hydrological model for predicting runoff from different land use areas. *Journal of Hydrology*, 217(3–4), 253–265. [https://doi.org/10.1016/S0022-1694\(98\)00280-7](https://doi.org/10.1016/S0022-1694(98)00280-7).
- Khan, U., Tuteja, N. K., Sharma, A., Lucas, S., Murphy, B., & Jenkins, B. (2016). Applicability of Hydrologic Response Units in low topographic relief catchments and evaluation using high resolution aerial photograph analysis. *Environmental Modelling & Software*, 81, 56–71. <https://doi.org/10.1016/j.envsoft.2016.03.010>.
- Khendek, F., & Gotzhein, R. (2019). In P. F. Casas, M.-R. Sancho, & E. Sherratt (Eds.), *System Analysis and modeling. Languages, methods, and tools for systems engineering: 10th international conference, SAM 2018, copenhagen, Denmark, october 15–16, 2018, proceedings* (1st ed.). Switzerland: Springer International Publishing.
- Kim, H., Kim, H. K., & Cho, S. (2020). Improving spherical k-means for document clustering: Fast initialization, sparse centroid projection, and efficient cluster labeling. *Expert Systems with Applications*, 150, 113288. <https://doi.org/10.1016/j.eswa.2020.113288>.
- Kling, C. L., Panagopoulos, Y., Rabotyagov, S. S., Valcu, A. M., Gassman, P. W., Campbell, T., ... Rabalais, N. N. (2014). LUMINATE: Linking agricultural land use, local water quality and gulf of Mexico hypoxia. *European Review of Agricultural Economics*, 41(3), 431–459. <https://doi.org/10.1093/erae/jbu009>.
- Latt, Z. Z., Wittenberg, H., & Urban, B. (2015). Clustering hydrological homogeneous regions and neural network based index flood estimation for ungauged catchments: An example of the chindwin river in Myanmar. *Water Resources Management*, 29(3), 913–928. <https://doi.org/10.1007/s11269-014-0851-4>.
- Lee, K. M., Yoo, J., Kim, S. W., Lee, J. H., & Hong, J. M. (2019). Autonomic machine learning platform. *International Journal of Information Management*, 49, 491–501. <https://doi.org/10.1016/j.ijinfomgt.2019.07.003>.
- Li, Q. L., Li, Z. J., Zhu, Y. L., Deng, Y. Q., Zhang, K., & Yao, C. (2018). Hydrological regionalisation based on available hydrological information for runoff prediction at catchment scale. *Innovative Water Resources Management - Understanding and Balancing Interactions between Humankind and Nature*, 379, 13–19. <https://doi.org/10.5194/iphhs-379-13-2018>.
- Lipor, J., & Balzano, L. (2020). Clustering quality metrics for subspace clustering. *Pattern Recognition*, 104, 107328. <https://doi.org/10.1016/j.patcog.2020.107328>.
- Lleti, R., Ortiz, M. C., Sarabia, L. A., & Sanchez, M. S. (2004). Selecting variables for k-means cluster analysis by using a genetic algorithm that optimises the silhouette. *Analytica Chimica Acta*, 515(1), 87–100. <https://doi.org/10.1016/j.jaca.2003.12.020>.
- Lotz, T., Opp, C., & He, X. (2018). Factors of runoff generation in the Dongting Lake basin based on a SWAT model and implications of recent land cover change. *Quaternary International*, 475, 54–62. <https://doi.org/10.1016/j.quaint.2017.03.057>.
- Lucke, J., & Forster, D. (2019). k-means as a variational EM approximation of Gaussian mixture models. *Pattern Recognition Letters*, 125, 349–356. <https://doi.org/10.1016/j.patrec.2019.04.001>.
- Machado, J. T., & Lopes, A. M. (2019). Multidimensional scaling and visualization of patterns in prime numbers. *Communications in Nonlinear Science and Numerical Simulation*, 83, 105128. <https://doi.org/10.1016/j.cnsns.2019.105128>.
- Machado, J. T., & Mehdipour, S. H. (2019). Multidimensional scaling analysis of the solar system objects. *Communications in Nonlinear Science and Numerical Simulation*, 79. <https://doi.org/10.1016/j.cnsns.2019.104923>. UNSP 104923.
- Mengistu, A. G., van Rensburg, L. D., & Woyessa, Y. E. (2019). Techniques for calibration and validation of SWAT model in data scarce arid and semi-arid catchments in South Africa. *Journal of Hydrology-Regional Studies*, 25. <https://doi.org/10.1016/j.ejrh.2019.100621>. UNSP 100621.
- Mesquita, D. P. P., Gomes, J. P. P., Souza, A. H., & Nobre, J. S. (2017). Euclidean distance estimation in incomplete datasets. *Neurocomputing*, 248, 11–18. <https://doi.org/10.1016/j.neucom.2016.12.081>.
- Naik, A., & Samant, L. (2016). Correlation review of classification algorithm using data mining tool: WEKA, rapidminer, tanagra, Orange and knime. In *International conference on computational modelling and security (cms 2016)* (Vol. 85, pp. 662–668). <https://doi.org/10.1016/j.procs.2016.05.251>.
- Pai, N., Saraswat, D., & Srinivasan, R. (2012). Field_SWAT: A tool for mapping SWAT output to field boundaries. *Computers & Geosciences*, 40, 175–184. <https://doi.org/10.1016/j.cageo.2011.07.006>.
- Qi, J. Y., Zhang, X. S., & Cosh, M. H. (2019). Modeling soil temperature in a temperate region: A comparison between empirical and physically based methods in SWAT. *Ecological Engineering*, 129, 134–143. <https://doi.org/10.1016/j.ecoleng.2019.01.017>.
- Ramos-Lima, L. F., Waikamp, V., Antonelli-Salgado, T., Passos, I. C., & Freitas, L. H. M. (2020). The use of machine learning techniques in trauma-related disorders: A systematic review. *Journal of Psychiatric Research*, 121, 159–172. <https://doi.org/10.1016/j.jpsychires.2019.12.001>.
- Rao, A. R., & Srinivas, V. V. (2006). Regionalization of watersheds by hybrid-cluster analysis. *Journal of Hydrology*, 318(1–4), 37–56. <https://doi.org/10.1016/j.jhydrol.2005.06.003>.
- Renjith, S., Sreekumar, A., & Jathavedan, M. (2020). Performance evaluation of clustering algorithms for varying cardinality and dimensionality of data sets. *Materials Today: Proceedings*. <https://doi.org/10.1016/j.matpr.2020.01.110>.
- Rousseeuw, P. J. (1987). Silhouettes - a graphical aid to the interpretation and validation of cluster-analysis. *Journal of Computational and Applied Mathematics*, 20, 53–65. [https://doi.org/10.1016/0377-0427\(87\)90125-7](https://doi.org/10.1016/0377-0427(87)90125-7).
- Sanzana, P., Jankowfsky, S., Branger, F., Braud, I., Vargas, X., Hirschfeld, N., et al. (2013). Computer-assisted mesh generation based on hydrological response units for distributed hydrological modeling. *Computers & Geosciences*, 57, 32–43. <https://doi.org/10.1016/j.cageo.2013.02.006>.
- Sharghi, E., Nourani, V., Soleimani, S., & Sadikoglu, F. (2018). Application of different clustering approaches to hydroclimatological catchment regionalization in mountainous regions, a case study in Utah State. *Journal of Mountain Science*, 15(3), 461–484. <https://doi.org/10.1007/s11629-017-4454-4>.
- Sheshukov, A. Y., Douglas-Mankin, K. R., Sinnathamby, S., & Daggupati, P. (2016). Pasture BMP effectiveness using an HRU-based subarea approach in SWAT. *Journal of Environmental Management*, 166, 276–284. <https://doi.org/10.1016/j.jenvman.2015.10.023>.
- Szegedy, C., Vanhoucke, V., Ioffe, S., Shlens, J., & Wojna, Z. (2016). Rethinking the inception architecture for computer vision. In *2016 IEEE conference on computer vision and pattern recognition (cvpr)* (pp. 2818–2826). <https://doi.org/10.1109/Cvpr.2016.308>.
- Tian, K., Li, J. H., Zeng, J. F., Evans, A., & Zhang, L. N. (2019). Segmentation of tomato leaf images based on adaptive clustering number of K-means algorithm. *Computers and Electronics in Agriculture*, 165. <https://doi.org/10.1016/j.compag.2019.104962>. ARTN 104962.
- Tongal, H., & Sivakumar, B. (2017). Cross-entropy clustering framework for catchment classification. *Journal of Hydrology*, 552, 433–446. <https://doi.org/10.1016/j.jhydrol.2017.07.005>.
- University of Ljubljana. (2019a). Orange data mining tool. Retrieved from <https://orange.biolab.si>.
- University of Ljubljana. (2019b). Image embedding inceptionV3. Retrieved from <https://orange3-imageanalytics.readthedocs.io/en/latest/widgets/image-embedding.html>.
- University of Ljubljana. (2019c). Silhouette plot. Retrieved from <https://orange-visual-programming.readthedocs.io/widgets/visualize/silhouetteplot.html>.
- Usgs (United States Geological Survey). (2019, May 18). Earth explorer digital elevation model. Retrieved from <https://earthexplorer.usgs.gov>.
- Wang, C., Chen, Z. L., Shang, K., & Wu, H. M. (2019). Label-removed generative adversarial networks incorporating with K-Means. *Neurocomputing*, 361, 126–136. <https://doi.org/10.1016/j.neucom.2019.06.041>.
- Wu, H. Q., Huang, Q., Xu, W., & Xi, S. F. (2015). Application of K-means cluster and rough set in classified real-time flood forecasting. *Advanced Materials Research*, 1092–1093, 734–741. <https://doi.org/10.4028/www.scientific.net/amr.1092-1093.734>.
- Yen, H., Park, S., Arnold, J. G., Srinivasan, R., Chawanda, C. J., Wang, R. Y., ... Zhang, X. S. (2019). IPEAT plus : A built-in optimization and automatic calibration tool of SWAT. *Water*, 11(8). <https://doi.org/10.3390/w11081681>. ARTN 1681.
- Zou, Q., Cui, P., He, J., Lei, Y., & Li, S. S. (2019). Regional risk assessment of debris flows in China-An HRU-based approach. *Geomorphology*, 340, 84–102. <https://doi.org/10.1016/j.geomorph.2019.04.027>.

GUIDE FOR AUTHORS

INTRODUCTION

Types of paper

Contributions falling into the following categories will be considered for publication: Original research papers, reviews, letters to the editor.

Please ensure that you select the appropriate article type from the list of options when making your submission. Authors contributing to special issues should ensure that they select the special issue article type from this list.

BEFORE YOU BEGIN

Ethics in Publishing

For information on Ethics in Publishing and Ethical guidelines for journal publication see <http://www.elsevier.com/publishingethics> and <http://www.elsevier.com/ethicalguidelines>.

Conflict of interest

All authors are requested to disclose any actual or potential conflict of interest including any financial, personal or other relationships with other people or organizations within three years of beginning the submitted work that could inappropriately influence, or be perceived to influence, their work. See also <http://www.elsevier.com/conflictsofinterest>.

Submission declaration

Submission of an article implies that the work described has not been published previously (except in the form of an abstract or as part of a published lecture or academic thesis), that it is not under consideration for publication elsewhere, that its publication is approved by all authors and tacitly or explicitly by the responsible authorities where the work was carried out, and that, if accepted, it will not be published elsewhere including electronically in the same form, in English or in any other language, without the written consent of the copyright-holder.

Changes to authorship

This policy concerns the addition, deletion, or rearrangement of author names in the authorship of accepted manuscripts:

Before the accepted manuscript is published in an online issue: Requests to add or remove an author, or to rearrange the author names, must be sent to the Journal Manager from the corresponding author of the accepted manuscript and must include: (a) the reason the name should be added or removed, or the author names rearranged and (b) written confirmation (e-mail, fax, letter) from all authors that they agree with the addition, removal or rearrangement. In the case of addition or removal of authors, this includes confirmation from the author being added or removed. Requests that are not sent by the corresponding author will be forwarded by the Journal Manager to the corresponding author, who must follow the procedure as described above. Note that: (1) Journal Managers will inform the Journal Editors of any such requests and (2) publication of the accepted manuscript in an online issue is suspended until authorship has been agreed.

After the accepted manuscript is published in an online issue: Any requests to add, delete, or rearrange author names in an article published in an online issue will follow the same policies as noted above and result in a corrigendum.

Copyright

[example: Upon acceptance of an article, authors will be asked to complete a 'Journal Publishing Agreement'. Acceptance of the agreement will ensure the widest possible dissemination of information. An e-mail will be sent to the corresponding author confirming receipt of the manuscript together with a 'Journal Publishing Agreement' form or a link to the online version of this agreement.

Permission of the International Research and Training Center on Erosion and Sedimentation or the China Water and Power Press is required for resale or distribution outside the institution and for all other derivative works, including compilations and translations (please consult paige.chyu@gmail.com or iswcr@foxmail.com). If excerpts from other copyrighted works are included, the author(s) must obtain written permission from the copyright owners and credit the source(s) in the article.]

Role of the funding source

You are requested to identify who provided financial support for the conduct of the research and/or preparation of the article and to briefly describe the role of the sponsor(s), if any, in study design; in the collection, analysis and interpretation of data; in the writing of the report; and in the decision to submit the paper for publication. If the funding source(s) had no such involvement then this should be stated. Please see <http://www.elsevier.com/funding>.

Language and language services

Please write your text in good English (American or British usage is accepted, but not a mixture of these). Authors who require information about language editing and copyediting services pre- and post-submission please visit <http://webshop.elsevier.com/languageediting> or our customer support site at <http://support.elsevier.com> for more information.

Submission

Submission to this journal proceeds totally online. Use the following guidelines to prepare your article. Via the homepage of this journal (http://www.evise.com/evise/faces/pages/navigation/NavController.jspx?JRNL_ACR=ISWCR) you will be guided stepwise through the creation and uploading of the various files. The system automatically converts source files to a single Adobe Acrobat PDF version of the article, which is used in the peer-review process. Please note that even though manuscript source files are converted to PDF at submission for the review process, these source files are needed for further processing after acceptance. All correspondence, including notification of the Editor's decision and requests for revision, takes place by e-mail and via the author's homepage, removing the need for a hard-copy paper trail. If you are unable to provide an electronic version, please contact the editorial office prior to submission [example: e-mail: paige.chyu@gmail.com or iswcr@foxmail.com; telephone: +86 10 68786416; or fax: 86 10 68411174].

Additional Information

Tables and figures may be presented with captions within the main body of the manuscript; if so, figures should additionally be uploaded as high resolution files.

PREPARATION

Use of wordprocessing software

It is important that the file be saved in the native format of the wordprocessor used. The text should be in single-column format. Keep the layout of the text as simple as possible. Most formatting codes will be removed and replaced on processing the article. In particular, do not use the wordprocessor's options to justify text or to hyphenate words. However, do use bold face, italics, subscripts, superscripts etc. When preparing tables, if you are using a table grid, use only one grid for each individual table and not a grid for each row. If no grid is used, use tabs, not spaces, to align columns. The electronic text should be prepared in a way very similar to that of conventional manuscripts (see also the Guide to Publishing with Elsevier: <http://www.elsevier.com/guidepublication>). Note that source files of figures, tables and text graphics will be required whether or not you embed your figures in the text. See also the section on Electronic illustrations.

To avoid unnecessary errors you are strongly advised to use the “spell-check” and “grammar-check” functions of your wordprocessor.

LaTeX

If the LaTeX file is suitable, proofs will be produced without rekeying the text. The article should preferably be written using Elsevier’s document class “elsarticle”, or alternatively any of the other recognized classes and formats supported in Elsevier’s electronic submissions system, for further information see <http://www.elsevier.com/wps/find/authorsview.authors/latex-ees-supported>.

The Elsevier “elsarticle” LaTeX style file package (including detailed instructions for LaTeX preparation) can be obtained from the Quickguide: <http://www.elsevier.com/latex>. It consists of the file: elsarticle.cls, complete user documentation for the class file, bibliographic style files in various styles, and template files for a quick start.

Article structure

Subdivision - numbered sections

Divide your article into clearly defined and numbered sections. Subsections should be numbered 1.1 (then 1.1.1, 1.1.2, ...), 1.2, etc. (the abstract is not included in section numbering). Use this numbering also for internal cross-referencing: do not just refer to “the text”. Any subsection may be given a brief heading. Each heading should appear on its own separate line.

Introduction

State the objectives of the work and provide an adequate background, avoiding a detailed literature survey or a summary of the results.

Material and methods

Provide sufficient detail to allow the work to be reproduced. Methods already published should be indicated by a reference: only relevant modifications should be described.

Theory/calculation

A Theory section should extend, not repeat, the background to the article already dealt with in the Introduction and lay the foundation for further work. In contrast, a Calculation section represents a practical development from a theoretical basis.

Results

Results should be clear and concise.

Discussion

This should explore the significance of the results of the work, not repeat them. A combined Results and Discussion section is often appropriate. Avoid extensive citations and discussion of published literature.

Conclusions

The main conclusions of the study may be presented in a short Conclusions section, which may stand alone or form a subsection of a Discussion or Results and Discussion section.

Appendices

If there is more than one appendix, they should be identified as A, B, etc. Formulae and equations in appendices should be given separate numbering: Eq. (A.1), Eq. (A.2), etc.; in a subsequent appendix, Eq. (B.1) and so on. Similarly for tables and figures: Table A.1; Fig. A.1, etc.

Essential title page information

- **Title.** Concise and informative. Titles are often used in information-retrieval systems. Avoid abbreviations and formulae where possible.
- **Author names and affiliations.** Where the family name may be ambiguous (e.g., a double name), please indicate this clearly. Present the authors’ affiliation addresses (where the actual work was done) below the names. Indicate all affiliations with a lower-case superscript letter immediately after the author’s name

and in front of the appropriate address. Provide the full postal address of each affiliation, including the country name, and, if available, the e-mail address of each author.

- **Corresponding author.** Clearly indicate who will handle correspondence at all stages of refereeing and publication, also post-publication. **Ensure that telephone and fax numbers (with country and area code) are provided in addition to the e-mail address and the complete postal address. Contact details must be kept up to date by the corresponding author.**
- **Present/permanent address.** If an author has moved since the work described in the article was done, or was visiting at the time, a “Present address” (or “Permanent address”) may be indicated as a footnote to that author’s name. The address at which the author actually did the work must be retained as the main, affiliation address. Superscript Arabic numerals are used for such footnotes.

Abstract

A concise and factual abstract is required. The abstract should state briefly the purpose of the research, the principal results and major conclusions. An abstract is often presented separately from the article, so it must be able to stand alone. For this reason, References should be avoided, but if essential, then cite the author(s) and year(s). Also, non-standard or uncommon abbreviations should be avoided, but if essential they must be defined at their first mention in the abstract itself.

Keywords

Authors are invited to submit keywords associated with their paper.

Abbreviations

Define abbreviations that are not standard in this field in a footnote to be placed on the first page of the article. Such abbreviations that are unavoidable in the abstract must be defined at their first mention there, as well as in the footnote. Ensure consistency of abbreviations throughout the article.

Acknowledgements

Collate acknowledgements in a separate section at the end of the article before the references and do not, therefore, include them on the title page, as a footnote to the title or otherwise. List here those individuals who provided help during the research (e.g., providing language help, writing assistance or proof reading the article, etc.).

Nomenclature and units

Follow internationally accepted rules and conventions: use the international system of units (SI). If other quantities are mentioned, give their equivalent in SI. Authors wishing to present a table of nomenclature should do so on the second page of their manuscript.

Math formulae

Present simple formulae in the line of normal text where possible and use the solidus (/) instead of a horizontal line for small fractional terms, e.g., X/Y. In principle, variables are to be presented in italics. Powers of e are often more conveniently denoted by exp. Number consecutively any equations that have to be displayed separately from the text (if referred to explicitly in the text).

Footnotes

Footnotes should be used sparingly. Number them consecutively throughout the article, using superscript Arabic numbers. Many wordprocessors build footnotes into the text, and this feature may be used. Should this not be the case, indicate the position of footnotes in the text and present the footnotes themselves separately at the end of the article. Do not include footnotes in the Reference list.

Table footnotes

Indicate each footnote in a table with a superscript lowercase letter.

Artwork

Electronic artwork

General points

- Make sure you use uniform lettering and sizing of your original artwork.
- Save text in illustrations as “graphics” or enclose the font.
- Only use the following fonts in your illustrations: Arial, Courier, Times, Symbol.
- Number the illustrations according to their sequence in the text.
- Use a logical naming convention for your artwork files.
- Provide captions to illustrations separately.
- Produce images near to the desired size of the printed version.
- Submit each figure as a separate file.

A detailed guide on electronic artwork is available on our website: <http://www.elsevier.com/artworkinstructions>

You are urged to visit this site; some excerpts from the detailed information are given here.

Formats

Regardless of the application used, when your electronic artwork is finalised, please “save as” or convert the images to one of the following formats (note the resolution requirements for line drawings, halftones, and line/halftone combinations given below):

EPS: Vector drawings. Embed the font or save the text as “graphics”.
TIFF: color or grayscale photographs (halftones): always use a minimum of 300 dpi.
TIFF: Bitmapped line drawings: use a minimum of 1000 dpi.
TIFF: Combinations bitmapped line/half-tone (color or grayscale): a minimum of 500 dpi is required.

If your electronic artwork is created in a Microsoft Office application (Word, PowerPoint, Excel) then please supply “as is”.

Please do not:

- Supply files that are optimised for screen use (like GIF, BMP, PICT, WPG); the resolution is too low;
- Supply files that are too low in resolution;
- Submit graphics that are disproportionately large for the content.

Color artwork

Please make sure that artwork files are in an acceptable format (TIFF, EPS or MS Office files) and with the correct resolution. If, together with your accepted article, you submit usable color figures then Elsevier will ensure, at no additional charge, that these figures will appear in color on the Web (e.g., ScienceDirect and other sites) regardless of whether or not these illustrations are reproduced in color in the printed version.

Figure captions

Ensure that each illustration has a caption. Supply captions separately, not attached to the figure. A caption should comprise a brief title (**not** on the figure itself) and a description of the illustration. Keep text in the illustrations themselves to a minimum but explain all symbols and abbreviations used.

Tables

Number tables consecutively in accordance with their appearance in the text. Place footnotes to tables below the table body and indicate them with superscript lowercase letters. Avoid vertical rules. Be sparing in the use of tables and ensure that the data presented in tables do not duplicate results described elsewhere in the article.

References

Citation in text

Please ensure that every reference cited in the text is also present in the reference list (and vice versa). Any references cited in the abstract must be given in full. Unpublished results and personal

communications are not recommended in the reference list, but may be mentioned in the text. If these references are included in the reference list they should follow the standard reference style of the journal and should include a substitution of the publication date with either “Unpublished results” or “Personal communication” Citation of a reference as “in press” implies that the item has been accepted for publication.

Web references

As a minimum, the full URL should be given and the date when the reference was last accessed. Any further information, if known (DOI, author names, dates, reference to a source publication, etc.), should also be given. Web references can be listed separately (e.g., after the reference list) under a different heading if desired, or can be included in the reference list.

References in a special issue

Please ensure that the words ‘this issue’ are added to any references in the list (and any citations in the text) to other articles in the same Special Issue.

Reference management software

This journal has standard templates available in key reference management packages EndNote (<http://www.endnote.com/support/enstyles.asp>) and Reference Manager (<http://refman.com/support/rmstyles.asp>). Using plug-ins to wordprocessing packages, authors only need to select the appropriate journal template when preparing their article and the list of references and citations to these will be formatted according to the journal style which is described below.

Reference style

The International Soil and Water Conservation Research (ISWCR) follows the Publication Manual of the American Psychological Association (APA) 6th for reference lists and text citation. The author are referred to the Publication Manual of the American Psychological Association, Fifth Edition, ISBN 1-55798-790-4, copies of which may be ordered from <http://www.apa.org/books/4200061.html> or APA Order Dept., P.O.B. 2710, Hyattsville, MD 20784, USA. or APA, 3 Henrietta Street, London, WC3E 8LU, UK. Details concerning this referencing style can also be found at <http://humanities.byu.edu/linguistics/Henrichsen/APA/APA01.html>.

Examples:

Text: All citations in the text should refer to:

One author

–Smith (2002) found...
–(Smith, 2002).

Two Authors:

–Smith and Jones (2003) found...
–(Smith & Jones, 2003).

Three or More Authors

–Smith et al. (2001) found...
– (Phelps et al., 2004)
–Smith et al. (2002) found...

Groups as Authors:

–1st Citation:
(American Psychological Association [APA], 2000).
–Subsequent Citations:
(APA, 2000).

Anonymous or No Author

–Use first few words of reference list entry (usually title):
(—Study Finds, 1995)
(TEA, 2007)

Authors with Same Surname

–Include initials: S. T. Smith (2000) and J. D. Smith (1999)

Two of more works within the same parentheses

–In order alphabetically, as they would appear in references, separated by semi-colons

(Jones, 2003; Thomas, 2010)

–If by same author, then by date

(Jones, 2003, 2007)

References should be arranged first alphabetically and then further sorted chronologically if necessary. More than one reference from the same author(s) in the same year must be identified by the letters “a”, “b”, “c”, etc., placed after the year of publication

Reference to a journal publication

Carlson, L. A. (2003). Existential theory: Helping school counselors attend to youth at risk for violence. *Professional School Counseling*, 6(5), 10-15.

Sagarin, B. J., & Lamer-Sagarin, K. A. (2005). Critically evaluating competing theories: An exercise based on the Kitty Genovese murder. *Teaching of Psychology*, 32(3), 167-169.

Hughes, J. C., Brestan, E. V., & Valle, L. A. (2004). Problem-solving interactions between mothers and children. *Child and Family Behavior Therapy*, 26(1), 1-16.

Journal with more than seven authors

Gilbert, D. G., McCleron, J. F., Rabinovich, N. E., Sugai, C., Plath, L. C., Asgaard, G., Botros, N. (2004). Effects of quitting smoking on EEG activation and attention last for more than 31 days and are more severe with stress. *Nicotine and Tobacco Research*, 6, 249-267.

Herbst-Damm, K.L., & Kulik, J.A. (2005). Volunteer support, marital status, and the survival times of terminally ill patients. *Health Psychology*, 24, 225-229. doi: 10.1037/0278-6133.24.2.225

Silick, T.J., & Schutte, N.S. (2006). Emotional intelligence and self-esteem mediate between perceived early parental love and adult happiness. *E-Journal of Applied Psychology*, 2(2), 38-48. Retrieved from <http://ojs.lib.swin.edu.au/index.php/ejap>.

Reference to a book

Beck, C. A. J., & Sales, B. D. (2001). *Family mediation: Facts, myths, and future prospects*. Washington, DC: American Psychological Association.

Johnson, R. A. (1989). Retrieval inhibition as an adaptive mechanism in human memory. In H. L. Roediger III & F. I. M. Craik (Eds.), *Varieties of memory & consciousness* (pp. 309-330). Hillsdale, NJ: Erlbaum.

English translation of a book:

Lang, P. S. (1951). *A philosophical essay on probabilities* (F. W. Truscott & F. L. Emory, Trans.). New York, NY: Dover. (Original work published 1814)

*In text, cite original date and translation date: (Lang, 1814/1951).

Dissertations and Theses

Caprette, C. L. (2005). *Conquering the cold shudder: The origin and evolution of snake eyes* (Doctoral dissertation). Ohio State University, Columbus, OH.

Pecore, J. T. (2004). *Sounding the spirit of Cambodia: The living tradition of Khmer music and dance-drama in a Washington, DC community* (Doctoral dissertation). Retrieved from Dissertations and Theses database. (UMI No. 3114720)

Caprette, C. L. (2005). *Conquering the cold shudder: The origin and evolution of snake eyes* (Doctoral dissertation). Retrieved from http://www.ohiolink.edu/etd/send-pdf.cgi?acc_num=osu1111184984

Online resource from group/government

U.S. Department of Health and Human Services. (2003). Managing asthma: A guide for schools. Retrieved from http://www.nhibi.nih.gov/health/prof/lung/asthma/asth_sch.pdf

Reference in other Language

Hughes, J. C., Brestan, E. V., & Valle, L. A. (2004). Problem-solving interactions between mothers and children. *Child and Family Behavior Therapy*, 26(1), 1-16. (In Chinese)

Journal abbreviations source

Journal names should be abbreviated according to

Index Medicus journal abbreviations: <http://www.nlm.nih.gov/tsd/serials/lji.html>;

List of title word abbreviations: <http://www.issn.org/2-22661-LTWA-online.php>;

CAS (Chemical Abstracts Service): <http://www.cas.org/sent.html>.

Submission checklist

The following list will be useful during the final checking of an article prior to sending it to the journal for review. Please consult this Guide for Authors for further details of any item.

Ensure that the following items are present:

One Author designated as corresponding Author:

- E-mail address
- Full postal address
- Telephone and fax numbers

All necessary files have been uploaded

- Keywords
- All figure captions
- All tables (including title, description, footnotes)

Further considerations

- Manuscript has been “spellchecked” and “grammar-checked”
- References are in the correct format for this journal
- All references mentioned in the Reference list are cited in the text, and vice versa
- Permission has been obtained for use of copyrighted material from other sources (including the Web)
- Color figures are clearly marked as being intended for color reproduction on the Web (free of charge) and in print or to be reproduced in color on the Web (free of charge) and in black-and-white in print
- If only color on the Web is required, black and white versions of the figures are also supplied for printing purposes

For any further information please visit our customer support site at <http://support.elsevier.com>.

AFTER ACCEPTANCE

Use of the Digital Object Identifier

The Digital Object Identifier (DOI) may be used to cite and link to electronic documents. The DOI consists of a unique alpha-numeric character string which is assigned to a document by the publisher upon the initial electronic publication. The assigned DOI never changes. Therefore, it is an ideal medium for citing a document, particularly ‘Articles in press’ because they have not yet received their full bibliographic information. The correct format for citing a DOI is shown as follows (example taken from a document in the journal *Physics Letters B*): doi:10.1016/j.physletb.2010.09.059 When you use the DOI to create URL hyperlinks to documents on the web, they are guaranteed never to change.

Proofs

One set of page proofs (as PDF files) will be sent by e-mail to the corresponding author (if we do not have an e-mail address then paper

proofs will be sent by post) or, a link will be provided in the e-mail so that authors can download the files themselves. Elsevier now provides authors with PDF proofs which can be annotated; for this you will need to download Adobe Reader version 7 (or higher) available free from <http://get.adobe.com/reader>. Instructions on how to annotate PDF files will accompany the proofs (also given online). The exact system requirements are given at the Adobe site: <http://www.adobe.com/products/reader/systemreqs>.

If you do not wish to use the PDF annotations function, you may list the corrections (including replies to the Query Form) and return them to Elsevier in an e-mail. Please list your corrections quoting line number. If, for any reason, this is not possible, then mark the corrections and any other comments (including replies to the Query Form) on a printout of your proof and return by fax, or scan the pages and e-mail, or by post. Please use this proof only for checking the typesetting, editing, completeness and correctness of the text, tables and figures. Significant changes to the article as accepted for publication will only be considered at this stage with permission from the Editor. We will do everything possible to get your article published quickly and accurately – please let us have all your corrections within 72 hours. It is important to ensure that all corrections are sent back to us in one communication: please check carefully before replying, as inclusion of any subsequent corrections cannot be guaranteed. Proofreading is solely your responsibility. Note that Elsevier may proceed with the publication of your article if no response is received.

Offprints

The corresponding author, at no cost, will be provided with a PDF file of the article via e-mail. For an extra charge, paper offprints can be ordered via the offprint order form which is sent once the article is accepted for publication. The PDF file is a watermarked version of the published article and includes a cover sheet with the journal cover image and a disclaimer outlining the terms and conditions of use.

More information about article offprint is available here: <http://webshop.elsevier.com/>

AUTHOR INQUIRIES

For inquiries relating to the submission of articles (including electronic submission) please visit this journal's homepage. Contact details for questions arising after acceptance of an article, especially those relating to proofs, will be provided by the publisher. You can track accepted articles at <http://www.elsevier.com/trackarticle>. You can also check our Author FAQs (<http://www.elsevier.com/authorFAQ>) and/or contact Customer Support via <http://support.elsevier.com>.

International Soil and Water Conservation Research (ISWCR)

Editorial Board

Editorial Managing Committee

Liu, Ning **Kuang, Shangfu** **Ying, Youfeng** **Liu, Jigen** **Fan, Haoming**
Ning, Duihu **Li, Zhongfeng** **Liu, Guangquan** **Duan, Xingwu**

Advisor

Blum, Winfried
University of Natural Resources and Life
Sciences, Austria

Critchley, William
CIS-Centre for International Cooperation,
Netherlands

Cui, Peng
Institute of Mountain Hazards and Environment,
Chinese Academy of Sciences

Delgado, Jorge A
USDA-ARS-SMSBRU, Soil Management and
Sugar Beet Research Unit, USA

Dumanski, Julian
World Bank; Gov't of Canada, Canada

El-Swaify, Samir
University of Hawai'i, USA

Lal, Rattan
Ohio State University, USA

Li, Rui
Institute of Soil and Water Conservation,
Chinese Academy of Sciences, China

Liu, Baoyuan
Beijing Normal University, China

Liu, Guobin
Institute of Soil and Water Conservation,
Chinese Academy of Sciences, China

Ni, Jinren
Peking University, China

Shao, Mingan
Institute of Geographic Science and Natural
Resources Research, Chinese Academy of
Sciences (CAS), China

Shen, Guofang
Beijing Forestry University, China

Sombatpanit, Samran
Department of Land Development Bangkok,
Thailand

Sun, Honglie
Institute of Geographic Science and Natural
Resources Research, Chinese Academy of
Sciences, China

Tang, Keli
Institute of Soil and Water Conservation,
Chinese Academy of Sciences, China

Yao, Wenyi
Yellow River Institute of Hydraulic Research,
China

Editor-In-Chief

Nearing, Mark
USDA-ARS Southwest Watershed Research Center, USA
mark.nearing@ars.usda.gov

Lei, Tingwu
China Agricultural University, China
leitngwu@cau.edu.cn

Associate Editors

Al-Hamdan, Osama
Texas A&M University,
Kingsville, USA

Baffaut, Claire
USDA-ARS Columbia, MO, USA

Borrelli, Pasquale
University of Basel, Switzerland

Bruggeman, Adriana
Energy, Environment and Water
Research Center of the Cyprus
Institute, Cyprus

Chen, Hongsong
Institute of Subtropical
Agriculture, Chinese Academy of
Sciences, China

Dazzi, Carmelo
University of Palermo, Italy

Fang, Hongwei
Tsinghua University, China

Fullen, Mike
University of Wolverhampton, UK

Golabi, Mohammad
University of Guam, USA

Golosov, Valentin
Kazan Federal University, Russia

Gomez, Jose Alfonso
Institute for Sustainable
Agriculture, CSIC, Cordob, Spain

Gomez Macpherson, Helena
Institute for Sustainable
Agriculture (IAS-CSIC), Spain

Guzmán, Gema
Universidad of Cordoba, Spain

Huang, Chi-hua
USDA-ARS National Soil Erosion
Research Laboratory, USA

Krecek, Josef
Czech Technical University, CZ

Licciardello, Feliciano
University of Catania, Italy

Lorite Torres, Ignacio
Centro Alameda del Obispo,
IFAPA, Junta de Andalucía, Spain

Merten, Gustavo
University of Minnesota Duluth,
USA

Napier, Ted
Ohio State University, USA

Nouwakpo, Sayjro
USDA -ARS Northwest Irrigation
and Soils Research Laboratory,
USA

Nunes, João
University of Lisbon, Portugal

Obando-Moncayo, Franco
Geographic Institute Agustin
Codazzi, Soil Survey Department,
Colombia

Oliveira, Paulo Tarso S.
Federal University of Mato
Grosso do Sul, Brazil

Osorio, Javier
Texas A&M University, USA

Pla Sentís, Ildefonso
Universitat de Lleida, Spain

Polyakov, Viktor
USDA-ARS Southwest Watershed
Research Center, USA

Reichert, Jose Miguel
Federal University of Santa
Maria, Brazil

Sadeghi, Seyed Hamidreza
Tarbiat Modares University, Iran

Sun, Weiling
Peking University, China

Wagner, Larry
USDA-ARS, Rangeland
Resources & Systems Research
Unit, USA

Walling, Des E.
University of Exeter, UK

Wei, Haiyan
Southwest Watershed Research,
USDA-ARS, USA

Williams, Jason
Southwest Watershed Research,
USDA-ARS, USA

Yin, Shuiqing
Beijing Normal University, China

Yu, Xinxiao
Beijing Forestry University,
China

Zhang, Guanghui
Beijing Normal University, China

Zhang, Qingwen
CAAS Institute of Agro-
Environment and Sustainable
Development, China

Zhang, Yongguang
International Institute for Earth
System Science, Nanjing
University, China

Zheng, Fenli
Institute of Soil and Water
Conservation, Chinese Academy
of Sciences, China

Zlatic, Moidrag
University of Belgrade, Serbia

Editorial Board Members

Cai, Qianguo, China
Chen, Yongqin David, China (Hong Kong)

Dazzi, Carmelo, Italy

Du, Pengfei, China

Duan, Xingwu, China

Fullhart, Andrew, USA

He, Binghui, China

Horn, Rainer, Germany

Kapur, Selim, Turkey

Kunta, Karika, Thailand

Li, Li, USA

Li, Yingkui, USA

Li, Zhanbin, China

Liang, Yin, China

Liu, Benli, China

Liu, Xiaoying, China

Lo, Kwong Fai Andrew, China (Taiwan)

McGehee, Ryan, USA

Miao, Chiyuan, China

Mrabet, Rachid, France

Mu, Xingmin, China

Oliveira, Joanito, Brazil

Ouyang, Wei, China

Paz-Alberto, Annie Melinda, Philippines

Peiretti, Roberto, Argentina

Ritsema, Coen, Netherlands

Shi, Zhihua, China

Sukvibool, Chinapat, Thailand

Surendran, Udayar, India

Tahir Anwar, Muhammad, Pakistan

Torri, Dino, Italy

Wang, Bin, China

Wu, Gaolin, China

Yu, Yang, China

Zhang, Fan, China

Zhang, Kebin, China

Managing Editors

Chyu, Paige (Executive Editor)
International Research and Training Center on Erosion
and Sedimentation, China
iswcr@foxmail.com

Li, Kang
China Water and Power Press, China
lk@waterpub.com.cn

Zhao, Ying
International Research and Training Center on Erosion and
Sedimentation, China
zhaoying@iwhr.com